To the Graduate Council:

I am submitting herewith a dissertation written by Changsheng Lu entitled " Geochemical Characterization of the Brewer Gold Hydrothermal System in Carolina Slate Belt, Jefferson, South Carolina." I have examined the final copy of this dissertation for form and content and recommend that it be accepted in partial fulfillment of the requirements for the degree of Doctor of Philosophy, with a major in Geology.

Kula C. Misra

Kula C. Misra, Major Professor

We have read this dissertation
and recommend its acceptance:

Lawrence A. Taylor

Craig E Barnes

Thomas C Jatcko

Accepted for the Council:

Lev Minkel

Associate Vice Chancellor
and Dean of The Graduate School

Geochemical Characterization of the Brewer Gold Hydrothermal System in Carolina Slate Belt, Jefferson, South Carolina

A Dissertation

Presented for the

Doctor of Philosophy

Degree

The University of Tennessee, Knoxville

Changsheng Lu

August, 1994

DEDICATION

This dissertation is dedicated to my parents

Jiahui Lu

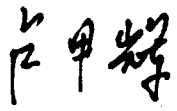

and

Tongmei Sun

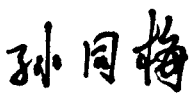

Who have shown their love throughout my life.

ACKNOWLEDGMENTS

I would like to thank my major professor, Dr. Kula Misra, for his guidance and patience throughout this study. He is always there when I need him, especially the last few month of the dissertation preparation. His help and moral support will always be remembered.

Thanks to my other committee members, Dr. Larry Taylor, Dr. Ted Labotka, and Dr. Craig Barnes, for their comments and assistance during various stages of this study. I would also like to thank other faculty and staff in the department, Dr. Otto Kopp, Dr. Claudia Mora, Dr. Don Byerly, and Mr. Allan Patchen, for their help on various mineralogical and chemical analyses. I especially like to thank all the friends and many fellow graduate students in the Department, who made my seemly endless life in the graduate school much more enjoyable. I also appreciate the help from Bob Bodnar of VPI, and Hank Julian and Steve Young of TVA.

This study has been supported financially by the research grants from the Geological Society of America, Sigma Xi, and Southeast GSA, and the Discretionary funds from the Department of Geological Sciences of the University of Tennessee.

I like to thank the Brewer Gold Co. and Westmont Mining Inc. for allowing me to work on this project and providing field assistance. I am especially grateful to Jae Stonehouse, Mark Zwaschka, and John Scheetz for their input and help in this study.

My loving parents have always shown their special love and encouragement, often from long distance, during my long school career, and I like to thank all they have done.

ABSTRACT

Gold mineralization in the Brewer mine in the Carolina slate belt, South Carolina, occurs in an intensely silicified zone, which constitutes the central part of hydrothermal alteration system more than 2 kilometers across. Mineralogic and petrographic studies indicate the following concentric alteration pattern: a silicic breccia center (quartz-pyrite-gold-enargite); an advanced argillic inner zone (quartz-alunite-andalusite); a sericitic outer zone (quartz-sericite); and a patchy propylitic outermost zone (chlorite-epidote-quartz) that grades into unaltered metavolcanic rocks. Geochemical analysis of the host volcanic rocks, including volcanic tuffs, flows, and breccias, indicates a rhyolitic composition within a tholeiitic suite. Compared to the unaltered volcanic rocks, the hydrothermally altered volcanic rocks are relatively enriched in SiO_2 and depleted in K_2O and Na_2O . The altered volcanic rocks also have relatively higher abundances of Sr, Cu, Mo, Pb, and Zr. SiO_2, Cu, and Mo are enriched toward the center of the system, whereas K_2O, Na_2O, Y, and V are depleted in the same direction.

Alunite in the Brewer mine is quite heterogeneous in composition and has extensive solid solution between alunite and natroalunite with compositional zonation of Na increasing from center to rim, as revealed by XRD and electron microprobe analyses. Sulfur isotope analyses of alunite and pyrite indicate a hypogene origin for the alunite and a magmatic hydrothermal environment for the acid sulfate alteration, which was broadly contemporaneous with the gold mineralization. The $\delta^{34}S$ values of the alunites, occurring as veinlets, replacements and disseminatations, range from 17.7 to 26.8 per mil. The $\delta^{34}S$ values of the pyrites of various modes of occurrence--euhedral crystals and finely

disseminated in the groundmass of the pyrite-quartz rocks and breccias, and quartz-pyrite veins-- range from 0.5 to 5.7 per mil. The narrow range of values in pyrite suggests that the sulfur was derived from the same source. That $\delta^{34}S$ values of the alunites are generally 15 to 22 ‰ larger than those of the pyrites suggests that alunite was a direct product of magmatic hydrothermal, acid sulfate alteration in an epithermal environment. Sulfuric acid was probably produced by the disproportionation of SO_2 with decreasing temperature, and equilibrium between aqueous H_2S and SO_4 formed by this disproportionation resulted in the alunite being enriched in ^{34}S relative to pyrite. Pyrite-alunite sulfur isotopic geothermometer gives temperatures of about 300-500 °C.

Microthermometric and microchemical analyses of fluid inclusions in the quartz reveal that the inclusion fluids are dominantly CO_2-bearing aqueous solutions. The majority of the primary and pseudosecondary inclusions are CO_2-bearing two-phase ($L+LCO_2$) or three-phase ($L+LCO_2+VCO_2$) inclusions at room temperature. Some CO_2-rich and aqueous primary and pseudosecondary fluid inclusions are also present, but the aqueous inclusions are mostly secondary in origin. Homogenization temperatures of primary and pseudosecondary fluid inclusions indicate that the hydrothermal fluids had temperatures between 160 and 330 °C. The widespread range probably reflects the effect of multiple- brecciation and hydrofracturing events during mineralization. The fluids have low to moderate salinity (<15 wt% NaCl. equiv.) and contain many trace components, including K, Ca, Ti, Cr, Mn, Fe, Ni, Cu, Zn, As, and Ba, as indicated by synchrotron X-ray fluorescence microprobe analysis. Laser Raman microprobe analysis on the fluid inclusions indicates that the fluids contain SO_4^{2-} in addition to CO_2.

The fluids for the Brewer gold mineralization differ compositionally from those of typical epithermal gold deposits and porphyry Au-Cu-Mo deposits, and a magmatic source appears to be the most likely source for the Brewer mineralizing fluids. Hydrofracturing and brecciation in the Brewer mine suggest that these processes most likely accompanied the release of aqueous fluids from a deep-seated felsic magma. The magma provided both the heat and fluid source for the mineralization. The Brewer hydrothermal system may represent a slightly deeper environment than the typical epithermal systems, with magmatic fluid playing a more important role than in the case of those in shallow environments. It is likely that meteoric water was involved in the process by mixing with the magmatic fluid, especially during the later stage of mineralization. Considering the widespread aluminosilcate alteration and other features in the Brewer mine, it is proposed that the Brewer hydrothermal system is a magmatic hydrothermal acid sulfate system which overlies or is related to a deep porphyry system.

Reaction-path calculations of the ore-forming processes indicate that fluid-rock reactions and mixing of magmatic fluids with cooler and diluted fluids were the dominant processes that contributed to the mineralization. These calculations, in response to the increase in pH and the decrease in temperature, produced sulfide mineral assemblages-- pyrite as the most abundant mineral and various amounts of bornite, chalcopyrite, enargite, covellite, tetrahedrite, and tennantite-- that are similar to those observed in the Brewer mine area. Speciation calculations show that chloride complexes are the dominant species for Fe, Cu, Zn, Pb, and Ag. $Au(HS)_2^-$ is the more abundant species for Au and $AuCl_2^-$ becomes more abundant only during the later stage of fluid-rock reaction.

The bisulfide complex of Au appears to be the dominant complex of gold under reduced conditions and chloride complex appears to be the more stable species under oxidized conditions. The primary mechanisms of gold precipitation appear to have been desulfidation resulting from precipitation of sulfide minerals and increase in pH due to either fluid-rock reaction or mixing with less acidic meteoric water.

TABLE OF CONTENTS

Part 1: Introduction

Part 2: Geochemical Signature of Alteration at the Brew Gold Mine, Jefferson, South Carolina

Part 3: Origin of Alunite and its Implication on the Environment of Hydrothermal Alteration and Gold Mineralization at the Brewer Gold Mine, Jefferson, South Carolina

Part 4: Fluid Evolution during Hydrothermal Gold Mineralization at the Brewer Mine, Jefferson, Carolina Slate Belt: Evidence from Fluid Inclusion Study

Part 5: Ore-forming Consequences and Gold Precipitation in Hypogene Acid Sulfate Environments--a Numerical Approach

Appendices

LIST OF TABLES

Table Page

LIST OF FIGURES

Figure Page

Part 1

Introduction

GENERAL BACKGROUND

The Brewer Gold Mine is located in Chesterfield County, South Carolina, about 2 kilometers southwest of Jefferson (Fig. 1). It is one of the oldest and most productive gold mine in the eastern United States. Gold was discovered at the Brewer Mine in 1828 and gold production from placers started that year. Subsequent mining activity in the Brewer area has occurred intermittently during 1844-1862, 1879-1894, and 1934-1940. Mining at Brewer was renewed in 1987 by the Brewer Gold Company and the production during the first year exceeded cumulative production prior to 1987.

The earliest description of the gold mineralization at Brewer in the context of its geologic setting was probably given by Nitze and Wilkens (1897). Since then, several papers have discussed the gold mineralization in the Brewer Mine and adjacent area. The most important of these include Graton (1906), Sloan (1908), Pardee and Park (1948), Minard (1971), Schmidt (1978, 1985), Spence et al. (1980), Worthington et al. (1980), Bell (1982), Butler (1985), Butler et al. (1988), Scheetz (1991), and Scheetz et al. (1991).

Graton (1908) discussed the gold mineralization at the Brewer Mine in his reconnaissance study of the southern Appalachians. He pointed out that the porphyritic rocks (brecciated) might have been acted on by silica- and ore-bearing solutions and identified the occurrence of topaz in the mine area. Pardee and Park (1948) discussed the early history of the mining at the Brewer Mine, the rock types and mineralization in the area, and a possible magmatic origin for the gold mineralization.

Recent studies in the Brewer Mine area are summarized in the papers by Butler (1985) and Butler et al. (1988). These papers discuss the geological features of the Brewer Mine, including structural, stratigraphic, petrologic, and mineralogical aspects, based mainly on mapping projects. Scheetz (1991) described in detail the mineralogy and textures of alterations and proposed a genetic model for the Brewer deposit. He also

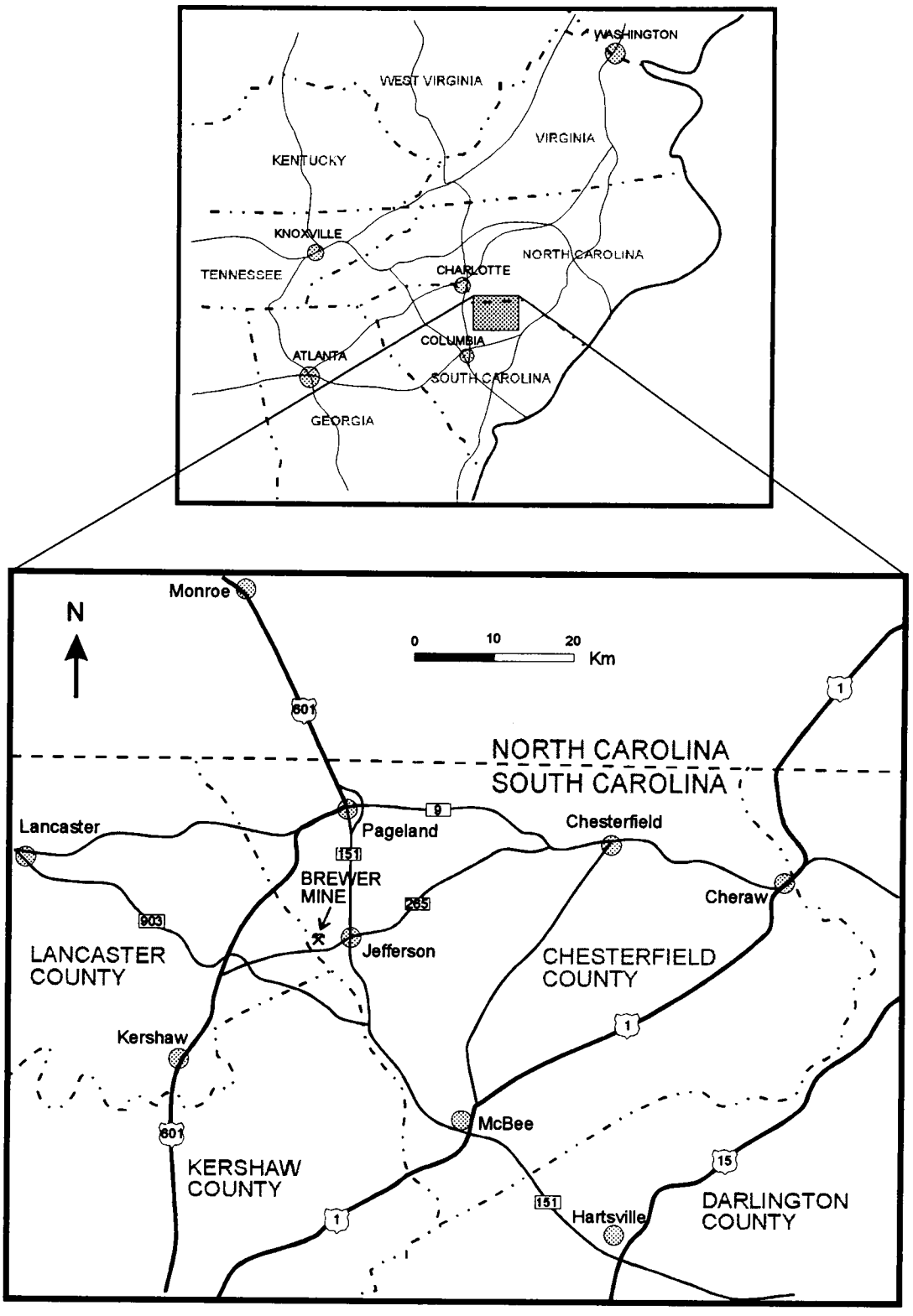

Fig. 1. Map showing location of the Brewer Gold Mine, Jefferson, South Carolina.

provided a complete annotated bibliography of past geological studies in the Brewer Mine area.

The mine area is located within the Carolina slate belt of the northeastern Piedmont of South Carolina, near the overlap of Coastal Plain sediments. The Carolina slate belt, one of the northeast-trending tectono-stratigraphic belts of the southern Appalachian Piedmont, is composed of Precambrian to Cambrian volcanic and sedimentary rocks that were metamorphosed to lower greenschist facies. The Carolina slate belt is considered to be an exotic terrane because its features (stratigraphy, structure, metamorphism, mineral deposits, and fauna) contrast sharply with those of nearby terranes. Paleomagnetic data also support the interpretation that the belt is an exotic terrane that was accreted to North America in early to middle Paleozoic time (Secor et al., 1983; Vick et al., 1983). Williams and Hatcher (1983) have suggested that the slate belt is a part of the Avalon terrane. Most tectonic models for the southern Appalachians (Hatcher, 1972; Rankin, 1975) have related the development of the Carolina slate belt stratigraphic sequence to a volcanic arc environment associated with subduction. An oceanic island-arc model for the Carolina slate belt was suggested by Whitney et al. (1978), based mainly on petrological and geochemical data. According to this model, the Carolina slate belt represents a primitive oceanic island-arc that was separated from a continent by a marginal basin. Rogers (1982) reviewed the relationship of geochemistry to tectonic setting and suggested a continental margin arc environment. Green et al. (1982) argued that the bimodal chemistry of the volcanic and volcanoclastic rocks supports such an interpretation. On the other hand, based on an isolated negative Bouguer gravity anomaly, Long (1979) has proposed that the Carolina slate belt may delineate the axis of an intracontinental rift zone filled with rift-stage volcanic and sedimentary rocks.

Various types of mineralization (Au, Cu, Pb, Zn, and Mo) have been found in the metavolcanic rocks of the Carolina slate belt (Feiss, 1985; Bell et al., 1980). Metallic mineral deposits in the slate belt are of four distinct types (Feiss, 1982): (1) polymetallic massive sulfide deposits, associated with extensive hydrothermal alteration of the host rocks; (2) remobilized massive sulfide deposits, characterized by recrystallization and deformation features; (3) vein-type mineralization of gold and minor base metal sulfides; and (4) postmagmatic hydrothermal veins of tungsten, molybdenum, and gold, related to granitoid intrusives.

Gold is especially abundant in the Carolina slate belt. Gold deposits in the Carolina slate belt may be classified into three broad groups (Feiss, 1985): volcanogenic deposits, metamorphic deposits, and placers. Many gold deposits in the Carolina slate belt are located at or near the contact between the lower volcanic unit and the upper sedimentary unit (Butler, 1985). Gold mining in the Carolina slate belt began in the early 1800's and the belt is still the main gold producer in the eastern United States.

The gold mineralization in the Brewer Mine occurs in an area characterized by intense silicification and is confined almost exclusively to the multiphase, eruptive breccia bodies or pipes in the Brewer area. The fragments within the breccia are composed of volcanic rocks, earlier phases of breccia, and earlier silica matrix types. The matrix of the breccia consists mainly of silica minerals, sulfides, and minor topaz. Sulfide minerals are dominanted by pyrite, with subordinate enargite. Other accessory minerals observed are sphalerite, chalcopyrite, tetrahedrite, bismuthinite, ilmenite, galena, bornite, cinnabar, native sulfur, covellite, chalcanthite, and gold (Scheetz, 1991; Butler, 1985; Butler et al., 1984, 1988; Pardee and Park, 1948). The sulfide minerals commonly make up 2-3% of the matrix in the breccia. Host rocks at the mine are hydrothermally altered and regionally metamorphosed felsic volcanic rocks. The felsic metavolcanic rocks are

overlain by fine-grained metasedimentary rocks that are generally unaltered and unmineralized.

The origin of the Brewer Gold Mineralization and related alteration features have been attributed to: (1) intrusion of the Pageland pluton exposed about 2 km northwest of the Brewer Mine (Pardee and Park, 1948); (2) an older buried intrusion lying at depth under the prospect, with the Brewer Mineralization representing leakage from a mushroom cap of mineralization (Worthington et al., 1980); (3) mineralization along a volcanic plug or explosion vein (Worthington et al., 1980); (4) a porphyry-type gold mineralization (Schmidt, 1985); (5) a fossil hot springs or fumarolic system that originated contemporaneously with the enclosing strata but has now been folded and tilted into its present position (Worthington et al., 1980; Butler et al., 1988); and (6) a pre-metamorphic acid sulfate type epithermal deposit (Scheetz, 1991).

Table 1 is a diagrammatic representation of the sequences in the Brewer area, as inferred from this study, as well as from earlier studies (Lu et al.; 1993, Scheetz, 1991; Butler, 1985; and Schmidt, 1985).

RESEARCH OBJECTIVES AND A GENERAL OVERVIEW

The development of genetic models for hydrothermal gold deposits must include a consideration of the nature and source of the mineralizing solution, source of the gold, and mechanisms of metal transport and deposition. Therefore, in order to understand the nature of mineralization in a specified deposit, it is essential to understand the hydrothermal system responsible for the mineralization. Thus, the central theme of this study is the characterization of the Brewer hydrothermal system in which gold mineralization occurs. This includes defining the mineralogic and geochemical signatures of the hydrothermal alteration, interpreting the formation environments (P, T, fluid characteristics, etc), and proposing viable mechanisms of gold transport and precipitation.

Table 1. Sequence of events at the Brewer mine area

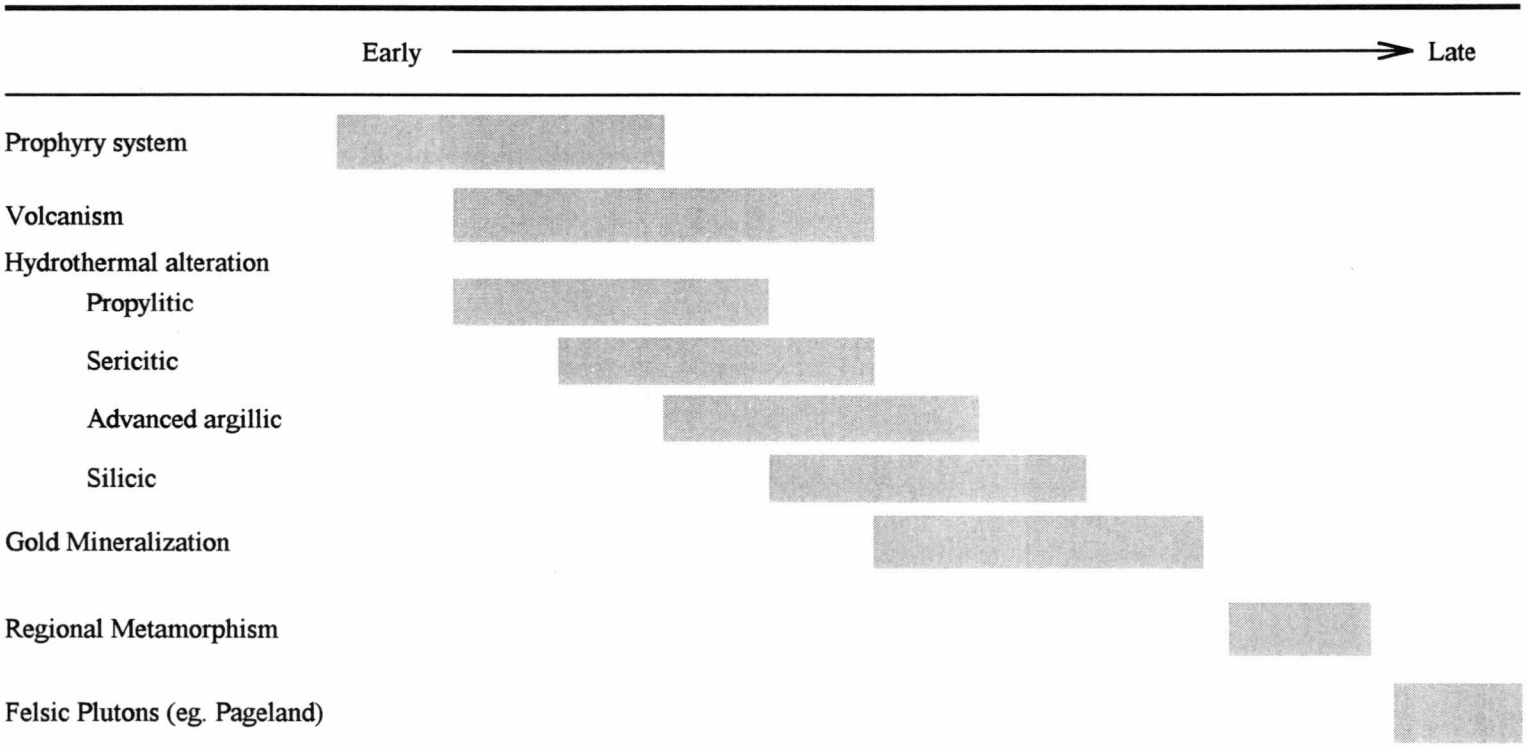

The research here involved aspects of field, petrography, mineralogy, stable isotope, and fluid inclusion studies. Numerical calculations have also been utilized to simulate the geochemical processes that may have contributed to the gold mineralization.

The dissertation consists of four journal-style papers from part 2 to part 5:

Part 2 is "Geochemical signature of alteration at the Brewer Gold Mine, Jefferson, South Carolina", which has already been published (Lu et al., 1993). It classifies the hydrothermal alteration types, defines the chemical affinity of the host rock, and discusses the major and trace elements variations among the alteration zones.

Part 3 is titled "Origin of alunite and its implication on the environment of hydrothermal alteration and gold mineralization at the Brewer Gold Mine, Jefferson, South Carolina". This paper describes the occurrence and petrography of alunite, discusses the mineralogical, chemical, and isotopic characteristics of alunite and associated pyrite, and proposes a genetic model for the hydrothermal alteration and gold mineralization. This paper will be submitted for publication on *Mineralium Deposita.*

Part 4, titled "Fluid evolution during hydrothermal gold mineralization at Brewer Mine, Carolina slate belt: evidence from fluid inclusion study", presents the results of microthermometric and microchemical analyses of fluid inclusions in the Brewer samples. The characteristics and evolution of hydrothermal fluids are discussed in this part. This paper will probably be sent to *Economic Geology* for publication.

Part 5 is "Ore-forming consequences and gold precipitation in hypogene acid-sulfate environments--a numerical approach". It utilizes reaction-path calculations to model the hydrothermal and ore-forming processes that may contribute to the gold mineralization in an epithermal environment, for example, the Brewer system. This part, combined with other modeling results, will be used for publication.

Appendices contain detailed petrographic, mineralogical, geochemical, and analytical data that were collected during this study.

REFERENCES

Bell, H., III, 1982, Strata-bound sulfide deposits, wall-rock alteration, and associated tin-bearing minerals in the Carolina slate belt, South Carolina and Georgia: Economic Geology, v. 77, p. 294-311.

Bell, H., III, Carpenter, R. H., and Feiss, P. G., 1980, Volcanogenic ore deposits of the Carolina slate belt: in Frey, R.W., ed., Excursions in southeastern geology, p. 149-178.

Butler, J. R., 1985, The Brewer mine: in Feiss, P. G., ed., Volcanic-hosted gold and high alumina rocks of the Carolina slate belt: Guidebook for field trip, 1985 SGE fall meeting and 1985 GSA annual meeting, p. 143-199.

Butler, J. R., Scheetz, J. M., Stonehouse, J. M., Tayler, D. R., and Callaway, R. Q., 1988, The Brewer gold mine, Chesterfield County, South Carolina: Guidebook for field trip of the annual GSA meeting, Southeastern section, 22p.

Feiss, P. G., 1985, Gold mineralization in the Carolina slate belt: Speculations on ore genesis: in Misra, K. C., ed., Volcanogenic sulfide and precious metal mineralization in the southern Appalachians: University of Tennessee, Department of Geological Sciences, Studies in Geology 16, p. 220-236.

Graton, L. C., 1906, Reconnaissance of some gold and tin deposits of the Southern Appalachians: U. S., Geological Survey Bulletin 293, 134 p.

Green, G. B., Cavaroe, V. V., Stoddard, E. F., and Abdelzahir, A. M., 1982, Volcanic and volcaniclastic facies in a part of the slate belt of North Carolina: Geological Society of America Special Paper 191, p. 109-124.

Hatcher, R. D., Jr., 1972, Development model for the southern Appalachians: Geological Society of America Bulletin, v. 83, p. 2735-2760.

Long, L. T., 1979, The Carolina slate belt-- Evidence of a continental rift zone: Geology, v. 7, p. 180-184.

Lu, C., Misra, K. C., Stonehouse, J. M., and Zwaschka, M. R., 1993, Geochemical signatures of alterations in Brewer gold mine, South Carolina: South Carolina Geology. v. 35, p. 37-54.

Minard, J. P., 1971, Gold occurrences near Jefferson, South Carolina: U. S. Geological Survey Bulletin 1334, p. 1-20.

Nitze, H.B.C. and Wilkens, H.A.J., 1897, Gold mining in North Carolina and adjacent south Appalachian regions: North Carolina Geological Survey Bulletin 10, 164p.

Pardee, J. T., and Park, C. F., Jr., 1948, Gold deposits of the southern Piedmont: U. S. Geological Survey Professional Paper 213, 156p.

Rankin, D. W., 1975, The continental margin of eastern North America in the southern Appalachians: The opening and closing of the proto-Atlantic Ocean: American Journal of Science, v. 275-A, p. 298-336.

Rogers, J. J., 1982, Critia for recognizing environments of formation of volcanic suites; Application of these critia to volcanic suites in the Carolina slate belt: Geological Society of America Special Paper 191, p. 99-107.

Scheetz, J. W., 1991, The geology and alteration of the Brewer gold mine, Jefferson, South Carolina: M.S. Thesis, University of North Carolina, Chapel Hill, 180p.

Scheetz, J. W., Stonehouse, J. M., and Zwaschka, M. R., 1991, Geology of the Brewer gold mine in South Carolina: Mining Engineering, v. 43. p. 38-42.

Schmidt, R. G., 1978, The potential for porphyry copper-molybdenum deposits in the eastern United States: U. S. Geological Survey Professional Paper 907-E, 31 p.

Schmidt, R. G., 1985, High-alumina hydrothermal systems in volcanic rocks and their significance to mineral prospecting in the Carolina slate belt: U. S. Geological Survey Bulletin 1562, 59 p.

Secor, D. T., Jr., Samson, S. L., Snoke, A. W., and Palmer, A. R., 1983, Confirmation of the Carolina Slate Belt as an exotic terrane: Science, v. 221, p. 649-651.

Sloan, E., 1908, Catalogue of the mineral localities of South Carolina: South Carolina Geological Survey Bulletin 2, 505 p.

Spence, W. H., Worthington, J. E., Jones, E. M., and Kiff, I. T., 1980, Origin of the gold mineralization at the Haile mine, Lancaster County, South Carolina: Mining engineering, v. 32, p. 70-72.

Vick, H. K., Channell, J. E. T., and Opdyke, N. D., 1987, Ordovician docking of the Carolina Slate Belt, paleomagnetic data: Tectonics, v. 6, p. 573-583.

Whitney, J. A., Parks, T. A., Carpenter, R. H., and Hartby, M. E., III, 1978, Volcanic evolution of the southern slate belt of Georgia and South Carolina-- a primitive island arc: Journal of Geology, v. 86, p. 173-192.

Williams, H., and Hatcher, R. D., Jr., 1983, Appalachian suspect terranes: Geological Society of America Memoir 158, p. 33-53.

Worthington, J. T., Kiff, I. T., Jones, E. M., and Chapman, P. E., 1980, Applications of the hot springs or fumarolic model in prospecting for lode gold deposits: Mining Engineering, v. 32, p. 73-79.

Part 2

Geochemical Signature of Alteration at the Brewer Gold Mine, Jefferson, South Carolina

ABSTRACT

Hydrothermal gold mineralization in the Brewer area is hosted by Late Precambrian to Cambrian metavolcanic rocks of the Persimmon Fork Formation of the Carolina slate belt. Geochemical analysis of these volcanic tuffs, flows, and breccias indicates a rhyolitic composition (SiO_2, 70-80%; Al_2O_3, 11-19%; Fe_2O_3, 2.0-4.1%; Na_2O, 0.1-5.1%; K_2O, 2.1-3.9%) within a tholeiitic suite (alkalies 3.0-7.0%). Metasedimentary rocks, stratigraphically overlying the metavolcanic rocks, have a different composition (SiO_2, 52-56%; Al_2O_3, 17-26%; Fe_2O_3, 5.7-12.3%; Na_2O, 0.1-1.7%; K_2O, 1.3-6.0%).

The gold mineralization is accompanied by hydrothermal alteration in the Brewer area. Mineral assemblages indicate the following alteration pattern in the area: a silicic center (quartz-pyrite breccia); an advanced argillic inner zone (quartz-andalusite-alunite rock); a sericitic outer zone (quartz-sericite rock); and a patchy propylitic outermost zone (chlorite-epidote-quartz rock) grading into unaltered metavolcanic rocks. Geochemical analysis of the unaltered and hydrothermally altered rocks reveals variations in element concentrations among alteration zones and a crude chemical zonation. Hydrothermally altered rocks are generally enriched in Si, Cu, Mo, Pb, Zn, and S and depleted in K, Mg, and Rb relative to host volcanic rocks. Si, Fe, Zn, Pb, Cu, and S are also generally enriched toward the center of the alteration halo, whereas K, Na, Mg, and Ba are depleted. Some small breccia pipes in southern part of the sericitic zone have compositions similar to the Brewer breccia rocks, implying that they might have formed as part of the same system as the main silicic central zone. Although Al_2O_3 is quite high in some andalusite-rich samples, the Al_2O_3 content in rocks from the advanced argillic zone is quite similar to rocks from other altered zones and the host metavolcanic rocks (10-20% Al_2O_3). Despite some differences, the tectonic setting, alteration pattern, and alteration types in the Brewer Mine area suggest that it is an epithermal acid-sulfate type

deposit. The lower greenschist facies metamorphism in the region during the Taconic orogeny does not seem to have significantly affected the chemistry of the Brewer rocks and the hydrothermal alteration pattern.

INTRODUCTION

Volcanic-hosted epithermal precious-metal deposits have been studied extensively because of their economic significance and their analogy to active hydrothermal systems (Hayba et al., 1985; Heald et al., 1987; Henley, 1985; Field and Fifarek, 1985; Bodnar et al., 1985). However, most of these studies have been conducted primarily in unmetamorphosed and young (Tertiary) volcanic terranes (Buchanan, 1981; Hayba et al., 1985; Silberman and Berger, 1985; Heald et al., 1987; Berger and Henley, 1988). There is little information on the older volcanic-hosted epithermal deposits, which may have been affected by later regional metamorphism and igneous activity. The deposits in metamorphic terranes may differ from those in unmetamorphosed terranes, especially in terms of mineral assemblages (Ririe, 1990a).

The Carolina slate belt is one of the most interesting and metallogenically significant terranes of the eastern U.S., as it hosts many different types of metallic and nonmetallic mineral deposits (Feiss, 1982, 1985; Feiss et al., 1991). Despite low-grade regional metamorphism and Paleozoic igneous activity, the Carolina slate belt, composed largely of Precambrian to Late Paleozoic volcanic and volcaniclastic rocks, has preserved a large number of epigenetic precious-metal deposits of subvolcanic origin, including the Brewer deposit. Worthington and Kiff (1970) suggested that these deposits are similar to the epithermal precious metal deposits which occur in Tertiary volcanic rocks of the western U.S. Feiss (1982) summarized the geochemistry of the volcanic rocks of the Carolina slate belt and suggested that they represent a calc-alkaline to tholeiitic bimodal suite emplaced in a subduction-related environment.

Gold mineralization in the Brewer area occurs in an intense silica-aluminosilicate alteration complex that is developed within Precambrian to Cambrian metavolcanic rocks (Persimmon Fork Formation) of the Carolina slate belt (Butler, 1985; Butler et al, 1988;

Nystrom, 1972; Schmidt, 1985). The Brewer deposit, mined intermittently over the last hundred years (Butler, 1985), is currently operated by the Brewer Gold Co. Earlier studies in the Brewer Mine area (Graton, 1906; Pardee and Park, 1948; Cherrywell and Butler, 1984; Butler, 1985; Schmidt, 1978, 1985; and Butler et al., 1988) focused mainly on reconnaissance mapping and field description. Jaacks (1986) conducted a geochemical survey of the ore zones and recently, Scheetz (1991) has provided a detailed account of the hydrothermal alteration in the area.

The purpose of this paper is to provide detailed information on the geochemical signatures of the Brewer deposit and its alteration zones and present a comparison of this metamorphosed deposit with epithermal acid-sulfate type deposits in unmetamorphosed terranes.

LOCAL GEOLOGY

The Brewer Gold Mine is located in Chesterfield County, South Carolina, 1.5 miles southwest of Jefferson. The mine lies on a topographic high that is bounded by the Lynches River to the west and its tributary, Little Fork Creek to the east. The deposit occurs in the Carolina slate belt, a NE-SW trending metamorphic terrane of the Piedmont Province in the southern Appalachians (Fig. 1). The Carolina slate belt consists of volcanic and sedimentary rocks of Late Proterozoic to Cambrian age that have been metamorphosed to lower greenschist facies and intruded by various plutons (Butler and Secor, 1991; Butler, 1985; Conley and Bain, 1965). Metavolcanic rocks include volcanogenic clast-dominated pyroclastics, epiclastics, and lava flows ranging up to 13 km in stratigraphic thickness. Metasedimentary rocks are dominated by mudstone, siltstone, and graywacke.

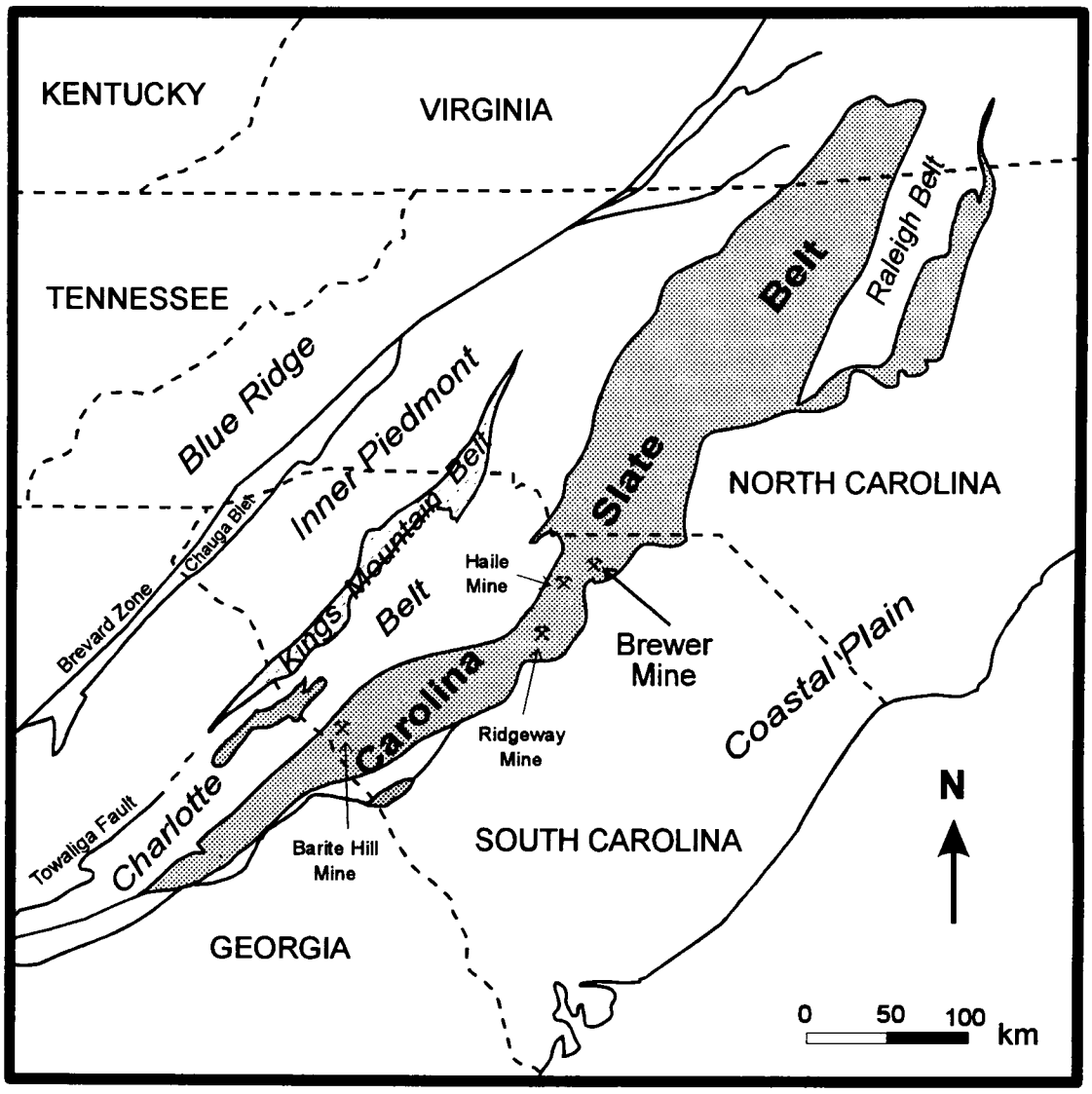

Fig. 1. General geologic map of the southern Appalachian Piedmont, showing the location of the Brewer Mine in the Carolina slate belt (after Butler, 1985).

In northern South Carolina, the Carolina slate belt consists of a predominantly felsic metavolcanic sequence, the Persimmon Fork Formation, that is overlain by metasedimentary rocks of the Richtex Formation (Secor, 1988). This belt is intruded by Paleozoic granitic bodies, such as the Pageland, Liberty Hill, and Lilesville plutons (Fig. 2). The geology of the Jefferson quadrangle, which includes the Brewer Mine area, has been described by Nystrom (1972) and Minard (1971). Metavolcanic rocks, considered equivalent to the Persimmon Fork Formation (Nystrom, 1972), consist of an interbedded mafic-felsic volcanic unit and a felsic volcanic unit. The metasedimentary rocks, mostly laminated slates, are correlated to the Richtex Formation. The "Pageland granite", a quartz monzonite pluton, is exposed northwest of the Brewer Gold Mine. Coastal Plain sediments overlap onto the Brewer area.

Metavolcanic rocks in the Brewer area include volcanic tuffs, flows, and breccias. Petrographic studies reveal that most of the pyroclastic rocks are felsic in composition. Volcanic tuffs include rhyolitic crystal and lithic tuffs. Crystal tuffs are composed of quartz, K-feldspar, and plagioclase crystals in a matrix of fine-grained quartz, sericite, and pumice fragments. Lithic tuffs consist of fragments of various types of volcanic rocks within a fine-grained matrix. Some of the tuffs contain both crystals and lithic fragments, and most show sorting and well-preserved stratification. Volcanic flows are not well stratified and contain blocks, lapilli, and ash with some individual blocks over 10 cm in diameter. Lapilli consist of both lithic fragments and crystals of quartz and feldspar. The matrix is composed of fine grained quartz, sericite, and hematite. Volcanic breccias contain angular lithic fragments (typically with composition similar to that of the matrix) and a matrix of quartz, sericite, and hematite. The volcanic flows and breccias suggest the presence of volcanic centers near the Brewer area.

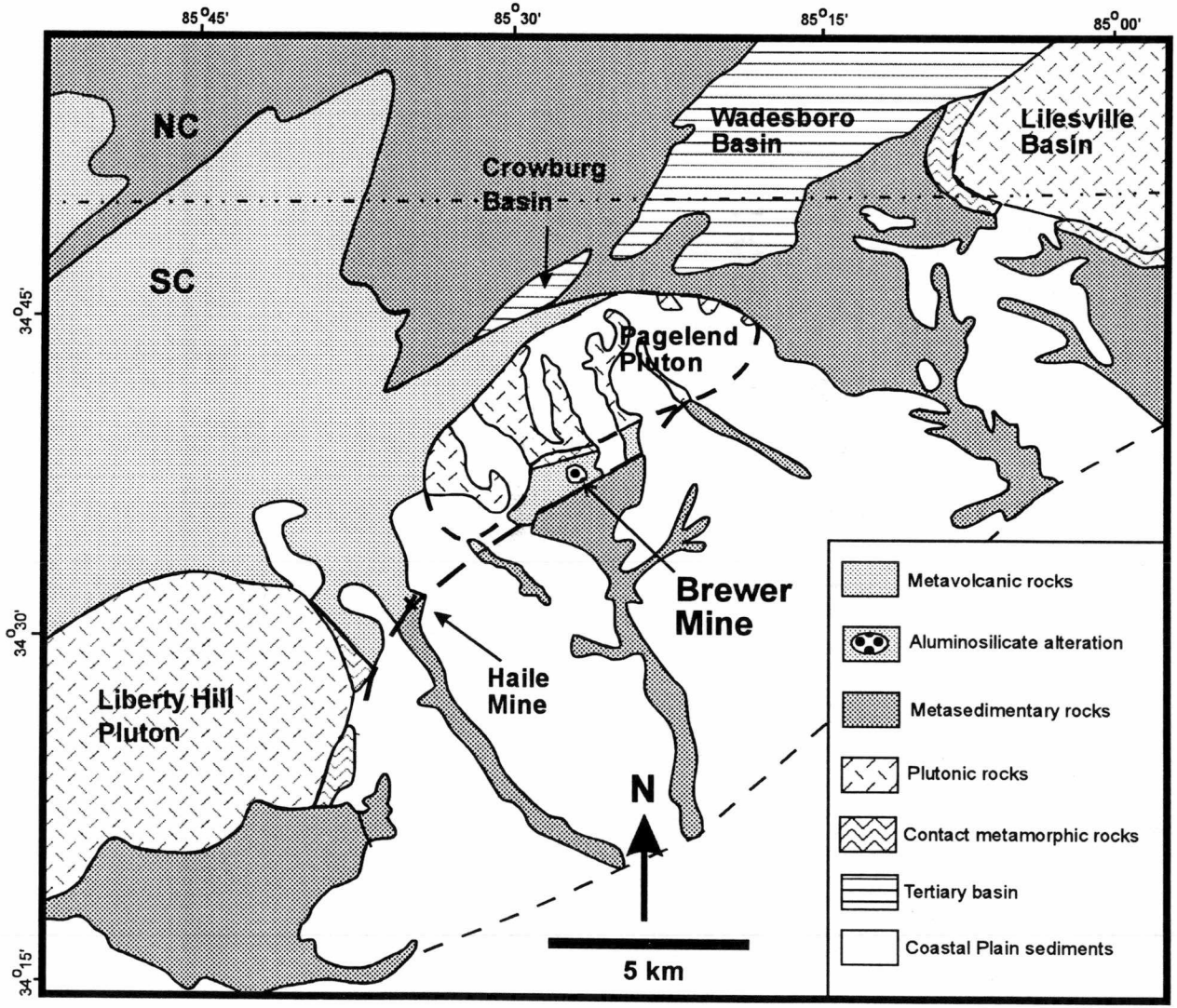

Fig. 2. Generalized geologic map of the Brewer area (after Bell and Popenoe, 1976; Butler et al., 1988; Scheetz, 1991).

Metasedimentary rocks in the Brewer area include mudstone, siltstone, and slate. The mudstone and siltstone are typically well laminated and, close to the Brewer Mine, are interlayered with volcanoclastics. Due to compositional and size differences, the interbedded rocks show distinct color layering in outcrop. Mudstones consist of fine-grained quartz, sericite, and clays. Slate, a product of regionally metamorphosed mudstone, has a mineral assemblage characterized by biotite, epidote, chlorite, quartz, and hematite.

The volcanic and sedimentary rocks have both been metamorphosed during a later regional metamorphic event, probably the Taconic orogeny. The metamorphic grade, based on the mineral assemblages present in the slate, is inferred to be lower-greenschist facies, as suggested earlier by Butler (1985). This is consistent with the overall metamorphic grade of the Carolina slate belt (Butler, 1991). Despite the metamorphism, many of the primary textures in the volcanic and sedimentary rocks, such as bedding planes and orientation of crystals and lithic fragments, are well preserved.

GOLD MINERALIZATION

The Brewer Mine occurs within the felsic volcanic rocks of the Carolina slate belt close to and partly under a thin edge of overlapping Coastal Plain sediments. Gold mineralization occurs in an intensely silicified zone composed of brecciated quartz-sulfide rocks, quartz-andalusite breccias, and massive sulfide-quartz rocks. Two ore bodies have been delineated (Scheetz et al., 1991): the main ore body of the Brewer pit, and a smaller body (B-6) which is located to the southeast of the main ore body. The main ore body in the Brewer pit is composed of quartz-pyrite breccias, quartz-andalusite breccias, and quartz-topaz rocks. The breccias are multi-phase, heterolithic, matrix- or clast-supported

breccias. Most clasts within the breccias consist of pre-existing breccia fragments. Fine-grained quartz, various sulfide minerals and topaz consist of the breccia matrix. The B-6 ore body is tabular, extending along a NWW-SSE direction, perhaps along a fault zone. The western part of the ore body is composed of intensely fractured breccia and quartz-andalusite rock and occurs along the contact of the two lithologies; the eastern part of the ore body was originally a massive sulfide rock containing some quartz, andalusite, kyanite, and topaz, but now is mainly represented as an aluminosilicate-bearing gossan.

Although quartz and pyrite are the dominant minerals in the mineralized zones, aluminosilicate minerals, such as andalusite and paragenetically later kyanite, may be locally abundant. Topaz occurs either in veins or as fine-grained matrix in the breccias. Enargite is also quite abundant in some quartz-sulfide breccias. Accessory minerals include sphalerite, chalcopyrite, bornite, cassiterite, chalcocite, tetrahedrite, galena, ilmenite, cinnabar, and native sulphur (Butler et al., 1988; Scheetz, 1991). Gold primarily occurs along grain boundaries.

HYDROTHERMAL ALTERATION

The gold-bearing silicic zone at Brewer is part of a much larger hydrothermal alteration system that extends over more than 2 kilometers across and has a near-circular shape in plan view (Fig. 3). Despite subsequent regional metamorphism, the hydrothermal alteration zones are easily discernible by their mineral assemblages, especially in the inner part of the system that has been subjected to mining. The alteration has been described in the literature as "widespread silicification and extensive development of pyrophyllite and sericite" (Pardee and Park, 1948), "massive quartzite"

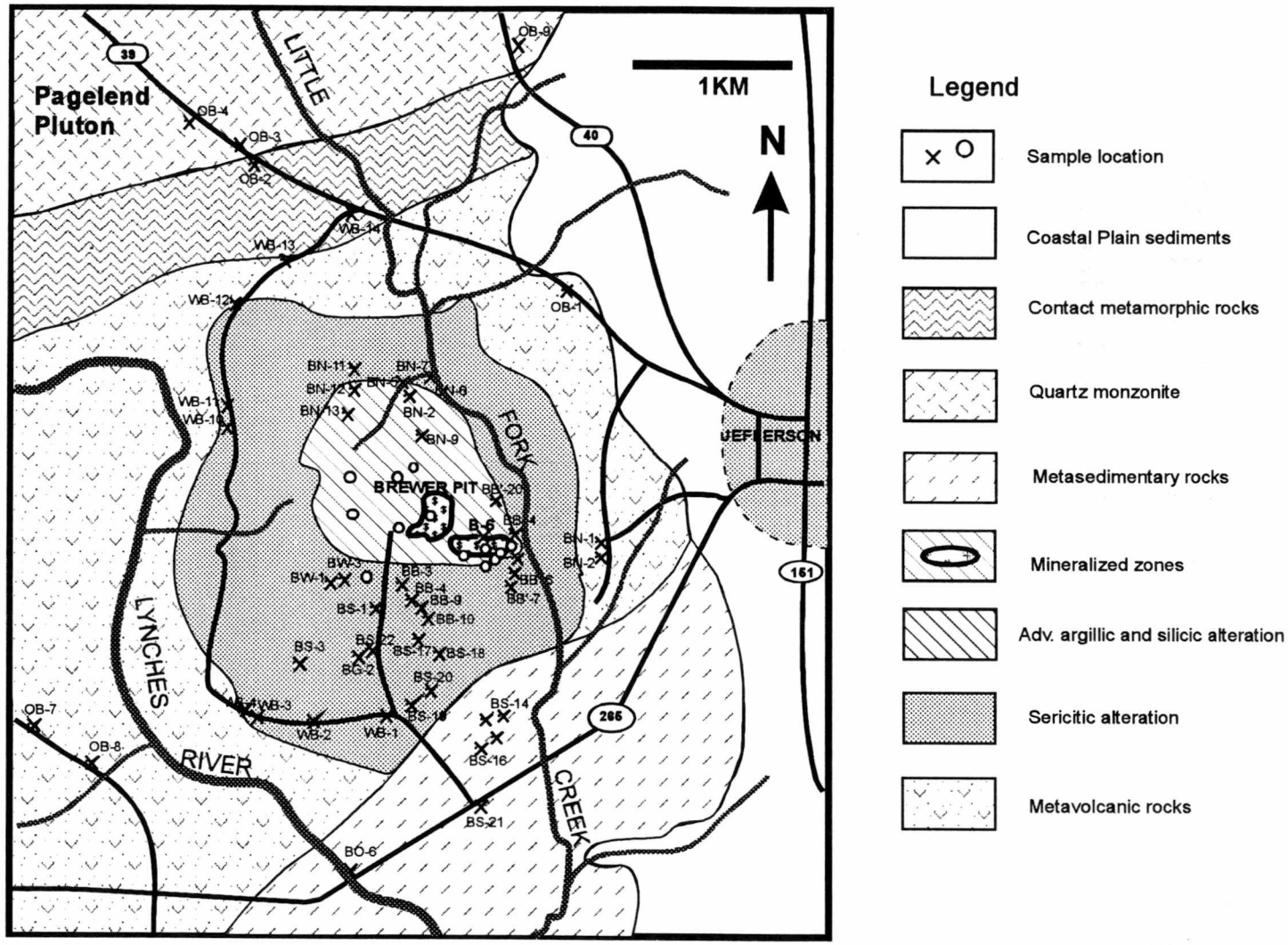

Fig. 3. Geologic map of the Brewer Mine, showing the distribution of hydrothermal alterations (modified after Schmidt, 1985; Nystrom, 1972; Scheetz, 1991). Note the concentric pattern of the silicic, advanced argillic, and sericitic alteration zones.

(Nystrom, 1972), "quartz granofels of high-fluorine subvolcanic alteration" (Schmidt, 1985), and most recently, "quartz-sulfide inner zone and quartz-sericite phyllite outer zone" (Scheetz et al., 1991). Scheetz (1991) described the alteration at the Brewer Mine in more detail in his M.S. thesis.

Based on mineralogical features used in the general classification of hydrothermal alteration summarized by Heald et al. (1987), four types of hydrothermal alteration can be recognized in the Brewer area: (a) silicic, (b) advanced argillic, (c) sericitic, and (d) propylitic. They are described below.

a. *Silicic alteration*

Silicic alteration in the Brewer Mine area is represented by quartz-sulfide rocks and it is confined to the central part of the alteration system. Geochemically, it is characterized by extreme abundance of silica, a hydrothermally introduced component. Quartz and pyrite are the dominant minerals with quartz often constituting more than 80 percent of the rock. Quartz and pyrite occur both in the clasts and matrix. Pyrite commonly occurs in the matrix of matrix-supported breccia and in the fractures of clast-supported breccia, behaving as a cementing material. Both quartz and pyrite are fine-grained, whereas the clasts are typically fine-grained aggregates of quartz and minor pyrite. Locally, topaz occurs in the matrix. Andalusite is also present locally, especially in the B-6 area, where andalusite can be quite abundant along with quartz and pyrite. Enargite is concentrated in certain phases of the brecciation. As discussed above, many accessory sulfide minerals are present in this zone. Pyrophyllite occurs along the fractures locally, typically associated with quartz veins. Gold mineralization is mainly confined to the silicic zone.

b. *Advanced argillic alteration*

Advanced argillic alteration is characterized by the assemblage quartz, alunite, and andalusite, with varying amounts of sericite, pyrophyllite, pyrite, topaz, diaspore, lazulite, and kaolinite. The rocks are typically quartz-andalusite rocks with local breccia texture present. Andalusite occurs as porphyroblasts in a fine-grained quartz-sericite matrix and as smaller grains within fractures. It is usually anhedral and, in some cases, is partially replaced by kyanite, quartz, and pyrophyllite. Alunite is present in three forms: microcrystalline aggregates, disseminations in the matrix, and vein-fillings. In microcrystalline aggregates, alunite and quartz apparently replaced phenocrysts in the original volcanic rocks, most likely feldspars. As disseminations in quartz-dominated matrix, alunite is fine-grained, tabular to columnar, and randomly oriented. Alunite, with quartz and andalusite, also occurs in veins. Quartz typically occurs as fine-grained, anhedral crystals that constitute the matrix, although some appear as aggregates. Kyanite occurs in the alteration zone, but only as replacement of andalusite, so it is probably a product of regional metamorphism.

c. *Sericitic alteration*

Sericitic alteration is represented by the assemblage quartz and sericite, with some pyrite and minor ilmenite. The rocks are commonly metamorphosed to quartz-sericite schist and phyllite, but original volcanic textures, such as pyroclastic and flow textures, are preserved locally. The schist is typically composed of fine-grained quartz- and or sericite-rich compositional layers. Quartz aggregates are also common along foliation. Fe-oxide stains mark foliation along pyrite-rich layers that parallel foliation. Sericite is preferably oriented along foliation planes, but the foliation penetrates sericite aggregates (Scheetz, 1991) indicating that the sericite is pre-tectonic. Chloritoid, occurring as

porphyroblasts in the quartz-sericite schist, exhibits syntectonic growth within the foliation, indicating a regional metamorphic origin.

A few breccia pipes were identified in southern part of the sericitic zone. These breccia pipe rocks have an assemblage of quartz, andalusite, pyrophyllite, sericite, and Fe-oxide, and they exhibit brecciated textures. The rocks are similar to brecciated andalusite-quartz rocks in the advanced argillic alteration zone.

d. *Propylitic alteration*

A mineral assemblage of quartz, epidote, calcite, chlorite, and pyrite defines the propylitic alteration. Sericite, K-feldspar, hematite, rutile, and ilmenite are present in minor amounts. The rocks exhibit volcanic pyroclastic textures (breccia and flow), similar to those observed in the volcanic country rocks not affected by hydrothermal alterations. Calcite occurs as replacement of plagioclase phenocrysts and as fine-grained aggregates in the matrix. Epidote is present as elongated crystals or as radiating aggregates. Chlorite constitutes only a minor component in the rocks.

The alteration types show a roughly concentric distribution (Figure 3). Silicic alteration forms the core of the hydrothermal system and is surrounded by a zone of advanced argillic alteration. These two zones broadly correspond to the "massive quartzite zone" of Nystrom (1972) and the "quartz granofels zone" of Schmidt (1985). They probably represent the center of a volcanic system - a cinder zone, a caldera, or a diatreme (Nystrom, 1972). Sericitic alteration surrounds the zone of advanced argillic alteration and grades outward to either propylitic alteration or unaltered volcanic rocks. The sericitic zone is described by Nystrom (1972) as sericite phyllite and by Schmidt (1985) as quartz-sericite-pyrite schist. Propylitic alteration occurs sporadically outside of the sericitic zone, mainly in the southern and southwestern parts of the system. The

alteration zoning pattern is similar to that of epithermal acid-sulfate deposits and its crude concentric pattern suggests a pre-metamorphic hydrothermal origin.

GEOCHEMISTRY OF THE ALTERATION ZONES

Analytical Procedure

About 90 samples from the Brewer Mine area have been analyzed for their major and trace elements in order to determine geochemical signatures of the alteration zones and possible geochemical associations. The samples are mainly from various alteration zones and unaltered volcanic rocks. A few samples of metasedimentary rocks, plutonic rocks, and contact metamorphic rocks were also analyzed. Analyses were performed on pressed pellets of finely ground powder by an in-house EG&G ORTEC Energy-dispersive X-ray Fluorescence Spectrometer (Johnson and King, 1987). The calibration protocol for XRF analysis was prepared using standard reference materials (Abbey, 1983) available from the U.S. Geological Survey, National Bureau of Standards, Canada Certified Reference Materials Projects, and other institutes. The LOI (loss on ignition) was determined gravimetrically and includes the loss of volatile substances, such as H_2O and CO_2, as well as any weight gain from stoichiometric oxygen through the oxidation of Fe^{2+} to Fe^{3+}.

All the major elements (Si, Al, Na, Mg, K, Ca, Fe, Ti, Mn, and P) are reported as oxide in percent (%) and trace elements (Cu, Zn, Pb, Mo, Ni, Cr, Co, V, Rb, Sr, Y, Zr, Nb, Ba) in parts per million (ppm). Table 1 lists all the average major and trace element compositions for the various rock types in the Brewer Mine area, as well as adjacent plutonic and contact metamorphic rocks.

Table 1. Major and trace element composition of lithologies within the Brewer mine area

	Metasedimentary rocks	Metavolcanic rocks	Sericitic	Advanced argillic	Silicic	Breccia pipes	Hornfels	Pageland granite
No. of Analysis	4	7	17	21	9	3	3	3
(%)								
Na_2O	0.54	1.42	0.77	1.07	0.63	0.60	3.05	3.96
K_2O	3.25	3.03	2.21	1.05	0.32	0.05	1.42	4.51
Al_2O_3	21.8	14.6	12.6	14.5	13.7	16.7	15.8	13.2
TiO_2	0.94	0.36	0.43	0.36	0.34	0.42	0.59	0.17
SiO_2	56.6	73.7	77.3	74.5	78.5	75.9	60.4	74.1
MgO	2.07	0.45	0.17	0.33	0.17	0.09	3.51	0.38
CaO	1.11	0.06	0.05	0.01	0.00	0.00	5.31	1.02
Fe_2O_3	8.36	2.79	3.09	1.97	1.71	3.10	6.42	1.78
MnO	0.06	0.03	0.03	0.02	0.02	0.03	0.12	0.02
P_2O_5	0.13	0.06	0.16	0.40	0.29	0.10	0.07	0.10
L.O.I.	5.46	2.87	2.61	6.31	4.22	3.10	2.16	0.93
Total	100.8	99.6	99.6	101.5	100.3	100.2	99.2	100.3
(ppm)								
Cu	38	17	19	21	22	15	37	18
V	*419	109	*204	114	98	154	53	0
Cr	30	4	4	9	6	7	65	6
Co	39	5	6	7	6	6	15	4
Ni	50	7	6	6	9	7	34	7
Zn	*203	52	64	*217	116	110	95	32
Pb	12	21	43	*108	26	21	9	24
Rb	82	92	45	14	10	0	56	228
Sr	100	93	200	451	114	113	321	92
Y	44	18	24	11	2	25	15	58
Zr	133	164	216	335	174	181	136	147
Nb	14	9	10	8	11	13	6	30
Mo	2	9	12	11	24	12	1	8
Ba	453	477	450	518	204	182	383	459

* Concentrations in some samples of the group are higher than the upper limit of calibration range.

Unaltered Metavolcanic and Metasedimentary Rocks

An important task in the geochemical characterization of alteration zones is determination of the protolith. The apparently unaltered metavolcanic rocks chosen for analysis are believed to represent samples of the volcanic protolith, because they were collected outside the area of pervasive hydrothermal alteration and have primary textures similar to altered volcanic rocks in the mine. The composition of the unaltered metavolcanic rocks -- SiO_2 mainly >70%, Al_2O_3 11-19%, Fe_2O_3 2.0-4.1%, MgO 0.1-0.8%, Na_2O 0.0-5.1%, and K_2O 2.1-3.9% (Fig.4) -- is similar to the average composition of rhyolite compiled by LeMaitre (1976) (SiO_2 72.8%, Al_2O_3 13.2%, Fe_2O_3 2.71%, MgO 0.39%, Na_2O 3.55%, K_2O 4.30%) and falls within the range of felsic volcanic rocks for the areas of Albemarle, North Carolina, and McCormick, South Carolina-Lincolnton, Georgia, reported by Feiss (1982). An important point is the narrow range of SiO_2 and Al_2O_3 for all the samples even though the rock type ranges from tuff to breccia and flow. The mafic unit reported by Nystrom (1972) was not analyzed in this study.

The metasedimentary rocks, stratigraphically overlying the metavolcanic rocks, have a different composition: SiO_2 52-56%, Al_2O_3 17-26%, Fe_2O_3 5.7-12.3%, MgO 0.4-4.3%, Na_2O 0.0-1.7%, and K_2O 1.3-6.0% (Fig. 4). The metasedimentary rocks (mudstone and argillite) have very low CaO, similar to the metavolcanic rocks (<0.2%). One sample of slate has a relatively higher CaO content (4.25%), probably reflecting the presence of epidote in the rock. Compared to the metavolcanic rocks, the metasedimentary rocks are slightly higher in TiO_2 and in some trace elements (V, Cr, Co, Ni, Zn; Table 1), but the available data do not permit a detailed correlation between the volcanic and sedimentary rocks.

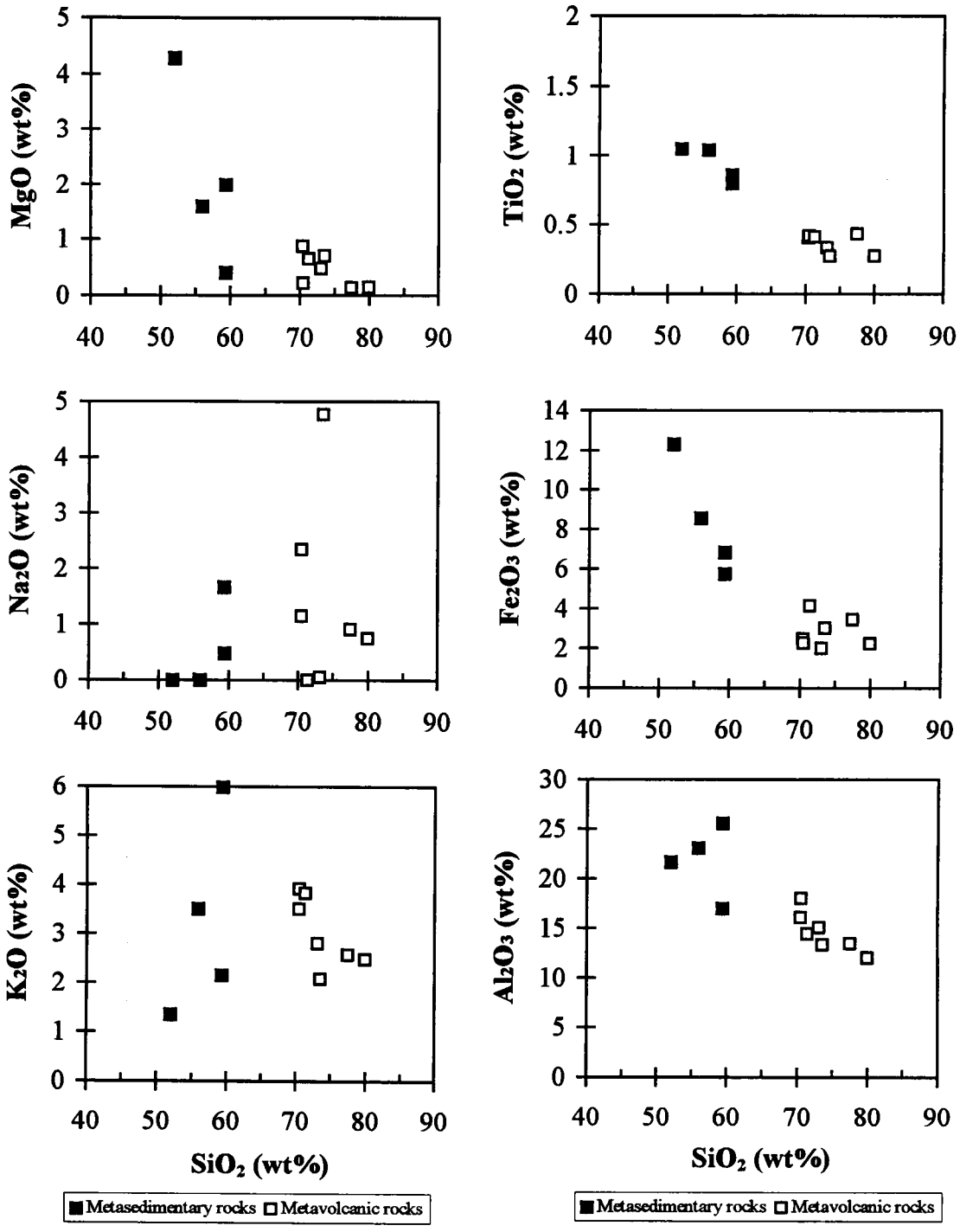

Fig. 4. Plots of various major elements vs. SiO_2 of hosting metavolcanic rocks and overlying metasedimentary rocks in the Brewer Mine area.

Geochemical Signatures of the Alteration Zones

Major element geochemistry

Overall, rocks within the Brewer alteration zone have a wide range of composition: 61-91% SiO_2, 7-25% Al_2O_3, 0.12-8.34% Fe_2O_3, 0.01-4.10% K_2O, 0.00-3.70% Na_2O, and 0.01-1.00% MgO. The rocks contain very little CaO (< 0.2%). Figure 5 is a Al_2O_3-SiO_2 plot for the unaltered and altered volcanic rocks. Rocks from the sericitic and advanced argillic alteration zones have a large range of SiO_2 compared to those from the silicic breccia zone. However, many of the silica-rich samples from the silicic zone are not represented here, because the high SiO_2 contents (typically > 90%) fall outside the SiO_2 range of calibration protocol. Petrographic studies indicate that these rocks are composed mainly of quartz with pyrite, as discussed in the previous section. The breccia pipes in the southern part of the sericitic zone have a similar composition as the silicic breccia rocks in the central zone.

Figure 6 illustrates the relationship between Fe_2O_3 and SiO_2. Fe_2O_3 varies widely in the rocks, especially in the sericitic and advanced argillic alteration zones, compared to the unaltered volcanic rocks. The relatively lower Fe_2O_3 of the silicic zone rocks probably reflects a bias in that many of the pyrite-rich samples were not analyzed.

Figure 7 is plots of K_2O-SiO_2, Na_2O-SiO_2, and MgO-SiO_2 for the rocks. The most obvious feature is the extremely low K_2O in the silicic zone and breccia pipes (Fig. 7a). The rocks from the sericitic and advanced argillic zone have a wide range of K_2O, but all altered rocks show some depletion relative to the unaltered volcanic rocks. Na_2O, for the most part, is also low (<2%) in the alteration zones (Fig. 7b). Alunite-bearing rocks have relatively higher Na_2O (2.3-3.6%), significantly higher than other rocks (<2%) in the same zone. The composition of alunite in the Brewer Mine is apparently a K-Na solid solution, as also indicated by X-ray diffractometric patterns. MgO is very low in the

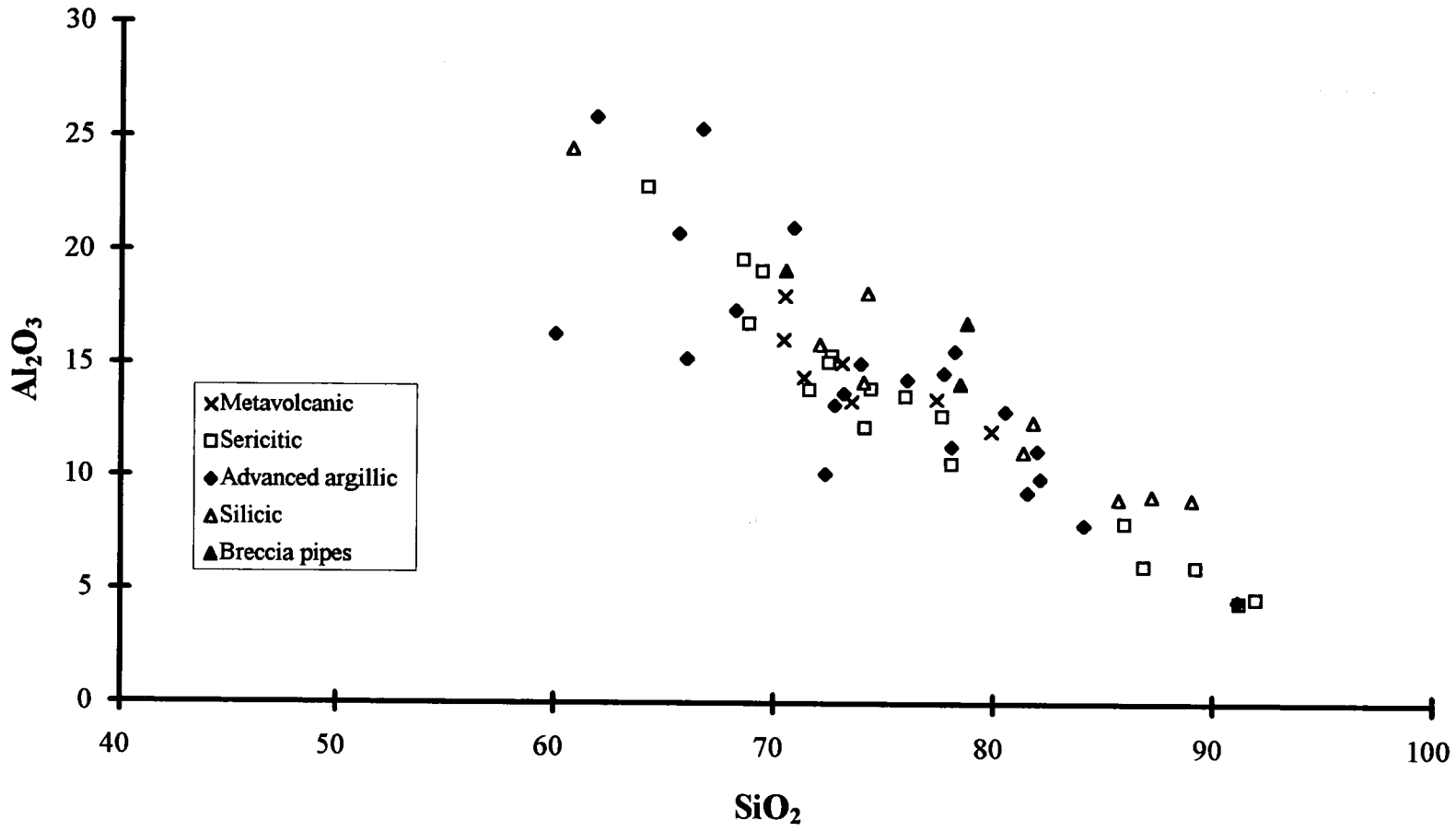

Fig. 5. A plot of Al_2O_3 vs. SiO_2 of the rocks from Brewer alteration zones. Note that the rocks are grouped based on the alteration types.

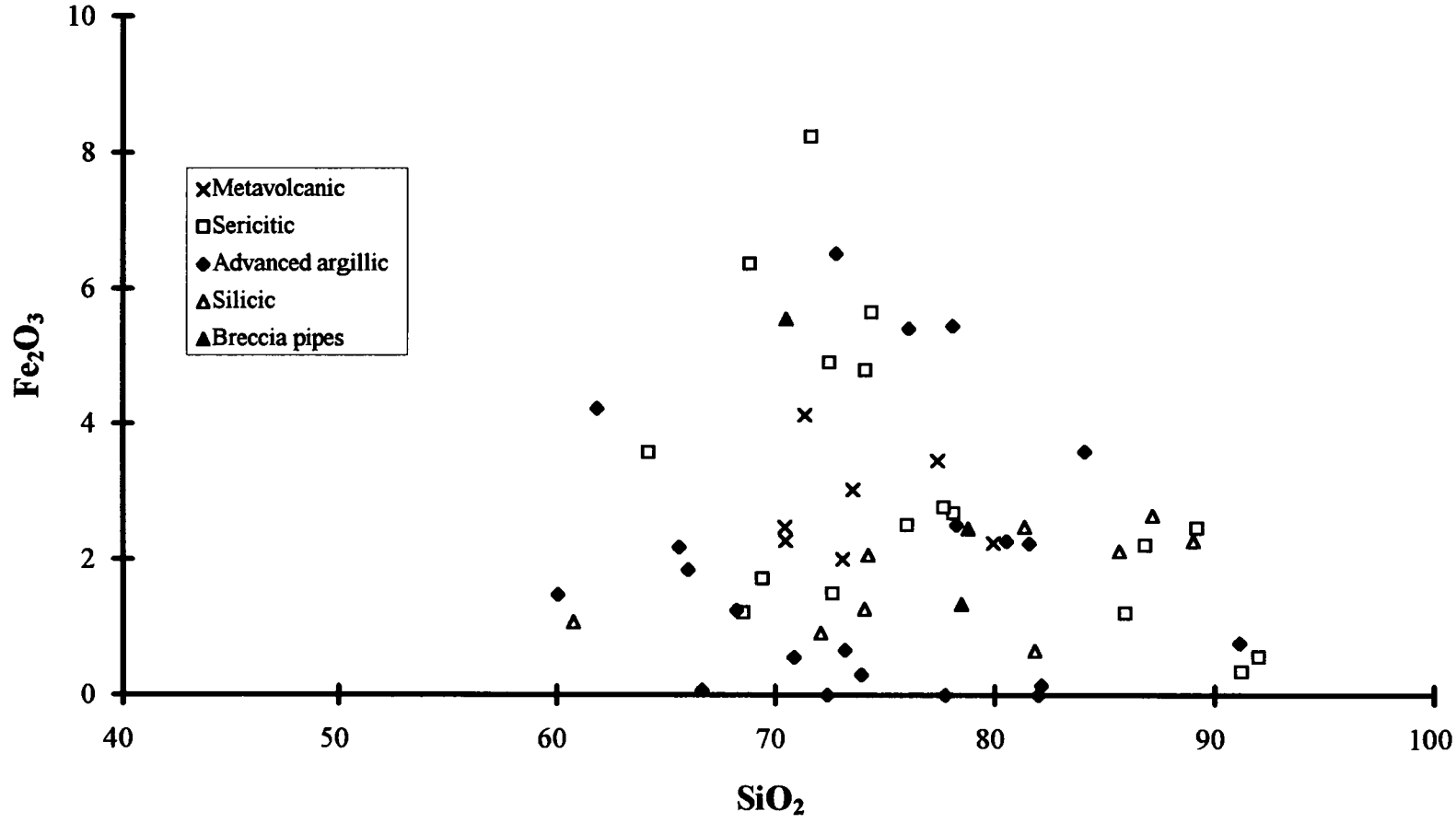

Fig. 6. A plot of Fe_2O_3 vs. SiO_2 of alteration rocks.

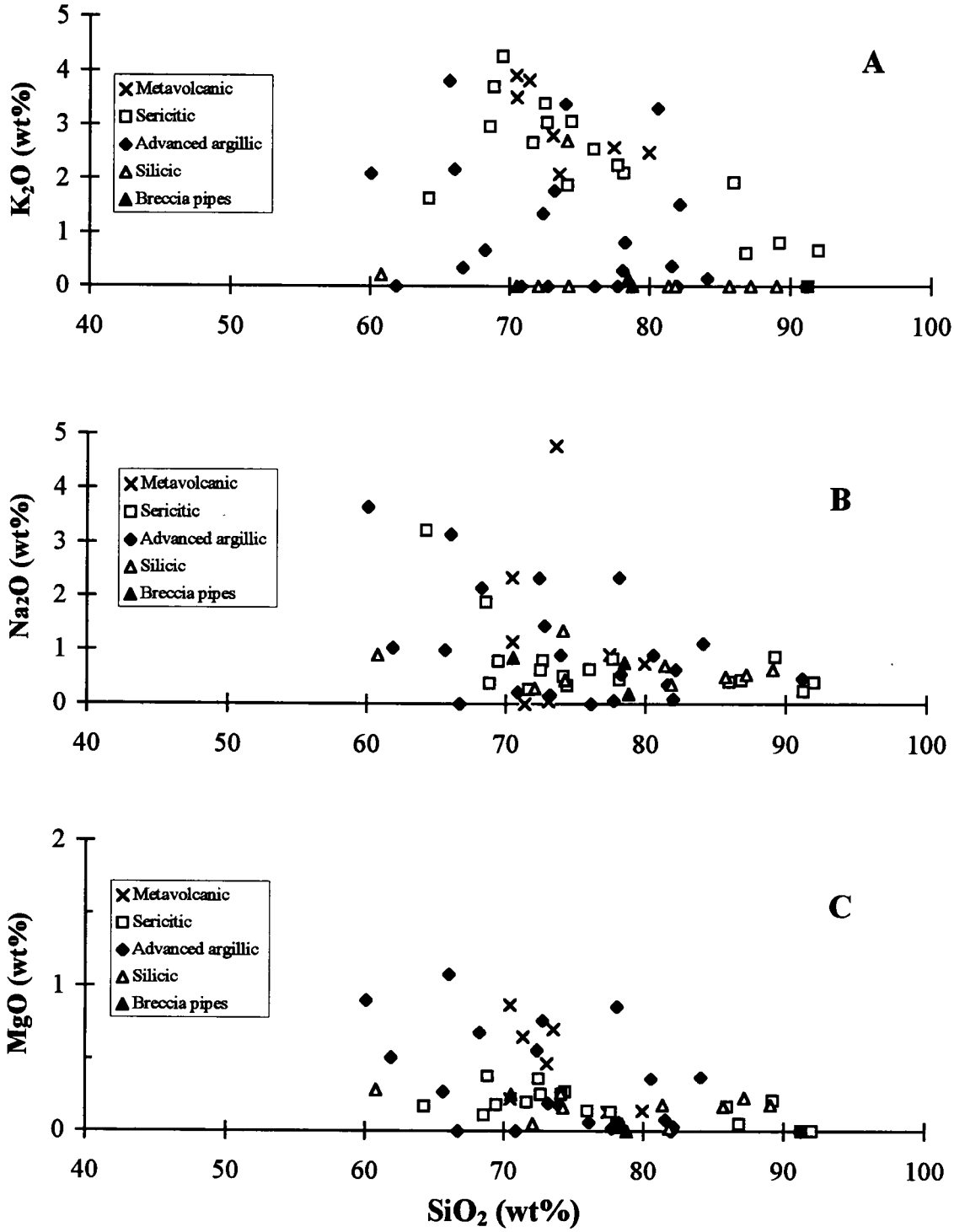

Fig. 7. Plots of K_2O, Na_2O, and Mgo vs. SiO_2 of altered rocks. Note that the silicic zone has very low concentrations of K_2O, Na_2O, and MgO.

rocks, mainly less than 1% (Fig. 7c). In the advanced argillic zone, MgO shows a relatively wider range, reflecting the distribution of Mg-bearing alteration minerals.

Overall, the hydrothermally altered rocks are depleted in alkali relative to unaltered volcanic rocks (Fig. 8). Alunite-bearing samples have higher alkali concentrations. Rocks from the silicic zone and breccia pipe are very low in alkali element. The metavolcanic rocks appear to be tholeiitic, similar to the volcanic rocks in the Albemarle area of North Carolina and the McCormick area of South Carolina-Lincolnton area of Georgia (Feiss, 1982).

A TiO_2-SiO_2 plot (Fig. 9) shows that TiO_2 varies mainly between 0.2 and 0.6% in altered rocks. The metasedimentary, contact metamorphic, and granitic rocks mainly have either higher or lower TiO_2.

The major elements show some systematic variations among the different alteration zones (Figure 10). SiO_2 increases slightly from the outer to the inner zone, whereas K_2O and Na_2O are depleted. Fe_2O_3 increases slightly in the sericitic zone, then decreases toward the advanced argillic zone. Al_2O_3 shows little variation throughout the zones, even though some andalusite-rich samples have relatively higher values. The same observation was noted with TiO_2. Ti and Al seem to have behaved as immobile elements during hydrothermal alteration assuming constant rock volume.

Trace element geochemistry

Fourteen trace elements (Cu, Zn, Pb, Mo, Ni, Cr, Co, V, Rb, Sr, Y, Zr, Nb, Ba) were analyzed. Based on the abundance, these elements fall into three groups. The first group, including Co, Cr, Ni, and Nb, is typically less than 10 ppm in most rocks. The second group, including Cu, Y, Mo, Pb, Rb, and Zn, has concentrations mainly between 10 and 100 ppm. The third group, consisting of Ba, Sr, Zr, and V, has concentrations mainly greater than 100 ppm (Fig. 11).

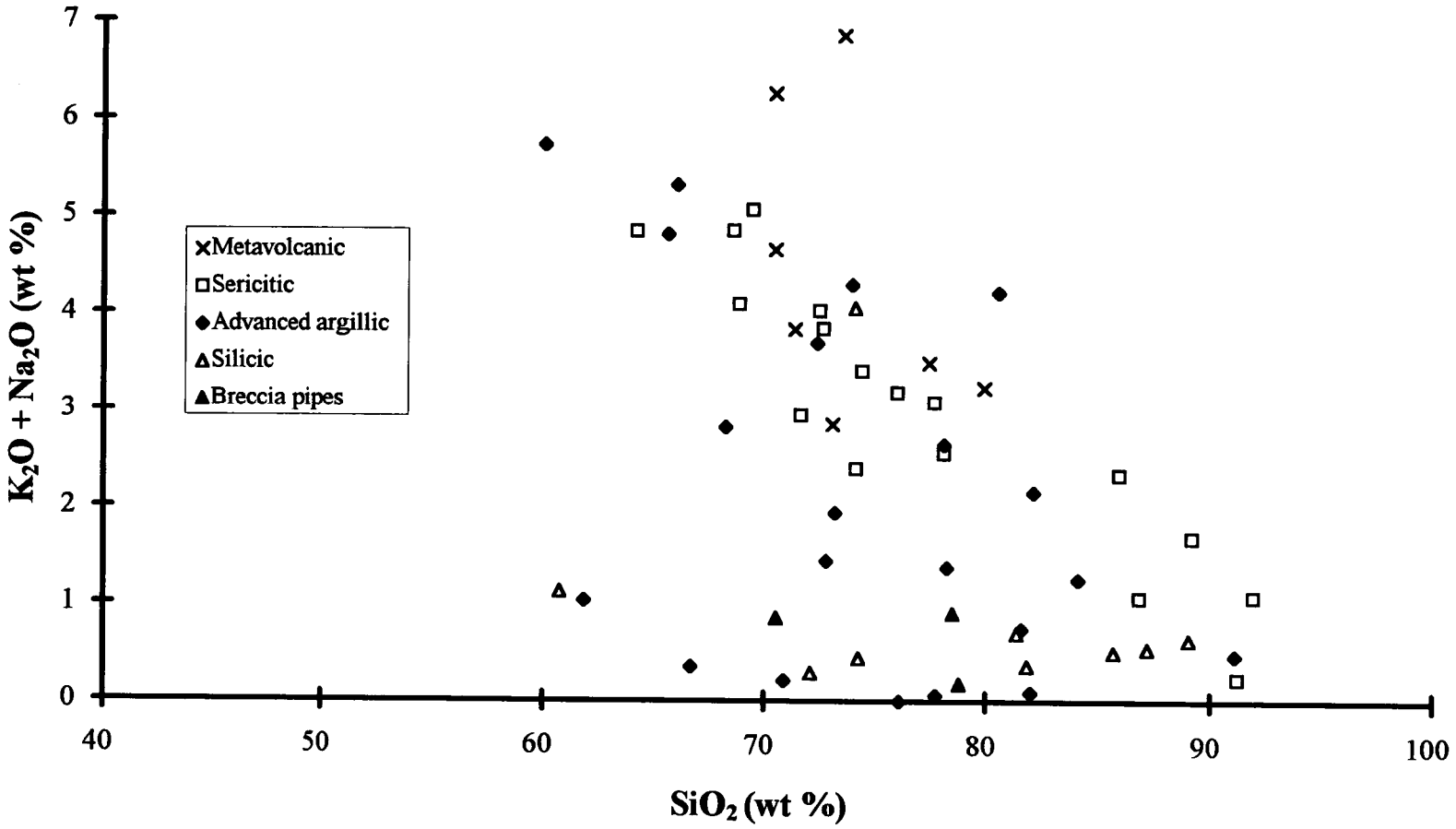

Fig. 8. An Alkali-SiO_2 plot of altered rocks showing the depletion of alkali (Na_2O+K_2O) toward the center of the Brewer system. The host volcanic rocks represent a tholeiitic suite.

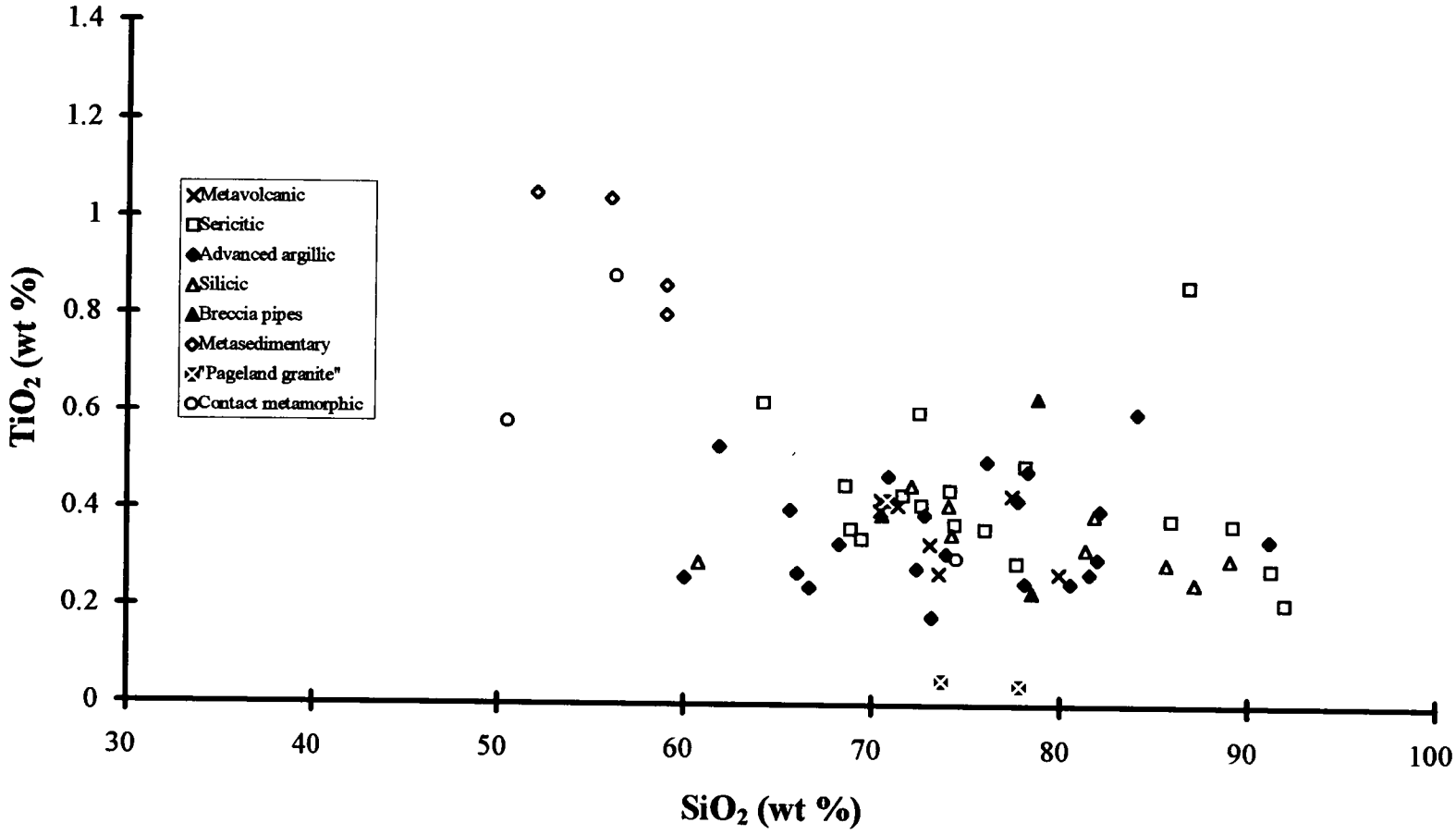

Fig. 9. TiO_2-SiO_2 plot showing the relatively uniform content of TiO_2 throughout the alteration zones.

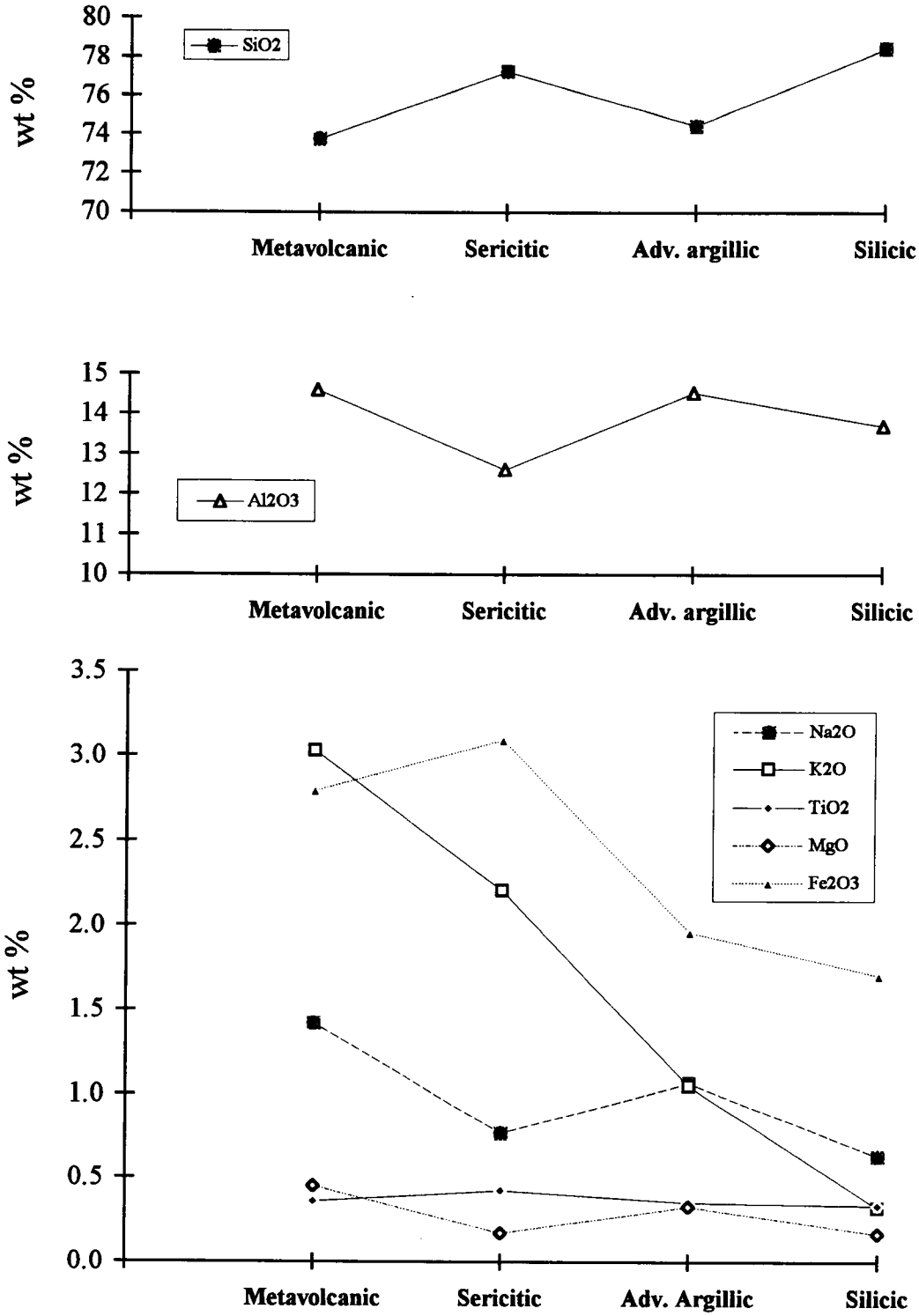

Fig. 10. Diagram showing the zoning of major elements in altered rocks. SiO_2 increases towards the center, whereas K_2O, Na_2O, MgO decrease. TiO_2 and Al_2O_3 are relatively constant. Note the depletion of most elements in the silicified zone (quartz+pyrite), suggesting leaching during hydrothermal alteration.

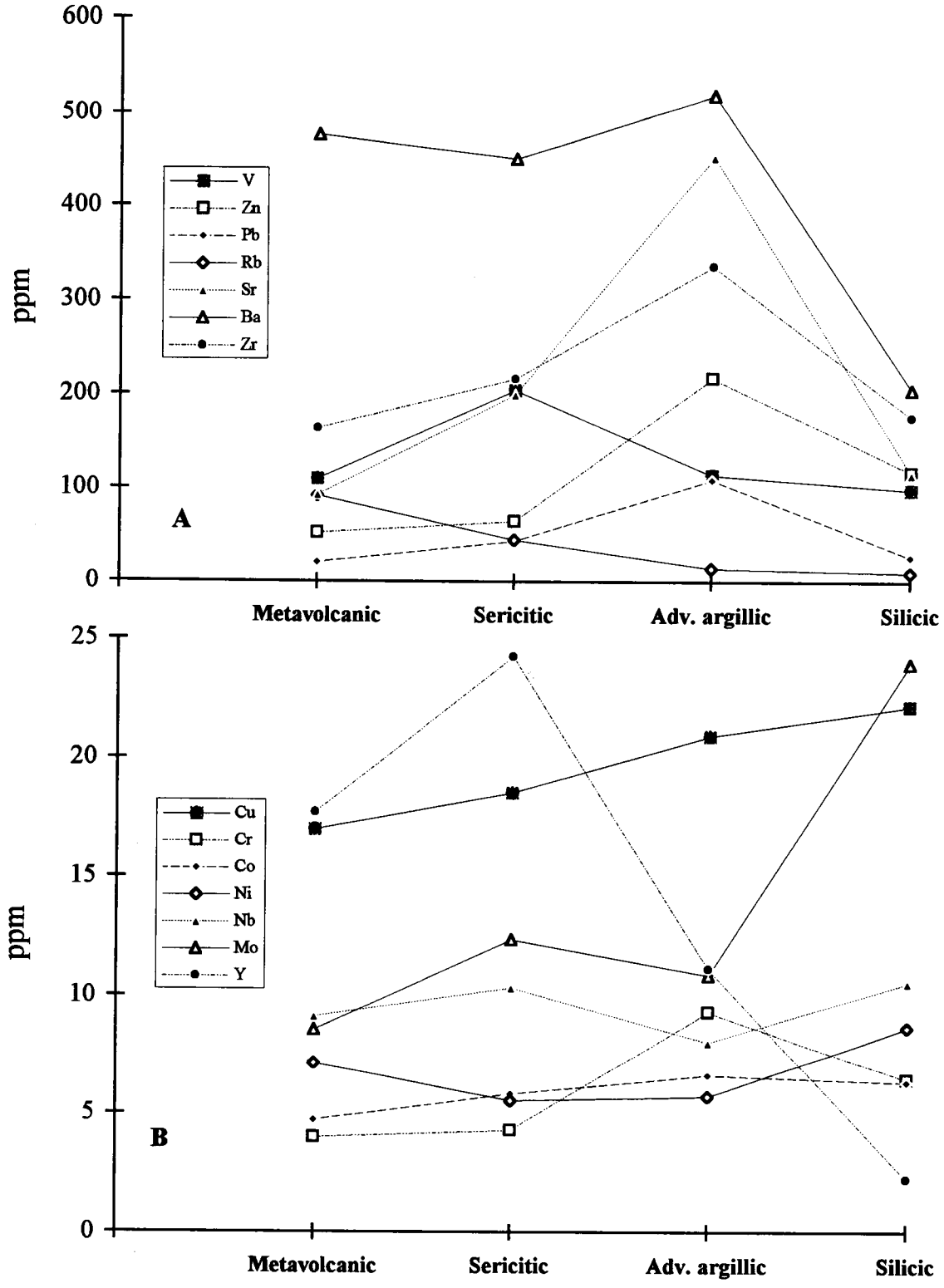

Fig. 11. Diagram showing the zoning of minor and trace elements in altered rocks.

From a geochemical orientation study in the interior part (silicic and advanced argillic zones) of the Brewer system, Jaacks (1986) concluded that the breccia has a distinctive chemical signature involving the elements Fe, Mn, Cu, Mo, As, Ag, Mg, Au, and Hg. Ti, V, Al, P, and Na were found to be strongly associated with the metavolcanic rocks adjacent to the breccia. Sr, Pb, Ba, Na, Al, and K showed a strong association with the metavolcanic rocks within structural zones. Ni, Co, and Zn were typically below detection limits. Mo, Cr, V, and Cu were mostly between 10 and 100 ppm, and Sr, Ba, and Pb were mostly greater than 100 ppm. This study shows similar concentrations of Co, Ni, Mo, Cu, Cr, Sr, and Ba, but Zn and V are much higher and the advanced argillic alteration zone is characterized by relatively abundant Sr, Zr, Zn, and Ba.

Figure 11 shows the variation of trace element abundances among the different alteration zones. One obvious trend is the depletion of many elements in the silicic zone. This could have been a result of a strong hydrothermal leaching process in the breccia zone leading to the removal of most of the elements, although the sample selection could also have introduced some bias. Overall, Cu, Sr, Zr, Pb, and Zn are enriched, whereas Rb and Y are depleted toward center of the system.

The trace element abundance in the rocks can vary greatly, even within the same zone. Some elements, like Pb, Zn, and Sr, can be quite high in some samples and fall outside of the calibration's upper limit. The true abundance of an element could not be determined in such cases although a minimum concentration could be estimated. The variations in abundance could have resulted from the mineral assemblages, channelized flow paths, and host rock compositions.

Plutonic and Contact Metamorphic Rocks

A few samples of Pageland pluton and contact metamorphic rocks were analyzed (Table 1). The Pageland pluton has a composition of typical granite (LeMaitre, 1976). The contact metamorphosed volcanic rocks, exhibit some chemical variations compared to the unaltered volcanic rocks. The most obvious differences are the relatively abundant MgO (3.51%) and CaO (5.31%) in the hornfels, represented by the abundance of epidote, amphibole, and calcite. The contact metamorphosed volcanic rocks have also higher Na_2O and lower SiO_2.

DISCUSSION

Formation of the Geochemical Zonation and Implication

The geochemical zonation in the Brewer area is the result of hydrothermal alteration. During hydrothermal alteration, fluids circulated and penetrated through the rocks, reacting with the original volcanic rocks and forming hydrothermal alteration minerals depending on the original rock composition, fluid composition, and P-T conditions.

The host volcanic rocks are quite heterogeneous, ranging from tuff to flow and breccia in the Brewer area. Many of these rocks may have formed at different phases in a single volcanic system, resulting in some variation of the original chemical compositions of the host rocks. The heterogeneity of the host rocks would certainly affect the geochemical signatures of the altered rocks. However, the volcanic rocks appear to be a reasonably cohesive group and originally felsic in composition (Figure 4).

The mineralizing hydrothermal fluids were probably acidic (low-pH) and sulfur-rich. This is suggested by the presence of abundant sulfide minerals, including pyrite and enargite (Cu_3AsS_4), and an acid-sulfate alteration mineral assemblage (quartz-alunite ($KAl_3(SO_4)_2(OH)_6$)) in the interior part of the hydrothermal system. Geochemical comparison between the hydrothermally altered and unaltered volcanic rocks suggests that the altered rocks are relatively enriched in Si, Cu, Mo, Zr, Sr, and Pb, all of which were introduced by the hydrothermal fluids. The dominance of pyrite-quartz breccia in the interior part of the system indicates that the mineralizing fluid was enriched in Fe and sulfur toward the end of the hydrothermal evolution. Many aspects of the hydrothermal system, fluid source and composition, metal transport, and precipitation mechanism will be discussed in later parts.

The P-T conditions of the Brewer hydrothermal alteration are not well understood. Temperatures as high as 300-400°C in the interior zone of the system are likely, based on andalusite-quartz mineral assemblage (Scheetz, 1991) and fluid inclusion study (Part 4). Scheetz (1991) suggested a shallow, near-surface emplacement for the Brewer system, based on the presence of layered siliceous sediments and siliceous clasts within andalusite-quartz rocks, quartz-sericite rocks, and metamudstones.

Effect of Regional Metamorphism on the Alteration Assemblages

The well preserved alteration zones and accompanying geochemical zonation indicate that the regional metamorphism has not significantly affected the chemistry of the rocks. Some metamorphic minerals, such as chloritoid and kyanite, are only present sporadically in the alteration halo. The composition of the chloritoid-bearing sericite schist is similar to other rocks in the sericite zone. In the central part of the system (silicic zone), metamorphic overprint is minimal. Around the central zone, the

metamorphic grade is only chlorite to biotite grade of lower greenschist facies. All this suggests that the rocks have been deformed to some degree, but the coeval metamorphism was perhaps an isochemical process. That is, there has been little chemical and mass transfer over a large area during the regional metamorphism, although some metals might have been remobilized along fracture zones on a local scale.

Comparison with Younger Epithermal Deposits

Many characteristics of the Brewer deposit, including structural setting, host rock, alteration type, alteration mineralogy, and sulfide mineralogy are similar to those of epithermal acid-sulfate type deposits (Hayba et al., 1985; Heald et al., 1987), even though some metamorphic features (metamorphic minerals and foliation) exist at the Brewer Mine (Table 2).

Hayba et al. (1985) and Heald et al. (1987) summarized the general characteristics of the epithermal acid-sulfate deposits. Acid-sulfate deposits are spatially related to intrusive centers, particularly ring-fracture volcanic domes on the margins of calderas. They are typically hosted by rhyodacitic volcanic rocks and are characterized by the occurrence of the vein mineral assemblage enargite+pyrite±covellite in an advanced argillic alteration zone, which is often coextensive with silicification and is surrounded by sericitic and propylitic alteration zones. The Brewer Gold Mine exhibits most of these features. The mine is hosted by felsic (rhyolitic) rocks in the center of a volcanic system, a cinder zone or a caldera (Nystrom, 1972). The gold mineralization, associated mainly with pyrite-quartz±enargite rocks, is accompanied by silicic, advanced argillic, sericitic and, to a limited degree, propylitic alteration zones in a concentrically zoned pattern.

Table 2. Comparison between the Brewer gold deposit and epithermal acid-sulfate deposits

	Epithermal Acid-sulfate Deposit	Brewer Mine
Host Rocks	rhyodacite to rhyolite	rhyolite
Sulfide Minerals	enargite, pyrite, gold, base-metal sulfides	enargite, pyrite, gold, base-metal sulfides
Alteration	silicic advanced argillic to argillic sericitic	silicic advanced argillic sericitic
Alteration Pattern	relatively small, equidimensional	concentric
Alteration Minerals	alunite, sericite, kaolinite,	alunite, sericite, kaolinite andalusite
Temperature	200 to 300 °C	200 to 350 °C (fluid inclusion data)
Fluid Composition	variable salinity (1-24 wt% NaCl equiv.) trace CO_2	H_2O-CO_2-variable salinity

However, some features, especially the widespread aluminosilicate alteration complex and the abundance of andalusite in the advanced argillic alteration zone of the Brewer area, are not present in typical acid-sulfate type deposits, which has led to the suggestion of different types of hydrothermal system (Schmidt, 1985; Worthington et al., 1980). The origin of the andalusite has been attributed to hydrothermal alteration in a porphyry system (Schmidt, 1978, 1985) and metamorphism (Ririe, 1990). More recently, Scheetz (1991) has suggested that much of the andalusite was formed during the prograde metamorphism after hydrothermal alteration has occurred. However, geochemical analysis presented here suggests that overall Al is not particularly enriched in the advanced argillic alteration zone.

CONCLUSIONS

1. Hydrothermal alteration associated with gold mineralization in the Brewer area produced a crude concentric zoning pattern, consisting of silicic (quartz-pyrite breccia), advanced argillic (alunite-quartz-andalusite), and sericitic (quartz-sericite) rocks. The geologic setting, alteration pattern, and alteration mineral assemblages suggest that the deposit is an epithermal acid-sulfate type deposit.

2. The protoliths of the metavolcanic rocks, the hosts for gold mineralization and hydrothermal alteration at Brewer, are mostly felsic volcanic rocks with an overall rhyolitic composition. The alkali index of the rocks suggests that they have a tholeiitic affinity. The metasedimentary rocks, overlying the metavolcanic rocks, are quite different in composition, characterized by lower SiO_2 and higher Al_2O_3, Fe_2O_3, and MgO.

3. The hydrothermal activity resulted in some chemical changes in the altered rocks. Overall, the hydrothermally altered volcanic rocks are relatively enriched in SiO_2

and depleted in K_2O and Na_2O compared to the unaltered volcanic rocks. The altered volcanic rocks also have relatively higher abundances of Sr, Cu, Mo, Pb, and Zr. Some elements show a systematic geochemical zonation. SiO_2, Cu, and Mo are enriched toward the center of the system, whereas K_2O, Na_2O, Y, Pb, and V are deleted.

4. The hydrothermal fluids were probably acidic and sulfur-rich, as indicated by the presence of high-sulfur minerals such as alunite, enargite, and abundant pyrite at the central alteration zone of the system. The hydrothermal fluids were probably also enriched in Fe, Cu, Mo, Zr, Pb, and other metals, as inferred from the geochemical signature of the rocks.

5. The well-preserved acid-sulfate type alteration pattern and mineral assemblage in the Brewer Mine area suggest that subsequent regional metamorphism did not significantly change the geochemical signature of the altered rocks, although it may have resulted in localized gold remobilization.

ACKNOWLEDGMENTS

I like to thank Otto Kopp of University of Tennessee for his help with XRF analyses. I also thank Westmont Mining Inc. and Brewer Gold Co. for providing field help during this study. John Scheetz kindly gave a field tour and showed some drill cores to the first author on a very hot summer day during early stage of the study. This study has been supported by a Geological Society of America research grant (1991), and a Sigma Xi research grant (1991), and Discretionary Funds of the Department of Geological Sciences at the University of Tennessee to the first author.

REFERENCES

Abbey, S., 1983, Studies in "standard samples" of silicate rocks and minerals 1969-1982: Geological Survey of Canada paper 83-15, 114p.

Bell, H., III, and Popenoe, P., 1976, Gravity studies in the Carolina slate belt near the Haile and Brewer mines, north-central South Carolina: Journal of Research, U. S. Geological Survey, v. 4, p. 667-682.

Berger, B. R. and Henley, R. W., 1988, Advances in the understanding of epithermal gold-silver deposits, with special reference to the western United States: in Keays, R. R. and Skinner, B. J., eds., The geology of gold deposits: the perspective in 1988, Economic Geology Monograph 6, p. 405-423.

Bodnar, R. J., Reynolds, T. J., and Kuehn, C. A., 1985, Fluid inclision systematics in epithermal systems: in Berger, B. R., and Bethke, P. M. (eds), Geology and Geochemistry of Epithermal Systems: Society of Economic Geologists, Reviews in Economic Geology, v. 2, P. 73-97.

Buchanan, L. L., 1981, Precious metal deposits associated with volcanic environments in the southwest: Arizona Geological Society Digest, v. 14, p. 237-261.

Butler, J. R., 1985, The Brewer mine: in Feiss, P. G., ed., Volcanic-hosted gold and high alumina rocks of the Carolina slate belt: Guidebook for field trip, 1985 SGE fall meeting and 1985 GSA annual meeting, p. 143-199.

Butler, J. R., 1991, Metamorphism: in J. W. Horton, Jr and V. A. Zulla, eds, The geology of Carolinas, University of Tennessee Press., p. 127-141.

Butler, J. R. and Howell, D. E., 1976, Geology of the Taxahaw quadrangle, Lancaster County, South Carolina: Division of Geology, South Carolina State Development Board, Geologic Notes, v. 20, p. 133-149.

Butler, J. R. and Secor, D. T., 1991, The Central Piedmont: in J. W. Horton, Jr and V. A. Zulla, eds, The geology of Carolinas, University of Tennessee Press., p. 59-78.

Butler, J. R., Scheetz, J. M., Stonehouse, J. M., Tayler, D. R., and Callaway, R. Q., 1988, The Brewer gold mine, Chesterfield County, South Carolina: Guidebook for field trip of the annual GSA meeting, Southeaster section, 22p.

Conley, J. F. and Bain, G. L., 1965, Geology of the Carolina slate belt west of the Deep River-Wadesboro Traiassic Basin, North Carolina: Southeastern Geology, v. 6, p. 117-138.

Feiss, P. G., 1982, Geochemistry and tectonic setting of the volcanics of the Carolina slate belt: Economic Geology, v. 77, p. 273-293.

Feiss, P. G., 1985, Gold mineralization in the Carolina slate belt: Speculations on ore genesis: in Misra, K. C., ed., Volcanogenic sulfide and precious metal mineralization in the southern Appalachians: University of Tennessee, Department of Geological Sciences, Studies in Geology 16, p. 220-236.

Feiss, P. G., Maybin, A. H., III, Riggs, S.R., and Grosz, A. E., 1991, Mineral resources of the Carolinas: in J. W. Horton, Jr and V. A. Zulla, eds, The geology of Carolinas, University of Tennessee Press., p. 319-345.

Field, C. W. and Fifarek, R. H., 1985, Light stable-isotope systematic in the epithermal environment: in Berger, B. R., and Bethke, P. M. (eds), Geology and Geochemistry of Epithermal Systems: Society of Economic Geologists, Reviews in Economic Geology, v. 2, P. 99-128.

Graton, L. C., 1906, Reconnaissance of some gold and tin deposits of the Southern Appalachians: U. S., Geological Survey Bulletin 293, 134 p.

Hayba, D. O., Bethke, P. M., Heald, P., and Foley, N. K., 1985, Geologic, mineralogic, and geochemical characteristics of volcanic- hosted epithermal precious-metal deposits: in Berger, B. R., and Bethke, P. M. (eds), Geology and Geochemistry of Epithermal Systems: Society of Economic Geologists, Reviews in Economic Geology, v. 2, p. 129-167.

Heald, P., Foley, N. K., and Hayba, D. O., 1987, Comparative anatomy of volcanic-hosted epithermal deposits: acid-sulfate and adularia-sericite types: Economic Geology, v. 82, p. 1-26.

Henley, R. W., 1985, The geothermal framework of epithermal deposits: in Berger, B. R., and Bethke, P. M. (eds), Geology and Geochemistry of Epithermal Systems: Society of Economic Geologists, Reviews in Economic Geology, v. 2, p. 1-24.

Jaacks, J. J., 1986, Geochemical orientation survey of the Brewer property, Chesterfield County, South Carolina: internal report of Westmont Mining, 56p.

Johnson, R. G. and King, B. L., 1987, Energy-dispersive X-ray Fluorescence Spectrometry: U. S. Geological Survey Bulletin 1770, F1-F5.

LeMaitre, R.M, 1976, The chemical variability of some common Igneous rocks: Journal of Petrology, v. 17, p. 589-637.

Minard, J. P., 1971, Gold occurrences near Jefferson, South Carolina: U. S. Geological Survey Bulletin 1334, p. 1-20.

Nystrom, P. G. Jr., 1972, Geology of the Catarra NW quadangle: Master's Thesis, University of South Carolina, 49p.

Pardee, J. T., and Park, C. F., Jr., 1948, Gold deposits of the southern Piedmont: U. S. Geological Survey Professional Paper 213, 156p.

Ririe, G. T., 1990a, A comparison of alteration assemblages associated with Archean gold deposits in Western Australia and Paleozoic gold deposits in the southeast United States: Can. J. Earth Sci., v. 27, p. 1560-1576.

Ririe, G. T., 1990, Characteristics of metamorphosed acid-sulfate gold deposits: (abstract) Geological Society of America, v. 22, p. A40.

Scheetz, J. W., 1991, The geology and alteration of the Brewer gold mine, Jefferson, South Carolina: M.S. Thesis, University of North Carolina, Chapel Hill, 180p.

Scheetz, J. W., Stonehouse, J. M., and Zwaschka, M. R., 1991, Geology of the Brewer gold mine in South Carolina: Mining Engineering, v. 43, p. 38-42.

Schmidt, R. G., 1978, The potential for porphyry copper-molybdenum deposits in the eastern United States: U. S. Geological Survey Professional Paper 907-E, 31 p.

Schmidt, R. G., 1985, High-alumina hydrothermal systems in volcanic rocks and their significance to mineral prospecting in the Carolina slate belt: U. S. Geological Survey Bulletin 1562, 59 p.

Secor, D. T., Jr., 1988, Review of the geology of the Carolina Slate Belt: in Secor, D. T., Jr., ed., 1988, Southeastern Geological Excursions: Guidebook for Geological Society of America, p. 1-18.

Secor, D. T., Jr., Snoke, A. W., and Dallmeyer, R. D., 1986, Character of the Alleghanian orogeny in the southern Appalachians: Part III. Regional tectonic relations: Geological Society of America Bulletin, v. 97, p. 1345-1353.

Silberman, M. L., and Berger, B. R., 1985, Relationship of trace- element patterns to alteration and morphology in epithermal precious-metal deposits; in Berger, B. R., and Bethke, P. M. (eds), Geology and Geochemistry of Epithermal Systems: Society of Economic Geologists, Reviews in Economic Geology, v. 2, p. 203-232.

Worthington, J. T., and Kiff, I. T., 1970, A suggested volcanogenic origin for certain gold deposits in the slate belt of the North Carolina Piedmont: Economic Geology, v. 65, p. 529-537.

Worthington, J. T., Kiff, I. T., Jones, E. M., and Chapman, P. E., 1980, Applications of the hot springs or fumarolic model in prospecting for lode gold deposits: Mining Engineering, v. 32, p. 73-79.

Part 3

Origin of Alunite and its Implication on the Environment of Hydrothermal Alteration and Gold Mineralization at the Brewer Gold Mine, Jefferson, South Carolina

ABSTRACT

Sulfur stable isotope analyses of alunite and pyrite from the Brewer Gold Mine, Jefferson, South Carolina, provide important information on the origin for the acid sulfate alteration and constraints on geochemical processes and conditions of accompanying gold mineralization. The Brewer Gold Mine is characterized by an acid sulfate alteration assemblage of alunite +quartz +andalusite +pyrite +enargite +other sulfide minerals. Hydrothermal alteration, which includes silicic, advanced argillic, sericitic, and limited propylitic alteration, exhibit a rough concentric zonation outward from center. Alunite is present in the mineralized breccia zones and nearby hydrothermally altered volcanic tuffs and breccias of advanced argillic alteration zone. Alunite occurs as fine-grained disseminations in groundmass, aggregates of interlocking mosaic of plates and tabular microcrystals, and small veins in volcanic rocks. It also occurs as large, rhombohedral crystals in pyrite-quartz rock. XRD and electron microprobe analyses indicate that the alunite has extensive solid solution between alunite and natroalunite with no jarosite component. Although the fine-grained alunites are mostly potassium-rich with K ranging from 0.51 to 0.87, the mineral compositions are quite heterogeneous, varying from grain to grain, even in a single sample. The relatively coarse, rhombohedral alunite crystals are mostly sodium-rich natroalunite with compositional zonation of increasing Na from center to rim.

$\delta^{34}S$ values of the alunites, including vein, replacement and disseminated forms, range from 17.7 to 26.8 per mil. $\delta^{34}S$ values of the pyrite, including euhedral crystals and fine-grained disseminations in the groundmass of the pyrite-quartz breccias, range from 0.5 to 5.7 per mil. Pyrite from the pyrite-quartz vein also has similar $\delta^{34}S$ values. The narrow range of $\delta^{34}S$ values suggests that the sulfur is likely from the same source. The $\delta^{34}S$ values of the alunites are generally 15 to 22 °/oo larger than that of the pyrites, suggesting that the alunite is a direct product of magmatic hydrothermal, acid sulfate

alteration in an epithermal environment. The sulfur stable isotope data support a magmatic hydrothermal environment where the sulfuric acid is likely produced by the disproportionation of SO_2 with decreasing temperature and the equilibrium between aqueous H_2S and SO_4 formed by the disproportionation results in that alunite is enriched in $\delta^{34}S$ relative to pyrite. The pyrite-alunite sulfur isotopic geothermometer gives temperatures of about 300-500°C, which is in agreement with the fluid inclusion data for the Brewer Mine. Considering the widespread aluminosilcate alteration and other features in the Brewer Mine, it is proposed that the Brewer hydrothermal system is a magmatic hydrothermal acid sulfate system, which overlies or is related to a deep porphyry system.

INTRODUCTION

Alunite [$KAl_3(SO_4)_2(OH)_6$] is the most characteristic mineral of acid sulfate alteration in volcanic-hosted epithermal precious-metal deposits (Hayba et al., 1985; Heald et al., 1987). Acid sulfate alteration, characterized by the assemblage alunite+kaolinite+quartz+pyrite, results from base leaching of wall-rock by fluids containing H_2SO_4. H_2SO_4 may be generated in three geologic environments: (1) by atmospheric oxidation of sulfides in the supergene environment; (2) by atmospheric oxidation at the water table in the steam-heated environment where H_2S released by deeper, boiling fluids; and (3) by the disproportionation of magmatic SO_2 to H_2S and H_2SO_4 during condensation of a magmatic vapor plume at intermediate depths in magmatic hydrothermal environments within silicic and andesitic volcanic terranes (Rye et al., 1992). Alunite is particularly important as an indicator of environments of formation, origins of chemical components, physical-chemical environments and temperatures of formation (Rye et al., 1992; Field, 1966, 1972; Hemley et al., 1969; Knight, 1977).

Supergene acid sulfate alteration may form over any sulfide zone when it is raised above the water table by tectonics or exposed by erosion. It may overprint earlier acid sulfate assemblages. Supergene alunite normally has $\delta^{34}S$ values virtually identical to precursor sulfides unless bacteriogenic reduction of aqueous sulfate takes place in standing pools of water. Acid sulfate alteration in steam-heated environments is characterized by pronounced vertical zoning. Most alunites of steam-heated origin has $\delta^{34}S$ values the same as those of precursor H_2S and related sulfides. Magmatic hydrothermal, acid sulfate alteration in near surface epithermal deposits is characterized by vertical orientation and horizontal zoning, and the presence of other Cu-As-Sb-S minerals. $\delta^{34}S$ values are typically 16 to 28 per mil larger than those for associated pyrite, reflecting equilibrium between aqueous H_2S and SO_4 formed by the disproportionation of

magmatically derived SO_2 (Rye et al., 1992). $\Delta^{34}S$ alunite-pyrite values provide reliable temperature estimates.

The Brewer Mine is a volcanic hosted gold deposit in the Carolina slate belt (Butler, 1985; Butler et al., 1988; Schmidt, 1978, 1985; Nystrom, 1972; Scheetz, 1991; Scheetz et al., 1991). Hydrothermal alteration, which probably occurred during Cambrian time, has produced an extensive aluminosilicate alteration zone that is represented by quartz, andalusite, kaolinite, and other aluminosilicate minerals (e.g., diaspore and pyrophyllite). The hydrothermal alteration is also accompanied by acid sulfate alteration that is characterized by an assemblage of alunite+quartz+pyrite +enargite. Gold mineralization occurs in hydrothermal breccia (silicic) that is surrounded by a zone of advanced argillic alteration. The gold mineralization is closely related to pyrite+quartz and is thus considered to be related to the hydrothermal alteration, which probably occurred in an epithermal environment.

Various geologic environments and genetic models have been proposed for the origin of the Brewer deposit (Butler, 1981; Butler et al., 1984, 1988; Worthing et al., 1970, 1980; Schmidt, 1978, 1985; Scheetz, 1991; Stonehouse, 1992). The presence of alunite in the Brewer Mine is mentioned by Butler et al. (1984, 1988) and is discussed by Scheetz (1991). The present study focuses on the acid sulfate alteration, which is the key to an understanding of the hydrothermal and mineralization environment of the Brewer system. The study places particular emphasis on the characterization of alunite and associated sulfides because they provide important informations on the hydrothermal process and environment (Rye et al., 1992; Field, 1966).

GEOLOGIC SETTING

The Brewer Gold Mine is located at southwest of Jefferson, Chesterfield County, South Carolina. It is within the Carolina slate belt, a northeast-southwest trending, low-grade metamorphic belt of the Piedmont in the southern Appalachians. The Carolina slate belt hosts numerous mineral deposits (Feiss, 1985) and has been a focus of gold exploration for more than a decade. Important gold deposits in the belt include those of Ridgeway, Haile, Barite Hill, and Brewer (Fig. 1).

The Carolina slate belt consists of Late Proterozoic to Cambrian volcanic and sedimentary rocks that have been metamorphosed to lower greenschist facies (Butler and Secor, 1991; Butler, 1985; Conley and Bain, 1965). The belt has been intruded by Late Paleozoic granitic bodies, such as the Pageland, Liberty Hill, and Lilesville plutons. Metavolcanic rocks include volcanogenic clast-dominated pyroclastic and epiclastic rocks, and lava flows, ranging up to 13 km in stratigraphic thickness. Metasedimentary rocks are dominated by mudstone, siltstone, and graywacke. The volcanosedimentary and volcanic rocks of the slate belt originated in continental margins or volcanic island arcs (Butler and Ragland, 1969; Glover and Sinha, 1973). Most of the gold deposits occur in the volcanic sequence near the contact with the volcaniclastic sedimentary sequence (Withington et al., 1980) and this contact has been a primary target of gold exploration in the belt.

In northern South Carolina, the Carolina slate belt consists of a predominantly felsic metavolcanic sequence, the Persimmon Fork Formation, that is overlain by metasedimentary rocks of the Richtex Formation (Secor, 1988). The geology of the Jefferson quadrangle, which includes the Brewer Mine area, has been described by Nystrom (1972) and Minard (1971). Metavolcanic rocks, considered equivalent to the Persimmon Fork Formation (Nystrom, 1972), consist of an interbedded mafic-felsic volcanic unit and a felsic volcanic unit. The metasedimentary rocks, mostly laminated

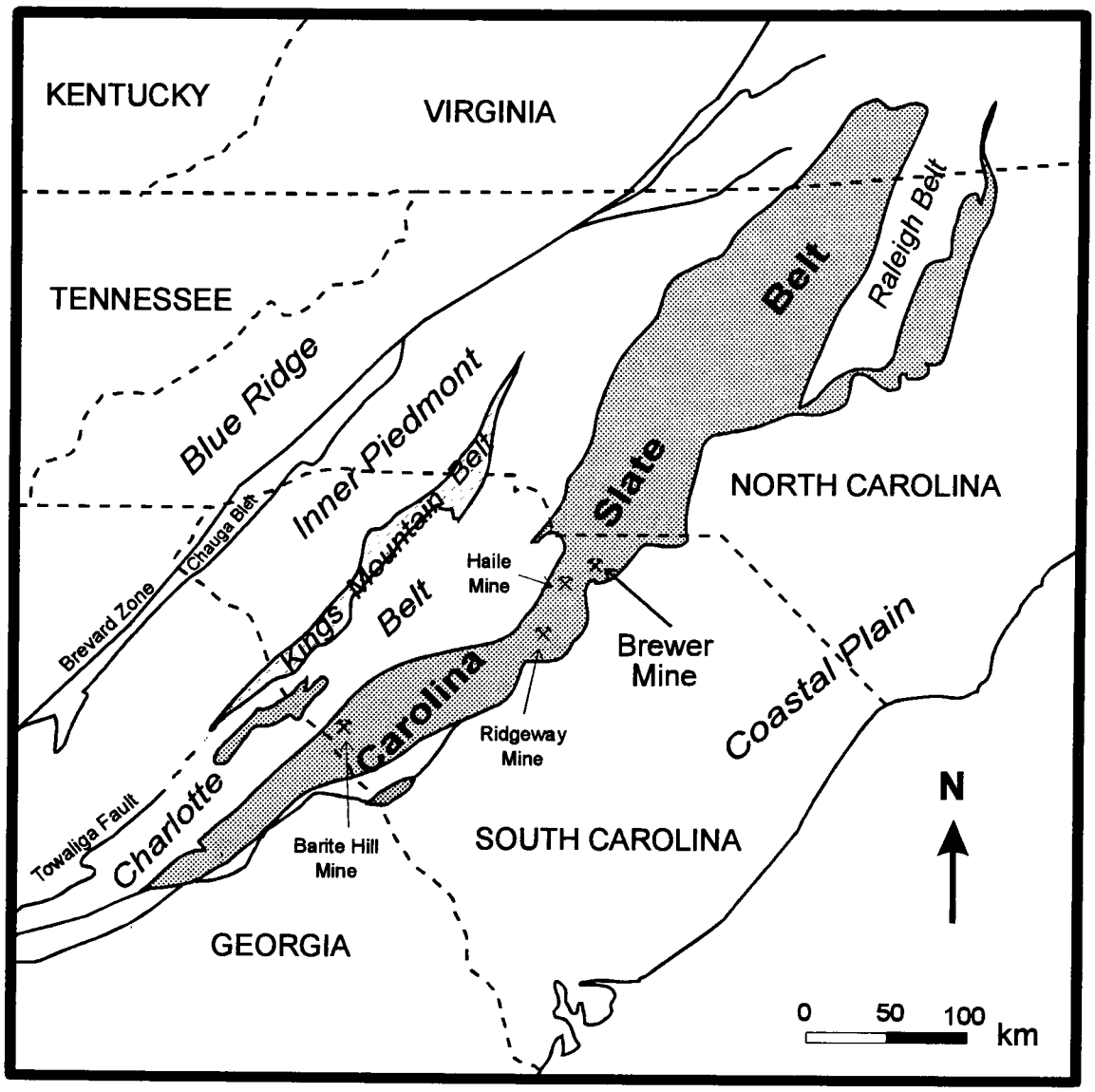

Fig. 1. Geological map showing the Carolina slate belt and location of the Brewer mine, South Carolina (After Butler, 1985).

slates, are correlated with the Richtex Formation. The Pageland granite, a quartz monzonite pluton, is exposed northwest of the Brewer Gold Mine. Coastal Plain sediments overlap the Brewer area. The volcanic and sedimentary rocks have been metamorphosed during a later regional metamorphic event, probably during the Taconic orogeny. The metamorphic facies, based on the mineral assemblages present in the slate, is inferred to be lower-greenschist facies (Butler, 1985), which is consistent with the overall metamorphic grade of the Carolina slate belt (Butler, 1991). Despite the metamorphism, many of the primary textures in the volcanic and sedimentary rocks, such as bedding planes and preferred orientation of crystals and lithic fragments, are well preserved.

Metavolcanic rocks in the Brewer area include volcanic tuffs, flows, and breccias. Petrographic studies reveal that most of the pyroclastic rocks are felsic in composition Scheetz, 1991; Lu et al., 1993). Volcanic tuffs include rhyolitic crystal and lithic tuffs. Crystal tuffs are composed of quartz, K-feldspar, and plagioclase crystals in a matrix of fine-grained quartz, sericite, and pumice fragments. Lithic tuffs consist of fragments of various types of volcanic rocks in a fine-grained matrix. Some of the tuffs contain both crystals and lithic fragments, and most show sorting and well-preserved stratification. Volcanic flows are not well stratified and contain blocks, lapilli, and ash with some individual blocks over 10 cm in diameter. Lapilli consist of both lithic fragments and crystals of quartz and feldspar. The matrix is composed of fine grained quartz, sericite, and hematite. Volcanic breccias contain angular lithic fragments (typically similar in composition to that of the matrix) and a matrix of quartz, sericite, and hematite. The volcanic flows and breccias suggest the presence of a volcanic center near the Brewer area.

Metavolcaniclastic sedimentary rocks in the Brewer area include mudstone and siltstone, which typically are well laminated and, close to the Brewer Mine, are

interlayered with volcanoclastics. Due to compositional and size differences, the interbedded rocks show distinct color layering in outcrop. Mudstones are composed of fine-grained quartz, sericite, and clay minerals.

THE BREWER GOLD MINE

Hydrothermal Alteration

The Brewer Mine occurs within the felsic volcanic rocks of the Carolina slate belt, close to and partly under a thin edge of overlapping Coastal Plain sediments (Fig. 2). The zone of gold mineralization at Brewer is part of a much larger hydrothermal alteration system that extends over more than 2 kilometers across and has a near-circular shape in plan view (Fig. 2). It probably represents the center of a volcanic system - a cinder cone, a caldera, or a diatreme (Nystrom, 1972). Despite subsequent regional metamorphism, the hydrothermal alteration zones are easily discernible by their mineral assemblages, especially in the inner part of the system that has been subjected to mining. In the central part of the alteration zone in the Brewer area, metamorphic effects seem to be minimal. The alteration has been described in the literature variously as "widespread silicification and extensive development of pyrophyllite and sericite" (Pardee and Park, 1948), "massive quartzite" (Nystrom, 1972), "quartz granofels of high-fluorine subvolcanic alteration" (Schmidt, 1985), and, most recently, as "quartz-sulfide and quartz-sericite phyllite zone" (Scheetz et al., 1991). Based on the characteristics summarized by Heald et al. (1987), four types of hydrothermal alteration can be recognized in the Brewer area: (a) silicic, (b) advanced argillic, (c) sericitic, and (d) propylitic. The alteration zones have a roughly concentric distribution pattern as shown in Fig. 2. Silicic alteration forms the core of the hydrothermal system and is surrounded by a zone of advanced argillic alteration. Sericitic alteration surrounds the zone of advanced argillic alteration and

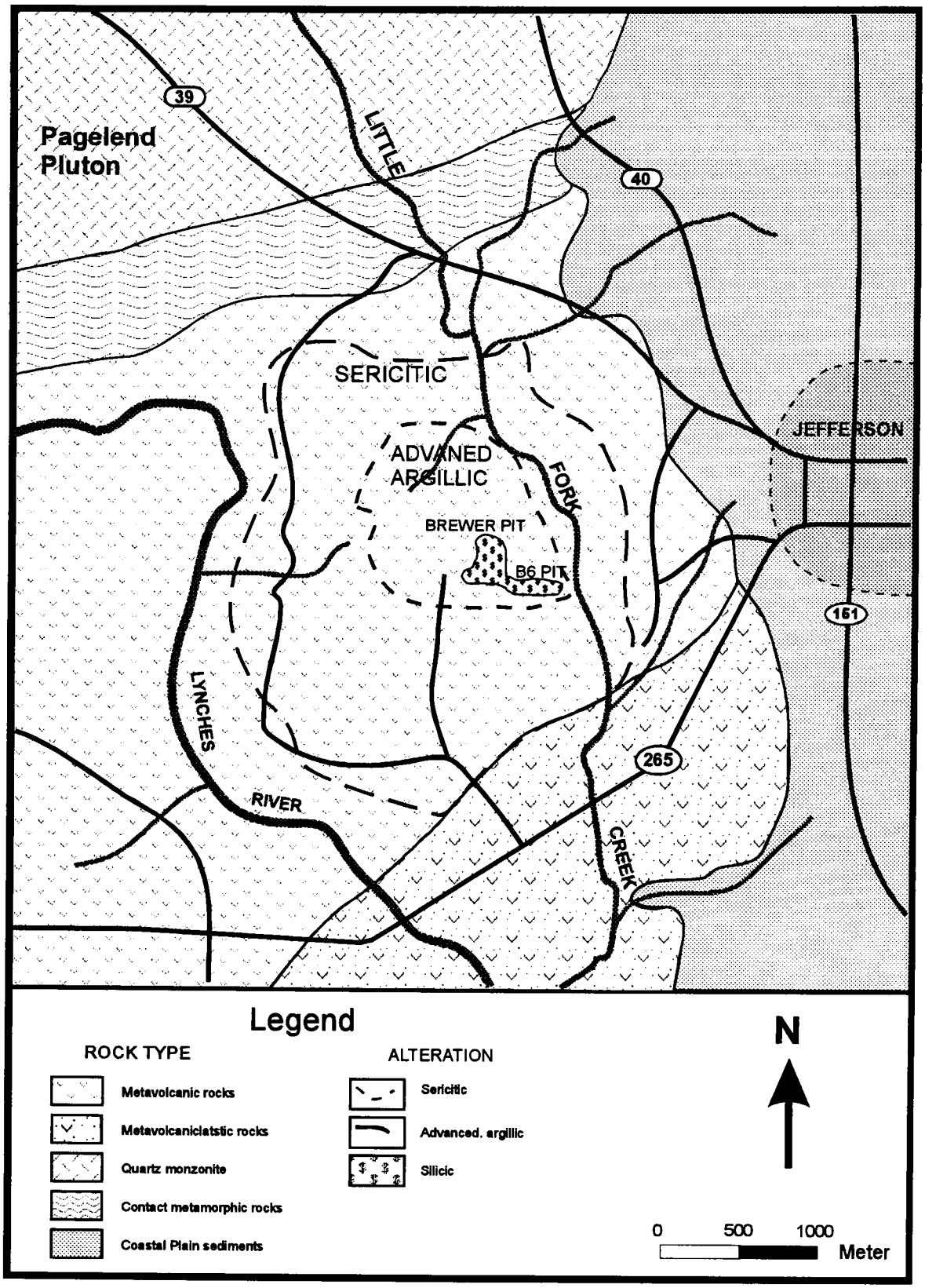

Fig. 2. Geologic map at the Brewer Mine area (After Schmidt, 1985; Nystrom, 1972; Scheetz, 1991). Note the hydrothermal alteration zones.

grades outward to either propylitic alteration or unaltered volcanic rocks. Propylitic alteration occurs sporadically outside the sericitic zone, mainly in the southern and southwestern parts of the system. The alteration zoning pattern is similar to that of epithermal acid sulfate deposits and its crude concentric pattern suggests a pre-metamorphic hydrothermal origin. The characteristics of the alteration zones is summarized below; detailed descriptions of the alteration mineral assemblages and their chemistry are given by Scheetz (1991) and Lu et al. (1993).

(a) Silicic alteration. Silicic alteration in the Brewer Mine area is represented by mineralized quartz-pyrite breccias, and it is confined to the central part of the alteration system. Geochemically, it is characterized by extreme abundance of silica, which is a hydrothermally introduced component. Quartz and pyrite are the dominant minerals, with quartz often constituting more than 80 percent of the rock. Enargite, topaz, and many sulfide minerals are present in places. Gold mineralization is mainly confined to the silicic zone.

(b) Advanced argillic alteration. Advanced argillic alteration is characterized by an assemblage of quartz, alunite, and andalusite, with varying amounts of sericite, pyrophyllite, pyrite, topaz, diaspore, and kaolinite. Andalusite occurs as porphyroblasts in a fine-grained quartz-sericite matrix and as smaller grains within fractures. Andalusite is usually anhedral and, in some cases, is partially replaced by kyanite, quartz, and pyrophyllite. Quartz typically occurs as fine-grained, anhedral crystals that constitute the matrix, although some appear as aggregates.

(c) Sericitic alteration. Sericitic alteration is represented by the assemblage quartz and sericite, with some pyrite and minor ilmenite. The rocks are commonly metamorphosed to quartz-sericite schist and phyllite, but original volcanic textures, such as pyroclastic and flow textures, are preserved locally. The quartz-sericite rock is typically composed of fine-grained quartz- and/or sericite-rich compositional layers.

Quartz "eyes" and aggregates are also common along foliation. Hematite stains mark foliation along pyrite-rich layers that are parallel to foliation.

(d) Propylitic alteration. A mineral assemblage of quartz, epidote, calcite, chlorite, and pyrite defines the propylitic alteration. Sericite, K-feldspar, hematite, rutile, and ilmenite are commonly present in minor amounts. The altered rock exhibits volcanic pyroclastic textures (breccia and flow), similar to those observed in the volcanic country rock not affected by hydrothermal alterations. Calcite occurs as replacement of plagioclase phenocrysts and as fine-grained aggregates in the matrix. Epidote is present as elongated crystals or as radiating aggregates. Chlorite constitutes a minor component of the rocks.

Geochemical analysis of the unaltered and hydrothermally altered rocks has revealed variations in element concentrations among alteration zones and a crude chemical zonation (Lu et al., 1993). Hydrothermally altered rocks are generally enriched in Si, Cu, Mo, Pb, Zn, and S and depleted in K, Mg, and Rb relative to host volcanic rocks. Si, Fe, Zn, Pb, Cu, and S are also generally enriched toward the center of the alteration halo, whereas Na, Mg, K and Ba are depleted.

Gold Mineralization

The Brewer deposit occurs within the felsic volcanic units (Fig. 2). Gold mineralization is restricted to the silicic zone composed of brecciated quartz-sulfide rocks, quartz-andalusite breccias, and massive sulfide-quartz rocks. Two ore bodies have been delineated (Scheetz et al., 1991): the main ore body of the Brewer pit, and a smaller body (B-6) which is located to the southeast of the main ore body (Fig. 3). The main ore body in the Brewer pit consists of quartz-pyrite breccia, quartz-andalusite breccia, and very minor quartz-topaz rock. The breccias are multi-phase, heterolithic, and matrix- or clast-supported. Most clasts within the breccias are pre-existing breccia fragments.

Fine-grained quartz, pyrite, and topaz, commonly comprise the breccia matrix. The B-6 ore body is tabular, extending along a NWW-SSE direction, perhaps along a fault or fracture zone. The western part of the ore body is composed of intensely fractured breccia and quartz-andalusite rock; the eastern part of the ore body was originally a massive sulfide rock containing quartz, andalusite, kyanite, and topaz but it is now represented by gossan. Quartz veins are abundant in the mineralized zone, ranging from tiny (centimeter-scale), discontinuous veinlets to large (up to meter scale) veins controlled by the structures, such as faults and fractures. Pyrite, enargite, muscovite, or pyrophyllite are present in some quartz veins.

Quartz and pyrite are the dominant minerals in the clasts and matrix. Pyrite commonly occurs in the matrix of matrix-supported breccia and in the fractures of clast-supported breccia, behaving as a cementing material. Both quartz and pyrite are fine-grained, whereas the clasts are typically fine-grained aggregates of quartz and minor pyrite. Although quartz and pyrite are the dominant minerals in the mineralized zones, aluminosilicate minerals, such as andalusite, may be locally abundant, especially in the B-6 area. Topaz occurs either in veins or as fine-grained matrix in the breccias. Locally, enargite is concentrated in some breccia phases, forming enargite-pyrite-quartz breccia (Fig. 3). Accessory minerals include sphalerite, chalcopyrite, bornite, cassiterite, chalcocite, tetrahedrite, galena, ilmenite, cinnabar, and native sulphur (Butler et al., 1988). Gold primarily occurs as micron-sized particles along grain boundaries, often associated with pyrite (Scheetz, 1991).

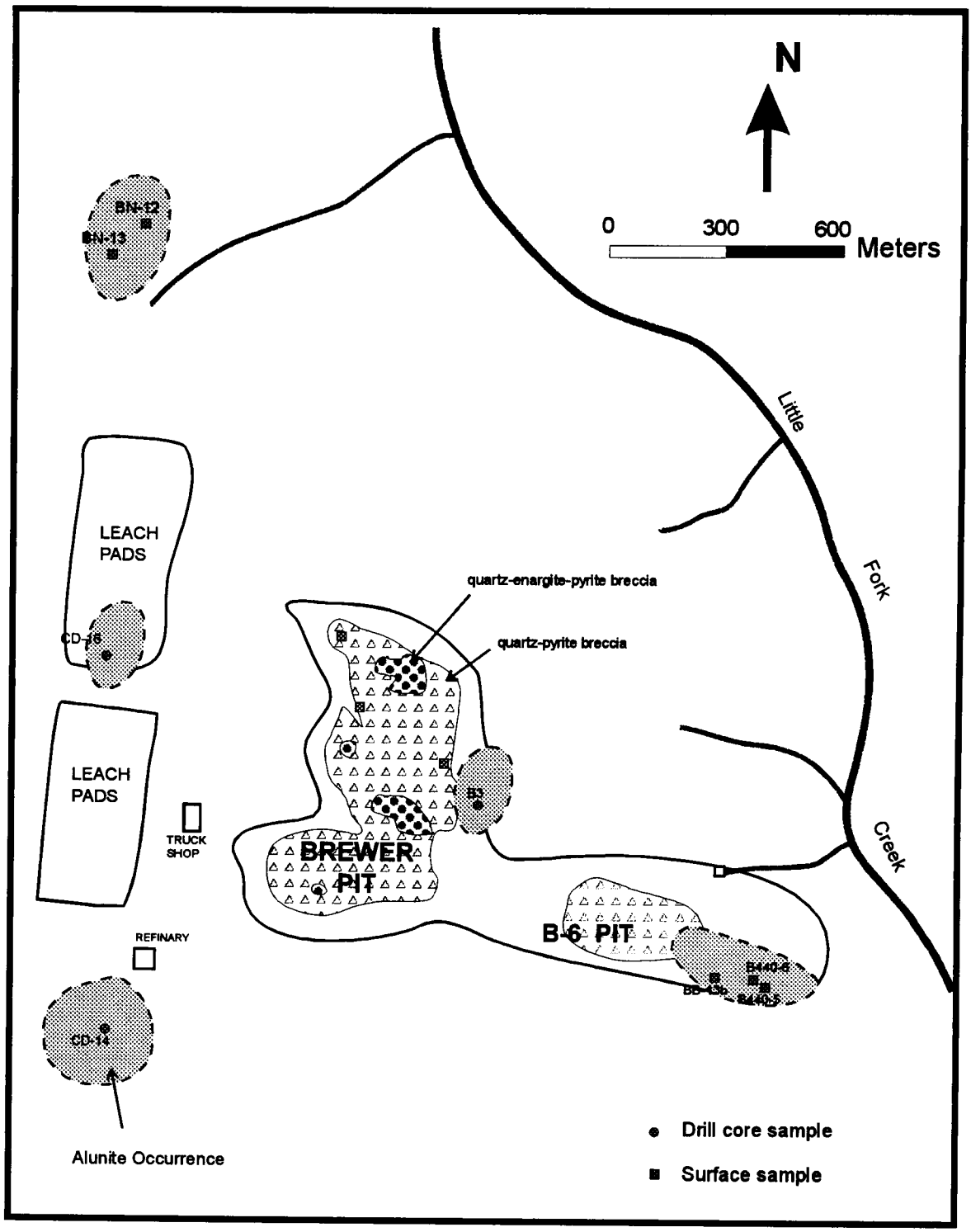

Fig. 3. Map of the Brewer Mine showing the occurrence of alunite within and surrounding the Brewer Pits. Based on mapping by the Brewer geologic staff and Scheetz (1991).

ALUNITE IN THE BREWER MINE AREA

Petrography

Alunite is present in the mineralized breccia zones and in the surrounding advanced argillic alteration zone. It is mostly observed to the north-west and southeast of the breccia zone (Fig. 3), occurring as discontinuous bodies. A direct correlation between the distribution of alunite and fracture pattern is difficult to establish, but the distribution of alunite bodies may be related to the structures that controlled the movement of hydrothermal fluids during alteration.

Alunite is most abundant in hydrothermally altered volcanic tuff and some pyrite-quartz breccia, although it is also observed in andalusite-quartz porphyry-like rock intersected in a deep drill hole. In the volcanic tuff, alunite occurs commonly as massive, microcrystalline pinkish aggregates and veins, constituting up to 30 % of the rock in some drill core samples. The alunite in the pyrite-quartz breccias is not recognizable in hand specimens but is easily identified in thin sections.

Alunite is present predominantly in three forms: microcrystalline aggregates in volcanic rock; disseminations in volcanic rock and pyrite-quartz rock; and vein-fillings in volcanic rock. In thin sections, alunite aggregates appear as an interlocking mosaics of platy and tabular micro-crystals of alunite and granular quartz (Fig. 4a) and are surrounded by a fine-grained groundmass composed mainly of quartz. Although some of the aggregates appear to be replacement of pre-existing phenocrysts of feldspar (Fig. 4b), other may represent fillings along fractures. As disseminations in quartz-dominated matrix, alunite occurs in volcanic rock and pyrite-quartz rock (Fig. 4c). The other minerals in the groundmass of the rocks are quartz and pyrite. The alunite occurs mostly as randomly oriented, small platy minerals, comprising < 5 to 50% of the groundmass in volume. Although disseminated alunite is mostly small, in a pyrite-quartz sample, the alunite appears as large rhombohedral and platy crystals in a groundmass of quartz and

Fig. 4(a-f). Photomicrographs of alunite-bearing rocks. Scale bars are shown on each photo. Abbreviations: Al, alunite; Py, pyrite; Qu, quartz; An, andalusite.

(4a). Fine-grained, tabular alunite crystals occur in rock-like mass, intermixed with fine grained quartz in alunite-quartz rock (Drill hole sample, CD-16-61). (crossed nicols).

(4b). Alunite aggregate in fine grained quartz matrix in hydrothermally altered volcanic rock (Drill hole sample, CD-16-84) in advanced argillic zone outside of the mineralized breccia center zone. The outline of the aggregate suggest that it either replaced preexisting phenocryst of feldspar or filled in the void of the volcanic tuff (crossed nicols).

(4c). Plate of alunite intermixed with quartz in the massive alunite rock (BB-13b)from the Brewer. The size of the alunite varies, range from fine- to medium-sized grains (crossed nicols).

(4d). Phenocrysts of alunite in quartz-pyrite breccia (B440-5) in the southeastern part of mineralized zone at Brewer. Note the large, euhedral to sub-euhedral forms of the alunite crystals, typically in flat rhombohedra (planar light).

(4e). Alunite vein cutting through fine-grained quartz-pyrite matrix in quartz-pyrite breccia (B440-6). (crossed nicols).

(4f). Fine-grained alunite with quartz in andalusite-bearing breccia (Drill hole sample, CD-16-100). Note the alteration of hydrothermal andalusite phenocryst. Alteration of andalusite crystals suggest that they formed earlier than the fine-grained groundmass (crossed nicols).

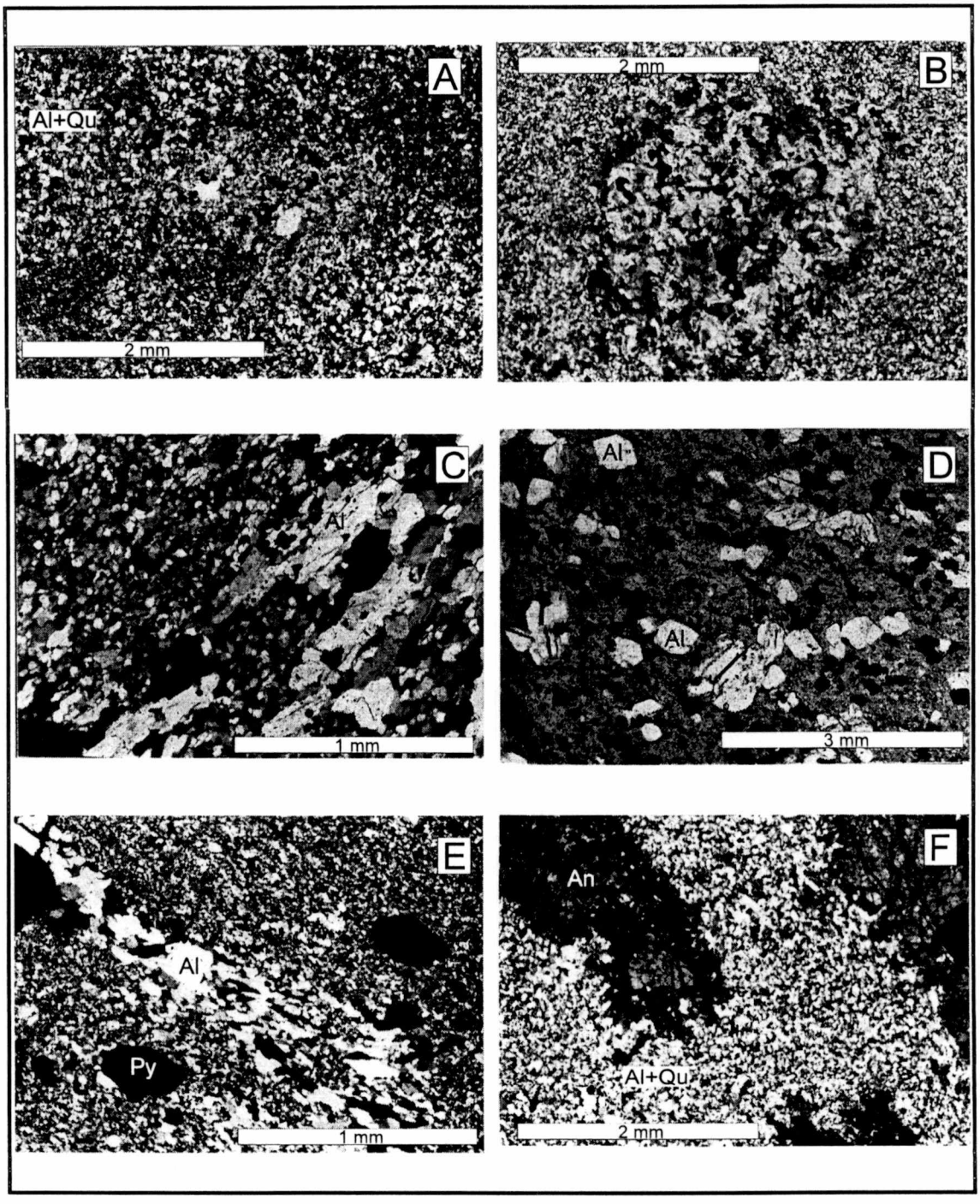
A
Al+Qu
2 mm
B
2 mm
C
Al
1 mm
D
Al
Al
3 mm
E
Al
Py
1 mm
F
An
Al+Qu
2 mm

pyrite (Fig. 4d). Alunite veinlets, up to 5 mm in width, are observed in volcanic tuff and breccia. The veinlets are composed either almost entirely of alunite or of alunite and quartz, with small amounts of pyrite. The alunite is typically tabular (Fig. 4e). The veinlets appear to represent fillings of fractures of the volcanic rocks.

Many other minerals are associated with alunite. Quartz is always present with alunite, either in groundmass or as veinlets and quartz "eyes". Pyrite coexists with alunite and quartz in quartz-pyrite rocks (Fig. 4e). The pyrite occurs as fine to medium grained, euhedral to anhedral crystals. The pyrite and alunite appear to have been coprecipitated and their coexistance is particularly important for the origin of the alunite. Sericite appears in some samples, commonly in the groundmass mixed with fine-grained quartz. Minor amounts of hematite are present in oxidized samples, apparently as an oxidation product of sulfides. Alunite is also present in the quartz-andalusite rock with an assemblage of quartz, alunite, andalusite, kyanite, sericite, pyrophyllite, kaolinite, and pyrite. The andalusite is coarsely crystallized and rimed by an alteration mineral assemblage of sericite and quartz. The alunite appears to replace andalusite in that it occurs along the fractures of andalusite (Fig. 4f).

All of the fine grained alunites of different modes of occurrence probably formed at the same time. This is suggested by the following observations: (1) the alunite veinlets typically taper out, apparently along fractures, but never cut the alunite disseminations in the groundmass; and (2) most of the alunite aggregates appear to be linked by small alunite veinlets. The coarse, rhombohedral and platy crystals of alunite in pyrite-quartz rock, however, have a distinct appearance.

Mineralogy and Chemistry of Alunite

Extensive solid solution typically exists between alunite [$KAl_3(SO_4)_2(OH)_6$] and natroalunite [$NaAl_3(SO_4)_2(OH)_6$]. Alunite can also have limited solid solution with

jarosite [$KFe_3(SO_4)_2(OH)_6$] (Parker, 1962; Battey, 1981). Powdered and grain-mount samples of alunite were analyzed by a Siemens D500 Diffractometer at the Department of Geological Sciences of the University of Tennessee, Knoxville, under conditions of 40 kV and 30 mA. XRD analysis confirmed the presence of alunite and indicated various amounts of natroalunite component in the alunite. Figure 5 shows the typical XRD pattern of alunite-bearing samples with peaks of alunite-natroalunite, quartz, and muscovite.

Chemical analysis of alunite was performed at the Department of Geological Sciences of the University of Tennessee with a fully automated Cameca SX-50 microprobe. Analytical conditions used were: 15 kV acceleration voltage, 10 or 20 nA current, 10 μm beam diameter , 20 second counting time for each element, and full ZAF correction.

The analysis (Table 1) indicates that the Brewer alunites belong to the alunite-natroalunite solid solution series, with essentially no jarosite component. The large compositional variations of alunite, in terms of K/Na ratios, is related to its texture (Fig. 6). The fine-grained, typically pinkish alunite, which occurs either as disseminations or aggregates, is K-rich, with K/(Na+K) mol ratio ranging from 0.51 to 0.87. The K content varies from grain to grain, even in a single sample. On the other hand, the coarse-grained, platy rhombohedral alunite is Na-rich natroalunite, with Na/(Na+K) mol ratio ranging from 0.55 to 0.75 (Fig. 6). The natroalunite is also compositionally zoned, with Na increasing from the center to the rim of grains (Fig. 7). P_2O_5 ranges up to 0.70 wt%, suggesting minor replacement of sulfur by phosphorus.

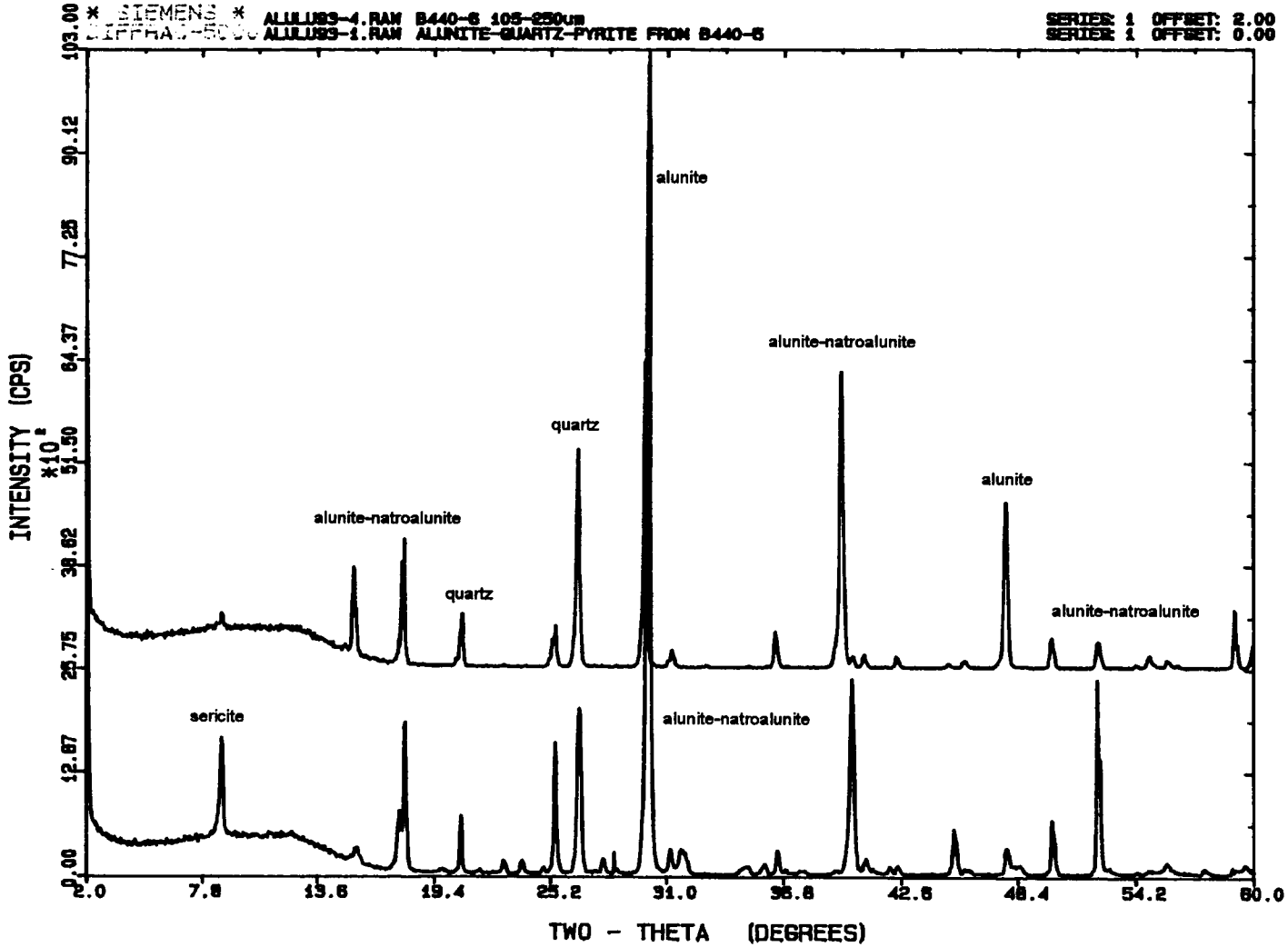

Fig. 5. XRD pattern of two alunite samples with small amounts of quartz and sericite. Location of the alunite peaks is typically between alunite-natroalunite standards, suggesting a solid solution series of alunite-natroalunite.

Table 1. Electron microprobe analyses of alunites from the Brewer mine area

Sample CD-16

Grain	1	2	3	4	5	6	7	8	9	10	11	12	13	min.	max.	average	std. dev.
Na_2O	2.54	2.39	3.72	2.03	1.86	3.06	2.57	1.00	2.77	3.18	2.89	3.06	2.60	1.00	3.72	2.59	0.68
K_2O	6.88	6.76	5.69	7.86	8.20	6.80	7.20	9.47	6.91	6.34	6.62	6.82	7.18	5.69	9.47	7.13	0.94
Al_2O_3	36.9	37.3	37.0	36.7	36.3	36.7	37.1	36.5	36.6	37.5	37.4	37.3	37.0	36.3	37.5	36.9	0.36
Fe_2O_3	<0.03	0.05	<0.03	0.05	0.04	<0.03	<0.03	0.05	0.05	<0.03	0.05	<0.03	0.05	0.04	0.05	0.05	0.01
SO_3	36.5	37.4	37.4	37.2	36.7	37.2	37.4	35.6	36.5	37.4	37.1	37.4	37.0	35.6	37.4	37.0	0.53
P_2O_5	0.33	0.34	0.56	0.49	0.36	0.42	0.40	0.70	0.33	0.42	0.46	0.31	0.50	0.31	0.70	0.43	0.11
Total(without H_2O)	83.1	84.3	84.3	84.4	83.5	84.2	84.7	83.4	83.2	84.8	84.4	84.9	84.3	83.1	84.9	84.1	0.62
Cations based on 6 (OH)																	
Na	0.349	0.324	0.502	0.276	0.256	0.416	0.348	0.123	0.382	0.428	0.391	0.412	0.354	0.123	0.502	0.351	0.09
K	0.624	0.602	0.506	0.703	0.744	0.608	0.640	0.867	0.627	0.561	0.590	0.605	0.643	0.506	0.867	0.640	0.09
Al	3.086	3.070	3.033	3.039	3.044	3.034	3.047	3.088	3.068	3.065	3.074	3.060	3.059	3.033	3.088	3.059	0.02
Fe	0.000	0.003	0.000	0.003	0.002	0.000	0.001	0.003	0.003	0.001	0.003	0.000	0.003	0.000	0.003	0.002	0.00
S	1.945	1.959	1.955	1.959	1.959	1.958	1.958	1.921	1.947	1.949	1.942	1.952	1.945	1.921	1.959	1.950	0.01
P	0.020	0.020	0.033	0.029	0.022	0.025	0.024	0.043	0.020	0.025	0.027	0.018	0.030	0.018	0.043	0.026	0.01
Total	6.024	5.978	6.028	6.009	6.026	6.041	6.018	6.045	6.046	6.028	6.027	6.047	6.033	5.978	6.047	6.027	0.02

Sample B440-5

	Grain a					Grain b			Grain c				
	rim	center	center	middle	rim	center	middle	rim	center	min.	max.	average	std. dev.
Na_2O	5.14	4.19	4.35	4.65	5.26	4.61	4.84	5.60	4.02	4.02	5.60	4.87	0.61
K_2O	3.47	5.09	4.78	4.49	3.37	4.18	4.24	2.86	5.05	2.86	5.05	3.94	0.85
Al_2O_3	37.6	37.8	37.7	37.7	37.5	37.9	37.7	38.0	36.4	36.4	38.0	37.5	0.64
Fe_2O_3	0.20	<0.03	<0.03	<0.03	<0.03	<0.03	<0.03	0.05	0.07	0.05	0.07	0.06	0.01
SO_3	37.6	37.9	36.8	37.2	37.7	38.4	38.1	37.3	37.4	37.3	38.4	37.8	0.47
P_2O_5	0.42	0.48	0.42	0.49	0.54	0.53	0.46	0.66	0.44	0.44	0.66	0.53	0.09
Total(without H_2O)	84.4	85.4	84.1	84.5	84.4	85.6	85.4	84.5	83.4	83.4	85.6	84.7	0.87
Cations based on 6 (OH)													
Na	0.688	0.557	0.588	0.624	0.703	0.609	0.641	0.747	0.548	0.548	0.747	0.650	0.08
K	0.305	0.445	0.425	0.397	0.296	0.363	0.370	0.251	0.452	0.251	0.452	0.346	0.08
Al	3.059	3.055	3.103	3.078	3.047	3.036	3.042	3.083	3.013	3.013	3.083	3.044	0.03
Fe	0.010	0.000	0.000	0.001	0.000	0.000	0.000	0.003	0.004	0.000	0.004	0.001	0.00
S	1.946	1.949	1.926	1.933	1.951	1.961	1.955	1.925	0.970	0.970	1.961	1.752	0.44
P	0.025	0.028	0.025	0.029	0.031	0.031	0.027	0.039	0.026	0.026	0.039	0.031	0.01
Total	6.033	6.034	6.067	6.062	6.028	6.000	6.034	6.048	6.013	6.000	6.048	6.024	0.02

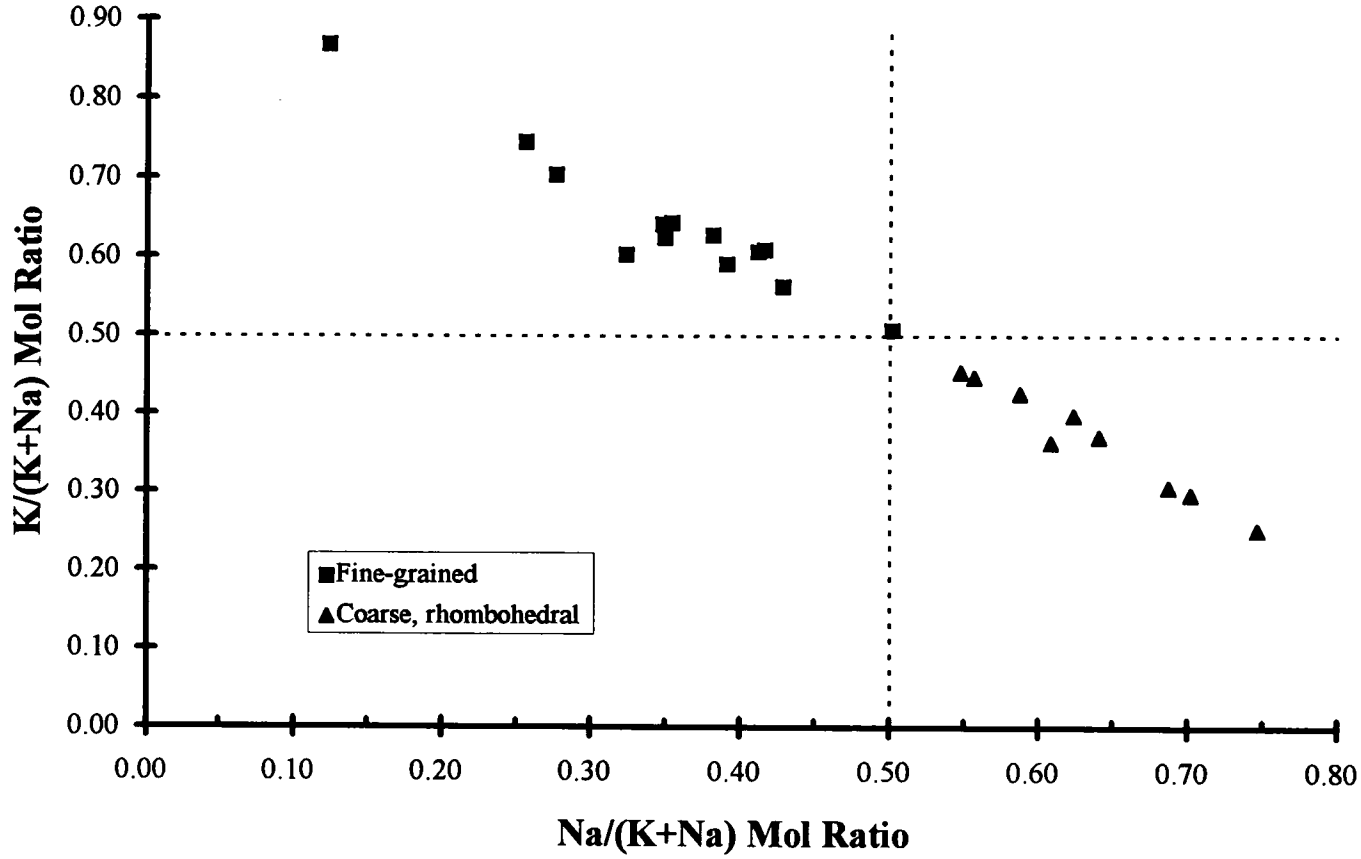

Fig. 6. Compositional variation of alunite, as revealed by electron microprobe analysis. The fine-grained alunites are K-rich, whereas the coarse, rhombohedral crystals are Na-rich natroalunite.

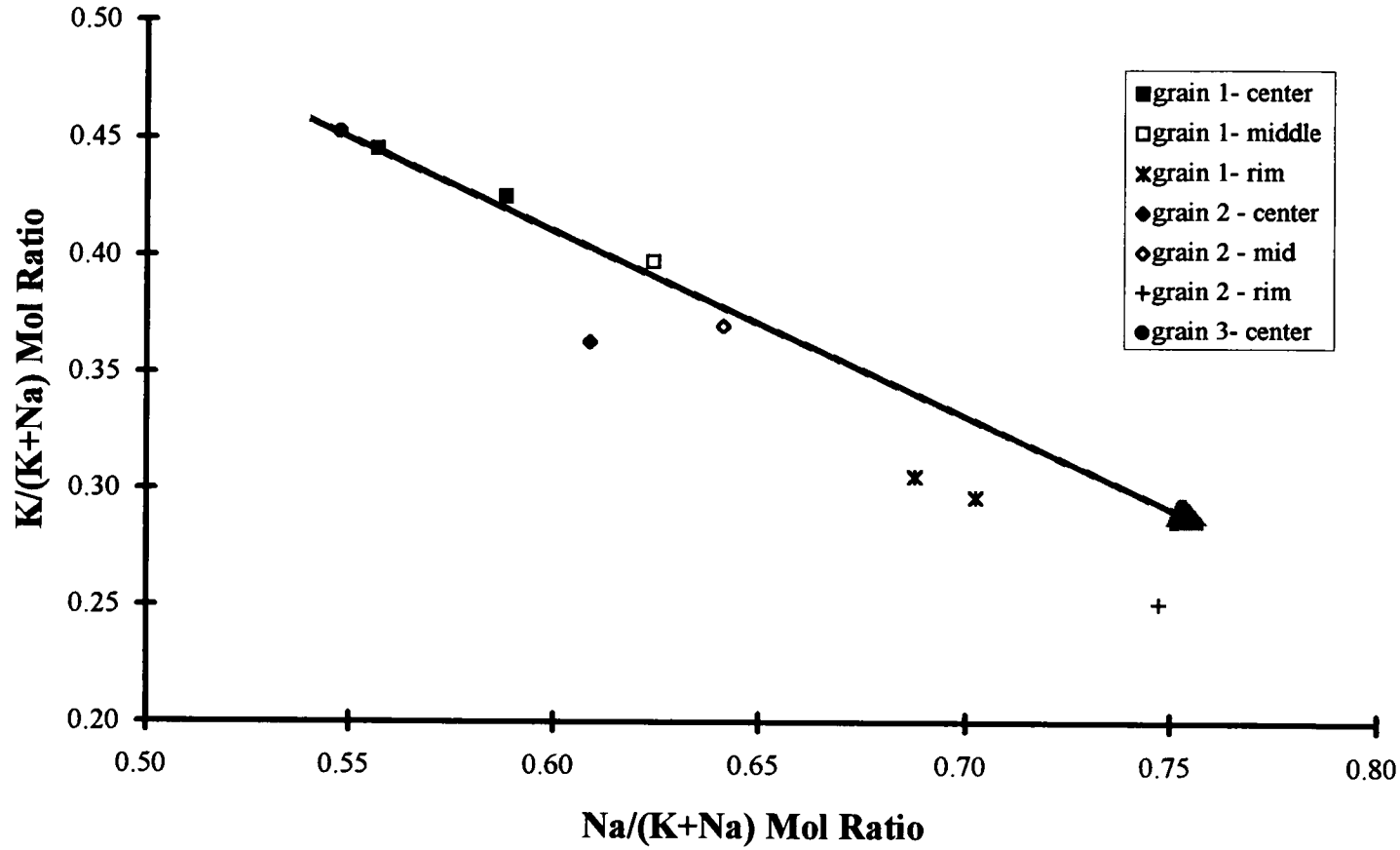

Fig. 7. Compositional zonation in natroalunite grains, which Na increasing from the center to the rim. The arrow shows the compositional trend.

SULFUR ISOTOPE GEOCHEMISTRY OF ALUNITE AND PYRITE

Analytical Procedure

Sulfur isotopic analysis was performed in the Department of Geology and Geochemistry of Stockholm University. Accuracy of analysis is better than ± 0.2 ‰. Both alunite and pyrite, hand-picked from surface and drill core samples, were crushed and sieved to a 106-500 μm size fraction. Different types of alunite samples --vein, replacement, and dissemination from volcanic rock and pyrite-quartz rock-- were selected for sulfur isotope analysis. Pyrite samples were selected from mineralized breccia, pyrite-bearing quartz vein, andalusite-pyrite rock, and volcanic tuff. Coexisting alunite and pyrite were separated first by heavy liquid, followed by hand-picking under binocular microscope. The pyrite separates were better than 95% pure. The alunite samples contained various proportions of alunite (10-80%), quartz, sericite, and trace amounts of pyrite in some samples.

Sulfur Isotope Results

The $\delta^{34}S$ values of alunite from the Brewer Gold Mine range from 17.7 to 26.8 per mil (Table 2 and Fig. 8) and average 22.6 per mil. Different types of alunite samples, including vein, phenocryst replacement and disseminated forms, have similar $\delta^{34}S$ values, between 21.3 and 26.8. The lower values (17.7 and 18.3 per mil) of two alunite samples could be due to pyrite contamination as they contain very fine-grained pyrite, often intergrown with alunite.

The $\delta^{34}S$ values of pyrite range from 0.5 to 5.7 per mil (Table 2, Fig. 8), with an average value of 3.4 per mil. Pyrite from the mineralized breccia of Brewer pit has $\delta^{34}S$ from 2.5 to 3.7 per mil. The relatively fine-grained pyrites from breccias have the same values as euhedral pyrite crystals in silicified volcanic rock and pyrite-andalusite rocks. The $\delta^{34}S$ values of pyrite from the massive pyrite rock and andalusite-pyrite rock of the

Table 2. Sulfur isotope data (per mil) for alunite and pyrite from the Brewer Gold Mine

Sample	Description	$\delta^{34}S$		$\Delta^{34}S$	T(°C)
		pyrite	alunite		
PYCRY	euhedral pyrite in silicified breccia	3.7			
B6PY	massive pyrite rock	3.4			
BQ-9	euhedral pyrite in quartz-pyrite vein	3.9			
BQ-9(b)	euhedral pyrite in quartz-pyrite vein	3.8			
BPQ	quartz-pyrite breccia	2.7			
BPQ-2	quartz-pyrite breccia	2.5			
BDH121-149	pyrite--quartz-andalusite breccia	2.4			
BDH61-777	pyrite in breccia	4.6			
BDH61-777(b)	pyrite in breccia	4.5			
B440-5	pyrite in pyrite-alunite rock	0.5			
B440-6	pyrite & alunite in pyrite-alunite rock	2.7	18.3	15.5	441.0
BB-13B	pyrite & alunite in pyrite-alunite rock	4.5	17.7	13.2	549.6
CD14-56	pyrite & alunite in pyrite-alunite rock	5.7	26.8	21.1	294.2
CD16-28	alunite vein in volcanic rock		24.9		
CD16-40	alunite vein in volcanic rock		25.3		
CD16-61	alunite in volcanic rock		24.3		
CD16-36	alunite aggregate in volcanic rock		25.3		
B3-236	alunite in volcanic rock		21.3		
B3-263	alunite in volcanic rock		21.3		
B3-263(b)	alunite in volcanic rock		21.3		

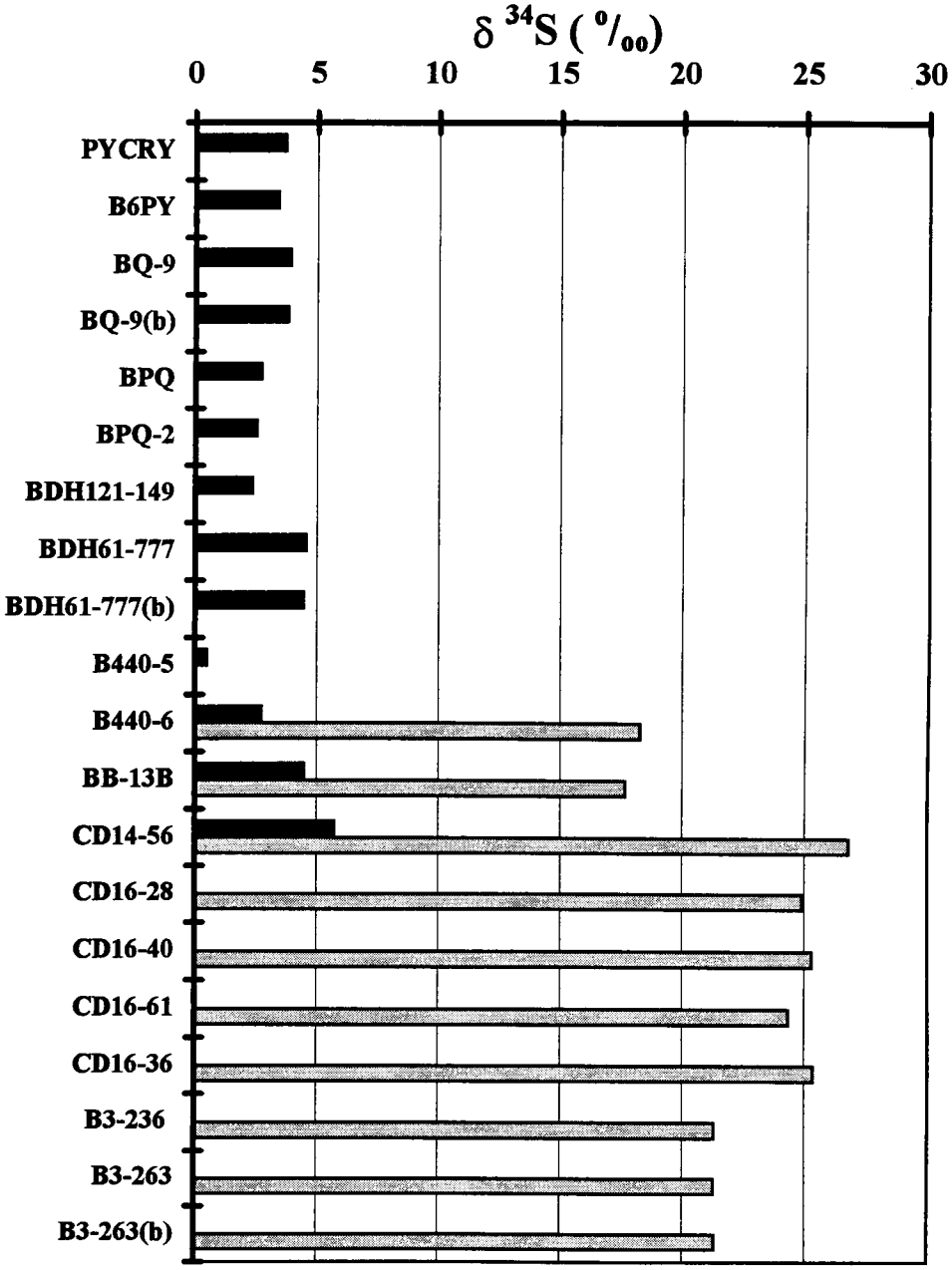

Fig. 8. $\delta^{34}S$ of alunite (shaded) and pyrite (black) from the Brewer Mine area. Both alunite and pyrite have relatively narrow ranges, but quite distinct ranges from each other. The $\delta^{34}S$ values of alunite are about 15 to 26 per mil larger than those of pyrite, suggesting a magmatic hydrothermal environment (see text).

B-6 ore body are between 0.5 and 4.5 per mil. Pyrite from quartz-pyrite veins has $\delta^{34}S$ of 3.8 and 3.9 per mil. One pyrite from alunite-bearing pyrite-quartz rock has $\delta^{34}S$ of 5.7 per mil. The pyrite from an andalusite-bearing breccia from deep part of the system is about 4.5 per mil. The similarity in the $\delta^{34}S$ ranges of the pyrites, irrespective of their texture and occurrence, implies that the pyrite-bearing quartz veins were the product of hydrothermal activity related to the gold mineralization in the Brewer area. The similar $\delta^{34}S$ values also indicate a common origin for the sulfur with little contamination or assimilation from the host rocks.

It is noteworthy that the $\delta^{34}S$ values of the pyrite from the Brewer Mine are similar to those of sulfide minerals from other epithermal deposits (-10 to +10 ‰; Field and Fifarek, 1985; Taylor, 1987; Ohmoto, 1986; Rye et al., 1992). As is the case with the pyrite and alunite from the Brewer, variations in the $\delta^{34}S$ values for either sulfates or sulfides in individual epithermal deposits rarely exceed 5 to 7 ‰. Compositionally distinct clusters present in some deposits can be related to source, age, and other unique conditions within a system (Field and Fifarek, 1985).

Interpretation

Origin of alunite

Because the acid sulfate alteration at the Brewer Mine, characterized by the occurrence of alunite+quartz±pyrite, is spatially related to the gold mineralization, the origin of the alunite is critical to the understanding of the conditions of mineralization. If the alunite at Brewer is of hypogene origin, the alunite would provide important information about the alterations accompanying the mineralization. On the other hand, if the alunite is of supergene origin and formed by oxidation of sulfides, the alunite would have no direct relationship with the gold mineralization. Because of the similarity in textures, mineralogy, and alteration forms associated with both supergene and hypogene

acid sulfate alteration, the $\delta^{34}S$ values of alunite and pyrite provide a potentially useful approach.

Supergene acid sulfate alteration may form over a sulfide zone when it is raised above the water table by tectonic uplift or exposed by erosion. It may overprint earlier acid sulfate assemblages. Field (1966) and Steiner and Rafter (1966) observed that sulfur undergoes little fractionation during supergene oxidation of sulfides and the formation of sulfate minerals. The small fractionation has also been confirmed by several experimental studies (Kaplan and Rittenberg, 1964; Nakai and Jensen, 1964; and Lewis and Krouse, 1969). Thus, supergene alunite normally has $\delta^{34}S$ values virtually identical to those of precursor sulfides, unless bacteriogenic reduction of aqueous sulfate takes place in standing pools of water (Rye et al., 1992). The $\delta^{34}S$ values of alunites from Brewer are generally 18 to 20 °/oo larger than those of pyrite (Table 2 and Fig. 8). Therefore, the alunites were likely to be hypogene in origin and part of the mineral assemblage formed during hydrothermal alteration accompanying the gold mineralization. The narrow range of $\delta^{34}S$ values of the alunites, 17.7 to 26.8 per mil, also indicates that they are cogenetic. The narrow ranges of $\delta^{34}S$ values and the lack of any overlap between alunites and pyrites suggest that the presence of supergene alunite that overprints earlier acid sulfate assemblages is highly unlikely.

Magmatic hydrothermal environment of the Brewer alunite

Hypogene alunite may be formed mainly in two different geologic environments: steam-heated and magmatic hydrothermal (Rye et al., 1992). Steam-heated environments typically occur in the upper portions of hydrothermal systems, where H_2S derived from underlying hydrothermal system and atmospheric oxidation of H_2S released by the magmatic boiling fluid to form sulfuric acid at and above water table result in the acid sulfate alteration. The acid sulfate alteration in steam-heated environment is characterized

by pronounced vertical zoning and the presence of extensive sinters. Because of a lack of isotopic fractionation in this oxidation process, the alunite from steam-heated environment has $\delta^{34}S$ values similar to those of the precursor H_2S and related sulfides (Rye et al., 1992). Magmatic hydrothermal acid sulfate environment, on the other hand, is characterized by an acid sulfate alteration that is developed in a hydrothermal system containing a significant magmatic component and driven by magmatic heat (Rye et al., 1992; Heald et al., 1987). In such an environment, SO_4^{2-} in the hydrothermal fluid is probably produced by the disproportionation of SO_2 by reaction such as (Holland, 1965; 1967) :

$$4SO_2 + 4H_2O = 4H_2SO_3 = 3H_2SO_4 + H_2S$$

The SO_2, derived from a magma and transported in a vapor plume consisting predominantly of water vapor, begins disproportionation with decreasing temperature. The SO_2 disproportionation becomes important at temperature below 400°C, depending on water pressure, producing increasing amounts of H_2SO_4 and H_2S with decreasing temperature (Rye et al., 1992). The equilibrium between aqueous H_2S and SO_4^{2-} formed by the disproportionation results in the enrichment of ^{34}S ($\delta^{34}S$=16 to 28 °/oo, depending on temperature) in alunite relative to pyrite.

At the Brewer Mine, the gold mineralization is confined to multi-episodic hydrothermal pyrite-quartz breccias, suggesting that the pyrite is a product of the mineralizing fluid. Thus, the $\delta^{34}S$ values of pyrite should represent the $\delta^{34}S$ values of H_2S in the fluid, and $\delta^{34}S$ values of pyrite and alunite would be similar if they were produced in a steam-heated environment. Other features of steam-heated environment lacking at Brewer include vertical zoning and extensive silica sinter. Boiling of fluid is common in steam-heated environment, but fluid inclusion studies (see Part 4) suggest that boiling was probably not a significant process in gold mineralization and hydrothermal activities at Brewer.

A magmatic hydrothermal acid sulfate environment for the Brewer is indicated by the alunite-pyrite sulfur isotopic data (discussed above) as well as by many other features. As is the case with many magmatic hydrothermal environments (Rye et al., 1992), the acid sulfate alteration is generally believed to be fracture controlled and is characterized by horizontal zoning of mineral assemblage, presence of abundant disseminated pyrite, enargite, and other Cu-As-Sb-S minerals, and high PO_4 contents of alunite. Many of these features are present in the Brewer Mine. The alteration zoning pattern in the Brewer, from the mineralized zone outward, is, silicic, advanced argillic, sericitic, and propylitic alteration. The alteration zoning pattern at Brewer, from silicic (mineralized zone) to propylitic (peripheral), probably developed around a volcanic caldera (Nystrom, 1972) and intense leaching by acidic fluids in the central part of the system resulted in a silicified zone. The distribution pattern of alunite bodies in the Brewer implies structural controls (fractures). The alunite in the alunite-quartz zone of the Brewer Mine, as mention earlier, occurs as aggregates of bladed or lathlike crystals replacing phenocrysts and as lathlike microcrystals intergrown with quartz in the groundmass. All these features, along with the presence of many sulfide minerals in the Brewer, strongly support a magmatic hydrothermal acid sulfate environment.

Temperature of hydrothermal alteration

Sulfur isotopic fractionation between alunite and pyrite in equilibrium ($\Delta^{34}S_{alunite\text{-}pyrite}$) during hydrothermal alteration is a potential geothermometer. In magmatic hydrothermal environment, alunite obtains its sulfate from sulfuric acid formed by the disproportionation of SO_2 derived from a magma. Equilibrium conditions in the fluid are likely at the high temperature and low pH of the environment and the $\delta^{34}S$ values of alunite and associated pyrite should reflect the H_2S/SO_4 ratio and temperature of the fluid. Thus, the $\Delta^{34}S_{alunite\text{-}pyrite}$ values should provide reliable temperature estimates

(Rye et al., 1992). Assuming equilibrium condition, the temperature of hydrothermal alteration at Brewer can be estimated from the $\delta^{34}S$ of the hypogenic alunite and pyrite using the fractionation equation (Ohmoto and Rye, 1979):

$$1000 \ln\alpha_{\text{alunite-pyrite}} = 4.86 * 10^6 T^{-2} + 6.0$$

where $\alpha_{\text{alunite-pyrite}}$ is the fractionation factor and T is the temperature (Kelvin). The $\Delta^{34}S_{\text{alunite-pyrite}}$ values in three pairs of coexisting pyrite and alunite are 13.2, 15.5, and 21.1. Using the above equation, the calculated temperatures are 549.6, 441.0, and 294.2 °C, respectively (Fig. 9). The highest temperature (549.6 °C) is probably too high considering the geologic environment in which acid sulfate alteration occurs. As discussed earlier, the $\delta^{34}S$ values of alunites in the samples are relatively low comparing to other alunite samples, which could be from some pyrite contamination.

The average $\delta^{34}S$ values of all alunite and pyrite, the $\Delta^{34}S_{\text{alunite-pyrite}}$ is 20.1, which gives a temperature of 314 °C. The average $\delta^{34}S$ values of all alunite and pyrite, excluding the distinctly lower pyrite value (0.51) and the two low alunite values (17.65 and 18.26), the $\Delta^{34}S_{\text{alunite-pyrite}}$ is 19.2, corresponding to a temperature of 333.7 °C, which is similar to the lower temperature range calculated from the coexisting alunite-pyrite pairs. Although the calculations are not based on strict coexistance, many of the alunite and pyrite samples are from the same small zones. Microthermometric analysis of fluid inclusions in the quartz from the Brewer indicates a homogenization temperature range of 160 to 330 °C. These temperatures are in general agreement with the lower end of alunite-pyrite geothermometer. However, the formation (trapping) temperature of the fluid inclusion should be somewhat higher at an elevated pressure. The temperatures estimated at Brewer are similar to those for other acid sulfate deposits, which lie between 200 and 300 °C (Hayba et al., 1985).

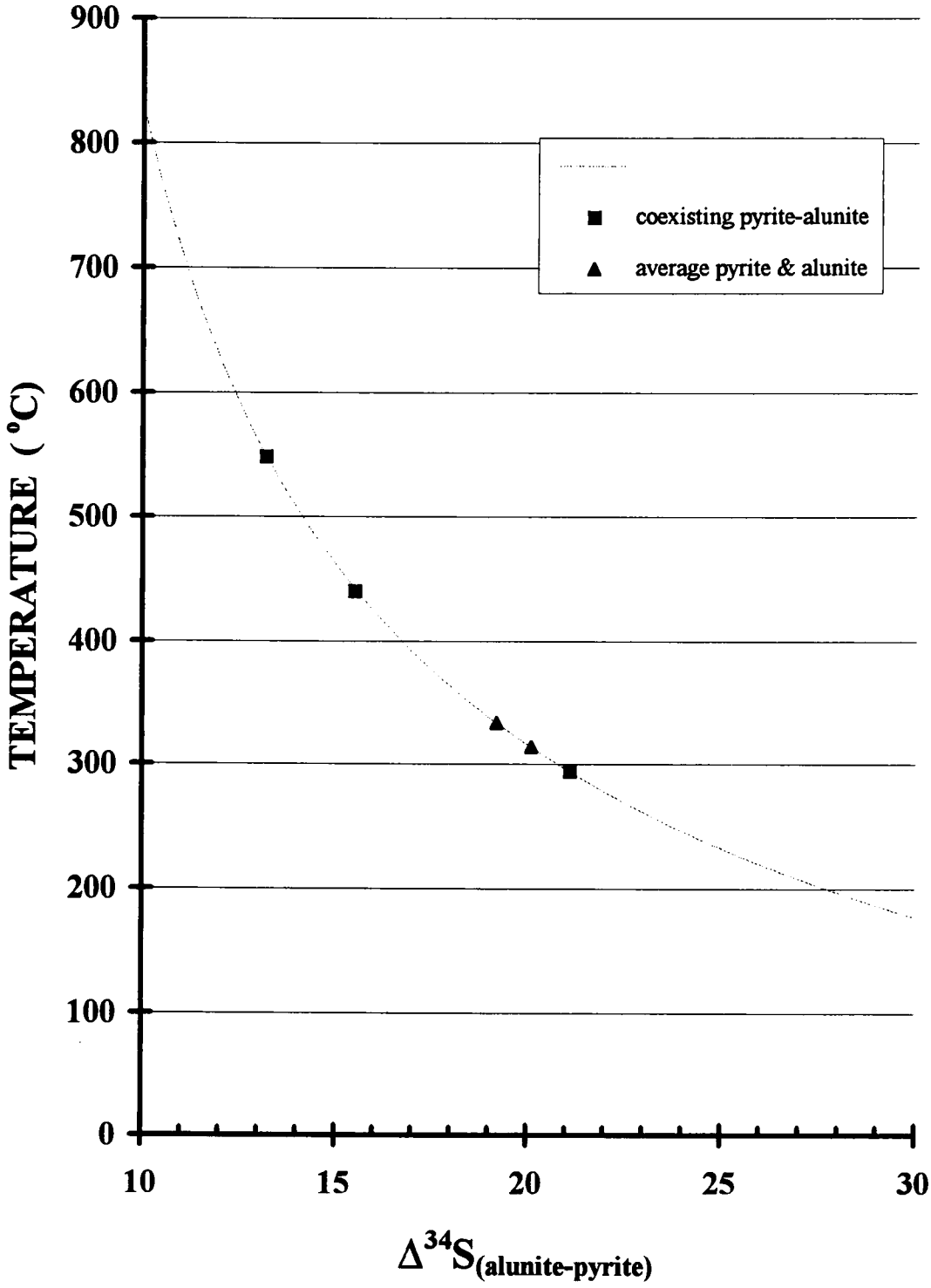

Fig. 9. Temperatures calculated from alunite-pyrite sulfur isotope geothermometer based on the equation of Ohmoto and Rye (1979). The temperature range for the acid sulfate alteration in Brewer is about 300-500 °C.

GENETIC MODEL

Hydrothermal Fluid Characterization and Geochemical Processes

The general hydrothermal fluid compositions and geochemical conditions for acid sulfate alteration have been extensively discussed in the literature (Hayba et al., 1985; Heald et al., 1987; Hemley et al., 1969; Knight, 1977; Rye et al., 1992; Raymahashay, 1968). The characteristic mineral assemblage of acid sulfate alteration--alunite, kaolinite, quartz, and pyrite--requires a hydrothermal fluid of low pH with significant concentrations of H_2SO_4 (Hemlay et al., 1969; Knight, 1977; Rye et al., 1992). An experimental study of alunite stability relations with other aluminosilicate minerals by Hemley et al. (1969) showed that a fairly high H_2SO_4 concentration was required before alunite could be produced in equilibrium with muscovite, kaolinite, or k-feldspar. A relatively high temperature environment favors the formation of alunite and kaolinite (or dickite or pyrophyllite), whereas higher temperature as well as higher K concentration are needed for the formation of alunite and muscovite. The activity of Na in the fluid does not significantly affect the acidity of the system. Knight (1977) studied the thermochemical relationship of alunite, enargite, and other copper-arsenic sulfates and concluded that the formation of alunite requires acid conditions and high sulfate activity and that the alunite-producing fluids may also produce high total sulfur mineralization at depth. If volcanic rocks above a porphyry intrusive are more oxidized than the intrusive, the fluid will oxidize as it moves upward. If the composition of the volcanic rocks is similar to that of the porphyry rock, decreasing temperature is possibly the predominant driving force for hydrothermal fluid-rock reactions along fluid pathlines. A relatively high temperature, acidic, and high sulfate environment favors the formation of alunite, quartz, enargite, and other copper-arsenic sulfosalts.

The presence of alunite, as well as of enargite and pyrite in the assemblage, suggests a S-rich fluid at Brewer. Moreover, fluid inclusions from the Brewer Mine

provide a direct evidence of S-rich fluid composition (see Part 4). Synchrotron X-ray fluorescence microprobe analysis of fluid inclusions at Brewer indicates the presence of S and Cl in the fluid. Laser Raman microprobe analysis of the fluid inclusions from the quartz in the mineralized breccia zone and advanced argillic (acid sulfate) zone of the Brewer Mine revealed the presence of SO_4^{2-} and CO_2 in the fluid (Fig. 10). No other sulfur species, such as HSO_4^-, H_2S, and HS^-, were detected in the fluid inclusions, implying that the fluids were relatively oxidized.

The mineral assemblage alunite-sericite-kaolinite-pyrophyllite-quartz in the advanced argillic alteration zone of the Brewer Mine suggests that the fluid probably had high K activity (Hemley et al., 1969). The compositional variation exhibited by the alunite-natroalunite from the Brewer area suggests a compositional evolution of the hydrothermal fluid toward Na enrichment during the alteration event, probably because of the change in T-P conditions and fluid-rock reactions along the fluid path. The effect of pressure on fluid compositional change is probably minimal (Hemley et al., 1969). Hemley et al. (1969) suggested that high aqueous Na/K ratios in the solution are required to form natroalunite because of considerably lower stability of natroalunite relative to the pure potassium phase. Increasing Na/K ratio in hydrothermal fluid may have resulted from the precipitation of K-bearing minerals, such as muscovite, kaolinite, K-feldspar, and pyrophyllite during hydrothermal alteration. The precipitation of K-bearing minerals could have lowered the K activity and relatively increased the Na/K ratio, so that the alunite-natroalunite became progressively more Na-rich. Considering the compositional variation of K-rich alunite, the overall trend appears to have been toward an increase in the Na/(Na+K) ratio, perhaps due to precipitation of other K-bearing minerals. K and other metals, including Ca, Ti, Cr, Mn, Fe, Ni, Cu, Zn, were detected in the hydrothermal fluid by Synchrotron X-ray fluorescence microprobe analysis of the Brewer

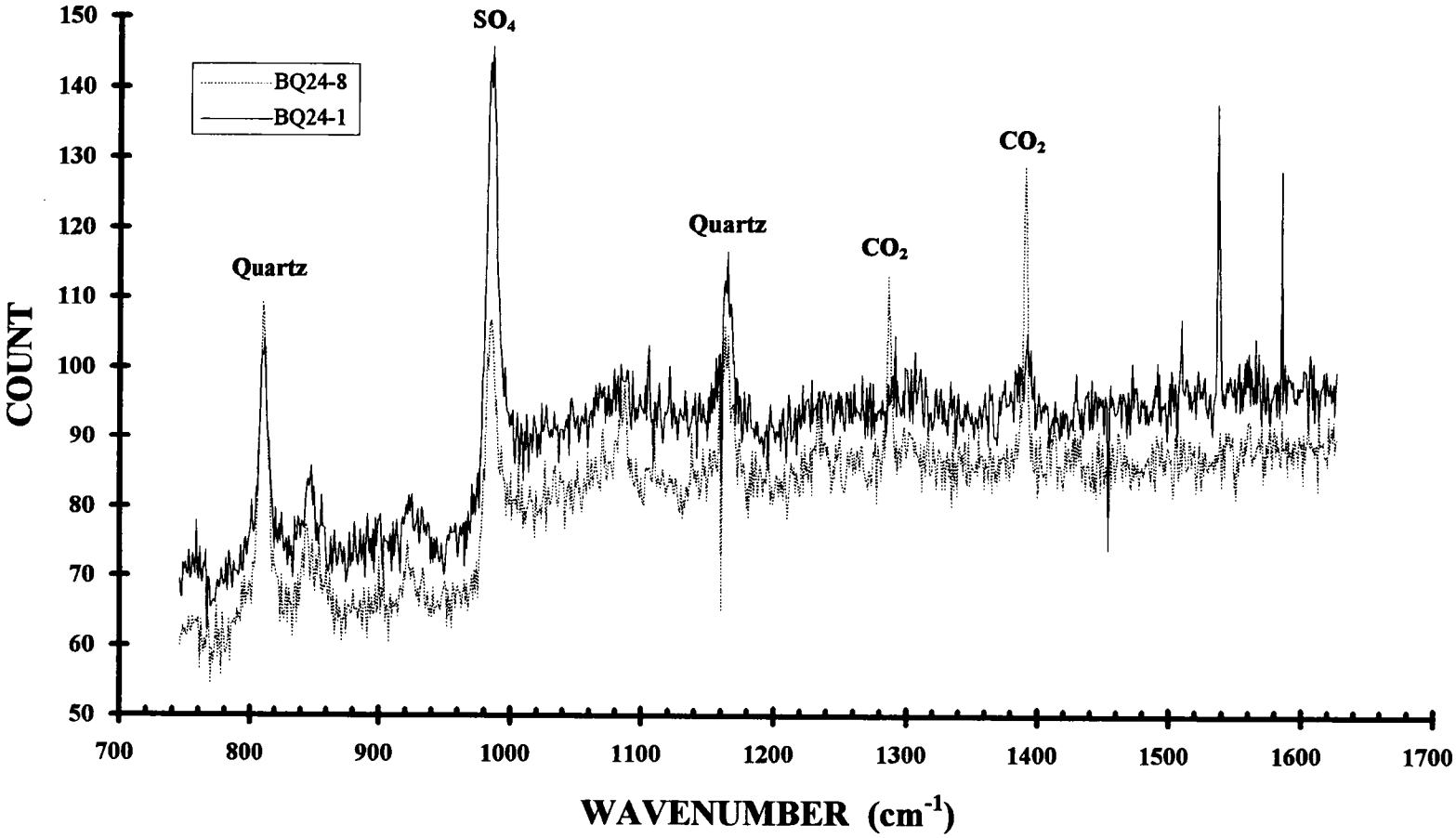

Fig. 10. Laser Raman microprobe analysis of fluid inclusions showing the SO_4^{2-} peaks near 980 cm^{-1}. The strong peaks indicate that the fluid is SO_4^{2-} -rich. Note that CO_2 is also present in the fluid.

fluid inclusions. Analytical limitation prevented the detection of Na, although it is likely to be present in the fluid.

Source of the fluids for the acid sulfate alteration is particularly important for understanding the geochemical processes that lead to the gold mineralization. Although the $\delta^{34}S$ values of individual sulfur-bearing minerals will not indicate the source of the fluid, the $\delta^{34}S$ value of total sulfur in the fluid may be diagnostic of its source (Ohmoto, 1986). In the Brewer hydrothermal system, possible sources of sulfur include direct magmatic, meteoric water, seawater, and the host-rock. The relatively indistinguishable $\delta^{34}S$ values of various pyrites in the Brewer deposit may suggest that there was little contribution from the wall rock. It is also possible that the mineralization was syn-volcanic in origin so that the $\delta^{34}S$ values are similar between host volcanic rock and magmatic hydrothermal fluid. The $\delta^{34}S$ values for total sulfur from magmatic sources such as volcanic rocks and/or magmatic intrusion are approximately 0 per mil (Ohmoto, 1972; 1986). The $\delta^{34}S$ values for total sulfur from Precambrian-Cambrian seawater sulfate are about 30 per mil (Holser and Kaplan, 1966; Holser, 1984). Meteoric water, which takes its isotopic signature from the oxidation and dissolution of sulfide and sulfate in the rock, has variable $\delta^{34}S$ values. The source of the sulfur may be dominated by magmatic, meteoric, and seawater sources based on X_{SO_4}/X_{H_2S} in the aqueous fluid. Nevertheless, magmatic fluid seems to have played an important role at Brewer.

The relatively low salinity and pH, high S, and CO_2-bearing hydrothermal fluid at the Brewer system implies that the gold may have been transported as various sulfide complexes (bisulfate or thioarsenide) in the hydrothermal fluid (Seward, 1973, 1984; Fyfe, 1986; Romberger, 1986, 1988; Cathles, 1985). Sulfide complexes are the most plausible transport mechanism for gold in epithermal environments. Acid sulfate type deposits are commonly relatively copper rich. At high H_2S concentrations, $Cu(HS)_2^-$ is the dominant copper-bearing complex (Barton et al., 1977). The chemistry of the

hydrothermal fluid is affected by temperature, pressure, activities of S_2 and O_2, pH, activity of Cl, and total sulfur concentration in the fluid (Heald et al., 1987). Therefore, oxidation, change in pH, decrease in sulfur activity will most likely cause gold precipitation; effect of temperature is uncertain (Romberger, 1988). Sulfur isotopic relationships between sulfate and sulfide minerals suggest that at temperatures below about 350°C, sulfide and sulfate precipitation is not caused by simple cooling, but rather by the mixing of sulfate-rich fluids (e.g., seawater) with hydrothermal fluid (Ohmoto, 1986). Because gold sulfide complexes are strongly affected by oxygen activity, mixing and fluid-rock interaction that produce oxidation of hydrothermal fluid may be a major mechanism of gold deposition.

Possible Relationship with a Cu-Mo Porphyry System

Although the evidence at Brewer is overwhelmingly in favor of a magmatic hydrothermal acid sulfate environment during the gold mineralization, many unique features at the Brewer suggest that the environment may have overlain, developed upon, or associated with a porphyry Cu-Mo environment. These features include the high-aluminosilicate alteration represented by andalusite and porphyry-like textures observed in the andalusite-bearing rocks of the deep part of the system (BDH-61) in this study and other core samples by Scheetz (1991). Andalusite is widespread in the mineralized breccia zone and advanced argillic alteration zone in the Brewer. It occurs as porphyritic crystals in volcanic rocks, euhedral platy crystals in massive pyrite rocks, and also as vein-filling or aggregates in the porphyry rock in the deeper part of system. It is usually highly fractured and surrounded by pyrophyllite fringes and pressure shadows in the rocks or in the veinlets. The porphyritic rock is composed of phenocrysts of quartz and andalusite and groundmass of quartz, sericite, pyrite, and apatite. Diaspore, corundum, kaolinite, and pyrophyllite are also present in the advanced argillic alteration zone.

Hydrothermal alteration containing andalusite and other high-alumina minerals is present at El Salvador, Chile (Gustafson and Hunt, 1975), La Granja, Peru (Schwartz, 1981), Butte, Montana (Brimhall, 1979; Meyer and Hemley, 1967), Elkhorn district, Montana (Steefel and Atkinson, 1984), Central Kazakhstan (summarized by Schmidt, 1985), and the Carolina slate belt (Klein and Criss, 1988). Many other gold deposits contain no andalusite but have other high aluminous minerals. Meyer and Hemley (1967) suggested that andalusite-bearing alteration assemblages are the high temperature equivalents of advanced argillic alteration assemblages. Some magmatic hydrothermal, acid sulfate systems many overlie deeper porphyry Cu or porphyry Mo environments (Silltoe, 1973, 1983; Wallace, 1979; Silltoe and Bonham, 1984; Bove et al., 1990).

Schmidt (1978; 1985) first proposed that some of the high-alumina hydrothermal systems in the volcanic rocks of the Carolina slate belt may be part of porphyry Cu-Mo system. He compared the high-alumina hydrothermal alteration in the belt -- represented by high-alumina minerals, such as andalusite, diaspore, and corundum, as well as by aluminous minerals, such as kaolinite and pyrophyllite -- with porphyry Cu-Mo deposits that contain aluminous alteration. Based on abundant high-alumina minerals and widespread silicification, he suggested that the Brewer was perhaps a porphyry gold deposit that is characterized by alumnosilicate alteration. Based on similarities in the style, mineralogy, and structural controls of mineralization between the Brewer and deposits worldwide, Stonehouse (1993) also suggested that the Brewer may be related to deep seated copper porphyry or skarn type mineralization.

Andalusite is either replaced or cut by hypogene alunite in the Brewer Mine, suggesting that the andalusite was likely formed before the acid sulfate alteration, probably during an early phase of the hydrothermal alteration. The low pH, K- and S-rich fluid during the subsequent acid sulfate alteration probably reacted with andalusite to form alunite and quartz:

$$3\ Al_2SiO_5 + 4\ H_2SO_4 + 2\ K^+ + 3\ H_2O = 2\ KAl_3(SO_4)_2(OH)_6 + 3\ SiO_2 + 2\ H^+$$

Using constraints of field, mineralogic, petrologic, chemical, and isotopic characteristics, the author proposes a generalized model for the Brewer as illustrated in Fig. 11. A felsic or felsic porphyritic magma was most likely the source of heat and fluid for the hydrothermal alteration. The magma was emplaced in a continental margin, probably an island-arc environment, and subsequent cooling resulted in the formation of porphyritic stocks and hydrothermal alteration minerals, including andalusite. The magmatic fluid with volatile components from the magma, probably rich in S, CO_2, H^+, K^+, and other metals, migrated upward along structural pathways and produced extensive hydrothermal alteration in the host volcanic rock. Sealing of channelways by deposition of sulfide minerals and silica caused an increase in the fluid pressure and led to the development of multi-phased hydrothermal breccias in the central silicic zone. Extensive leaching of base metals in the central portion of the system formed the aluminosilicate zone, probably including some andalusite, such as those in massive pyrite-andalusite rock, during acid sulfate alteration. The hydrothermal fluid, driven from the magmatic source, mixed with meteoric water and reacted with wall rock, causing the precipitation of gold and sulfide minerals.

CONCLUSIONS

The gold mineralization at the Brewer Mine of the Carolina slate belt, South Carolina, is accompanied by extensive hydrothermal aluminosilicate alteration and advanced argillic alteration. Sulfur stable isotope analyses of alunite and pyrite from the mine have provided important information of origin for the acid sulfate alteration and constraints on geochemical processes and conditions of accompanying gold mineralization. The $\delta^{34}S$ values of the alunites, including veinlets, replacements and

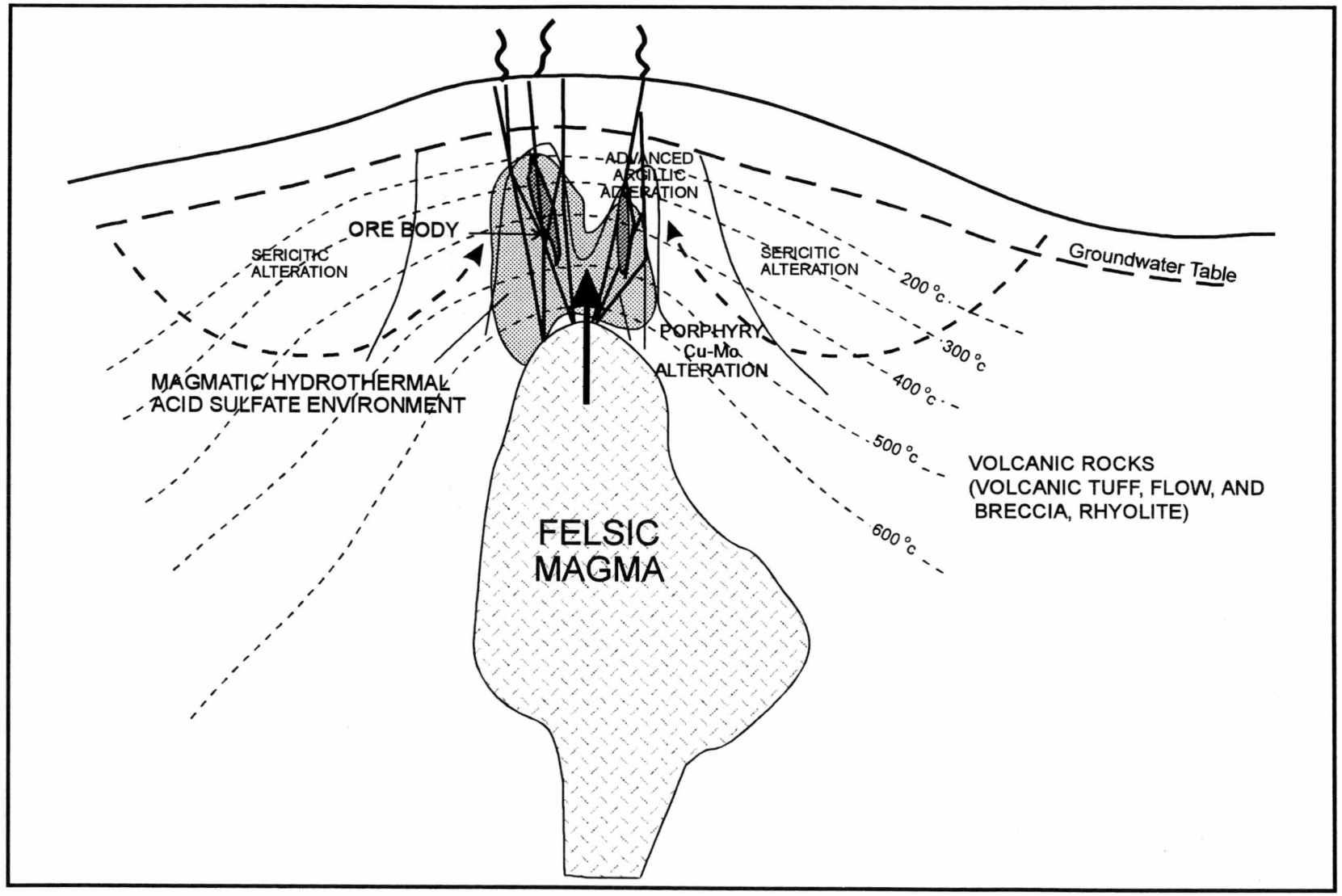

Fig. 11. Schematic diagram of conceptual model of the environment for the Brewer hydrothermal acid sulfate alteration system.

disseminatations, range from 17.7 to 26.8 per mil. The $\delta^{34}S$ values of the pyrites, including euhedral crystals and fine-grained in the groundmass of the pyrite-quartz rocks and breccias, and quartz-pyrite veins, range from 0.5 to 5.7 per mil. The narrow range of values in pyrite suggests that the sulfur was likely from a same fluid source. Distinct $\delta^{34}S$ ranges between alunites and pyrites indicate a hypogene origin for the Brewer alunite. The acid sulfate alteration is related to the magmatic hydrothermal alteration which is believed to be contemporaneous with the gold mineralization.

That $\delta^{34}S$ values of the alunites are generally 15 to 22 °/oo larger than that of the pyrite suggests a direct product of magmatic hydrothermal, acid sulfate alteration in an epithermal environment where the sulfuric acid was likely produced by the disproportionation of SO_2 with decreasing temperature, and the equilibrium between aqueous H_2S and SO_4 formed by the disproportionation resulted in that alunite is enriched in $\delta^{34}S$ relative to pyrite. Pyrite-alunite sulfur isotopic geothermometer gives temperatures about 300-500 °C that is in general agreement with the fluid inclusion data (see Part 4) of the Brewer Mine.

Extensive solid solution between alunite and natroalunite exhibited by the Brewer alunite probably reflects a complex fluid evolution during the hydrothermal alteration. The hydrothermal fluid was apparently enriched in K but Na appeared to be enriched toward to the later stage of hydrothermal alteration, as indicated by the compositional zonation of alunite-natroalunite. Presence of SO_4 and many other metals in the fluids suggests that a relatively oxidized condition prevailed during later stage of hydrothermal alteration and mineralization.

Considering the unique features, such as widespread aluminosilicate alteration and porphyritic textures, in the Brewer Mine area, it is likely that the Brewer magmatic hydrothermal system was linked to a porphyry Cu-Mo environment.

ACKNOWLEDGMENTS

Allan Patchen kindly provided assistance for the electron microprobe analysis of alunite. The author thanks Westmont Mining Inc. and Brewer Gold Co. for providing access to the mine and field assistance. It is particularly grateful to Jae Stonehouse, Mark Zwaschka, and John Scheetz of the Brewer Gold Company for valuable and helpful discussions of the geology of the Brewer Mine. Research grants from the Geological Society of America (1991), and Sigma-Xi (1991), Geological Society of America Southeastern Section (1992), and Discretionary Funds of the Department of Geological Sciences at the University of Tennessee are acknowledged.

REFERENCES

Barton, P. B. Jr., Bethke, P. M., and Roedder, E., 1977, Environment of ore deposition in the Creede Mining District, San Juan Mountains, Colorado: Part III. Progress toward interpretation of the chemistry of the ore-forming fluid for the OH vein: Economic Geology, v. 72, p. 1-24.

Bove, D. J. and Hon, K., 1990, Compositional changes induced by hydrothermal alteration at the Red Mountain alunite deposit, Lake City, Colorado: U.S.G.S Open-File report 90-0235, 29p.

Brimhall, G. H. Jr., 1979, Lithologic determination of mass transfer mechnisms of multi-stage porphyry copper mineralization at Butte, Montana: vein formation by hypogene leaching and enrichment of potassium-silicate protore: Economic geology, v. 74, p. 556-689.

Butler, J. R. and Ragland, P. C., 1969, A petrochemical survey of plutonic intrusions in the Piedmont, Southern Appalachians, USA: Contributions to Mineralogy and Petrology, v. 24, p. 164-190.

Butler, J. R. and Secor, D. T., 1991, The Central Piedmont: in J. W. Horton, Jr and V. A. Zulla, eds, The geology of Carolinas, University of Tennessee Press., p. 59-78.

Butler, J. R., 1985, The Brewer mine: in Feiss, P. G., ed., Volcanic-hosted gold and high alumina rocks of the Carolina slate belt: Guidebook for field trip, 1985 SGE fall meeting and 1985 GSA annual meeting, p. 143-199.

Butler, J. R., Scheetz, J. M., Stonehouse, J. M., Tayler, D. R., and Callaway, R. Q., 1988, The Brewer gold mine, Chesterfield County, South Carolina: Guidebook for field trip of the annual GSA meeting, Southeastern section, 22p.

Buttey, M. H., 1981, Mineralogy for students: 2nd ed., Longman, 355 p.

Cathles, L. M., 1986, The geologic solubility of gold from 200-350 °C, and its implications for gold-base metal ratios in vein and stratiform deposits: in Clark, L. A., ed., Gold in the western shield, p. 187-210.

Conley, J. F. and Bain, G. L., 1965, Geology of the Carolina slate belt west of the Deep River-Wadesboro Traiassic Basin, North Carolina: Southeastern Geology, v. 6, p. 117-138.

Feiss, P. G., 1985, Gold mineralization in the Carolina slate belt: Speculations on ore genesis: in Misra, K. C., ed., Volcanogenic sulfide and precious metal mineralization in the southern Appalachians: University of Tennessee, Department of Geological Sciences, Studies in Geology 16, p. 220-236.

Field, C. W. and Fifarek, R. H., 1985, Light stable-isotope systematic in the epithermal environment: in Berger, B. R., and Bethke, P. M. (eds), Geology and Geochemistry of Epithermal Systems: Society of Economic Geologists, Reviews in Economic Geology, v. 2, P. 99-128.

Field, C. W., 1966, Sulfur isotopic method for discriminating between sulfates of hypogene and supergene origin: Economic Geology, v. 61, p. 1428-1435.

Field, C. W., 1972, Surfur isotopic evidence for the supergene origin of alunite deposits, Tolfa district, Italy: Mineral Deposita, v. 7, p. 113-125.

Fyfe, W. S., 1986, The transport and deposition of gold: in Clark, L. A., ed., Gold in the western shield, p. 156-167.

Glover, L. III., and Sinha, A. K., 1973, The Virgilina deformation, a Late Precambrian to Early Cambrian (?) orogenic event in the central piedmont of Virginia and North Carolina: in L. Glover and P. H. Ribbe, eds., The Byron Cooper Volume, American Journal of Science, v. 273-A, p. 234-251.

Gustafson, L.B. and Hunt, J.P., 1975, The porphyry copper deposit at El Salvador, Chile: Economic geology, v. 70, p. 857-912.

Hayba, D. O., Bethke, P. M., Heald, P., and Foley, N. K., 1985, Geologic, mineralogic, and geochemical characteristics of volcanic- hosted epithermal precious-metal deposits: in Berger, B. R., and Bethke, P. M. (eds), Geology and Geochemistry of Epithermal Systems: Society of Economic Geologists, Reviews in Economic Geology, v. 2, p. 129-167.

Heald, P., Foley, N. K., and Hayba, D. O., 1987, Comparative anatomy of volcanic-hosted epithermal deposits: acid-sulfate and adularia-sericite types: Economic Geology, v. 82, p. 1-26.

Hemley, J. J., Hostertler, P. B., Gude, A. J., and Mountjoy, W. T., 1969, Some stability relations of alunite: Economic Geology, v. 64, p. 599-612.

Hemley, J. W., Montoya, J. W., Marinenko, J. W., and Luce, R. W., 1980, Equilibria in the system Al_2O_3-SiO_2-H_2O and some general implications for alteration/mineralization processes: Economic Geology, v. 75, p. 210-228.

Holland, H. D., 1965, Some applications of thermochemical data to problems of ore deposits, II. Mineral assemblages and the composition of ore-forming fluids: Economic Geology, v. 60, p. 1101-1166.

Holland, H. D., 1967, Gangue minerals in hydrothermal deposits, in Barnes, H.L., ed., Geochemistry of hydrothermal ore deposits: New York, p. 382-436.

Holser, W. T., 1984, Gradual and abrupt shifts in ocean chemistry during Phanerozoic time, in Holland, H. D., and Trendall, A. F., ed., Patterns of change in earth evolution. p. 123-143.

Holser, W. T. and Kaplan, I. R., 1966, Isotope geochemistry of sedimentary sulfates: Chemical Geology, v. 1, p. 93-135.

Kaplan, I. R. and Rittenburg, S. C., 1964, Microbiological fractionation of sulfur isotopes: Journal of General Microbiology, v. 34, p. 195-121.

Klein, T. L., and Criss, R. E., 1988, An oxygen isotope and geochemical study of meteoric-hydrothermal systems at Pilot Mountain and selected other localities, Carolina slate belt: Economic Geology, v. 83, p. 801-821.

Knight, J. E., 1977, A thermochemical study of alunite, enargite, luzonite, and tannantite deposits: Economic Geology, v. 72, p. 1321-1336.

Lewis, J. S. and Krouse, H. R., 1969, Isotopic composition of sulfur and sulfate produced by oxidation of FeS_2: earth Planet. Sci. Letters, v. 5, p. 425-453.

Lu, C., Misra, K. C., Stonehouse, J. M., and Zwaschka, M. R., 1993, Geochemical signatures of alterations in Brewer gold mine, South Carolina: South Carolina Geology. v. 35, p. 37-54.

Meyer C. and Hemley, J. J., 1967, Wall rock alteration: in Barnes, H. L., ed., Geochemistry of Hydrothermal Ore Deposits,, John Wiley and Sons, New York, p. 166-235.

Minard, J. P., 1971, Gold occurrences near Jefferson, South Carolina: U. S. Geological Survey Bulletin 1334, p. 1-20.

Nakai, N. and Jensen, M. L., 1964, The kinetic isotope effect in the bacterial reduction and oxidation of sulfur: Geochemica Cosmochimica Acta, v. 28, p. 1893-1912.

Nystrom, P. G. Jr., 1972, Geology of the Catarra NW quadangle: Master's Thesis, University of South Carolina, 49p.

Ohmoto, H. and Rye, R. O., 1979, Isotopes of sulfur and carbon: in Barnes, H. L., ed., Geochemistry of Hydrothermal Ore Deposits, 2nd edition, John Wiley and Sons, New York, p. 509-567.

Ohmoto, H., 1972, Systematic of sulfur and carbon isotopes in hydrothermal ore deposits: Economic Geology, v. 67, p. 551-578.

Ohmoto, H., 1986, Stable isotope geochemistry of ore deposits: in Valley et al., ed. Stable isotopes in high temperature geological processes, Review in Mineralogy, v. 16, p. 491-559.

Pardee, J. T., and Park, C. F., Jr., 1948, Gold deposits of the southern Piedmont: U. S. Geological Survey Professional Paper 213, 156p.

Parker, R. L., 1962, Isomorphous substitution in nature and synthetic alunite: American Mineralogist, v. 47, p. 127-136.

Romberger, S. B., 1986, The solution chemistry of gold applied to the origin of hydrothermal deposits: in Clark, L. A., ed., Gold in the western shield, p. 168-112.

Romberger, S. B., 1988, Geochemistry of gold in hydrothermal deposits: U. S. Geological Survey Bulletin 1857-A, p. 9-25.

Rye, R. O., Bethke, P. M., and Wasserman, M. D., 1992, The stable isotope geochemistry of acid sulfate alteration: Economic Geology, v. 87, p. 225-262.

Scheetz, J. W., 1991, The geology and alteration of the Brewer gold mine, Jefferson, South Carolina: M.S. Thesis, University of North Carolina, Chapel Hill, 180p.

Scheetz, J. W., Stonehouse, J. M., and Zwaschka, M. R., 1991, Geology of the Brewer gold mine in South Carolina: Mining Engineering, v. p. 38-42.

Schmidt, R. G., 1978, The potential for porphyry copper-molybdenum deposits in the eastern United States: U. S. Geological Survey Professional Paper 907-E, 31 p.

Schmidt, R. G., 1985, High-alumina hydrothermal systems in volcanic rocks and their significance to mineral prospecting in the Carolina slate belt: U. S. Geological Survey Bulletin 1562, 59 p.

Schwartz, M. O., 1981, The geochemistry of leached capping of the La Granja porphyry copper deposit, Peru: Journal Geochemical Exploration, v. 15, p. 93-113.

Secor, D. T., Jr., 1988, Review of the geology of the Carolina Slate Belt: in Secor, D. T., Jr., ed., 1988, Southeastern Geological Excursions: Guidebook for Geological Society of America, p. 1-18.

Seward, T. M., 1973, Thio complexes of gold and transport of gold in hydrothermal ore solutions: Geochimica Cosmochimica Acta, v 37, 379-399.

Seward, T. M., 1984, The transport and deposition of gold in hydrothermal systems: in Foster, R. P., ed., Gold'82; The geology, geochemistry and genesis of gold deposits: Rotterdam, A. A. Balkema, p. 165-179.

Sillitoe, R. H. and Bonham, H. F., Jr., 1984, Volcanic landforms and ore deposits: Economic Geology, v. 79, p. 1286-1298.

Sillitoe, R. H., 1973, The tops and bottoms of porphyry copper deposits: Economic Geology, v. 68, p. 799-815.

Sillitoe, R. H., 1983, Enargite-bearing massive sulfate deposits high in porphyry copper deposits: Economic Geology, v. 78, p. 348-352.

Sillitoe, R. H., 1985, Ore-related breccias in volcanoplutonic arcs: Economic Geology, v. 80, p. 1467-1514.

Steefel, C. I., and Atkinson, W. W., Jr., 1984, Hydrothermal andalusite and corundum in the Elkhorn district, Montana: Economic Geology, v. 79, p. 573-579.

Steiner, A., and Rafter, T. A., 1966, Sulfur isotopes in pyrite, pyrrhotite, alunite and anhydrate from steam wells in the Taupo volcanic zone, New Zealand: Economic Geology, v. 61, p. 1115-1129.

Stonehouse, J. M., 1992, Potential exploration implications of structural, mineralogical, and morphological features of the Brewer Au-Cu occurrence, Jefferson, S.C.: (Abstract) Geological Society of America Southeastern Section Meeting at Winston-Salem, North Carolina, v. 24, p. 68.

Taylor, B. E., 1987, Stable isotope geochemistry of ore-forming fluids, in Kyser, T. K., ed., Stable isotope geochemistry of low-temperature processes, Mineralogical Association of Canada Short Course Handbook, V. 13, p. 337-417.

Wallace, A. B., 1979, Possible signatures of buried porphyry-copper deposits in middle to late Tertiary volcanic rocks of western Virginia Range, Washoe, Storey, and Lyon Counties, Nevada: Economic Geology, v. 83, p. 864-874.

Worthington, J. T., and Kiff, I. T., 1970, A suggested volcanogenic origin for certain gold deposits in the slate belt of the North Carolina Piedmont: Economic Geology, v. 65, p. 529-537.

Worthington, J. T., Kiff, I. T., Jones, E. M., and Chapman, P. E., 1980, Applications of the hot springs or fumarolic model in prospecting for lode gold deposits: Mining Engineering, v. 32, p. 73-79.

Part 4

Fluid Evolution during Hydrothermal Gold Mineralization at the Brewer Mine, Jefferson, Carolina Slate Belt: Evidence from Fluid Inclusion Study

ABSTRACT

Gold mineralization at the Brewer Mine, South Carolina, occurs in an intensely silicified zone composed primarily of multi-stage hydrothermal quartz-pyrite breccias that are accompanied by extensive hydrothermal alterations. The inner part of the aluminosilicate hydrothermal system is predominantly an acid-sulfate alteration assemblage characterized by quartz, pyrite, alunite, enargite, topaz, and andalusite. The brecciation and hydrothermal alteration have produced abundant matrix quartz and quartz veins in the mineralized zone and in the surrounding hydrothermally altered, host rhyolitic volcanic breccia, flow, and tuff of the Carolina slate belt.

Fluid inclusions in the quartz were analyzed to determine the fluid composition and the physicochemical conditions of gold mineralization. Quartz occurs in many forms: (a) as very fine-grained disseminations and aggregates in the breccia fragments; (b) as fine- to medium-grained clear crystals in the breccia, often with pyrite and enargite; (c) as fine- to coarse-grained aggregates and discontinuous veins containing sulfide minerals in the breccia; and (d) as barren veins in both mineralized and unmineralized host volcanic rocks. The majority of the primary and pseudosecondary inclusions are CO_2-bearing two-phase ($L+LCO_2$) or three-phase ($L+LCO_2+VCO_2$) inclusions, with CO_2 occupying about 10 to 30% of the inclusions by volume at room temperature, although some primary and pseudosecondary CO_2-rich and mostly secondary aqueous fluid inclusions are also present. The fluid inclusions have homogenization temperatures and decrepitation temperatures between 160 and 330 °C, ice-melting temperatures between -13.7 and -1.0 °C, and clathrate-melting temperatures between 1.1 and 9.9 °C. CO_2 homogenization temperatures range from -3 to 31 °C. Microthermometric and microchemical analyses of the fluid inclusions indicate H_2O+CO_2 fluids with relatively low salinity (< 15 wt% NaCl equiv.). Laser Raman microprobe analysis on the fluid inclusions indicates that the inclusion fluids contain SO_4^{2-} in addition to CO_2.

Synchrotron x-ray fluorescence microprobe analysis of selected individual inclusions has revealed the presence of Cl, S, Ca, K, Fe, Ti, Cu, Zn, As, and Br. The fluids for the Brewer Gold Mineralization differ compositionally from those of typical epithermal gold and porphyry Au-Cu-Mo deposits, and may have been derived from a deep-seated felsic magma at the time of volcanism and mineralization.

INTRODUCTION

The Carolina slate belt is one of the most metallogenically significant terranes in the eastern United States. Various types of mineralization (Au, Cu, Pb, Zn, and Mo) have been found in the metavolcanic rocks of the belt (Feiss, 1985; Feiss et al., 1991; Bell et al., 1980). Gold mineralization is especially abundant in the Carolina slate belt. Most of the gold deposits in the belt are located at or near the contact between the lower volcanic unit and the upper sedimentary unit (Worthington et al., 1980; Butler, 1985). They are hosted by the volcanic sequence, and are commonly associated with rhyolitic horizons (Worthington, 1993). Features of volcanogenic and structurally controlled mineralization in many of the deposits have led several authors to propose a subvolcanic origin for the gold deposits (Worthington and Kiff, 1970; Worthington et al., 1980). Worthington and Kiff (1970) first suggested that these deposits are similar to the epithermal precious metal deposits that occur in Tertiary volcanic rocks of the western United States (Buchanan, 1981). However, due to the complex geological setting of many of these gold deposits, studies of the gold mineralization in some individual deposits have led to other theories on the origin of these gold deposits, such as hydrothermal veins (Feiss, 1985) and hydrothermal emplacements in shear zones (Tomkinson, 1988; Duckett et al., 1989). Some mineralized quartz veins, parallel to the regional metamorphic cleavage and with little alteration, are also present in the belt. These veins are found in spatial proximity to the environments of volcanogenic gold deposits, thus they may represent the remobilization of volcanogenically derived gold by high temperature, possibly CO_2-rich metamorphic fluids (Ford, 1981; Miller, 1982).

The Brewer Gold Mine is hosted by hydrothermally altered and regionally metamorphosed felsic volcanic rocks of the Carolina slate belt in northeastern Piedmont of South Carolina (Fig. 1). The felsic metavolcanic rocks are overlain by fine-grained volcanoclastic metasedimentary rocks that are generally unaltered and unmineralized. The

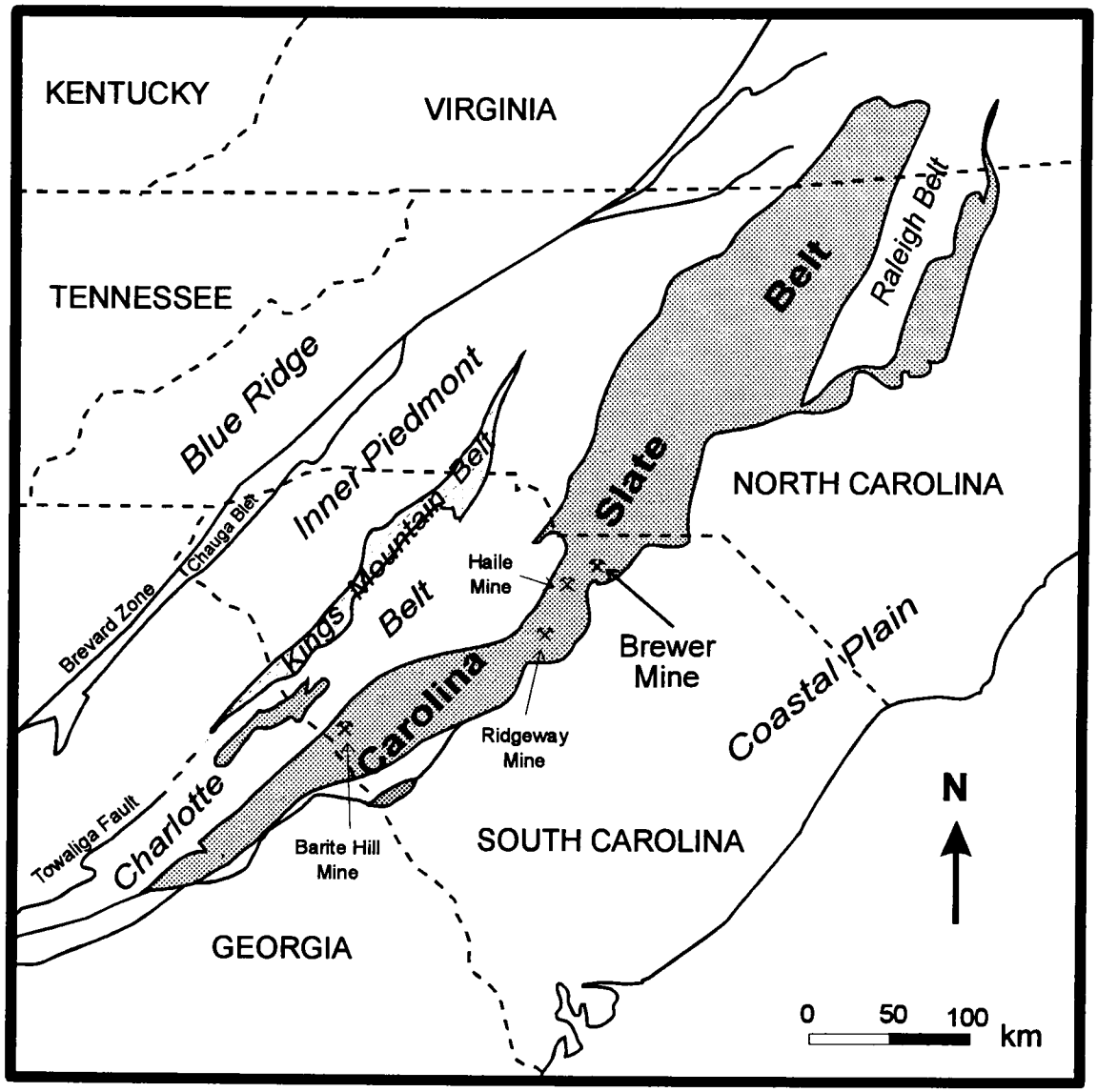

Fig. 1. Geological map showing the Carolina slate belt and location of the Brewer Mine, South Carolina (After Butler, 1985).

gold mineralization at Brewer occurs in an intensely silicified zone that is characterized by multi-stage brecciation, and a distinctive mineralogy dominated by quartz and pyrite with enargite, topaz, alunite, and andalusite, and with abundant quartz veins. Although the mineralization has been correlated with the volcanic activity that produced the brecciation and hydrothermal alteration (Worthington et al., 1980; Butler, 1985; Schmidt, 1979, 1985; Butler et al., 1988; Scheetz, 1991), little information is available on mineralizing fluids and physiochemical conditions of the hydrothermal alteration and mineralization. This is in sharp contrast to the volcanic-hosted epithermal precious-metal deposits in the younger (Tertiary) volcanic terranes of western United States from which most of the genetic models have been formulated (Hayba et al., 1985; Heald et al., 1987; Henley, 1985; Field and Fifarek, 1985; Bodnar, et al., 1985; Buchanan, 1981; Silberman and Berger, 1985; Berger and Henley, 1988).

Understanding the nature and source of the mineralizing fluid is a key to the development of genetic models for a hydrothermal gold deposit. The present study tries to characterize the mineralizing fluid composition, the physiochemical conditions, and fluid evolution at the Brewer hydrothermal system during the hydrothermal mineralization.

GEOLOGY AND HYDROTHERMAL GOLD MINERALIZATION

Regional and Local Geology

The Carolina slate belt is composed largely of Precambrian to Early Paleozoic volcanic and volcaniclastic sedimentary rocks that have undergone low-grade regional metamorphism and been intruded by many Paleozoic igneous plutons. The slate belt in northeastern South Carolina contains an extensive unit of predominantly felsic metavolcanic rocks that is overlain by a mixed volcano-sedimentary sequence. The volcanic rocks of the slate belt are probably a bimodal suite of calc-alkaline to tholeiitic

rocks of both shallow submarine and subaerial facies (Feiss, 1982). Intrusives in the Carolina slate belt are predominately granitic plutons that range in age from 265 to 650 m.y. (Butler and Ragland, 1969), although small mafic bodies are also present. Rocks of the Carolina slate belt were folded and metamorphosed up to lower-greenschist facies, ranging from chlorite to biotite grade, during the early to middle Paleozoic time (Taconic orogeny) (Butler, 1991). The belt is considered to be an exotic terrane because its features (stratigraphy, structure, metamorphism, mineral deposits, and fauna) contrast sharply with those of nearby terranes (Secor et al., 1983; Vick et al., 1983; Williams and Hatcher, 1983). It probably developed in a volcanic arc environment associated with subduction (Hatcher, 1978; Rankin, 1975), in an oceanic island arc setting (Whitney et al., 1978), or a continental margin arc environment (Rogers,1982), or in a rift zone (Long, 1979).

The Brewer Gold Mine is hosted within felsic volcanic rocks that are near the contact of overlying volcaniclastic sedimentary rocks (Fig. 2). The volcanic rocks consist of flows, tuffs, breccias, and pyroclastics. Volcanic tuffs include rhyolitic crystal and lithic tuffs. Some of the tuffs contain both crystals and lithic fragments, and most show sorting and well-preserved stratification. Volcanic flows are not well stratified and contain blocks, lapilli, and ash with some individual blocks over 10 cm in diameter. Volcanic breccias contain angular lithic fragments (typically with composition similar to that of the matrix) and a matrix of quartz, sericite, and Fe-oxides. The widespread volcanic flows and breccias suggest the presence of a volcanic center near the Brewer area. The sedimentary rocks in the Brewer area are mostly mudstone and siltstone that are typically well laminated and, close to the Brewer Mine, interlayered with volcanoclastics. The Pageland porphyritic granite batholith is located two kilometers northwest of the Brewer Mine. Many folds and faults are developed in the Brewer area (Butler, 1985; Scheetz, 1991).

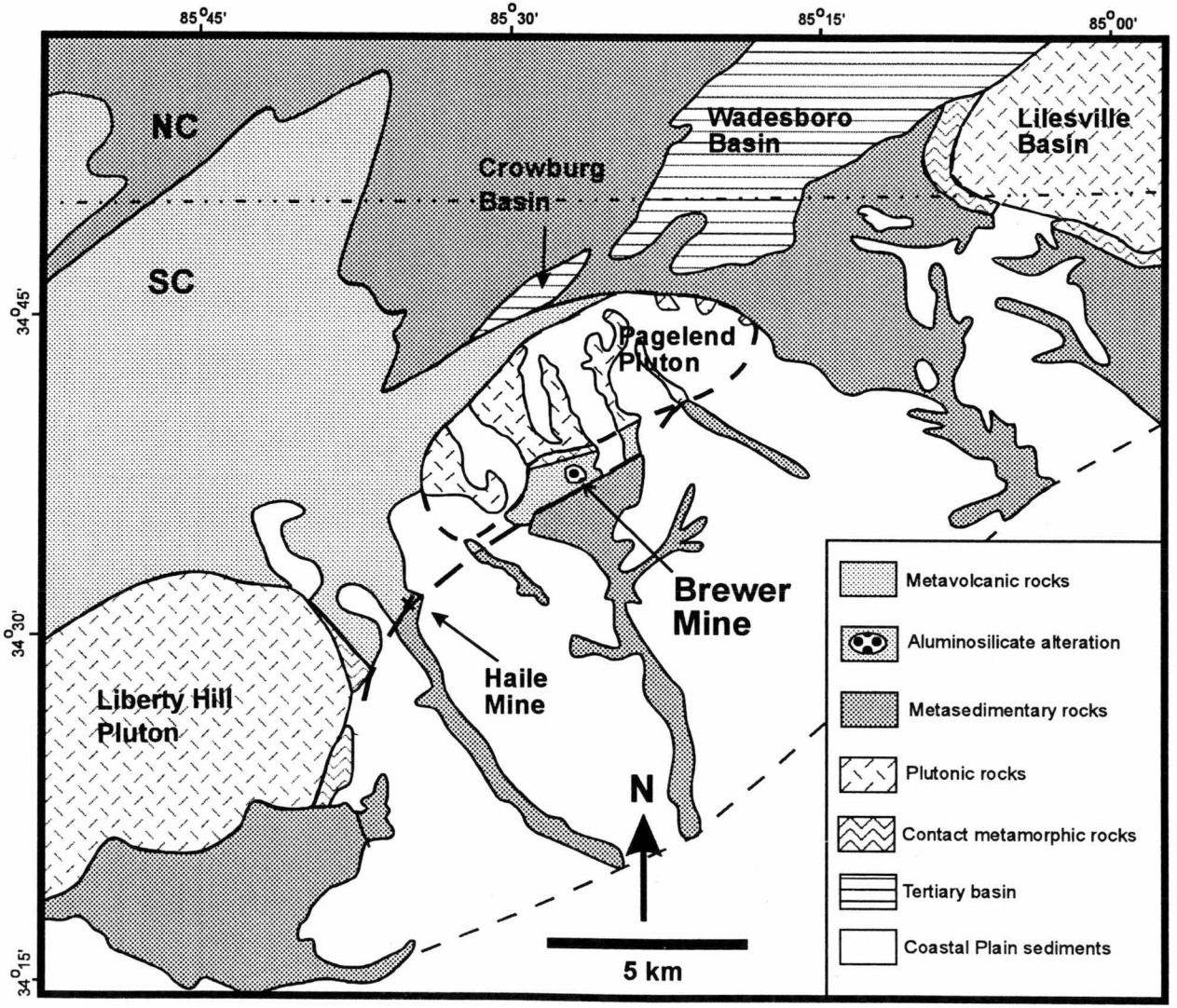

Fig. 2. Generalized geologic map of the Brewer area (after Bell and Popenoe, 1976; Butler et al., 1988; Scheetz, 1991).

Hydrothermal Alteration and Gold Mineralization

Gold mineralization in Brewer occurs in an intensely silicified zone, which constitutes the central part of a much larger hydrothermal alteration system that extends over more than 2 kilometers across and has a near-circular shape in plan view, which probably represents the center of a volcanic system - a cinder zone, a caldera, or a diatreme (Nystrom, 1972). Extensive hydrothermal activities have formed a concentric alteration pattern which consists of, outward from the interior, zones of silicic, advanced argillic, sericitic, and sporadically distributed propylitic alteration (Lu et al., 1993). Silicic alteration in the Brewer Mine area is represented by quartz-sulfide heterolithic breccia rocks that are characterized by extreme abundance of hydrothermally introduced SiO_2. Advanced argillic alteration is characterized by the assemblage quartz, hypogene alunite, and andalusite, with varying amounts of sericite, pyrophyllite, pyrite, topaz, diaspore, and kaolinite. The assemblage quartz+pyrite+alunite$\pm$other aluminosilicate minerals also indicates that the gold mineralization was accompanied by acid sulfate alteration. Sericitic alteration is represented by the assemblage quartz and sericite, with some pyrite and minor ilmenite. A mineral assemblage of quartz, epidote, calcite, chlorite, and pyrite defines the propylitic alteration. More detailed descriptions about the mineralogy and hydrothermal alteration have been given by Scheetz (1991) and Lu et al. (1993).

Gold mineralization is confined almost exclusively to the multiphase, eruptive breccia bodies or pipes in the central part of the alteration zone (Fig. 3). The heterolitic, matrix- or clast-supported breccias include quartz-sulfide breccias, quartz-andalusite breccias, and minor massive sulfide rocks. The fragments within the breccia vary in size from 25 cm to less than 1 mm and are composed of volcanic rocks, earlier phases of breccia, and earlier silica matrix. The matrix of the breccia consists mainly of quartz, sulfides, and minor topaz. Sulfide minerals are dominantly of pyrite, with subordinate

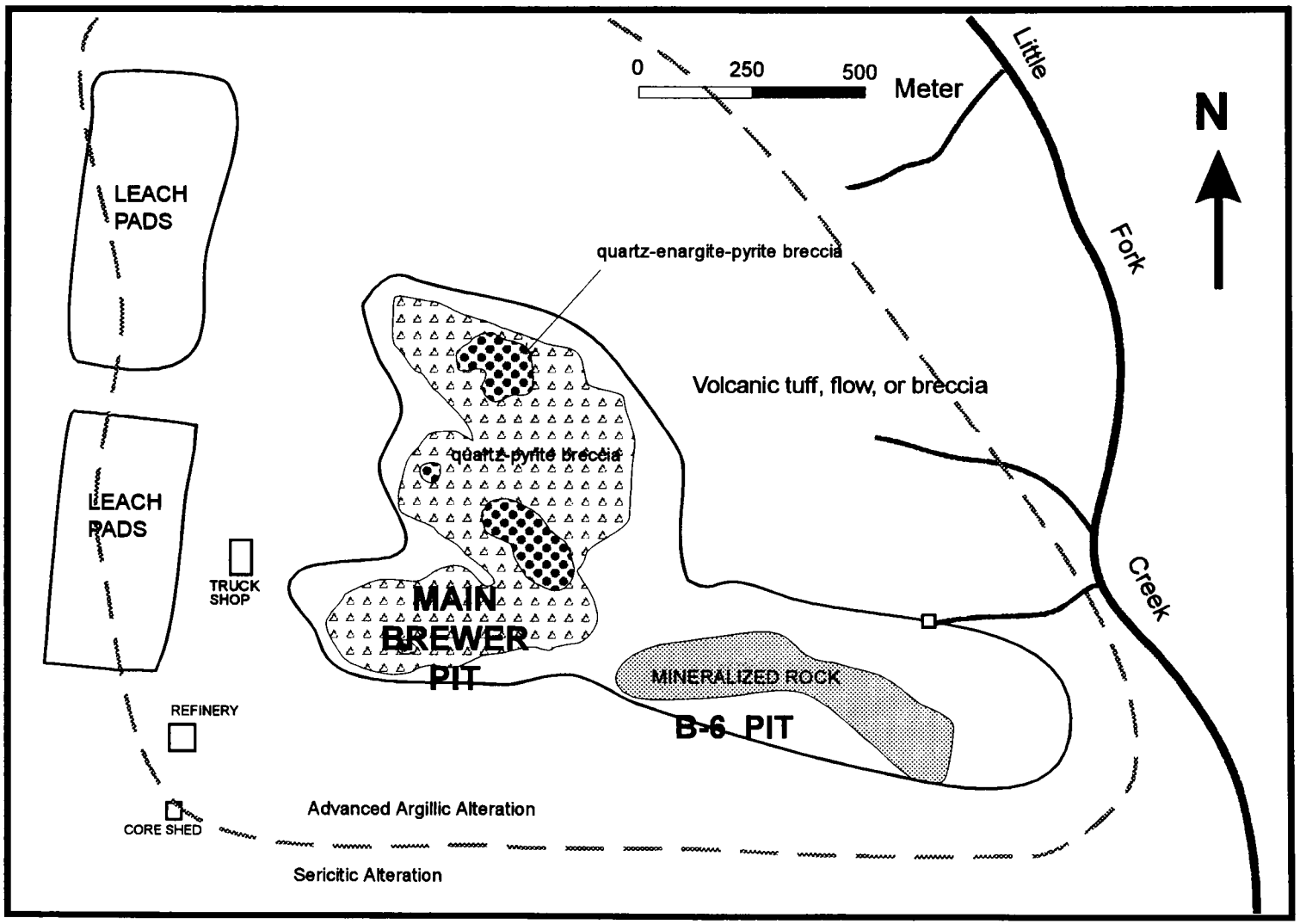

Figure 3. Geologic map of mineralized zone at the Brewer mine (modified after Scheetz, 1991).

amounts of enargite and chalcopyrite. Other accessory minerals observed are sphalerite, tetrahedrite, bismuthinite, ilmenite, galena, bornite, cinnabar, native sulfur, covellite, chalcanthite, and gold (Scheetz, 1991; Butler, 1985; Butler et al., 1988; Pardee and Park, 1948). The sulfide minerals commonly make up 2-3% or more of the matrix in the breccia The gold primarily occurs along grain boundaries associated with pyrite in the breccias and visible gold is also found in quartz-pyrite veins in the breccia zone (Scheetz, 1991). Two main ore bodies are in the mineralized zone: the main Brewer and the B-6 (Fig. 3). The main Brewer pit is mostly hydrothermal quartz-sulfide breccias and the B-6 pit is associated with alumina-bearing gossan and fracture controlled mineralization. The emplacement and localization of the orebodies appear to have been controlled by structures; the breccia pipes are often localized by the intersections of faults/fractures. Several episodes of brecciation and silicification are apparent within the orebody, but not all breccias have gold mineralization. The breccias at Brewer are probably hydromagmatic (hydrovolcanic) breccias based on general classification features listed by Sillitoe (1985). The characteristic in support of this interpretation include: (1) the presence of variable sized breccia pipes; (2) multiple stages of silicification and brecciation; (3) structural control on brecciation; and (4) silicification that is characterized by widespread occurrence of quartz as both pervasive replacement of, and cement to, breccia fragments. Quartz veins are abundant in the mineralized zone, ranging from tiny discontinuous vein to large vein that is controlled by fractures. In some quartz veins, pyrite, enargite, sericite, or pyrophyllite are present.

FLUID INCLUSIONS

Petrography of the Host Quartz

All fluid inclusions analyzed in this study are hosted by quartz crystals. Very few suitable fluid inclusions were observed in other minerals. Quartz in the Brewer Mine

occurs in four different forms: (a) as very fine-grained disseminations and aggregates in the breccia fragments; (b) as fine- to medium-grained clear crystals in the breccia, often with pyrite and enargite, probably as vug fillings; (c) as fine- to coarse-grained aggregates and discontinuous veins containing sulfide minerals in the breccia; and (d) as barren veins in both mineralized and unmineralized host volcanic rocks.

Fluid inclusions suitable for microthermometric analysis are present in all varieties of quartz, except in the very fine-grained quartz. Mineralized quartz veins are mostly within the breccia zone, often occurring as small, irregular, and discontinuous veins. A few mineralized quartz veins are up to several centimeters in thickness, and some contain euhedral pyrite. In the mineralized quartz veins and quartz aggregates, pyrite is the most abundant mineral; enargite is also abundant in some veins, especially in the pyrite-enargite breccia pipes. Minor sphalerite and covellite are present in some samples. Visible gold is also found in quartz-pyrite veins (Scheetz, 1991). Barren quartz veins are widespread in the mineralized breccia zone, hydrothermal alteration zones, and host volcanic rocks. The size and geometry of the veins vary greatly. Most of them seem to be controlled by either fractures or faults. Orientation of the veins is complex, particularly in or near the breccia zone (see Appendix E). The quartz veins seem to tread mostly NE-SW with dips to SE, although NW-SE stiking veins are quite common. The correlation of the veins with the regional structural trend, which is mostly NE-SW, is difficult, and the age relationship among the quartz veins remain ambiguous especially in and near the breccia zone. Most of the quartz veins are probably related to hydrothermal alteration. Although the quartz in the Brewer Mine is typically anhedral, some large, euhedral quartz crystals (up to 25 cm in length) were observed in a fracture zone. The varied morphology of the vein quartz in the Brewer area -- microcrystalline, breccia-fill, and aggregate -- is analogous to what has been considered by Dowling and Morrison (1988) to be typical of quartz veins formed in an epithermal environment.

Most of the fluid inclusions analyzed in this study were in the quartz from the mineralized zones; a few were from the surrounding hydrothermally altered rocks near the mineralized zone. One quartz vein sample was from the volcanoclastic unit which probably overlies the volcanic rock in the Brewer area.

Fluid Inclusion Types

The fluid inclusions occur in many different modes: randomly isolated, 3-D randomly distributed, and along microfractures (Figs. 4a-4k). Some microfractures are apparently sealed within the quartz gains, some cut into grains and cut across grain boundaries. Because of the lack of identifiable growth zones and, in some cases, grain boundaries, the primary versus secondary origin of the fluid inclusions along some fractures could not be established with confidence. The form of the inclusions varies from highly irregular to perfectly shaped negative crystals mirroring the geometry of host quartz. Large fluid inclusions, often isolated, tend to be irregular in form, whereas small inclusions, often along fractures, are commonly spheroidal or oblate in shape (Fig. 4-b). However, fluid inclusions large enough for microthermometric analysis (> 5 μm) are present in most samples. In some samples, fluid inclusions are extremely abundant and are relatively large in size. Overall, the fluid inclusions range from <2 to 30 μm in size with some up to 50 μm.

Some inclusions show necking-down phenomenon (Fig. 4j) and appear to have been decrepitated (Fig. 4i). Some are star-shaped, suggesting that the natural decrepitation was probably related to a subsequent thermal or deformation event. These types of inclusions were excluded from microthermometric analysis.

At room temperature (20 °C), most fluid inclusions consist of two phases (Figs. 4a, 4d, and 4j) although one-phase (Fig. 4e) and three-phased inclusion (Fig. 4c) are present in some samples. No daughter minerals were observed in the inclusions, except in

Fig. 4(a-k). Photomicrographs of the fluid inclusions. Scale bar is marked on each photograph.

(4a). Primary two-phase ($L+LCO_2$) fluid inclusions in quartz of breccia (BP-LV). Note the pyrite intergrowth. The inclusions have negative crystal forms and uniform phase ratios.

(4b). Primary and secondary inclusions (BPQ-4). Note the large primary two-phase ($L+LCO_2$) inclusions and the small one-phase aqueous (H_2O) inclusions along a microfracture.

(4c). A three-phase ($L+LCO_2+VCO_2$) inclusion in sample (BQ-1).

(4d). Primary inclusions in sample (BQ-24). Note the negative crystal forms.

(4e). CO_2-rich fluid inclusions in sample (BDH-61-893). Most of them appear to be one-phased liquid CO_2 in a sealed fracture.

(4f). Three-dimensionally distributed two-phase inclusions (BDH-96-70). Note the random distribution of the inclusions. The dark dots represent inclusions below the plane of focus.

(4g). A group of two-phased primary inclusions in hydrothermal quartz (BP-LV). Other tiny inclusions are mostly pseudosecondary, occurring in sealed fractures.

(4h). Secondary H_2O-rich inclusions (BPQ-X). Most of them are small and irregular in shape, containing a very small water bubble. They occur in a fracture zone.

(4i). Primary inclusions that were probably subjected to stress. Note the irregular shape and preferred orientation (BQ-1).

(4j). Primary two-phase ($L+LCO_2$) fluid inclusions in quartz occur as isolated inclusions and along a sealed fracture. The arrow points to an inclusion subjected to necking-down (BP-V).

(4k). Pseudosecondary CO_2-rich inclusions in a sealed fracture (BDH-96-70). Note the small (secondary) inclusions along the later fractures.

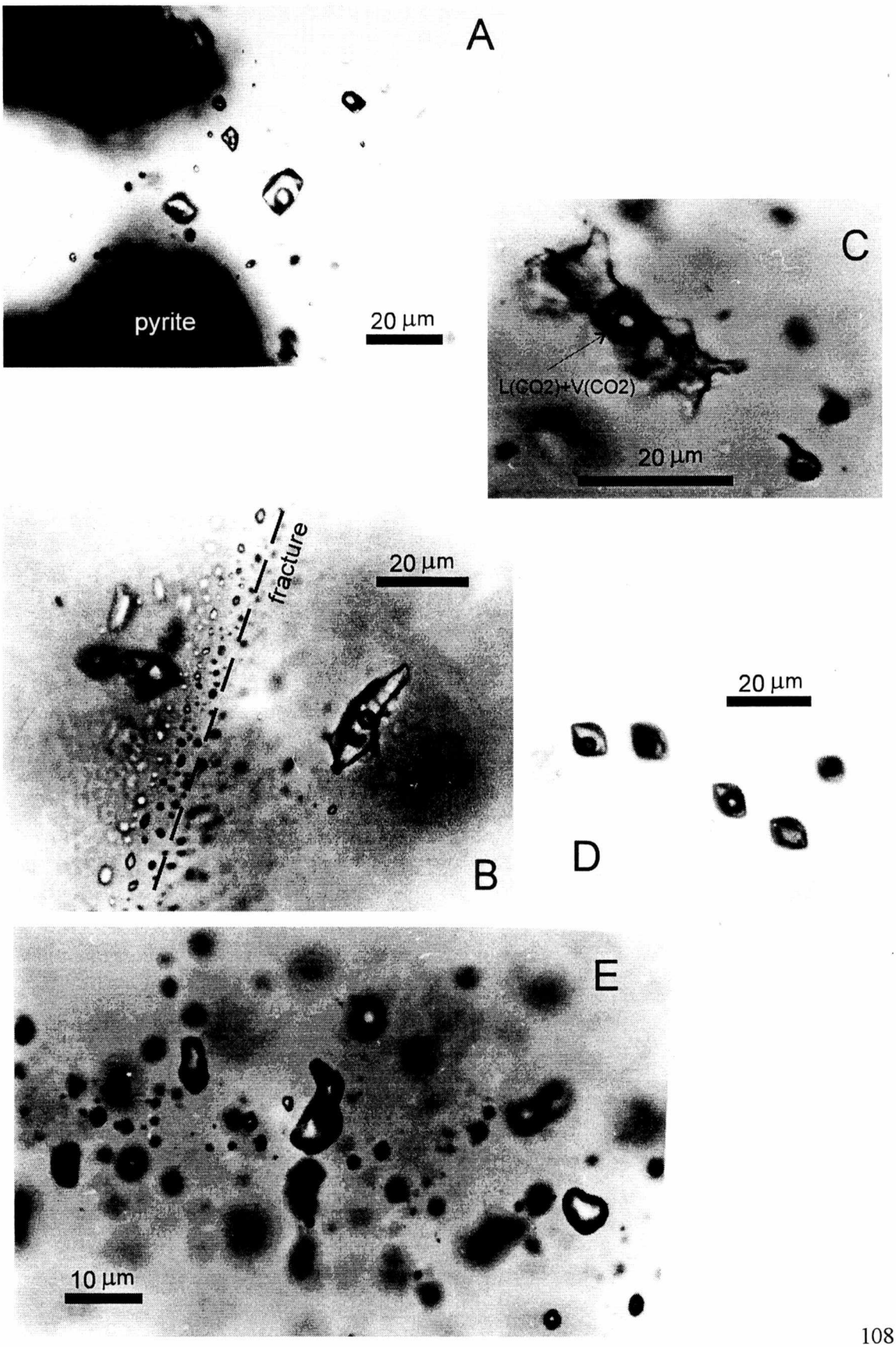
A
pyrite
20 μm
C
L(CO2)+V(CO2)
20 μm
fracture
20 μm
B
20 μm
D
E
10 μm

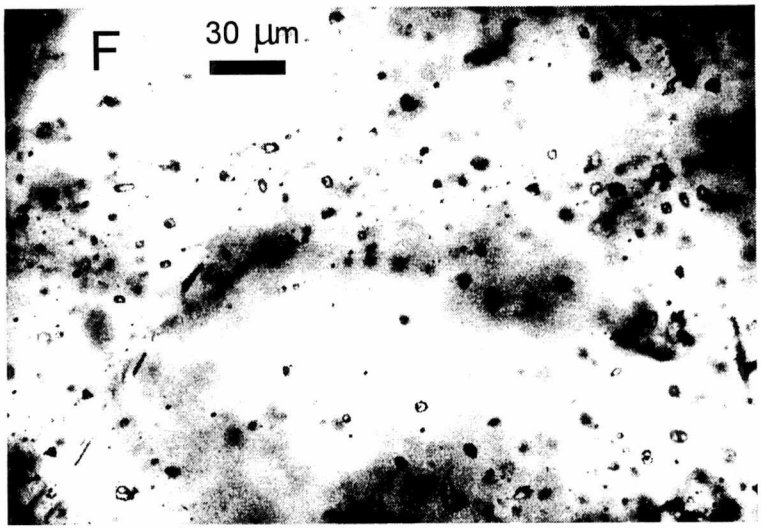
F
30 µm

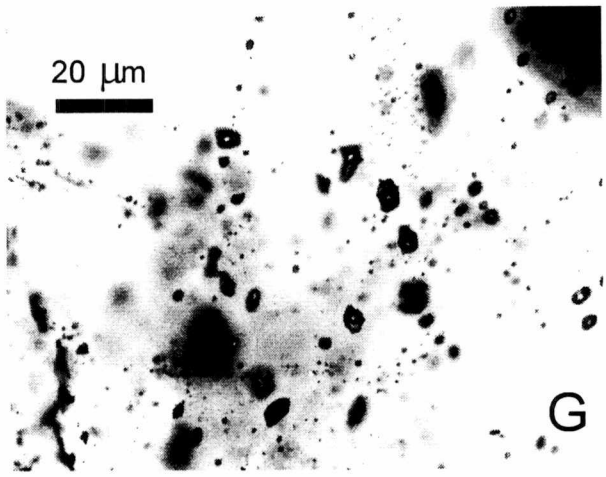
20 µm
G

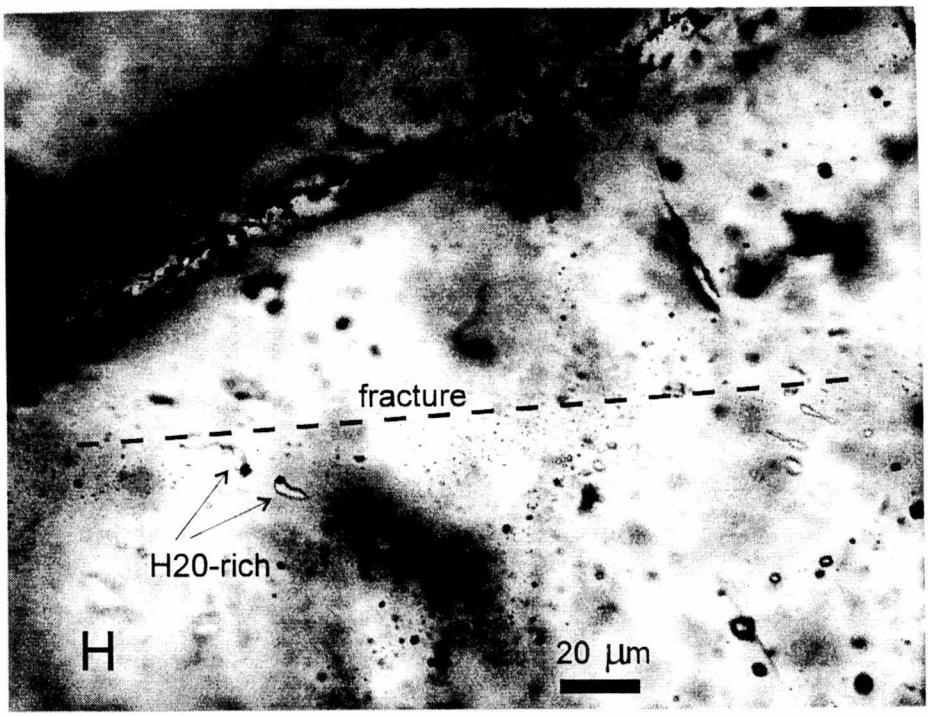
fracture
H20-rich
H
20 µm

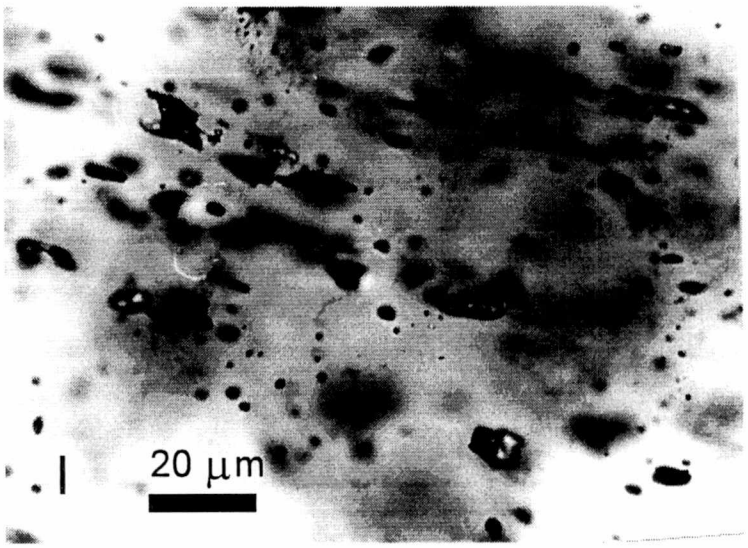
I
20 µm

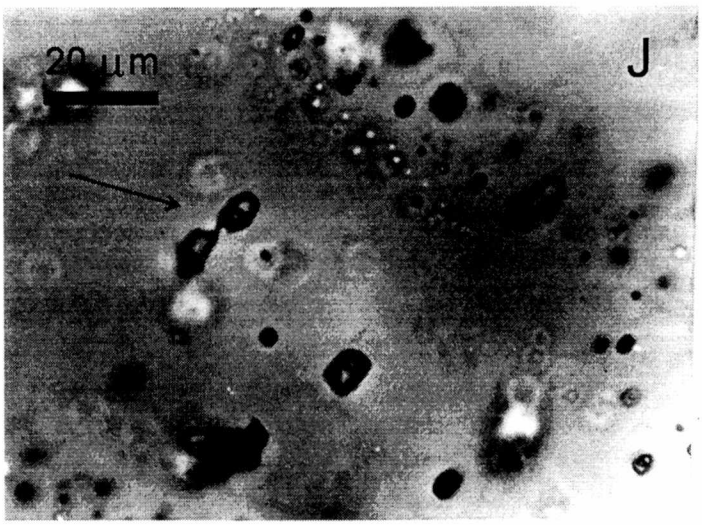
20 µm
J

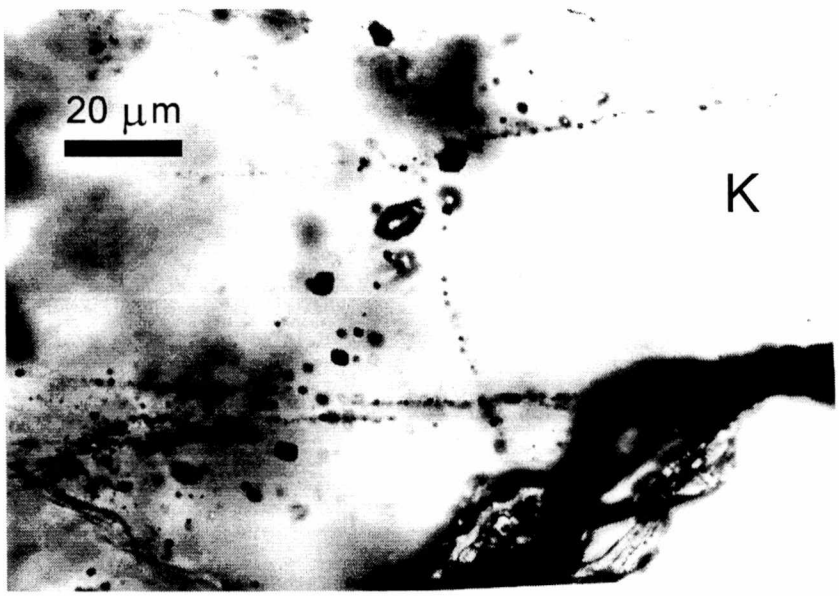
20 µm
K

one or two inclusions where solids phases, likely quartz and sulfide, are present probably due to incident trapping. Heating of three-phase inclusions showed phase transformations typical of H_2O-CO_2 inclusions, for example, the disappearance of CO_2 gas phase when heated by a hair dryer. Simple cooling by spraying acetone on the samples caused appearance of CO_2 gas bubble from the one or two-phased inclusions, indicating the presence of CO_2. Crushing test on the three-phase and the two-phase inclusions also confirmed the presence of CO_2.

Based on the present phases in the fluid inclusions at room temperature and their behavior during simple cooling and heating treatment, the fluid inclusions may be classified into three groups: CO_2-rich (Group 1); H_2O+CO_2 (Group 2); and H_2O-rich (group 3).

Group 1 (CO_2-rich) fluid inclusions are composed of either pure CO_2 or CO_2+H_2O with CO_2 greater than 50% in volume at room temperature (Fig. 4e and 4k). Most are either liquid CO_2 (LCO_2) or liquid CO_2 + liquid H_2O (LCO_2+LH_2O) at room temperature. Some of them appear to be liquid CO_2 + vapor CO_2 (LCO_2+VCO_2) with a small volume of the gas phase, whereas some are LCO_2+LH_2O+VCO_2 (Table 1). These inclusions are abundant mostly in the breccia zone, in the quartz of both the breccias and veins. Most of them appear to be in sealed fractures (Fig. 4k), although some also extend to the grain boundary. A few occur in randomly isolated mode. The inclusions vary in size from < 2 μm to 30 μm and in form from negative crystal to tabular and spheroidal shapes to irregular forms. Irregular shapes are very common for CO_2-rich inclusion. Most of group 1 inclusions are considered to be either primary or pseudosecondary according to criteria cited by Roedder (1984) and Shepherd et al. (1985) and were apparently trapped during the growth of the quartz crystals.

Some fluid inclusions appear to be pure liquid CO_2 (Fig. 4e), but may contain some amount of H_2O. CO_2 inclusions can contain up to 15 vol.% H_2O, but the H_2O may

not be obvious because the H_2O tends to adhere to the inclusion wall as a thin film and the CO_2 tends to form a thick dark rim (Kreulen, 1980; Oslen, 1988; Hollister, 1988, 1990; Craw, 1990). Most pure CO_2 inclusions from Brewer appear to have dark rims (fig. 4e).

Group 2 (H_2O+CO_2) inclusions are the most abundant in the Brewer samples. They appear to be either two-phase (LH_2O+LCO_2) (Fig. 4-a) or the typical three-phase (LH_2O+LCO_2+VCO_2) inclusions (Fig. 4c). CO_2 phases (LCO_2+VCO_2) occupy about 5-30% (mostly 10-20 %) of the inclusion volume. The VCO_2/LCO_2 ratio varies, but the CO_2 gas phase usually constitutes a small percentage of the CO_2 phase at room temperature. When slightly heated (<31°C), all three-phase inclusions become two-phase inclusions. The fluid inclusions mostly have forms from negative crystal to irregular. The inclusions occur in 3-D random and isolated modes as well as along fracture planes. 3-D random inclusions are particularly abundant in some grains (Fig. 4-f). Some inclusions concentrate in a zone without apparently fracture control. Most of the inclusions along the fractures appear to be sealed although some fractures seem to cut to grain boundary. Most inclusions of this group are primary or pseudosecodary; some may be secondary in origin although they could also be related to the same hydrothermal event.

Group 3 (H_2O-rich) fluid inclusions are either two-phase water and vapor (LH_2O+V) or one-phased water (LH_2O) inclusions at room temperature (Fig. 4h). Neither CO_2 nor clathrate was observed during cooling of the inclusions. The group 3 inclusions are generally small, mostly less than 5 μm, with a few up to 20 μm in size. The inclusions occur in many forms from spheriodal to irregular. The vapor phase usually occupies a small percentage of the inclusion volume, typically less than 5% and mostly about 2%. Most of the inclusions lie along well-defined fractures and the fractures often crosscut the other two group inclusions. Group 3 inclusions are most likely secondary in origin. These inclusions, common in the breccia zone, may represent a later hydrothermal fluid.

Some generalization are possible about the fluid inclusion types and their abundance. The quartz samples from the mineralized breccia zone have relatively abundant, large inclusions; most of the barren quartz veins have smaller inclusions. One sample from the deeper part of the system has mostly CO_2-rich inclusions. However, the fluid inclusions in the samples from the main pit and the B-6 pit are similar in type and mode of occurrence, suggesting that the two ore zones may belong to a single system. Although a sample may contain inclusions belonging to more than one of the three groups, each group usually has its own characteristic pattern. In most samples, the inclusions occurring along a fracture or concentrated in an area belong to be the same type and show fairly uniform H_2O:CO_2 phase ratio, although there are some exceptions.

Microthermometric Analysis

Microthermometric analysis of fluid inclusions was performed with a Fluid Inc. version of the USGS Gas Flow Heating/Freezing System at the Fluid Inclusion Laboratory of the Department of Geological Sciences, the University of Tennessee. The system was calibrated using synthetic fluid inclusions of pure H_2O and H_2O+CO_2 with 25% CO_2. Temperature measurements with the equipment is reproducible to better than $\pm$0.2 °C between -56.6 and 0 °C and within $\pm$1 °C up to 370 °C. various heating and cooling rates were used in the measurements, but invariably a very slow rate was used near the homogenization and other phase changes to record the temperature accurately. Repeated measurements on the same inclusion was performed on most inclusions. To avoid decrepitation of CO_2-bearing inclusions during heating, freezing runs preceded heating runs. Although primary and pseudosecondary inclusions, considered to be related to the hydrothermal event, were the main target of this study, some secondary inclusions were also analyzed for possible useful information. The results of microthermometric analysis are summarized in Table 1.

Table 1. Summary of microthermometric analysis data of fluid inclusions

Sample #	Inclusion phases & types				Microthermometric Data					
	Inclusion type	Number	CO_2 or vapor %		Tm-CO_2		Te		Tm-ice	
			Range	Ave.	Range	Ave.	Range	Ave.	Range	Ave.
BDH-61-893 -- quartz in deep porphyry-like rock										
	Lc	6			-56 - -55.8	-56.0				
	Lc+Vc	3			-56.0	-56.0				
	Lc+L	3	60 - 80	70	-55.7	-55.7				
	L+Lc	16	5 - 40	18	-55.7 - -60.0	-56.9	-35.0	-35.0	-0.6 - -5.0	-2.2
	L+Lc+Vc	1	10							
BP-B1 -- quartz in breccia										
	Lc+L	4	60 - 80	70						
	Lc+L+Vc	1	70	70						
	L+Lc	5	5 - 15	10						
QV-E -- quartz in breccia from BP										
	Lc+L	1	60							
	L+Lc+Vc	4	10	10						
BPQ-X -- quartz in breccia										
	Lc+L	8	60 - 80	70	-57.8 - -56	-57.0				
	L+Lc+Vc	17	5 - 30	15	57.0	57.0				
	L+V	11	0-2	2			-30 - -31	-30.2	-11.0 - -3.0	-6.8
BPQ-4 -- small quartz vein in breccia										
	Lc	3								
	L+Lc	1	10				-30.0		-5.1	
	L+Lc+Vc	6	10 - 20	11			25.0 - -28.0	26.0		
	L+V	1	10				-26.0			
BPQ-7 -- small quartz vein in breccia										
	L+Lc	2	5 - 20	13						
	L+Lc+Vc	10	10	20	-55.0	-55.0	-28.0	-28.0	-11.2 - -3.0	-7.1
	L+V	3	2 - 5	4						
BPQ-SV -small mineralized vein in breccia										
	L+Lc+Vc	8	10 - 15	13			-25.0	-25.0	-5.0 - -4.2	-4.2
	L+V	2	5 - 7	6			-30.0	-30.0	-3.5 - -1.3	-2.4
BP-LV -- mineralized quartz vein in breccia										
	L+Lc	8	10 - 40	17	-56.7 - -58.9	-57.8				
	L+Lc+Vc	6	25	18	-57.6		-31.0 - -30.0	-30.0	-8.8 - -6.0	-7.5
	L+V	1	5	5			-26.0	-26.0	-1.1	-1.1
BPV -- quartz in quartz-andalusite-pyrite rock										
	L+Lc	4	5 - 40	16			-24.0	-24.0		
	L+Lc+Vc	11	10 - 30	16	-56.0 - -56.1	-56.0	-26.0 - -30.0	-27.5	-13.7 - -1.2	-7.6
BQ-36 -- quartz vein in breccia										
	Lc+Vc	3	10 - 15	13.0						
	L+Lc	19	7 - 35	21	-57.0	-57.0				
	L+Lc+Vc	3	15 - 20	19	57.0	57.0	-30.0	-30.0	-0.5	-0.5
	L+V	2	10	10			-30.0	-30.0	-0.7 - -2.4	-1.5
BQ-45 -- quartz vein in breccia										
	Lc	1			-57.0					
	Lc+L	2	60 - 70	65	-56.6	-56.6				
	Lc+L+Vc	1	60		-57.0					
	L+Lc	10	15 - 30	24					-0.2	-0.2
	L+Lc+Vc	1	30		-57.0					
BQ-43 -- quartz vein in breccia										
	L+Lc	5	5 - 40	22						
	L+Lc+Vc	1	20	20						
BNQ-19 -- quartz vein in andalusite-bearing rock										
	Lc+L	3	60 - 80	74	-57.0	-57.0	-30.0	-30.0	-8.5	-8.5
	L+Lc	15	10 - 40	19	-57.0	-57.0	30.0 - 33.0	-32.0	-10.1 - -1.0	-7.0
	L+Lc+Vc	1	10				-30.0		-8.5	
	L+V	1	15						-8.0	

Table 1 (continued)

Sample #	Microthermometric Data							
Inclusion type	Tm-clath		$Th\text{-}CO_2$		Th		Td	
	Range	Ave.	Range	Ave.	Range	Ave.	Range	Ave.
BDH-61-893 -- quartz in deep porphyry-like rock								
Lc			-3.2 - 4.5	0.2				
Lc+Vc			23.0 - 24.0	23.7				
Lc+L			4.4 - 4.6	4.5	232.0	232.0		
L+Lc	1.1 - 8.0	4.60	1.0 - 14.0	5.23	198.3 - 242.0	219.70	302.0	302.0
L+Lc+Vc					195.6			
BP-B1 -- quartz in breccia								
Lc+L					280.0 - 290.2	284.6		
Lc+L+Vc			30.9		288.0			
L+Lc					205.0 - 220.0	208.7		
QV-E -- quartz in breccia from BP								
Lc+L							250.2	
L+Lc+Vc			28.4 - 30.0	29.4			295.1 - 337.6	324.8
BPQ-X -- quartz in breccia								
Lc+L			4.8 - 11.7	8.7	226.0 - 249.2	244.2	257.0 - 271.9	264.5
L+Lc+Vc			22.7 - 28.7	25.4	227.0 - 245.0	234.4	195.0 - 245.0	223.8
L+V					106.0 - 110.4	107.7		
BPQ-4 -- small quartz vein in breccia								
Lc			13.6 - 14.1	13.9				
L+Lc	8.0		18.1					
L+Lc+Vc	1.5	1.5	21.0 - 30.0	25.3				
L+V								
BPQ-7 -- small quartz vein in breccia								
L+Lc					226.2	226.2	187.4	187.4
L+Lc+Vc	6.1 - 8.0	7.3	21.0 - 29.8	24.4	213.7 - 271.0	236.7	206.3 - 270.0	235.4
L+V					108.0 - 141.7	122.2		
BPQ-SV -small mineralized vein in breccia								
L+Lc+Vc	3.1 - 8.6	4.4	24.0 - 27.0	25.1	193.0 - 242.9	209.7		
L+V					165.0	165.0		
BP-LV -- mineralized quartz vein in breccia								
L+Lc	4.0 - 6.0	5.0	10.2 - 18.6	14.4	197.0 - 308.0	252.5		
L+Lc+Vc	4.0 - 6.1	5.2	26.0 - 30.0	27.0	192.0 - 224.9	202.7	196.7 - 255.0	216.2
L+V					151.0	151.0		
BPV -- quartz in quartz-andalusite-pyrite rock								
L+Lc	1.1	1.1			271.0	271.0	245.0 - 288.8	272.0
L+Lc+Vc	2.9 - 6.0	4.5	25.2 - 30.9	28.6	223.4 - 280.0	245.8	245.0 - 277.0	263.0
BQ-36 -- quartz vein in breccia								
Lc+Vc			26.7 - 29.0	28.0				
L+Lc			20.0	20.0	185.0 - 262.4	225.4	223.6 - 250	231.9
L+Lc+Vc					225.1 - 242.5	235.4		
L+V					190.0	190.0		
BQ-45 -- quartz vein in breccia								
Lc			17.4					
Lc+L					320.0	320.0		
Lc+L+Vc			29.6					
L+Lc					184.0 - 314.6	268.9	280.0 - 300.0	290.0
L+Lc+Vc			25.6					
BQ-43 -- quartz vein in breccia								
L+Lc			1.8 - 2.0	2.0	150.0 - 326.2	246.4		
L+Lc+Vc	9.9		30.9		242.5			
BNQ-19 -- quartz vein in andalusite-bearing rock								
Lc+L			10.0 - 12.0	11.0	270.0	270.0		
L+Lc					208.6 - 326.7	259.0	226.6 - 300.0	262.0
L+Lc+Vc	4.3				301.8			
L+V								

Table 1 (continued)

Sample #	Geochemical data							
Inclusion type	$X(H_2O)$		$X(CO_2)$		X(NaCl)		Density (CO_2)	
	Range	Ave.	Range	Ave.	Range	Ave.	Range	Ave.
BDH-61-893 -- quartz in deep porphyry-like rock								
Lc			1.000	1.000			0.900 - 0.946	0.927
Lc+Vc			1.000	1.000			0.726 - 0.739	0.730
Lc+L	0.404 - 0.537	0.471	0.463 - 0.596	0.530			0.899 - 0.901	0.900
L+Lc	0.803 - 0.931	0.880	0.057 - 0.197	0.120	0.012	0.012	0.831 - 0.922	0.890
L+Lc+Vc								
BP-B1 -- quartz in breccia								
Lc+L								
Lc+L+Vc	0.661		0.339				0.532	
L+Lc								
QV-E -- quartz in breccia from BP								
Lc+L								
L+Lc+Vc	0.714 - 0.974	0.908	0.026 - 0.286	0.092			0.586 - 0.647	0.615
BPQ-X -- quartz in breccia								
Lc+L	0.547 - 0.657	0.616	0.343 - 0.453	0.384			0.849 - 0.898	0.870
L+Lc+Vc	0.885 - 0.984	0.950	0.016 - 0.115	0.049			0.639 - 0.743	0.701
L+V					0.015 - 0.052	0.030		
BPQ-4 -- small quartz vein in breccia								
Lc							0.830 - 0.834	0.831
L+Lc	0.953		0.035		0.012		0.794	
L+Lc+Vc	0.942	0.942	0.058	0.058			0.596 - 0.763	0.696
L+V								
BPQ-7 -- small quartz vein in breccia								
L+Lc								
L+Lc+Vc	0.886 - 0.955	0.924	0.032 - 0.114	0.070	0.012 - 0.023	0.016	0.604 - 0.763	0.715
L+V								
BPQ-SV -small mineralized vein in breccia								
L+Lc+Vc	0.913 - 0.961	0.927	0.030 - 0.050	0.042	0.008 - 0.038	0.031	0.677 - 0.726	0.709
L+V								
BP-LV -- mineralized quartz vein in breccia								
L+Lc	0.803 - 0.908	0.856	0.058 - 0.177	0.118	0.020 - 0.033	0.027	0.789 - 0.860	0.825
L+Lc+Vc	0.881 - 0.954	0.909	0.013 - 0.088	0.064	0.022 - 0.034	0.028	0.596 - 0.696	0.672
L+V								
BPV -- quartz in quartz-andalusite-pyrite rock								
L+Lc								
L+Lc+Vc	0.863 - 0.977	0.940	0.023 - 0.091	0.047	0.006 - 0.046	0.026	0.513 - 0.709	0.620
BQ-36 -- quartz vein in breccia								
Lc+Vc			1.000	1.000			0.631 - 0.683	0.654
L+Lc	0.904	0.904	0.096	0.096			0.774	0.774
L+Lc+Vc								
L+V								
BQ-45 -- quartz vein in breccia								
Lc							0.800	
Lc+L								
Lc+L+Vc	0.725		0.275				0.611	
L+Lc								
L+Lc+Vc	0.890		0.110				0.702	
BQ-43 -- quartz vein in breccia								
L+Lc	0.861 - 0.973	0.936	0.027 - 0.139	0.064			0.916 - 0.917	0.916
L+Lc+Vc	0.947		0.052		0.001		0.532	
BNQ-19 -- quartz vein in andalusite-bearing rock								
Lc+L	0.417 - 0.654	0.536	0.346 - 0.583	0.465			0.847 - 0.862	0.855
L+Lc								
L+Lc+Vc								
L+V								

Table 1 (continued)

Sample #	Geochemical data					
Inclusion type	Density (aq.)		Density (bulk)		wt% NaCl equiv.	
	Range	Ave.	Range	Ave.	Range	Ave.
BDH-61-893 -- quartz in deep porphyry-like rock						
Lc	0.900 - 0.946	0.927	0.900 - 0.946	0.927		
Lc+Vc	0.726 - 0.739	0.730	0.726 - 0.739	0.730		
Lc+L			0.919 - 0.930	0.925		
L+Lc	1.022	1.022	0.958 - 0.994	0.980	0.99 - 3.95	2.20
L+Lc+Vc						
BP-B1 -- quartz in breccia						
Lc+L						
Lc+L+Vc			0.670			
L+Lc						
QV-E -- quartz in breccia from BP						
Lc+L						
L+Lc+Vc			0.785 - 0.956	0.912		
BPQ-X -- quartz in breccia						
Lc+L			0.904 - 0.938	0.917		
L+Lc+Vc			0.908 - 0.979	0.948		
L+V			0.981 - 1.044	1.010	4.86 - 14.98	9.91
BPQ-4 -- small quartz vein in breccia						
Lc						
L+Lc	1.022		0.999		3.95	
L+Lc+Vc			0.916	0.916		
L+V						
BPQ-7 -- small quartz vein in breccia						
L+Lc						
L+Lc+Vc	1.019 - 1.048	1.029	0.912 - 1.016	0.950	3.95 - 7.31	5.17
L+V						
BPQ-SV -small mineralized vein in breccia						
L+Lc+Vc	0.677 - 1.076	0.792	0.040 - 1.021	0.814	2.77 - 11.74	9.66
L+V					2.14 - 5.62	3.88
BP-LV -- mineralized quartz vein in breccia						
L+Lc	1.051 - 1.075	1.063	0.946 - 1.043	0.995	7.48 - 10.58	9.03
L+Lc+Vc	1.047 - 1.069	1.058	0.969 - 10.45	0.988	7.31 - 10.47	8.96
L+V					1.82	1.82
BPV -- quartz in quartz-andalusite-pyrite rock						
L+Lc						
L+Lc+Vc	1.005 - 1.103	1.054	0.928 - 1.018	0.962	1.98 - 14.77	8.33
BQ-36 -- quartz vein in breccia						
Lc+Vc			0.631 - 0.683	0.654		
L+Lc			0.942	0.942		
L+Lc+Vc					0.83	0.83
L+V					1.16 - 3.92	2.54
BQ-45 -- quartz vein in breccia						
Lc						
Lc+L						
Lc+L+Vc			0.764			
L+Lc						
L+Lc+Vc			0.905			
BQ-43 -- quartz vein in breccia						
L+Lc			0.973 - 0.974	0.973		
L+Lc+Vc	0.989		0.898		0.22	
BNQ-19 -- quartz vein in andalusite-bearing rock						
Lc+L			0.876 - 0.946	0.896		
L+Lc					1.65 - 14.05	9.00
L+Lc+Vc					12.29	
L+V					11.70	

Table 1 (continued)

Sample #	Inclusion phases & types				Microthermometric Data					
	Inclusion type	Number	CO_2 or vapor %		$Tm\text{-}CO_2$		Te		Tm-ice	
			Range	Averag	Range	Averag	Range	Averag	Range	Average
BDH-121-X -- quartz in massive pyrite										
	L+Lc	10	10 - 25	16	-57.0	-57.0	-25.0 - -28.0	-27.0	-0.1 - -2.8	-1.5
	L+Lc+Vc	7	10 - 20	16	-54.6	-54.6	-30.0	-30.0	-3.6	-3.6
	L+V	1	10	10			-28.0	-28.0		
BQ-5 -- quartz in breccia										
	Lc+Vc	1	25		-55.7	-55.7				
	L+Lc	1	10				-30.0	-30.0		
	L+Lc+Vc	2	10 - 15	13						
	L+V	8	5 - 10	6			-30.0 - -25.0	-27.3	-6.0 - 0.0	-1.8
BQ-1 -- quartz vein in altered volcanic rock										
	Lc+L	2	50 - 60	55						
	L+Lc	8	15 - 40	21						
	L+Lc+Vc	1	15	15						
BQ-30 -- quartz vein in altered volcanic rock										
	L+Lc	6	5 - 30	18						
BQ-24 -- quartz vein in B-6 area										
	L+Lc	7	10 - 40	24						
	L+Lc+Vc	13	10 - 25	18	-55.0 - 54.0	-54.8	-32.0 - 22.0	-26.5	- 6.0 - -3.5	-4.8
BQ-6 -- quartz vein in B-6 altered volcanic rock										
	L+Lc	5	10 - 15	11						
BQ-9(S) -- pyrite-quartz vein in B-6 area										
	L+Lc	12	15 - 30	20						
	L+Lc+Vc	3	15 - 20	18						
BDH-96-45 -- quartz vein in volcanic rock										
	L+Lc	4	15 - 20	19						
	L+Lc+Vc	3	5 - 20	12						
	L+V	2	5	5						
BDH-96-70 -- quartz in pyrite-als rock										
	L+Lc	4	10 - 20	14						
BDH-96-160 -- quartz vein in breccia										
	L+Lc	6	5 - 15	12						
BDH-96-226 -- vein in pyritic silicified rock										
	L+Lc+Vc	8	10 - 25	19	-55.6 - -55.9	-55.8			-5.7 - -2.9	-4.4
QV -- quartz vein in B-6										
	L+Lc+Vc	3	25	25						
BDH-96-117(b) -- quartz vein in B-6 breccia										
	L+V	5	5 - 10	7			-26.0 - 25.0	-25.6	-5.1 - -4.5	-4.8
BS-10 -- quartz vein in volcaniclastic rock (clay pit)										
	L+Lc	10	10 - 15	11						
	L+V	3	10 - 15	12			-28 - -30	-28.7	-5.3 - -7.0	-6.0

Abbreviation:

Phases: Lc - liquid CO_2; Vc - vapor CO_2; L - liquid H_2O, V - vapor H_2O

Temperatures: $Tm\text{-}CO_2$ - CO_2 melting; Te - ice melting; Tm-ice - last ice melting; $Th\text{-}CO_2$ - CO_2 homogenization; Th - total homogenization; Td - decrepitation

Table 1 (continued)

Sample #	Microthermometric Data							
Inclusion type	Tm-clath		Th-CO_2		Th		Td	
	Range	Averag	Range	Averag	Range	Averag	Range	Average
BDH-121-X -- quartz in massive pyrite								
L+Lc	6.5 - 10.0	8.9	15.0 - 19.1	16.4	220.0 - 243.2	235.5	322.0	322.0
L+Lc+Vc	8.5 - 10.0	9.1	30.0 - 30.9	30.4	210.0 - 233.9	220.6		
L+V								
BQ-5 -- quartz in breccia								
Lc+Vc			28.5	28.5				
L+Lc	6.0	6.0			194.5	194.5		
L+Lc+Vc			29.0	29.0			249.0	249.0
L+V					126.9 - 201.6	184.4		
BQ-1 -- quartz vein in altered volcanic rock								
Lc+L					314.2 - 319.4	316.8		
L+Lc					209.2 - 270.1	238.9		
L+Lc+Vc							323.0	323.0
BQ-30 -- quartz vein in altered volcanic rock								
L+Lc					190.0 - 249.3	227.9	267.0 - 271.0	269.0
BQ-24 -- quartz vein in B-6 area								
L+Lc					220.0 - 235.0	227.8	230.0	230.0
L+Lc+Vc	5.0 - 10.0	7.6	29.0 - 29.6	29.5	156.0 - 236.0	215.1		
BQ-6 -- quartz vein in B-6 altered volcanic rock								
L+Lc					188. - 222.7	199.7	223.0	223.0
BQ-9(S) -- pyrite-quartz vein in B-6 area								
L+Lc					227.1 - 288.0	256.1	300.0	300.0
L+Lc+Vc					225.0 - 253.2	235.8		
BDH-96-45 -- quartz vein in volcanic rock								
L+Lc					204.0 - 206.4	204.9		
L+Lc+Vc					189.5 - 208.8	201.3		
L+V					180.0 - 198.1	189.0		
BDH-96-70 -- quartz in pyrite-als rock								
L+Lc					286.5 - 297.9	292.3		
BDH-96-160 -- quartz vein in breccia								
L+Lc					199.9 - 229.4	219.7		
BDH-96-226 -- vein in pyritic silicified rock								
L+Lc+Vc	7.2 - 8.2	8.0	27.8 - 29.5	28.8	240.1 - 264.9	251.7	240.1 - 278.3	265.5
QV -- quartz vein in B-6								
L+Lc+Vc			28.4	28.4	313.0	313.0	311.0	311.0
BDH-96-117(b) -- quartz vein in B-6 breccia								
L+V					110.6 - 266.4	190.7		
BS-10 -- quartz vein in volcaniclastic rock (clay pit)								
L+Lc					169.0 - 214.0	188.5		
L+V					170.0	170.0		

Abbreviation:

Phases: Lc - liquid CO_2; Vc - vapor CO_2; L - liquid H_2O, V - vapor H_2O

Temperatures: Tm-CO_2 - CO_2 melting; Te - ice melting; Tm-ice - last ice melting; Th-CO_2 - CO_2 homogenization; Th - total homogenization; Td - decrepitation

Table 1 (continued)

Sample #	Geochemical data							
Inclusion type	$X(H_2O)$		$X(CO_2)$		X(NaCl)		Density (CO_2)	
	Range	Averag	Range	Averag	Range	Averag	Range	Average
BDH-121-X -- quartz in massive pyrite								
L+Lc	0.906 - 0.961	0.929	0.036 - 0.078	0.063	0.001 - 0.020	0.008	0.783 - 0.822	0.809
L+Lc+Vc	0.933 - 0.975	0.957	0.025 - 0.058	0.040	0.008 - 0.009	0.009	0.513 - 0.596	0.572
L+V								
BQ-5 -- quartz in breccia								
Lc+Vc							0.644	0.644
L+Lc								
L+Lc+Vc	0.956 - 0.972	0.964	0.028 - 0.044	0.036			0.631	0.631
L+V	9.970 - 0.990	0.982			0.010 - 0.030	0.018		
BQ-1 -- quartz vein in altered volcanic rock								
Lc+L								
L+Lc								
L+Lc+Vc								
BQ-30 -- quartz vein in altered volcanic rock								
L+Lc								
BQ-24 -- quartz vein in B-6 area								
L+Lc								
L+Lc+Vc	0.911 - 0.957	0.939	0.043 - 0.061	0.055	0.000 - 0.028	0.014	0.612 - 0.631	0.617
BQ-6 -- quartz vein in B-6 altered volcanic rock								
L+Lc								
BQ-9(S) -- pyrite-quartz vein in B-6 area								
L+Lc								
L+Lc+Vc								
BDH-96-45 -- quartz vein in volcanic rock								
L+Lc								
L+Lc+Vc								
L+V								
BDH-96-70 -- quartz in pyrite-als rock								
L+Lc								
BDH-96-160 -- quartz vein in breccia								
L+Lc								
BDH-96-226 -- vein in pyritic silicified rock								
L+Lc+Vc	0.930 - 0.960	0.926	0.028 - 0.081	0.062	0.010 - 0.016	0.012	0.615 - 0.661	0.635
QV -- quartz vein in B-6								
L+Lc+Vc	0.919	0.919	0.081	0.081			0.647	0.650
BDH-96-117(b) -- quartz vein in B-6 breccia								
L+V								
BS-10 -- quartz vein in volcaniclastic rock (clay pit)								
L+Lc								
L+V								

Abbreviation:

Phases: Lc - liquid CO_2; Vc - vapor CO_2; L - liquid H_2O, V - vapor H_2O

Temperatures: Tm-CO_2 - CO_2 melting; Te - ice melting; Tm-ice - last ice melting; Th-CO_2 - CO_2 homogenization; Th - total homogenization; Td - decrepitation

Table 1 (continued)

Sample #	Geochemical data					
Inclusion type	Density (aq.)		Density (bulk)		wt% NaCl equiv.	
	Range	Average	Range	Average	Range	Average
BDH-121-X -- quartz in massive pyrite						
L+Lc	0.991 - 1.043	1.011	0.957 - 0.992	0.977	0.17 - 6.63	2.61
L+Lc+Vc	1.009 - 1.012	1.011	0.899 - 0.955		2.60 - 3.00	2.84
L+V						
BQ-5 -- quartz in breccia						
Lc+Vc						
L+Lc						
L+Lc+Vc			0.938 - 0.956	0.947		
L+V			0.904 - 0.941	0.920	3.28 - 9.19	5.78
BQ-1 -- quartz vein in altered volcanic rock						
Lc+L						
L+Lc						
L+Lc+Vc						
BQ-30 -- quartz vein in altered volcanic rock						
L+Lc						
BQ-24 -- quartz vein in B-6 area						
L+Lc						
L+Lc+Vc	0.988 - 1.055	1.021	0.913 - 0.970	0.934	0.02 - 8.97	5.51
BQ-6 -- quartz vein in B-6 altered volcanic rock						
L+Lc						
BQ-9(S) -- pyrite-quartz vein in B-6 area						
L+Lc						
L+Lc+Vc						
BDH-96-45 -- quartz vein in volcanic rock						
L+Lc						
L+Lc+Vc						
L+V						
BDH-96-70 -- quartz in pyrite-als rock						
L+Lc						
BDH-96-160 -- quartz vein in breccia						
L+Lc						
BDH-96-226 -- vein in pyritic silicified rock						
L+Lc+Vc	1.016 - 1.031	0.100	0.919 - 0.981	0.943	3.57 - 5.41	4.04
QV -- quartz vein in B-6						
L+Lc+Vc			0.909	0.910		
BDH-96-117(b) -- quartz vein in B-6 breccia						
L+V					7.10 - 7.96	7.53
BS-10 -- quartz vein in volcaniclastic rock (clay pit)						
L+Lc						
L+V					8.24 - 10.48	9.17

Abbreviation:

Phases: Lc - liquid CO_2; Vc - vapor CO_2; L - liquid H_2O, V - vapor H_2O

Temperatures: Tm-CO_2 - CO_2 melting; Te - ice melting; Tm-ice - last ice melting; Th-CO_2 - CO_2 homogenization; Th - total homogenization; Td - decrepitation

Freezing

The fluid inclusions from the Brewer Mine exhibited complex phase changes during freezing. The CO_2-bearing inclusions often developed as many as five phases on freezing: aqueous liquid, ice, gas hydrates, solid CO_2, CO_2-rich liquid, and CO_2-rich vapor. For these inclusions, it was possible to measure several temperatures -- CO_2 melting (Tm-CO_2), ice eutectic (Te), final ice-melting (Tm-ice), clathrate melting (Tm-clath), and CO_2 homogenization (TCO_2) -- although not all of these in every inclusion.

In order to detect and freeze all the CO_2 phases, the inclusions were cooled below -100 °C. During the freezing, two apparent phase transitions could be observed in most inclusions: the freezing of aqueous phases and the freezing of CO_2 phases. The temperatures of the freezing of aqueous phases ranged from -30 to -50 °C and those of the freezing of liquid CO_2 ranged from -70 to -100 °C. The freezing temperatures could not be determined more precisely because of the relatively fast cooling rate and the overcooling commonly associated with the cooling process. Various phase-change temperatures were measured by slow heating of the frozen inclusions.

Solid CO_2 melting temperatures (Tm-CO_2) -- Temperatures of solid CO_2 melting, measurable in most group 1 and group 2 inclusions, are between -60 and -54 °C, and mostly around -56 to -57 °C (Fig. 5-a). The temperatures are very close to the pure solid CO_2 melting temperature of -56.7 °C, indicating the lack of significant amounts of CH_4 or N_2 (Burruss, 1981).

Eutectic temperatures (Te) -- Eutectic temperature, the temperature at which ice starts to melt, is usually difficult to measure. It is often underestimated because of the poor optics of the fluid inclusions and the prior presence of liquid CO_2 in the CO_2-bearing inclusions. Most of the Te measurements are from group 2 and group 3 inclusions, although a few are also from group 1 inclusions. Te ranges from -35 to -23 °C (Fig. 6-a)

and lies in the range expected for a Na, K, Mg, and Ca-bearing chloride salt-water solution (Shephred et al., 1985).

Last ice-melting temperatures (Tm-ice) -- The last ice-melting temperatures, measured mostly in group 3 and in some group 2 inclusions, range from -13.7 to -0.1 °C, with majority of the values being greater than -6 °C (Fig. 6-b). Despite similar ranges, the group 2 inclusions appear to have relatively lower Tm-ice than the group 3 inclusions. Overall, the last ice-melting temperatures indicate relatively low fluid salinities for the Brewer system.

Clathrate melting temperatures (Tm-clath) -- Temperatures of clathrate ($CO_2.5 3/4 H_2O$) melting range from 1.1 to 10.0 °C (Fig. 5-b), with the majority being greater than 6 °C. Because the clathrate can lock up some amount of water, the final ice melting temperatures would be lower in the presence of clathrate (Collins, 1979). The clathrate melting temperature, however, can be used for estimating salinity of the fluid (Collins, 1979; Bowers and Helgeson, 1985; Brown and Lamb, 1989).

CO_2 homogenization temperatures (Th-CO_2) -- Temperatures of CO_2 homogenization vary greatly depending on the fluid inclusion type, ranging from -2 to 31 °C (Fig. 5-c). All inclusions homogenize into liquid state. Monophase CO_2 and CO_2-rich inclusions (group 1) and some group 2 inclusions have CO_2 homogenization temperatures below room temperature, ranging from -2 to 20 °C. Homogenization temperatures of three-phase (group 2) and two-phase CO_2-rich (group 1) inclusions are above room temperature, so they were measured during heating.

Heating

CO_2 homogenization temperatures (Th-CO_2) -- The Th-CO_2 of two- and three-phased inclusions at room temperature range from 21 to 30 °C (Fig. 5-c). CO_2 homogenized into liquid state in all inclusions. The CO_2 homogenization temperatures fall

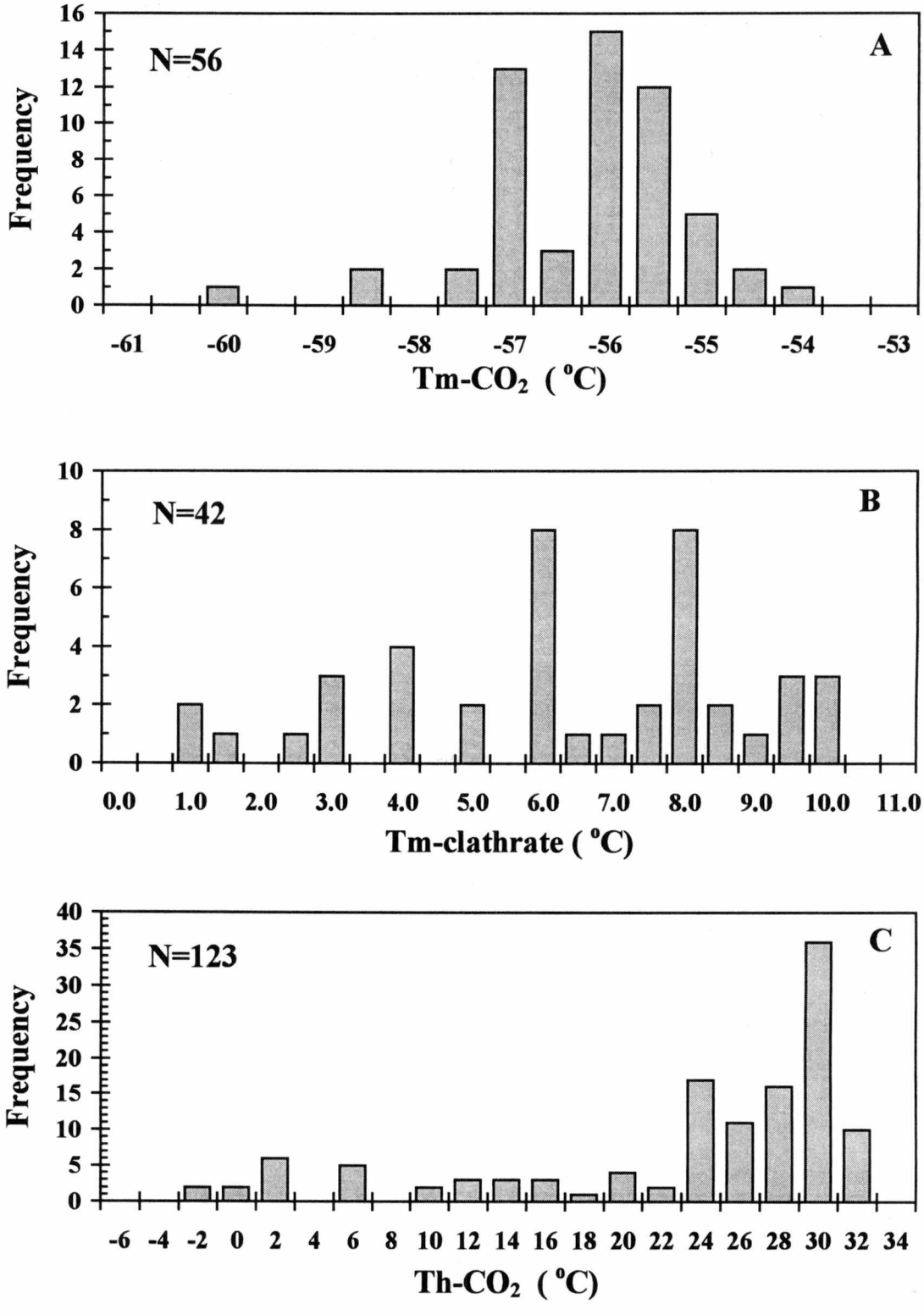

Fig. 5. Histograms of temperatures of phase change for H_2O-CO_2 inclusions. a) Solid CO_2 melting; b) Clathrate ($CO_2.5^{3/4}H_2O$) melting; c) CO_2 homogenization (V-> L).

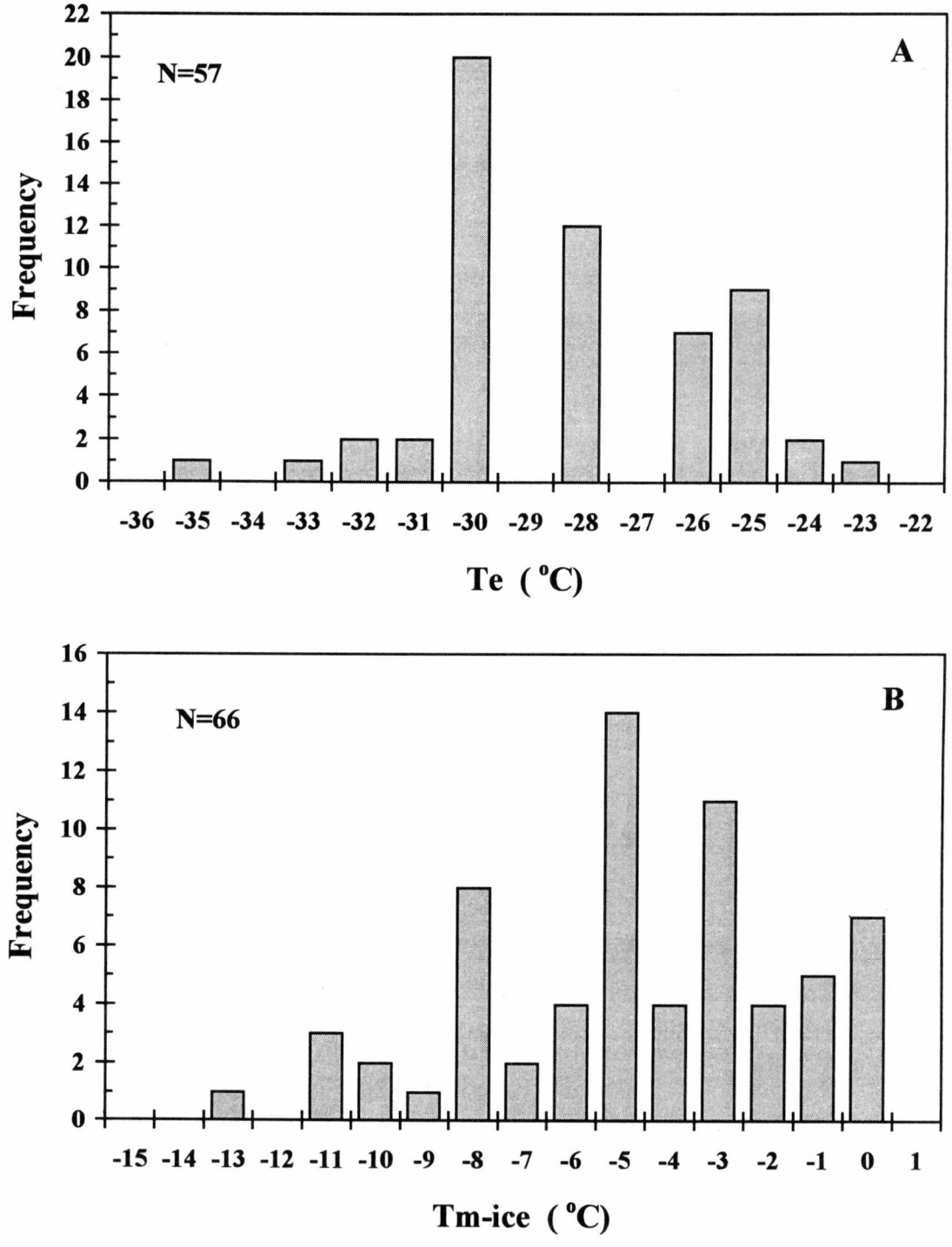

Fig. 6a. Histogram of the temperatures of initial ice-melting (eutectic).
6b. Histogram of the temperatures of last ice-melting.

into three sets; -4 to 4 °C, 10 to 20 °C, and 20 to 31 °C. Most of the CO_2-rich inclusions appear to have lower Th-CO_2.

Total homogenization temperatures (Th) and decrepitation temperatures (Td) -- Figure 7-a shows the homogenization temperatures and decrepitation temperatures of the three groups of fluid inclusions. Overall, the homogenization temperatures range from 106.0 °C to 326.7 °C, but lie mostly between 190 and 280 °C with a single mode. The group 3 (H_2O-rich) inclusions, which invariably homogenized into liquid phase, have distinct lower temperatures, mostly less than 200 °C, although a few homogenized at higher temperatures, up to 260 °C. The Th histogram of the H_2O-rich group 3 inclusions shows a crude bimode distribution--<120 °C and 140 to 220 °C-- which could have resulted from two different hydrothermal fluids. The group 2 inclusions have the most measurements and the widest range, from 150 to 330 °C, but with a strong mode at 190-240 °C. The CO_2 phase in group 2 inclusions always homogenized into H_2O phase. The temperature range for group 1 inclusions (220 - 330 °C) is distinctly higher than that for group 3, but overlaps with that of group 2 inclusions. Some of the group 1 inclusions homogenized into H_2O phase and some of the near-pure CO_2 inclusions appeared to homogenize into CO_2 phase, but most of the them decrepitated before observable homogenization.

Decrepitation before homogenization occurred in CO_2-bearing inclusions of both group 1 and group 2, especially in the CO_2-rich inclusions. This is due to the high internal pressure of the fluid inclusions (Shepherd et al, 1985; Roedder, 1984). The negative crystal-shaped inclusions tended to rupture in direction along the long axis of inclusions. Although the Td is not the true Th, nevertheless, the temperature of decrepitation provides a minimum estimate of homogenization temperature. Figure 7-b shows the relationships of temperatures of homogenization and decrepitation of the inclusions. Overall, the ranges of Th and Td are similar. Decrepitation also occurred

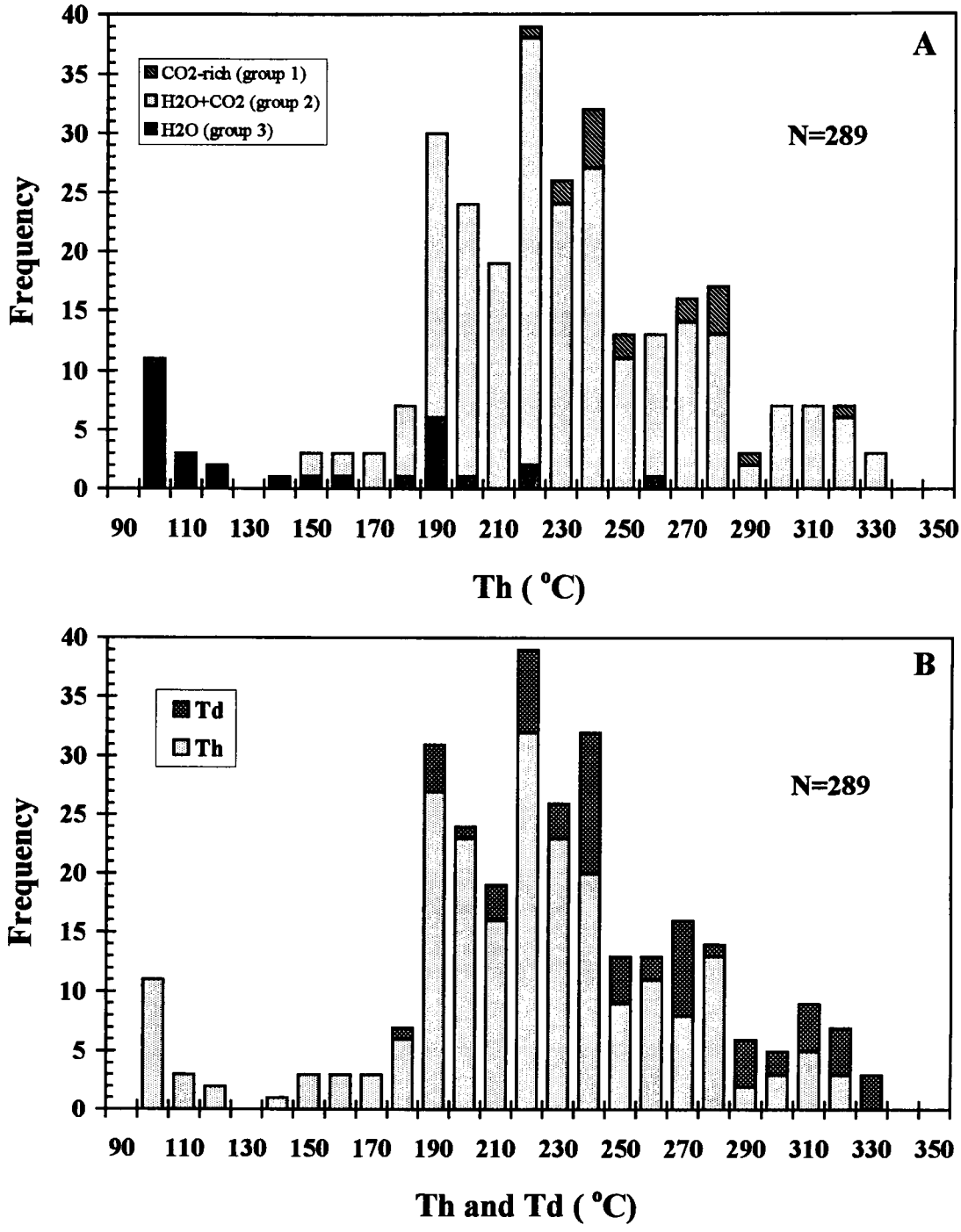

Fig. 7. Histograms of the temperatures of homogenization and decrepitation.

a). Histogram of the temperatures of homogenization (including decrepitation) of the three group fluid inclusions. Group 3 inclusions have mostly lower temperatures.

b). Histogram showing the distribution of Th and Td. Th and Td appear to have a similar range.

after homogenization when overheating. The ruptured inclusions seem to have larger volume percent of CO_2 and invariably have higher Th's compared to prior measurements on the same inclusions.

The samples from the central part of the system, the B-6 ore zone, and the volcanic rocks have no discernible difference in Th range. This may be the result of multiple episodes of hydrothermal alteration that produced large variation in Th's, even in a single sample (Table 1).

Density of CO_2 and XCO_2 in the fluid

The appearance of CO_2-bearing inclusions at room temperature and the homogenization state of CO_2 are related to bulk density of the CO_2 phase in the fluid inclusions (Valakovich and Altunim, 1968). Therefore, the density of CO_2 fluid in the fluid inclusions can be calculated from Th-CO_2 temperatures. The CO_2 densities range from 0.95 to 0.51 g/cm^3 (Fig. 8). In general, CO_2-rich inclusions (typically one- or two-phased CO_2 inclusions at room temperature) have higher densities.

The bulk density of the fluid and the CO_2 content in H_2O-CO_2 inclusions can be calculated using volumetric property of CO_2-H_2O phases, salt content in H_2O, and Th-CO_2 (Brown and Lamb, 1989; Bowers and Helgeson, 1983). The composition and volumetric property of mixed CO_2-H_2O inclusions with < 6 wt% NaCl can also be determined by a graphic technique (Schwartz, 1989). This is especially useful for the inclusions that lack complete microthermometric measurements. The bulk densities of the inclusion fluids were calculated using the FLINCOR program (Brown, 1989) which utilizes the equations of state given by Brown and Lamb (1989) (see Table 1). The bulk densities of the fluid inclusions range from 0.68 to 1.08 g/cm^3. As expected, CO_2-rich inclusions generally have lower bulk densities, whereas the H_2O-rich and relatively saline inclusions (group 3 and some group 2 inclusions) have higher bulk densities. The calculated XCO_2 values range from 0.275 for CO_2-rich inclusions to 1.00 for nearly pure

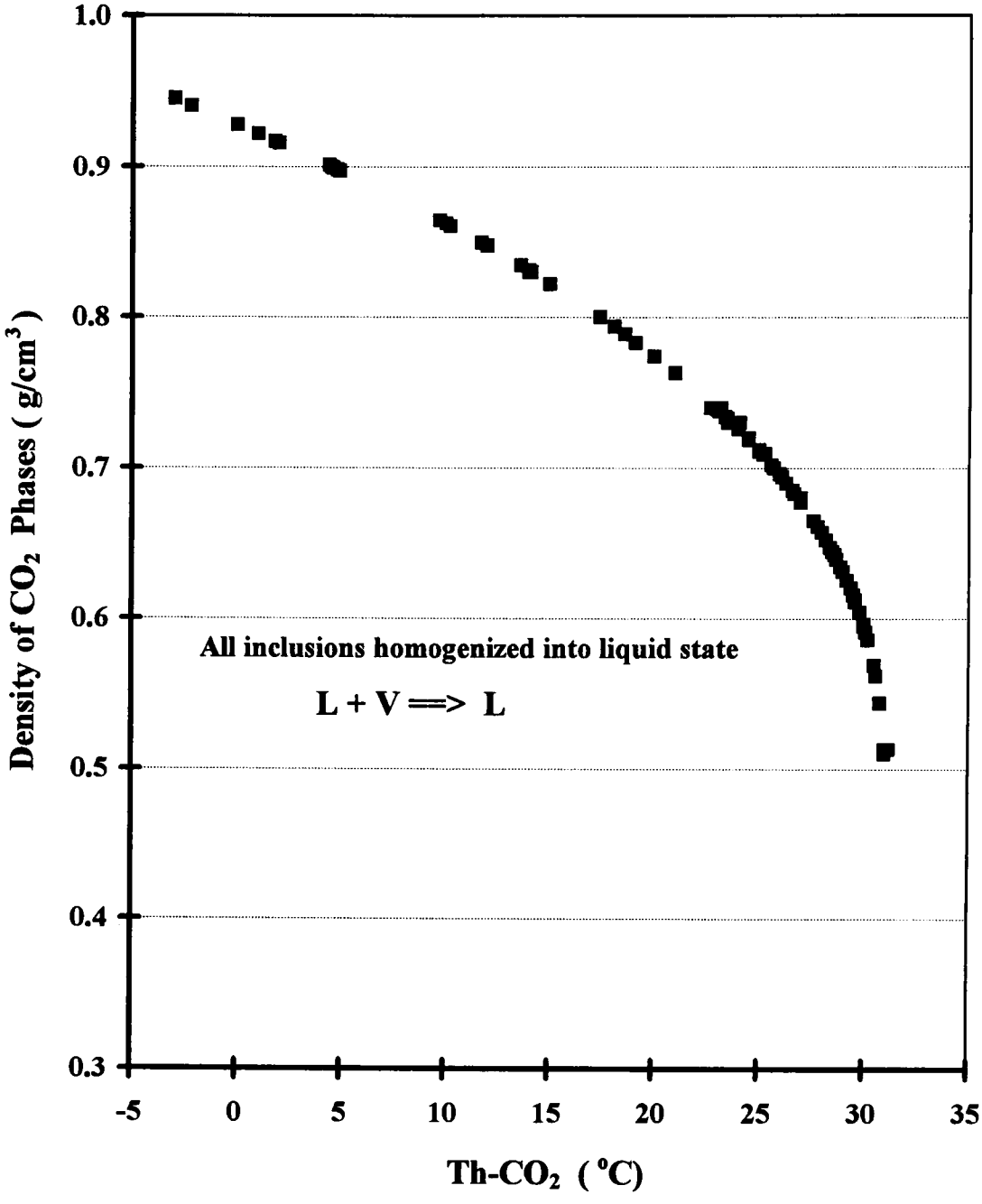

Fig. 8. CO_2 densities calculated from Th-CO_2 for the Brewer fluid inclusions. All inclusions homogenized into liquid phase.

CO_2 inclusions (group 1). The group 2 H_2O+CO_2 inclusions have XCO_2 from 0.02 to 0.177.

Salinity of the fluids

Salinity of the fluid inclusions can be calculated based on the chemical system that the fluid inclusions represent. Based on the behavior of phase changes during freezing and heating, the composition of group 2 and some group 1 fluid inclusions may be approximated by the H_2O-CO_2-NaCl system. Group 3 inclusions mostly have a H_2O-NaCl composition, possibly with small amounts of KCl, MgCl and $CaCl_2$ and even minor CO_2. Salinity of the fluid inclusion was calculated using the equation of Brown and Lamb (1989) for a H_2O-CO_2-NaCl system by the computer program FLINCOR (Brown, 1991). For the H_2O-rich inclusions (group 3), salinity calculations were based on NaCl-H_2O system (Zhang and Fratz, 1985). Using the freezing point depression method of calculating salinities as NaCl equivalents for Ca-Na-K-Mg-chloride solutions generally introduces less than 5% error (Clynne and Potter, 1977).

The calculated salinities of the inclusion fluids range from 0.02 to 14.98 wt% NaCl equivalent. Salinity of group 2 H_2O-CO_2 inclusions varies from 0.02 to 14.77 and from 1.16 to 14.98 wt% NaCl equivalent for group 3 inclusions (H_2O-rich). The salinities of the inclusions vary considerably not only among samples, but also in a single sample, suggesting a complex history for the fluid inclusions. There seems to be a general trend that inclusions with higher Th have relatively lower Tm-ice and higher salinity (Fig. 9). This trend may be attributed to the mixing of deeper hydrothermal fluid with cooler, less saline meteoric water during its ascent to the site of mineralization.

The importance of CO_2 on freeze point measurement, hence on salinity, of fluid inclusions has been well studied (Collins, 1979; Hendenquist and Henley, 1985; Browne, et al, 1976). Collins (1979) discussed the effects of relatively high CO_2 concentrations on the depression of ice-melting temperature. If CO_2 is present, formation of invisible

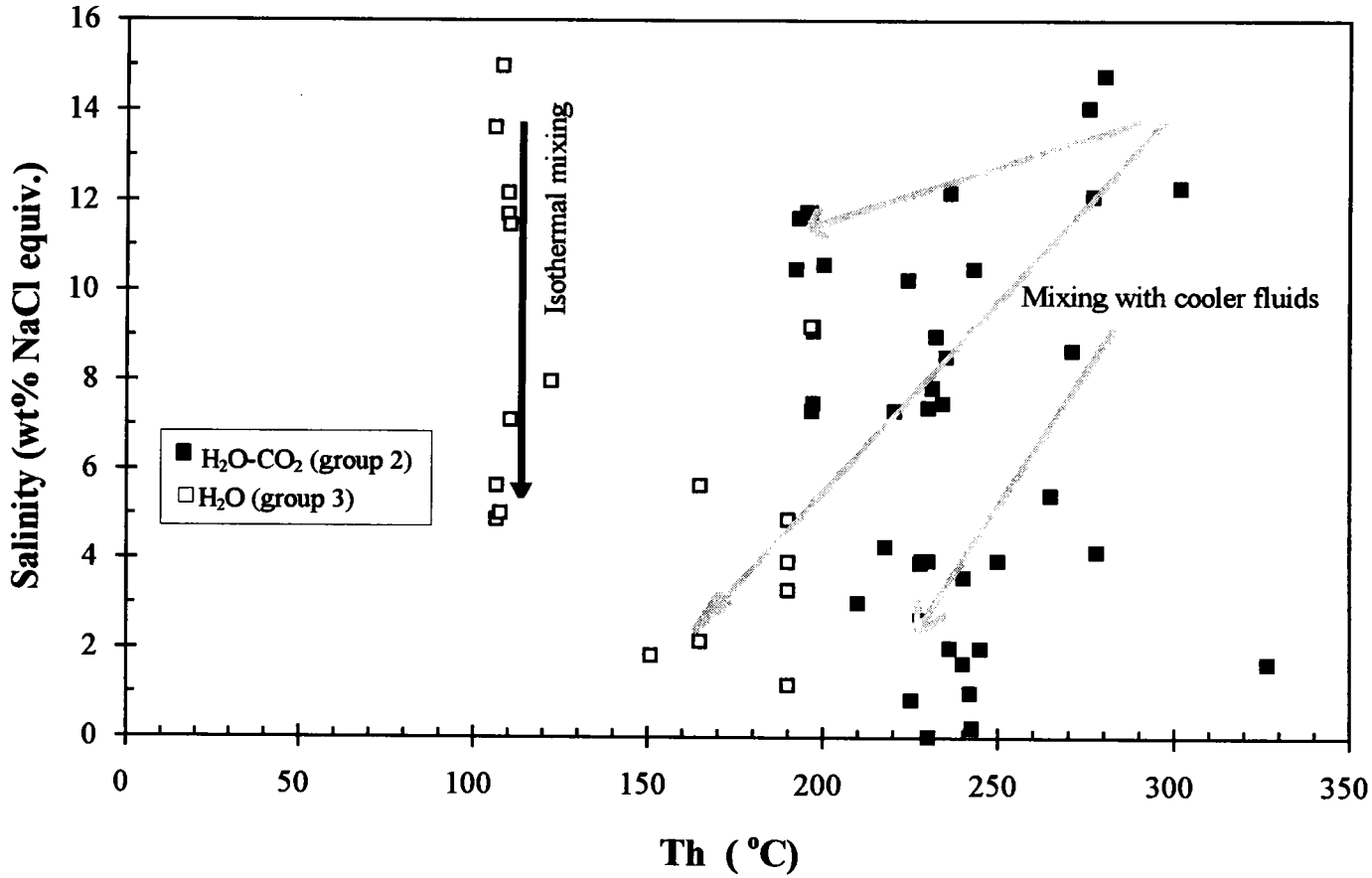

Fig. 9. Salinity-Th relationship showing the possible fluid evolution paths. The salinity of H_2O-CO_2 (group 2) inclusions (filled square) is calculated from Tm-clath in a H_2O-CO_2-NaCl system whereas that of H_2O-rich (group 3) inclusion (open square) is calculated from Tm-ice in a H_2O-NaCl system. H_2O-rich inclusions in one sample show widespread salinities within a narrow temperature range, suggesting isothermal mixing of fluids with contrasting salinities. Other data may be best explained by fluid-mixing processes.

clathrate crystals on cooling can result in serious overestimation of the salinity. Small amounts of CO_2 in fluid inclusions often not detectable during thermometric analysis. Hendenquist and Henley (1985) showed that a lower CO_2 content (no visible CO_2 phase) in the fluid inclusions also causes a relatively higher estimation of salinity. Fluid inclusion containing up to 9 wt% CO_2 may not show a visible CO_2 phase (Hendenquist and Henley, 1985). Therefore, it is possible that the salinity of the fluid is actually lower than estimated from the cooling-heating measurements of the H_2O-rich inclusions.

Possible deformation effects

Several mechanisms can result in the formation of pure and nearly pure CO_2 inclusions (Hollister, 1988; 1990): selective extraction of H_2O from a homogeneous CO_2-H_2O fluid following immiscible separation; selective leakage of H_2O from CO_2-H_2O fluid inclusions through incorporation of H_2O into the crystal structure of the host quartz; and ductile strain-induced leakage of H_2O from mixed CO_2+H_2O fluid inclusions due to difference in wetting properties. CO_2 and H_2O have different wetting properties (Roedder, 1984; Ramboz et al., 1982; Watson and Brenan, 1987). Because H_2O preferentially wets the walls of inclusions and mineral surfaces, H_2O may escape during deformation and leave CO_2-dominated, or even pure CO_2, inclusions (Crawford and Hollister, 1986; Watson and Brenan, 1987). At Brewer, the CO_2-rich inclusions, which occur in fractures or sealed fractures, could have formed as the result of escape of H_2O from the H_2O-CO_2 inclusions.

Chemical Microanalyses of Fluid Inclusions

Laser Raman microprobe analysis

Analytical method

Multichannel laser Raman microprobe (LRM) analysis was performed at the Fluids Research Laboratory of the Department of Geological Sciences at the Virginia

Polytechnic and State University at Blacksburg, Virginia. The principle of Laser Raman spectroscopy is summarized by Etz (1979) and the application of Laser Raman microprobe on fluid inclusions has been discussed by many authors (Rosasco and Roedder, 1979; Touray et al., 1985; Mernagh and Wilde, 1989; Pasteris et al., 1988). Because Raman radiation is produced by the vibration of bonds between atoms, the analysis is restricted to polyatomic species such as SO_4^{2-}, CO_2, CH_4, CO, HS, and SO_2. For this study, fluid inclusions in 14 samples (doubly polished thin sections) were analyzed. Due to the limited penetration of laser Raman, only those inclusions close to the surface could be analyzed.

Chemical components in the fluids

Laser Raman microprobe analysis revealed the presence of CO_2, SO_4^{2-}, and possibly SO_2 and H_2S+HS^- in the Brewer fluid inclusions (Table 2). Apparently, CO_2 and SO_4^{2-} are the dominant components of the fluid inclusions. In most inclusions, CO_2, either as gaseous phase or as dissolved species in the aqueous phase, appeared to be the most important component in the fluid, showing distinct CO_2 peaks (1388 and 1288 cm^{-1}) (Fig. 10a and 10c). CO_2 was detected in most of the inclusions from the samples, although very weak CO_2 peaks in some inclusions indicated only minor amounts of CO_2. SO_4^{2-} was detected in some samples, with distinct SO_4^{2-} peak (980 cm^{-1}) and it appeared to be the predominant peaks in some inclusions (Fig. 10b), indicating that it is the most abundant component in some inclusions. All SO_4^{2-}-bearing samples are from the breccia zone and B-6 ore zone, suggesting that the mineralizing fluids were enriched in sulfate.

H_2O is clearly shown by the presence of a broad O-H stretching bend of H_2O at near 3400 cm^{-1} range in the Raman spectra (Fig. 10a). The exact positions of the peak are variable, ranging from 3419 to 3462 cm^{-1}. The shift of the maximum peaks may be related to the salinity of the fluid. Mernagh and Wilde (1989) showed that the O-H

Table 2. Summary of laser Raman microprobe data

Sample #	Inclusion Type		Peaks (cm^{-1})						
	Phases	CO_2 or vapor %	Quartz	SO_4^{2-}	SO_2	CO_2	N_2	H_2S+HS^-	H_2O
			464, 695, 1161	980	1151	1288, 1388	2331	2580	~3430
BDH-121-X	L								x
	L+Lc	10-40	x	x	?	x			x
	L+Lc+Vc	10-15	x	x		x			x
	Lc+L	70	x			x			x
	quartz		x						
BPQ-X	L+Lc	5-35	x			x	?		x
	L+Lc+Vc	5-20	x			x			x
	Lc		x			x	?		x
	quartz		x						
BP vein	L+Lc+Vc	10-40	x	x	?	x			x
	Lc					x			
	Lc+L	70-75	x			x			
	quartz		x				x		
BS-10	L								x
	L+V	5-10	x			?	?		x
	L+Lc+Vc	40	x						x
	quartz		x						
B61-893	L								x
	L+Lc	20	x			x			
	L+Lc+Vc	10-15	x		x	x	x		x
	Lc					x			
	Lc+L	50-60	x			x			
	quartz		x		x				
BQ-24	L								x
	L+Lc	15	x	x		x			x
	L+Lc+Vc	10-30	x	x	?	x			x
	quartz		x		x				
BNQ-19	L								x
	L+Lc	10		x		x			
	L+Lc+Vc	10-15	x	x		x	x		x
	Lc		x			x			
	Lc+L	60				x			
	quartz		x						
B96-70	L								x
	L+Lc	15	x	x					x
	L+Lc+Vc	10-20	x	x	x	x			x
	Lc+L	60	x			x			
	quartz		x		x				
BPQ-4	L								x
	L+Lc+Vc	8-15	x		x	x		?	x
	L+V	5-10	x		x				x
	Lc+L	50	x			x			
	quartz		x				x		
BQ-1	L+Lc+Vc	20	x			x			x
	Lc		x			x			
	quartz		x						
BPLV	L+Lc	20	x		x	x			x
	L+Lc+Vc	10-25	x		x	x	x		x
	quartz		x						
BPQ-7	L								x
	L+Lc	10-20	x			x			x
	L+Lc+Vc	10-20	x			x	?		x
	Lc					x			
	Lc+L	70				x			
	quartz		x		x				
BP	L								x
	L+Lc	5							x
	L+Lc+Vc	15-20							x
	quartz		x						
BQ-5	L+Lc	15				x			x
	L+Lc+Vc	15				x			x
	Lc					x			x
	quartz		x						

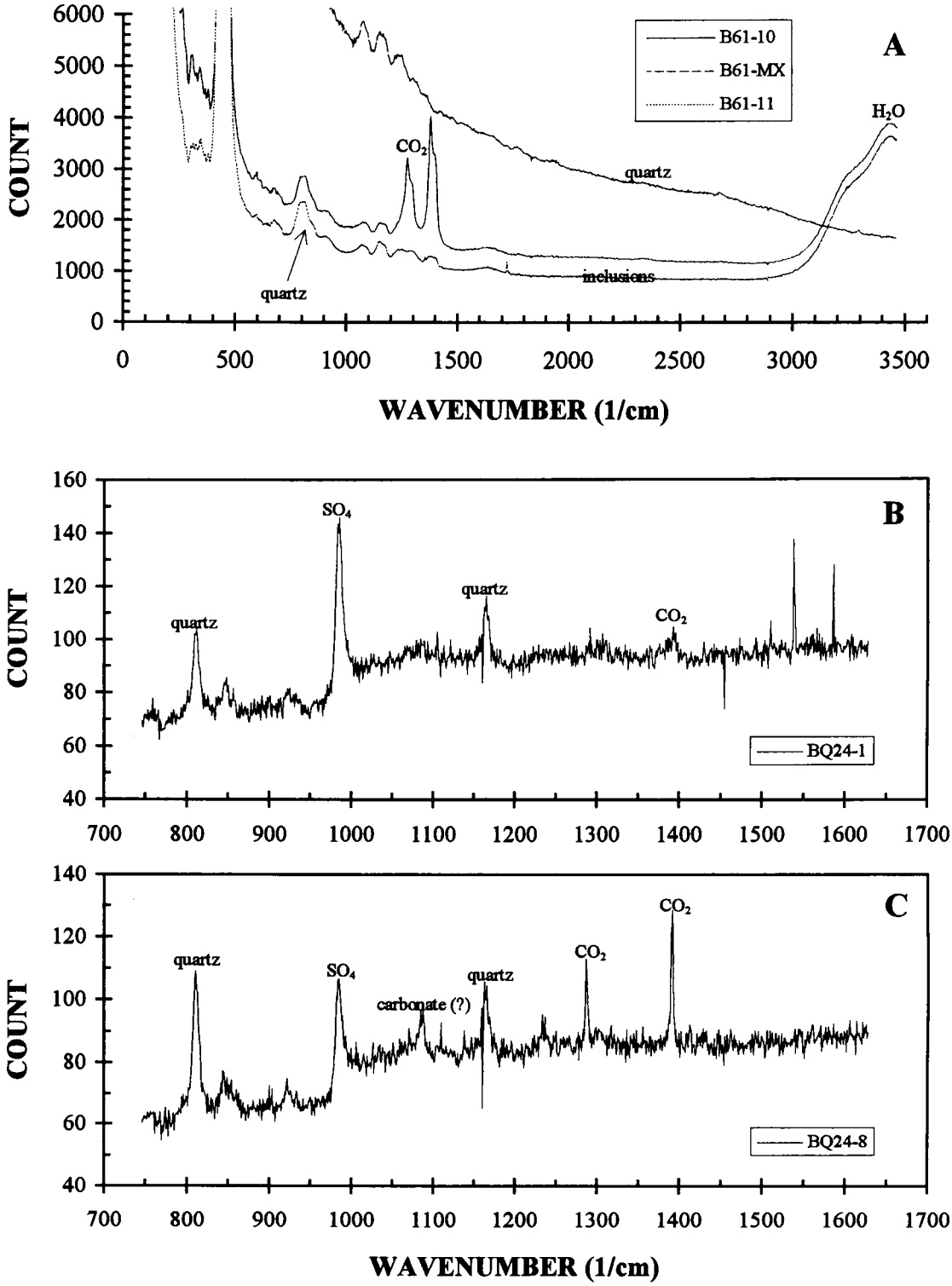

Fig. 10. Raman spectra of fluid inclusions revealed by laser Roman microprobe. a) host quartz, a CO_2-H_2O inclusion, and a fluid inclusion with a small amount of CO_2. b) a fluid inclusion contains SO_4^{2-} and a minor amount of CO_2. c) a fluid inclusion contains CO_2 and SO_4^{2-}. It also shows spectra of carbonate minerals.

stretching region (2800-3800 cm^{-1}) in Raman spectra of aqueous solutions is sensitive to changes in the salt concentration.

Small amounts of several other chemical constitutes may be in the inclusion fluids, are suggested by their relatively weak peaks. These include N_2, SO_2, and possibly H_2S+HS^-. The N_2 peak (at 2331 cm^{-1}), present in about 10 analyses of both inclusions and host quartz, may be a reflection of N_2 picked up from the air as the analyses were done under atmosphere conditions. However, it is also possible that it is actually a minor constituent of inclusion fluids. Some inclusions showed a weak peak near the characteristic peak of SO_2 (1151 cm^{-1}), so minor amounts of SO_2 may also be present in the fluid inclusions. However, the SO_2 peak strongly overlap with the Raman scattering spectrum of host quartz at 1161 cm^{-1} and thus may be spurious. Only one inclusion showed a peak close to the position of H_2S+HS^- (2580 cm^{-1}) and no positive identification could be made because of its weak intensity. No CO or CH_4 could be identified in the Brewer inclusions, although they are often present in CO_2-bearing fluids (Thomas and Spooner, 1989; Smith, et al, 1984; Burruss, 1981). The lack of detection of these compounds probably reflects their extremely low concentrations in the inclusion fluids.

A few inclusions have peaks around 1080-1100 cm^{-1} (Fig. 10c), close to characteristic Raman spectra of carbonate group minerals. No carbonate minerals were observed in the fluid inclusions. However, tiny calcite crystals in the fluid inclusion, especially growth on the inclusion wall, would be difficult to detect.

There appears to be some systematic variation in the composition of inclusion fluids. Group 1 (CO_2-rich) inclusions have little SO_4^{2-} in the fluids, whereas group 2 (H_2O+CO_2) inclusions contain CO_2 and SO_4^{2-} in varying proportion, and possibly small amount of SO_2. The SO_4^{2-} appears to be preferably concentrated in the H_2O phase, because the SO_4^{2-} peaks were observed to be higher when the probe point was placed on

the H_2O phase. Group 3 inclusions (H_2O-rich) have mostly only the H_2O peak, but two inclusions have weak CO_2 peaks suggesting the possibility of minor amount of CO_2. As H_2O-rich (group 3) inclusions often cut the other two groups of inclusions, it is highly likely that the CO_2 in group 3 inclusions was derived locally from the pre-existing CO_2-bearing inclusions. However, the lack of CO_2 peaks for most group 3 inclusions strongly suggests a extremely low concentration of CO_2 content in the inclusion fluids.

Synchrotron x-ray fluorescence microprobe analysis

Analytic procedure

Synchrotron X-ray fluorescence (SXRF) microprobe analysis of fluid inclusions from the Brewer Mine was performed at the National Synchrotron Light Source (NSLS), Brookhaven National Laboratory, Upton, New York. The samples used were doubly polished thin sections. A collimated white beamline was used for the analysis; the X-ray energy used ranged up to 20 keV.

Various studies (Frantz et al., 1988; Rankin et al., 1992) have shown the usefulness of SXRF microprobe in analyzing fluid inclusion compositions, particularly trace metals and monoatomic species in the fluid. Synchrotron radiation has a very high intensity from the tube source and the beam is well-collimated, so the intensity remains high away from source. Synchrotron radiation is highly linearly polarized which minimizes the scattered radiation. Therefore, non-destructive, trace level analyses of a wide range of elements with high spatial resolution and low power deposition when analyzing volatile-rich specimens have been the main advantages of synchrotron X-ray fluorescence. This makes the SXRF microprobe well suited for nondestructible trace element analyses of nanogram samples, such as fluid inclusions.

Results

K, Ca, Ti, Cr, Mn, Fe, Ni, Cu, Zn, As, Ba, S, and Cl were detected in fluid inclusions--Fe, Mn, and Ca in all the inclusions analyzed, and others in some of the

inclusions. Table 3 summarizes the analytical results and figure 12 show the X-ray pattern of two fluid inclusions.

In order to distinguish the effect of the background, the host quartz was also analyzed. The quartz showed recognizable Cu, Fe, and Mn peaks, most likely because of tiny fluid inclusions in the background and/or tiny sulfide solid inclusions in the quartz. Pyrite, and sometimes enargite, are abundant in some parts of the thin sections. Because of the strong penetrating ability of synchrotron X-ray radiation, these sulfide minerals deep below the surface could have produced a source of contamination. An analysis on a sulfide mineral (enargite) show the presence of Fe, Cu, and As (Table 3).

The inclusions appears to have some differences in chemical components. A H_2O-rich H_2O-CO_2 inclusion showed the presence of many chemical constituents, including S, Cl, K, Ca, Ti, Cr, Mn, Fe, Ni, Cu, Zn, As, and Br (Fig. 11a). On the other hand, a CO_2-rich 3-phase (Lc+L+Vc) inclusion, which was probed on the CO_2 phase, had only low-intensity of Mn, Fe and Ca (?) peaks and no Cl peak (Fig. 11b). The higher metal content in the H_2O phase than in CO_2 phase suggests that the metals and other constituents may have stayed preferentially in H_2O phase.

HYDROTHERMAL FLUID CHARACTERIZATION AND EVOLUTION

Physiochemical Conditions during Mineralization

Trapping of the fluid inclusions

Variable CO_2:H_2O ratios in fluid inclusions in a deposit could result from either heterogeneous trapping of fluids or episodic boiling (phase separation) of a homogeneous fluid. Under condition of CO_2 as the dominant dissolved gas in hydrothermal fluid, phase separation will take place at 300 °C and 1.5 kb if the CO_2 content of the H_2O-CO_2-NaCl fluid exceeds 15 mol% (Naden and Shepherd, 1989). CO_2 boiling (or phase seperation) is indicated by that variable phase ratios fluid inclusions homogenize into both vapor and

Table 3. Summary of SXRF microprobe data

Elements	Peaks		Energy (keV)	BP-LV			BQ-24				
				L+Lc	Lc+L+Vc	sulfide	L+Lc	L+Lc	L+Lc	L+Lc	quartz
S	Kα		2.307	**		***			**		
Cl	Kα		2.622	**					**		
K	Kα		3.312	**			*	*	**	*	
Ca	Kα		3.690	***	*		**	**	***	**	**
		Kβ	4.012	**					**		
Ti	Kα		4.508	**				*	**	**	
		Kβ	4.931	*					**		
Cr	Kα		5.411	**				*	**		
		Kβ	5.947								
Mn	Kα		5.895	**	**		**	**	**	**	
		Kβ	6.492								
Fe	Kα		6.400	***	**	***	***	***	***	***	***
		Kβ	7.059	**		***	**	**	**	**	
Ni	Kα		7.472	**					**		
		Kβ	8.265	*							
Cu	Kα		8.041	**		***	**	**	**	**	**
		Kβ	8.907			***					
Zn	Kα		9.631	**			**	**	**	*	**
		Kβ	9.572								
As	Kα		10.532	**		**					
		Kβ	11.729								
Br	Kα		11.907	**	**						
		Kβ	13.296								

Note: *** -- large peak (prominent)

** -- medium peak (easily identified)

* -- small peak (not distinguishable but recognizable)

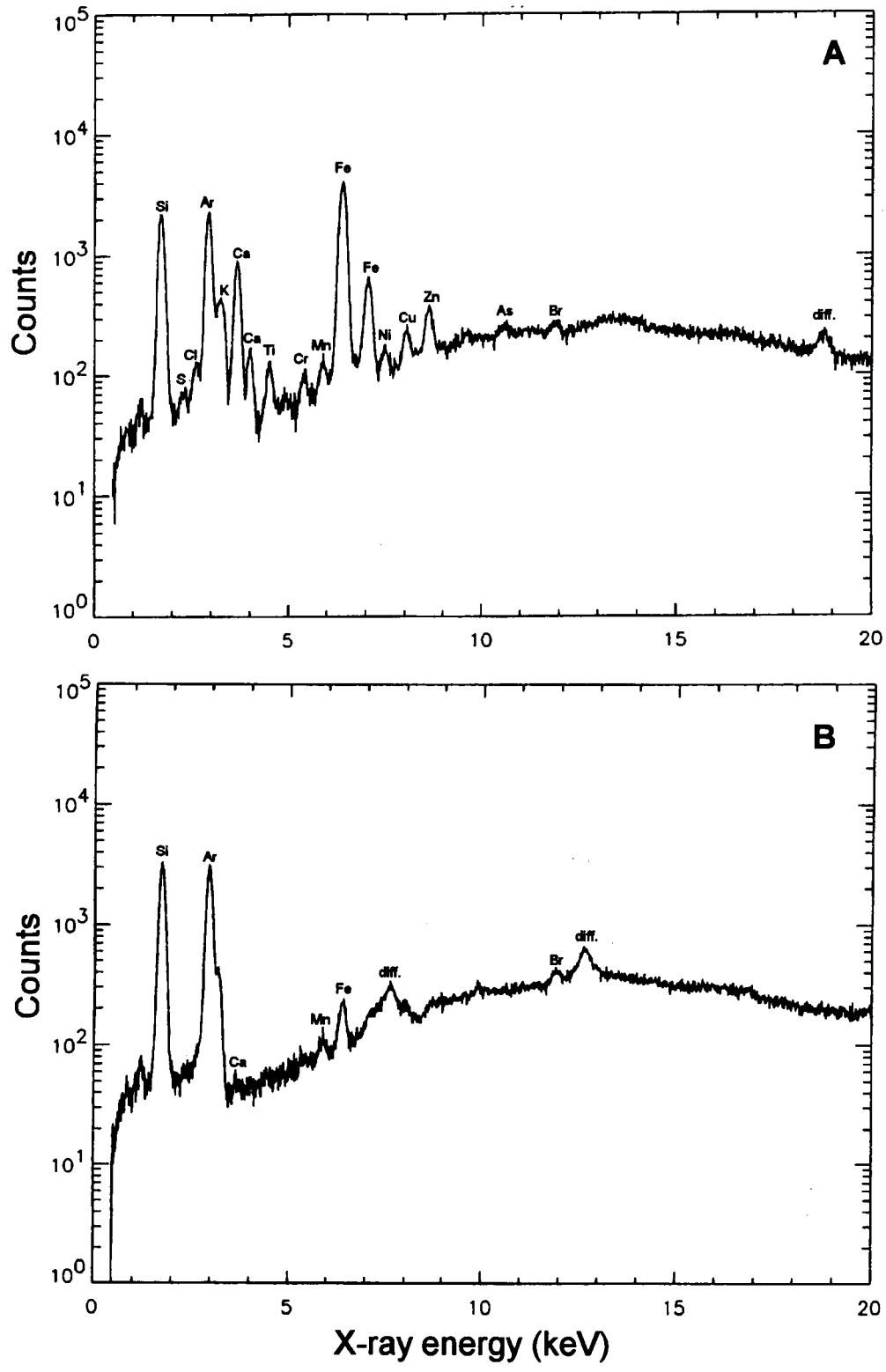

Fig. 11. Synchrotron XRF patterns of two fluid inclusions: a) a two-phased H_2O-rich H_2O-CO_2 inclusion containing many metal and other components; b) a three-phased CO_2-rich inclusion containing only Fe and Mn (see text).

liquid (or liquid water and liquid CO_2) phases at a same temperature. Heterogeneous trapping is also indicated by coexisting inclusions with varying proportion and composition of phases, but the inclusions may homogenize into either one or two phases at different temperatures.

The occurrence and heating-cooling behavior of the fluid inclusions in the Brewer system suggest that heterogeneous trapping was probably the predominant process that resulted in the variable CO_2:H_2O ratios in fluid inclusions, especially for the abundant H_2O-CO_2 inclusions. Evidence in favor of the conclusion include: 1) although fluid inclusions of variable CO_2:H_2O ratios occurs in a single sample, they usually do not occur in the same fracture or zone; 2) CO_2 gas phase invariably homogenizes into CO_2 liquid phase; 3) CO_2 phase homogenizes into H_2O aqueous phase; and 4) the inclusions often have a large spread of homogenization temperature; and 5) the multiple brecciation and hydrothermal fracturing in the mineralized zone where fluids with different composition can be formed in a rapidly changed physiochemical conditions through processes such as fluid mixing and fluid-rock reaction.

On the other hand, episodic boiling (phase separation) could have played some role in the formation of CO_2-rich inclusions. Extremely CO_2-rich inclusions are not very common in geologic environments and they can be formed from a relatively low-CO_2 fluid through boiling. The relatively limited occurrence of CO_2-rich inclusions in the Brewer Mine suggests that boiling did not occur extensively during the trapping of the inclusions, but may have occurred locally or was limited to some episodes of brecciation.

Fluid immiscibility in the system H_2O-CO_2-NaCl significantly affects the phase equilibria. The immiscible field (H_2O-CO_2 solvus) varies greatly depending on the salinity and pressure of the fluids. Bowers and Helgeson (1983) showed that increasing NaCl content causes an extension of the immiscibility field, especially on the H_2O-rich side; increasing pressure has the opposite effect. Figure 12 is a XCO_2-Th plot for the fluid

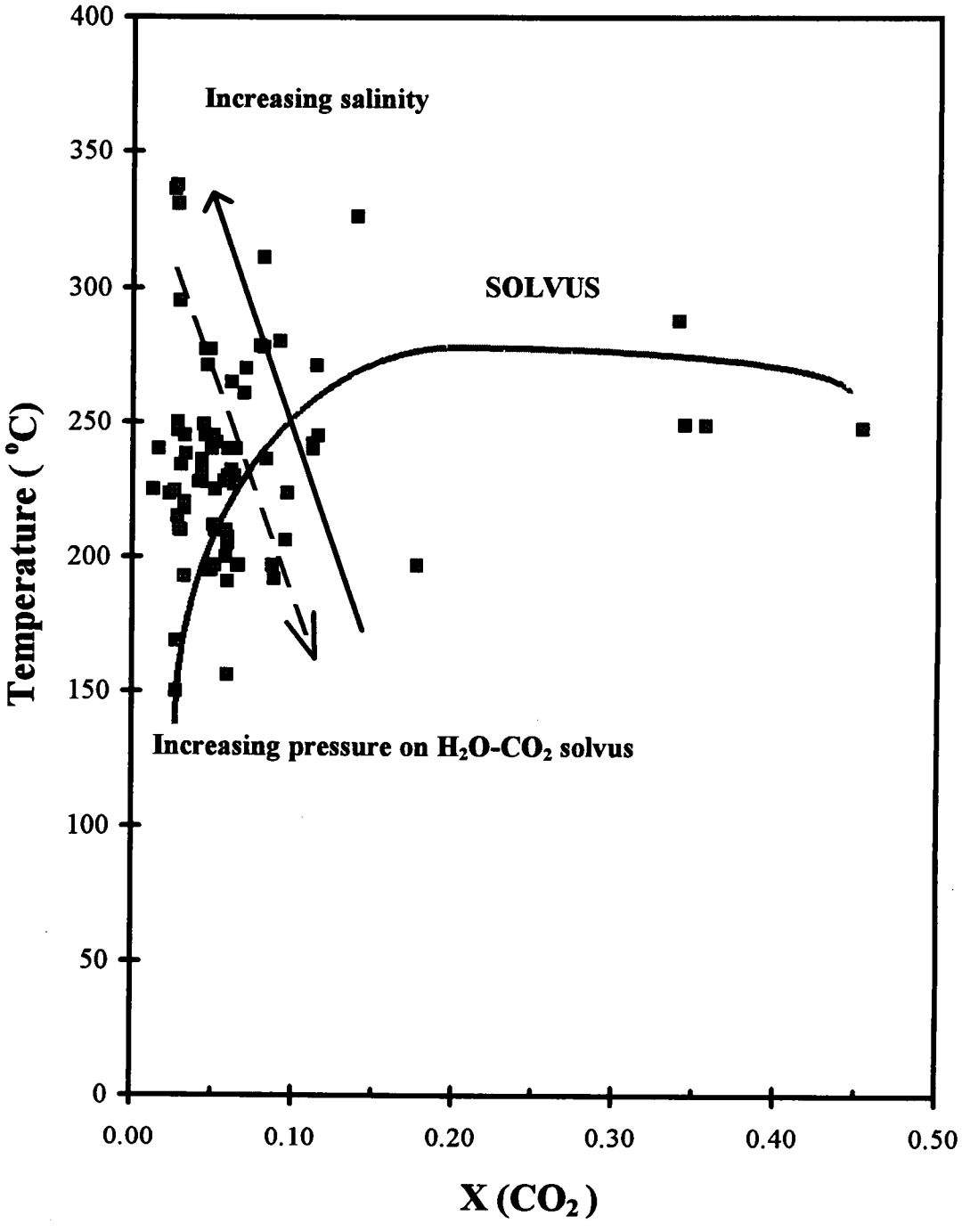

Fig. 12. X(CO_2)-Th relationship of the fluid inclusions from Brewer. Increasing salinity or pressure of the fluid could result in the movement of CO_2-H_2O solvus, thus a large field of CO_2-H_2O homogenization temperature.

inclusion data in the Brewer Mine, which shows that the Th has a large range in the H_2O-rich side. This could be attributed to variations either in fluid pressure or fluid salinity, both of which are compatible with the widespread multi-episodic breccias in the mineralized zone at the Brewer Mine. The multi-stage brecciation occurred probably in response to the cyclic buildup and release of fluid pressure in the volcanic system (magma), and repeated episodes of brecciation could have also led to variation in the fluid salinity by fluid-fluid mixing.

Temperature of fluid

Homogenization temperatures of the group 1 and 2 primary and pseudosecondary fluid inclusions indicate a temperature of 190 to 330 °C for the hydrothermal fluids. The homogenization temperatures, however, provide only a minimum trapping temperature of the fluid. The mostly secondary, H_2O-rich fluid inclusions (group 3) have lower homogenization temperatures, suggesting that they were trapped either during the waning stage of the mineralization or during a later another hydrothermal or metamorphic episode. However, the occurrence of the quartz, many of them in the breccia cement and aggregate and small quartz vein, implies it is more likely that they were formed during later mineralization alteration stage as H_2O becomes more prominent.

The temperature range obtained by fluid inclusion microthermometric analysis is consistent with that obtained from the pyrite-alunite sulfur isotope geothermometer (see Part 3). At Brewer, The $\delta^{34}S$ values of alunites range from 17.7 to 26.8 per mil. The $\delta^{34}S$ values of pyrites range from 0.51 to 5.70 per mil, with a much more restricted range (2.53 to 3.68 per mil) for the pyrite from the mineralized breccia. That the $\delta^{34}S$ values of alunites are generally 15 to 22 ‰ larger than that of the coexisting pyrite suggests that the alunite was a direct product of magmatic hydrothermal, acid sulfate alteration in an epithermal environment where the sulfuric acid was probably produced by the disproportionation of SO_2 with decreasing temperature. The equilibrium between

aqueous H_2S and SO_4^{2-} formed by the disproportionation resulted in alunite enriched in ^{34}S relative to pyrite. The temperature range of about 300-500 °C obtained from the $\Delta^{34}S_{alunite\text{-}pyrite}$ values in coexisting pyrite and alunite, overlaps at the higher end of the temperature estimated from the fluid inclusions.

Further constraint on the temperature of the mineralizing fluids is given by mineral assemblages. At Brewer, the hydrothermal mineral assemblage of andalusite, diaspore, kaolinite, and pyrophyllite suggests that the temperature range is about 250 to 400 °C at 1 and 2 kb H_2O pressure in the system of Al_2O_3-SiO_2-H_2O (Hemley et. al., 1980) (Fig. 13).

The formation of various forms of silica may be attributed to the temperature variation during mineralization (Fournier, 1988). Slow cooling of a hydrothermal solution generally will result in the deposition of quartz if initial temperatures are between about 200 °C and 340 °C. Rapid cooling allows supersaturated silica solutions to form. Slight silica supersaturation with respect to quartz is required for chalcedony to precipitate directly from solution, whereas large degrees of supersaturation are required for precipitation of amorphous silica. The widespread presence of quartz in the mineralized zone at Brewer suggests that the hydrothermal fluid did not undergo very rapid cooling.

Pressure estimation

The fluid inclusion Th and its corresponding pressure along a univariant phase boundary provide the minimum pressure and temperature conditions of mineralization. At Brewer, the pressure and temperature that prevailed during mineralization were probably somewhat higher, defined by some point on the isochore for a known fluid composition. Unfortunately, no independent geobarometer is available for pressure estimation. However, the observation that many CO_2-bearing (group 1 and some group 2) inclusions decrepitated before homogenization during heating provides some crude information about the internal pressure of the fluid inclusions. Studies have shown that

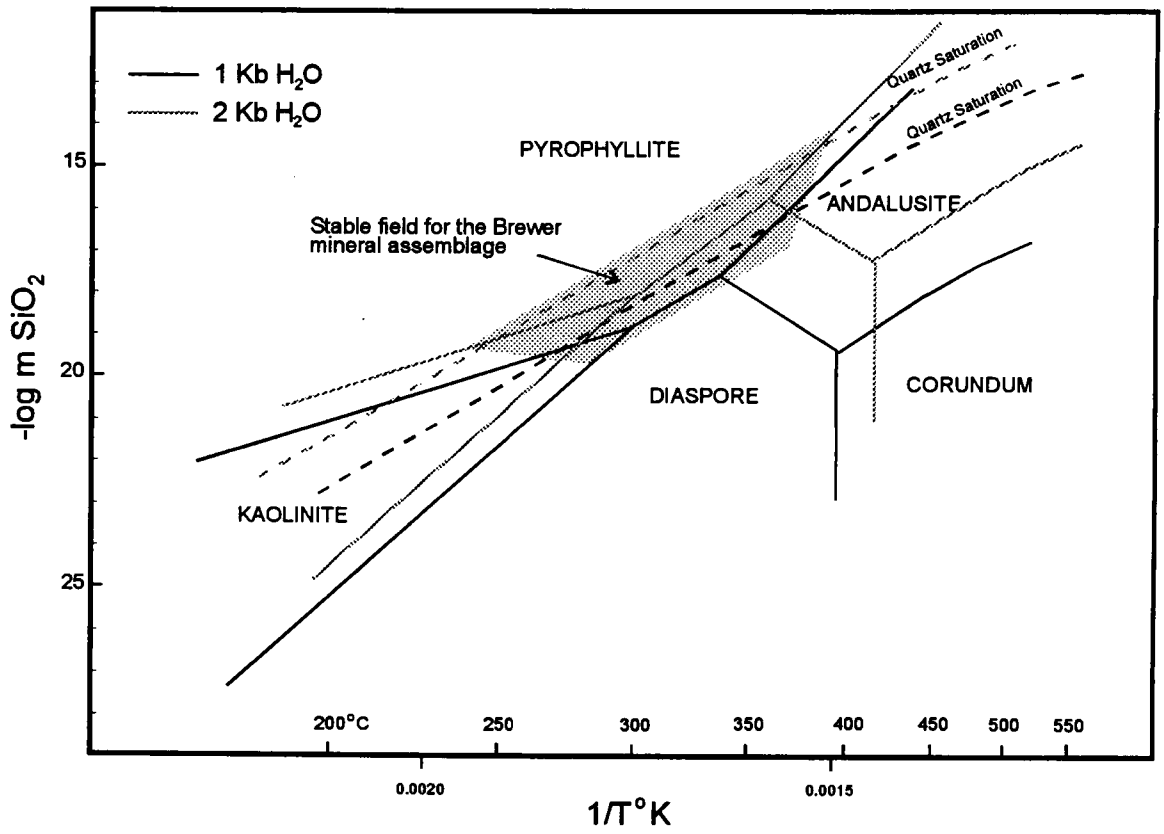

Fig. 13. Mineral equilibrium constraint on the formation temperatures based on system Al_2O_3-SiO_2-H_2O at 1 and 2 kb (After Hemley et al., 1980).

decrepitation for a specific sized inclusion in a mineral during heating is related to internal pressure (Naumov et al., 1966; Leroy, 1979; Swanenberg, 1980; and Roedder, 1966). Medium-sized inclusions (~35 μm) in quartz generally decrepitate at 850 bars internal pressure, and smaller inclusions (~12 μm) rupture at about 1200 bars. Thus, the internal pressure required for decrepitation of CO_2-bearing inclusions (mostly between 8 to 15 μm) in the Brewer samples would probably be in excess of 1000 bars. Using isochores by Bowers and Helgeson (1983) for the system H_2O-CO_2-NaCl, with CO_2 and NaCl contents applicable to the Brewer, the trapping temperatures of fluid inclusion at a pressure of 1 to 1.5 kb would lie between 300 to 500 °C, about 100 °C higher than the homogenization temperatures.

The experimentally established boiling curve for H_2O-CO_2 system can be used for pressure estimates from fluid inclusions with known CO_2 contents (Roedder and Bodnar, 1980). The pressure estimated for the Brewer samples ranges from about 300 to 1000 bars. The method of intersecting CO_2 and H_2O isochores (Roedder and Bodnar, 1980) gives pressures in the order of 500 to 1200 bars.

Geochemistry of Mineralizing Fluid

The fluid inclusion data suggest that the fluids related to the gold mineralization in the Brewer Mine were H_2O-CO_2 fluids with variable CO_2 contents. The fluids had low to moderate salinity (<15 wt% NaCl. equiv.), contained many metal components, and probably were SO_4^{2-}-rich, especially during late stage of the mineralization.

The presence of SO_4^{2-} in the fluid inclusion and generally lack of HS^- and H_2S may suggest that the fluid was relatively oxidized during the trapping. Alternatively, the reduced sulfur may have been consumed to precipitate pyrite and other sulfides in the central part of the hydrothermal system (the mineralized breccia zone), leaving the fluid

relatively enriched in SO_4^{2-}. The lack of CO and CH_4 may also be attributed to an relatively oxidized environment favoring CO_2.

As described earlier, SXRF analysis has revealed the presence of many alkaline and metal components (K, Ca, Ti, Cr, Mn, Fe, Ni, Cu, Zn, As and Br) in the fluid, which is consistent with mineral assemblages presented in the mineralized zone. A geochemical survey (Jaack, 1986) showed that the breccias have distinctive chemical signature of Fe, Mn, Mg, Cu, As, Mo, Ag, Au, and Hg enrichment. The mineralization zone also showed the enrichment of the many these elements in the hydrothermally altered rocks and breccias (Lu et al., 1993). Fe was apparently the most dominant metal in the fluids, as indicated by the high Fe intensity in SXRF pattern (Fig. 11) and by widespread pyrite in the mineralized breccia zone. Although Ca was detected in the inclusion, very few Ca-bearing minerals were observed in the mineralized breccia zone, implying that the Ca might move to the outer alteration zone, e.g. the propylitic zone, to precipitate as calcite and epidote.

The fluid characteristics and P-T conditions permit some speculation about the possible gold precipitation mechanism. The gold likely is transported as predominantly sulfide-complexed forms in the high S and relatively lower salinity fluid , although some could be in chloride-complexed forms (Seward, 1991, 1984, and 1973; Romberger, 1986, 1988). Deposition of gold from a hydrothermal system can be caused by many physical and chemical changes, such as decreasing in temperature and/or pressure, an increasing in fO_2, and a change of fluid composition through such reactions:

$$Au(HS)_2^- + O_2 + H_2O \Longrightarrow Au + H^+ + SO_4^{2-} \quad \text{(oxidation)}$$

$$Au(HS)_2^- + H_2O \Longrightarrow Au + H^+ + HS^- + SO_4^{2-} \quad \text{(pH increase)}$$

Overall, the fluids for the Brewer gold mineralization differ compositionally from those of typical epithermal gold deposits, porphyry Au-Cu-Mo deposits, and Archean Lode gold deposits (Table 4). Although the tectonic setting, hydrothermal alteration

Table 4. Comparison of the fluid characteristics of Brewer with major types of gold deposits

Deposit Type	Fluid Composition	Salinity(wt% NaCl)	CO_2 Density	Th (°C)	Fluid Sources
Epithermal Au	H_2O+(NaCl) CO_2 (minor)	low (<5%)	low	< 350	meteoric + (magmatic)
Porphyry Au-Cu-Mo	H_2O CO_2 (minor)	moderate-high (up to 75%)	low	up to 750	magmatic
Archean Lode Gold	H_2O CO_2	low (<5%)	high	200-400	metamorphic magmatic-meteoric
Brewer	H_2O-CO_2-NaCl	2-14%	moderate-high	150-320	magmatic + (meteoric)

pattern, mineralization style, and alteration mineral assemblages all indicate epithermal acid-sulfate environment for the gold mineralization at Brewer, the fluid composition is somewhat different from the typical Tertiary epithermal precious metal deposits (Bodnar et al., 1985; Heald et al., 1987; Berger and Henley, 1981; and Henley et al., 1985) for its higher CO_2 content in the fluid.

Fluid Sources

Epithermal precious metal deposits are typically associated with lower CO_2, either boiling or non-boiling, low-salinity fluids of mostly meteoric origin (Bodnar et al., 1985; Heald et al., 1987). However, CO_2 is a common constituent of active geothermal and fossil ore-forming fluids (Hendenquist and Henley, 1985; Henley and Ellis, 1983; Cunningham, 1982). CO_2 is the dominant constituent of the dissolved gases in geothermal fluids, and in some geothermal systems, its dissolved component, such as HCO_3^-, even exceeds that of chloride (Hendenquist and Henley, 1985). CO_2 in geothermal systems may originate from decarbonation reactions from carbonate rocks and from dispersed organic matter, from meteoric water, or from magmatic sources.

CO_2-bearing fluid has often been mentioned in metamorphic deposits and Archean Lode gold deposits and the mineralizing fluids have been attributed to sources of metamorphic fluids, meteoric water, magmatic fluids, or combined fluids (Colvine et al., 1984; Smith et al., 1984; Rushton et al., 1993; Mckeag and Craw, 1989; Hostler, 1981). Some of the Archean gold mineralization, typically in quartz veins, indicate oxidized hydrothermal fluids. Because of their oxidized nature, the most likely general source for the fluids may be felsic magmas (Cameron and Hattori, 1987). Felsic magmas could have expelled CO_2-rich fluids responsible for many of the gold mineralization in Archean quartz veins in Canada, such as McIntyre-Hollinger, Canada (Smith et al., 1984) and Newfoundland (Kay and Strong, 1983).

CO_2-bearing inclusions have been also found in many other environments, including some epithermal (Moore et al., 1992), porphyry Mo (Gallagher et al., 1992) and Cu-Mo breccia mineralization (Norman and Sawkins, 1985), plutonic and volcanic related deposits (Henley and Ellis, 1983; Thomas and Spooner, 1992), and acid-sulfate deposits (Rodalquilar, Spain; Oepon et al., 1990). CO_2-rich fluid is also present in some epithermal systems that overprint an earlier higher temperature system (Summitville, Colorado), and the fluid may actually represent earlier magmatic fluids (Bodnar et al., 1985). Baker and Andrew (1991) studied a gold-bearing breccia pipe at Kidston, Australia in which CO_2-rich inclusions are present. They concluded that the CO_2 fluid is introduced from a cooling rhyolitic magma based on carbon stable isotope data. Gallagher et al. (1992) studied porphyry molybdenum mineralization in Galway granite in Ireland. The fluid inclusions in quartz veins, H_2O-CO_2-NaCl in composition, homogenized in the range 100-350 °C and have a salinity of 1-13 wt% NaCl equivalent. The CO_2-bearing fluids were produced by decompression-activated unmixing of a weakly mineralized H_2O-CO_2 fluid from a dense Mo-bearing NaCl-H_2O-CO_2 fluid which migrated from the magma chamber into overlying joints to form the vein-hosted mineralization. Low-salinity (<2 wt% NaCl), CO_2-H_2O fluids are present in gold-bearing quartz veins in the Mother Lode vein system, California. The mineralization was from magmatic activity associated with a subducting slab (Weir and Kerrick, 1987).

Although metamorphic fluid is often CO_2-rich, the fact that the mineralization is prior to the metamorphism makes this source unlikely. Meteoric water was probably present at the time of mineralization, but the mostly rhyolitic volcanic host rock, in which meteoric water circulates, in not likely to have provided the CO_2-bearing fluid, especially the CO_2-rich fluid. Magmatic fluid appears to be the most feasible source for the Brewer Mineralizing fluids. In the volcanic-hosted deposits that contain enargite+gold as components of advanced argillic alteration, such as at Brewer, magmatic-hydrothermal

fluids could have been important at least during earlier stages of mineralization (Sillitoe, 1989). Hydrofracturing and brecciation in the Brewer Mine suggest that these processes most likely accompanied the release of aqueous fluids from magma. However, to produce CO_2-bearing fluid, a deep-seated felsic magma (high aluminosilicate melt) may be needed. The magma probably provided both the heat and fluid source for the mineralization, as well as was responsible for the volcanic activities in the area, either during or prior to the mineralization.

Experimental study by Burnham (1972) suggested that an aluminosilicate melt could release CO_2-H_2O fluid. Because CO_2 is less readily dissolved than H_2O in aluminosilicate melts (felsic magmas), the earlier separated fluid from magma could be CO_2-rich (Burnham, 1979). A high-CO_2 magma would permit the separation of a mineralizing aqueous phase at a greater depth than a CO_2-poor magma. Metals that form strong S complexes, including Au, may partition into the S-rich, H_2O-CO_2 fluid, where metals that complex strongly with Cl, such as base metals, partition into the saline aqueous liquid.

Many I-type magmas are S-rich and are associated with porphyry Cu-Mo. Because of the high concentration of SO_2 relative to H_2S (0.1 to 10 fugacity ratios) in magmatic aqueous phases, increasing fO_2 and decreasing pressure may produce a highly sulfur-rich fluid capable of transporting significant amounts of heavy metal chloride complexes (Burnham and Ohmoto, 1980). Volatile and incompatible elements, such as CO_2,Cl, S, and base and precious metals, partition into the fluid. S separates into the fluid as SO_2 and H_2S, the relative amounts being determined by fO_2 (Carroll and Rutherford, 1985). SO_2 will be dominant in a relatively oxidized magma. SO_2 begins the disproportionation of SO_2 with decreasing temperature according to the reaction (Holland, 1965, 1967):

$$4SO_2 + 4H_2O = 4H_2SO_3 = 3H_2SO_4 + H_2S$$

and contributes to the formation of sulfide and sulfate minerals. Precipitation of pyrite does not mandate a strongly reduced fluid due to its wide fO_2 stability. The S stable isotope data of pyrite and associated alunite from the Brewer suggest that they have the same sulfur source. The widespread aluminosilicate minerals at the Brewer Mine raise the possibility of an underlying porphyry environment (see Part 3).

The extent of meteoric water contribution to the hydrothermal fluids at Brewer is difficult to assess from the fluid inclusion data although the group 3 inclusions, mostly secondary in nature, have somewhat lower salinity than the group 2 inclusion, suggesting contribution from meteoric water. As an extension of their geochemical and oxygen isotope study of the hydrothermal alteration in the Pilot Mountain of Carolina slate belt, Klein and Criss (1988) suggested the possibility of a significant meteoritic water component in the Brewer hydrothermal fluids ($\delta^{18}O$ of 8.2 to 9.3 ‰ for whole-rock) based on limited samples from the Brewer area. However, because of the multi-phase magmatic-hydrothermal brecciation and fracturing during the mineralization, the meteoric water contribution could have varied greatly in time and space.

The Brewer hydrothermal system may represent a slightly deeper environment than the typical epithermal system. The magmatic fluid may have played a more predominant role than in a shallow environment where meteoric water may be dominant, such as a near surface system. The CO_2 that released from the magma in miscible with H_2O was trapped in the system before the CO_2 escape. Meteoric water was probably introduced into system to form lower salinity, H_2O-rich hydrothermal fluid during late stage of the mineralization.

CONCLUSIONS

Microthermometric and microchemical analyses of fluid inclusions in the Brewer Mine have revealed the characteristics of the mineralizing fluid and physiochemical

conditions of mineralization and hydrothermal alteration. The information provides important constraints on the gold transport and precipitation mechanism and the genetic model for the Brewer Mine.

1. Homogenization temperatures of primary and pseudosecondary fluid inclusions indicate that the hydrothermal fluids are likely have temperatures between 160 and 330 °C. The widespread range in temperatures probably reflects the multiple-phased, repeated brecciation and hydrofracturing during mineralization. The temperatures could be up to 100 °C higher if relatively higher fluid pressure prevails during mineralization. The fluid pressure required for decrepitation of CO_2-rich inclusions that is common in the Brewer samples would probably be in excess of 1000 bars.

2. The fluid inclusion data suggest that the fluids related to the gold mineralization in the Brewer are H_2O-CO_2 fluids with various CO_2 contents. The fluids have low to moderate salinity (<15 wt% NaCl. eq.) and contain many metal components, including K, Ca, Ti, Cr, Mn, Fe, Ni, Cu, and Zn. The fluids are probably SO_4^{2-}-rich, at least during late stage of the mineralization and relatively oxidized. The fluids have high Fe and may contain As and F.

3. Heterogeneous trapping is probably the dominant process for the variable fluid inclusions and CO_2:H_2O ratio. However, boiling (phase seperation) could have played some roles for the formation of CO_2-rich inclusions.

4. A magmatic source appears to be the most feasible source for the mineralizing fluids. Hydrofracturing and brecciation in the Brewer Mine suggest the processes most likely accompany the release of aqueous fluids from a deep-seated felsic magma (high aluminosilicate melt). The magma probably provides both the heat and fluid source for the mineralization, as well as responsible for the volcanic activities in the area, either during or prior to the mineralization. The mineralization at Brewer probably is syn-volcanic origin.

5. The Brewer hydrothermal system may represent a slightly deeper environment than the typical epithermal system, with magmatic fluid probably played a more predominant role than these in a shallow environment. Meteoric water is likely involved in the process by mixing with the magmatic fluid, especially during later stage of mineralization, as indicated by salinity-Th relationship and presence of mostly secondary H_2O-rich aqueous inclusion.

ACKNOWLEDGMENTS

Thanks to Bob Bodnar and Frank Harrison of Virginia Tech for helping the LRM analysis. Mark Rivers, Steve Sutton, Sasa Bajt of Brookhaven National Laboratory, and Tom Skulski of Rensselaer Polytechnic Institute helped in the SXRF microprobe analysis. I thank Westmont Mining Inc. and Brewer Gold Co. for providing access to the mine and field assistance. Mark Zwaschka, Jae Stonehouse, and John Scheetz of the Brewer Gold Co. gave some insights of the Mine geology. The following grants supported this study: Geological Society of America (1991), Sigma Xi (1991), Geological Society of America Southeastern Section (1992), and Discretionary Funds of the Department of Geological Sciences at the University of Tennessee (1991 and 1992).

REFERENCES

Baker, E. M. and Andrew, A. S., 1991, Geologic, fluid inclusion, and stable isotope studies of the gold-bearing breccia pipe at Kidston, Queensland, Australia: Economic Geology, v. 86, p. 810-830.

Bell, H., III, Carpenter, R. H., and Feiss, P. G., 1980, Volcanogenic ore deposits of the Carolina slate belt: in Frey, R.W., ed., Excursions in southeastern geology, p. 149-178.

Berger, B. R. and Henley, R. W., 1988, Advances in the understanding of epithermal gold-silver deposits, with special reference to the western United States: in Keays, R. R. and Skinner, B. J., eds., The geology of gold deposits: the perspective in 1988, Economic Geology Monograph 6, p. 405-423.

Bodnar, R. J., Reynolds, T. J., and Kuehn, C. A., 1985, Fluid inclision systematics in epithermal systems: in Berger, B. R., and Bethke, P. M. (eds), Geology and Geochemistry of Epithermal Systems: Society of Economic Geologists, Reviews in Economic Geology, v. 2, P. 73-97.

Bowers, T.S., and Helgeson, H.C., 1983, Calculation of the thermodynamic and geochemical consequences of non-ideal mixing in the system H_2O-CO_2-NaCl on the phase relations in geologic systems: equation of state for H_2O-CO_2-NaCl fluids at higher temperatures and pressures. Geochimica et Cosmochimica. Acta, v. 45, p. 225-228.

Brown, P. E., 1989, FLINCOR: a microcomputer program for the reduction and investigation of fluid inclusion data. American Mineralogist, v. 74, p. 1390-1393.

Brown, P. E., and Lamb, W. M., 1989, P-V-T properties of fluids in the system H_2O+CO_2+NaCl: New graphical presentations and implications for fluid studies: Geochimica et Cosmochimica. Acta, v. 53, p. 1200-1021.

Browne, P.R.L., Roedder, E., and Wodzicki, A., 1976, Comparison of past and present geothermal waters, from a study of fluid inclusions, Boardland Field, New Zealand. In Cadek, J., Paces, T., ed., Proceedings International Symposium on Water-rock Interaction, Czechoslovakia, 1974, Geol. Survey, Prague, p. 140-149.

Buchanan, L. L., 1981, Precious metal deposits associated with volcanic environments in the southwest: Arizona Geological Society Digest, v. 14, p. 237-261.

Burnham, C. W., and Ohmoto, H., 1980, Late-stage processes of felsic magmatism., Soc. Mining Geol. Japan, Special Issue 8, p. 1-11.

Burnham, C. W., 1979, Magma and hydrothermal fluids. In Geochemistry of hydrothermal ore deposits, 2nd ed., H.L. Barnes, ed., J. Wiley and Sons, New York, p. 71-136.

Burnham, C. W., 1985, Energy release in subvolcanic environments: implications for breccia formation: Economic Geology, v. 80, p. 1515-1522.

Burruss, R. C., 1981, Analysis of phase equilibria in C-O-S fluid inclusions: in Hollister, L.S. and Crawford, M. L., eds, Fluid inclusion: Application to Petrology, p. 39-74.

Butler, J. R. and Secor, D. T., 1991, The Central Piedmont: in J. W. Horton, Jr and V. A. Zulla, eds, The geology of Carolinas, University of Tennessee Press., p. 59-78.

Butler, J. R., 1985, The Brewer mine: in Feiss, P. G., ed., Volcanic-hosted gold and high alumina rocks of the Carolina slate belt: Guidebook for field trip, 1985 SGE fall meeting and 1985 GSA annual meeting, p. 143-199.

Butler, J. R., 1991, Metamorphism: in J. W. Horton, Jr and V. A. Zulla, eds, The geology of Carolinas, University of Tennessee Press., p. 127-141.

Butler, J. R., Scheetz, J. M., Stonehouse, J. M., Tayler, D. R., and Callaway, R. Q., 1988, The Brewer gold mine, Chesterfield County, South Carolina: Guidebook for field trip of the annual GSA meeting, Southeastern section, 22p.

Cameron, E. M. and Hattori, K., 1987, Archean gold mineralization and oxidized hydrothermal fluids: Economic Geology, v. 82, p. 1177-1191.

Cathles, L. M., 1986, The geologic solubility of gold from 200-350°C, and its implications for gold-base metal ratios in vein and stratiform deposits: in Clark, L. A., ed., Gold in the western shield, p. 187-210.

Clynne, M. A., and Potter, R. W., II, 1977, Freezing point depression of synthetic brines (abstract). Geol. Soc. Am. Abstr. programs, v. 9, 930.

Collins, P. I. F., 1979, Gas hydrates in CO_2-bearing fluid inclusions and the use of freezing data for estimation of salinity: Economic Geology, v. 74, p. 1435-1444.

Colvine, A. C., Andrews, A. J., Cherry, M. E., Durocher, M. E., Fyon, A. J., Lavigne, M. J., Jr., MacDonald, A. J., Marmont, S., Poulsen, K. H., Springer, J. S., and Troop, D. G., 1984, An integrated model for the origin of Archean Lode gold deposits: Ontario Geological Survey Open File Report 5524, 84p.

Crawford M. L. (1981) Phase equilibria in aqueous fluid inclusions. Mineral. Assoc. Canada Short Course Handbook 6, 75-100.

Cunningham, C, G., Arribas, Jr. A., Rytuba, J.J., and Arribas, A., 1990, Mineralized and unmineralized calderas in Spain; Part I, evolution of the Los Frailes caldra: Mineral deposita, v. 25 (suppl.), p. S21-S28.

Dowling, K. and Morrison, G., 1988, Application of quartz textures to the classification of gold deposits using North Queensland examples: in Keays, R. R. and Skinner, B. J., eds., The geology of gold deposits: the perspective in 1988, Economic Geology Monograph 6, p. 342-355.

Duckett, R.P., Evans, P. H., and Gillon, K. A., 1988, Economic geology of the Ridgeway gold deposits, Fairfoield County, South Carolina: in Secor, D.T., Jr., ed., Southeastern geological excursions: GSA Southeastern Section, p. 4--44.

Etz, E. S., 1979, Raman microprobe analysis: principles and application: Scanning Electron Microscopy, p. 67-82.

Feiss, P. G., 1982, Geochemistry and tectonic setting of the volcanics of the Carolina slate belt: Economic Geology, v. 77, p. 273-293.

Feiss, P. G., 1985, Gold mineralization in the Carolina slate belt: Speculations on ore genesis: in Misra, K. C., ed., Volcanogenic sulfide and precious metal mineralization in the southern Appalachians: University of Tennessee, Department of Geological Sciences, Studies in Geology 16, p. 220-236.

Feiss, P. G., Maybin, A. H., III, Riggs, S.R., and Grosz, A. E., 1991, Mineral resources of the Carolinas: in J. W. Horton, Jr and V. A. Zulla, eds, The geology of Carolinas, University of Tennessee Press., p. 319-345.

Field, C. W. and Fifarek, R. H., 1985, Light stable-isotope systematic in the epithermal environment: in Berger, B. R., and Bethke, P. M. (eds), Geology and Geochemistry of Epithermal Systems: Society of Economic Geologists, Reviews in Economic Geology, v. 2, P. 99-128.

Fleming, A. W., Handley, G. A., Williams, K. L., Hills, A. L., and Corbett, G. J., 1986, The Porgera gold deposit, Papua New Guinea: Economic Geology, v. 81, p. 660-680.

Ford, M. M., 1981, A fluid inclusion and petrographic study of barren and gold-mineralized quartz veins in the central and southern Carolina slate belt, North Carolina: M.S. Thesis, University of North Carolina, Chapel Hill, North Carolina, 72p.

Fournier, R, O., 1988, Silica minerals as indicators of conditions during gold deposition: in Tooker, E. W., ed., Geologic characteristics of sediment- and volcanic-hosted disseminated gold deposits--search for an occurrence model; U. S. Geological Survey Bulletin 1646, p. 15-26.

Frantz, J. D., Mao, H. K., Zhang, Y., Wu, Y., Thompson, A.C., Underwood, J.H., Giauque, R.D., Jones, K.W., and Rivers, M.L., 1988, Analysis of fluid inclusions by X-ray fluorescence using synchrotron radiation: Chemical Geology, v. 69, p. 235-244.

Fyfe, W. S., 1986, The transport and deposition of gold: in Clark, L. A., ed., Gold in the western shield, p. 156-167.

Fyfe, W. S., and Kerrich, R., 1984, Gold: natural concentration processes: in Foster, R. P., ed., Gold'82; The geology, geochemistry and genesis of gold deposits: Rotterdam, A. A. Balkema, p. 99-127.

Gallaher, V., Feely, M., Hodelsberger, H., Tenkin, G.R.T., and Fallick, A. E., 1992, Geological, fluid inclusion and stable isotope studies of Mo mineralization, Galway granite, Ireland: Mineral Deposita, v. 27, p. 314-325.

Hatcher, R. D., Jr., 1972, Development model for the southern Appalachians: Geological Society of America Bulletin, v. 83, p. 2735-2760.

Hayba, D. O., Bethke, P. M., Heald, P., and Foley, N. K., 1985, Geologic, mineralogic, and geochemical characteristics of volcanic- hosted epithermal precious-metal deposits: in Berger, B. R., and Bethke, P. M. (eds), Geology and Geochemistry of Epithermal Systems: Society of Economic Geologists, Reviews in Economic Geology, v. 2, p. 129-167.

Heald, P., Foley, N. K., and Hayba, D. O., 1987, Comparative anatomy of volcanic-hosted epithermal deposits: acid-sulfate and adularia-sericite types: Economic Geology, v. 82, p. 1-26.

Hedenquist, J. W., and Henley, R. W., 1985, The importance of CO_2 on freezing point measurements of fluid inclusions: Evidence from active geothermal systems and implications for epithermal ore deposition: Economic Geology, v. 80, p. 1379-1406.

Hemley, J. W., Montoya, J. W., Marinenko, J. W., and Luce, R. W., 1980, Equilibria in the system Al_2O_3-SiO_2-H_2O and some general implications for alteration/mineralization processes: Economic Geology, v. 75, p. 210-228.

Henley, R. W. and Ellis, A. J., 1983, Geothermal systems ancient and modern: a geochemical review: Earth Sciences Review, v. 19, p. 1-50.

Henley, R. W., 1985, The geothermal framework of epithermal deposits: in Berger, B. R., and Bethke, P. M. (eds), Geology and Geochemistry of Epithermal Systems: Society of Economic Geologists, Reviews in Economic Geology, v. 2, p. 1-24.

Henley, R. W., 1991, Epithermal gold deposits in volcanic terranes: in Foster, R.P. ed., Gold metallogeny and exploration, p. 133-164.

Holland, H. D., 1965, Some applications of thermochemical data to problems of ore deposits, II. Mineral assemblages and the composition of ore-forming fluids: Economic Geology, v. 60, p. 1101-1166.

Holland, H. D., 1967, Gangue minerals in hydrothermal deposits, in Barnes, H.L., ed., Geochemistry of hydrothermal ore deposits: New York, p. 382-436.

Hollister, L. S., 1988, On the origin of CO_2-rich fluid inclusions in migmatites: Journal of metamorphic Geology, V. 6, p. 467-474.

Hollister, L. S., 1990, Enrichment of CO_2 in fluid inclusions in quartz by removal of H_2O during crystal-plastic deformation: Journal of Structural Geology, v. 12, p. 895-901.

Jaacks, J. J., 1986, Geochemical orientation survey of the Brewer property, Chesterfield County, South Carolina: internal report of Westmont Mining, 56p.

Kilinc I. A. and Burham C. W. (1972) Partitioning of chloride between a silicate melt and coexisting aqueous phase from 2 to 8 kilobars. Econ. Geol. 67, 231-235.

Klein, T. L., and Criss, R. E., 1988, An oxygen isotope and geochemical study of meteoric-hydrothermal systems at Pilot Mountain and selected other localities, Carolina slate belt: Economic Geology, v. 83, p. 801-821.

Krupp, R. E. and Seward, T. M., 1987, The Rotokawa geothermal system, New Zealand: an active epithermal gold-depositing environment: Economic Geology, v. 82, p. 1109-1129.

Lipman, P. W., Fisher, F. S., Mehnert, H. H., Naeser, C. W., Luedke, R. G., and Steven, T. A., 1976, Multiple ages of Mid-Tertiary mineralization and alteration in the western San Juan Mountains, Colorado: Economic Geology, v. 71, p. 571-588.

Long, L. T., 1979, The Carolina slate belt-- Evidence of a continental rift zone: Geology, v. 7, p. 180-184.

Lu, C., Misra, K. C., Stonehouse, J. M., and Zwaschka, M. R., 1992, Geochemical signatures of alteration in Brewer gold mine, South Carolina: South Carolina Geology. v. 35, p. 37-54.

McKeng, S. A. and Craw, D., 1989, Contrasting fluid in gold-bearing quartz vein systems formed progressively in a rising metamorphic belt: Otago Schist, New Zealand: Economic Geology, v. 84, p. 22-33.

Mernagh, T. P. and Wilde, A. R., 1989, The use of the laser Raman microprobe for the determination of salinity in fluid inclusions: Geochimica et Cosmochimica Acta, v. 53, p. 765-771.

Miller, B. M., 1982, A petrographic and fluid inclusion study of some Scheelite-bearing quartz veins, Cabarrus County, North Carolina: M.S. Thesis, University of North Carolina, Chapel Hill, North Carolina, 85p.

Moore, J. H., Adams, M. C., and Lexeux, M. M., 1992, The formation and distribution of CO_2-enriched fluid inclusiond in epithermal environments: Geochimica et Cosmochimica Acta, v. 56, p. 121-135.

Nader, J. and Shepherd, T.J., 1989, Role of methane and carbon dioxide in gold deposition: Nature, v. 342, p. 793-795.

Norman, D. I. and Sawkins, F. J., 1985, The Tribag breccia pipes: Precambrian Cu-Mo deposits, Batchawana Bay, Ontario: Economic geology, v. 80, p. 1593-1621.

Oepen, P.Sanger-von, Friedich, G., and Kisters, A., 1990, Comparison between the fluid characteristics of the Rodalquilar and two neighboring epithermal gold deposits in Spain: Mineral Deposita, v. 25(suppl.), p. 36-41.

Pasteris, J. D., Wopenka, B., and Seitz, J. C., 1988, Practical aspects of quantitative laser Raman microprobe spectroscopy for the study of fluid inclusions: Geochimica et Cosmochimica Acta, v. 52, p. 979-988.

Potter R. W., II, 1977, Pressure corrections for fluid-inclusion homogenization temperatures based on the volumetric properties of the system NaCl-H_2O. J. Res. USGS 5, 5:603-607.

Poutiainen, M., 1993, Fluid inclusion geochemistry of the early Proterozoic Pirila gold deposit in Rantasalmi, southeastern Finland: Mineral Deposita, v. 28, p. 129-135.

Ramboz, C., Pichavant, M., and Weisbrod, A., 1982, Fluid immiscibility in natural processes. use and misuse of fluid inclusion data. II. Interpretation of fluid inclusion data in terms of immiscibility: Chemical Geology, v. 37, p. 29-48.

Rankin, A. H., Ramsey, M.H., Coles, B., Langevelde, F. Van, and Thomas, C.R., The composition of hypersaline, iron-rich granitic fluids based on laser-ICP and Synchrotron-XRF microprobe analysis of individual fluid inclusions in topaz, Mole granite, eastern Australia: Geochimica et Cosmochimica Acta, v. 56, p. 67-79.

Rankin, D. W., 1975, The continental margin of eastern North America in the southern Appalachians: The opening and closing of the proto-Atlantic Ocean: American Journal of Science, v. 275-A, p. 298-336.

Robert, F., and Kelly, W. C., 1987, Ore-forming fluids in Archean gold-bearing quartz veins at the Sigma Mine, Abitibi greenstone belt, Quebec, Canada: Economic Geology, v. 82, p. 1464-1482.

Roedder E. and Bodnar, R.J., 1980, Geologic pressure determination from fluid inclusion studies. Annual Review Earth Planetary Sciences, v. 8, p. 263-301.

Roedder E., 1984, Fluid inclusions. Review in Mineralogy No. 12. Mineral. Soc. Amer.

Roedder, E., 1967, Fluid inclusions as samples of ore fluids: In H.L. Barnes, ed., Geochemistry of hydrothermal ore deposits. Rinehart & Winston, New York, p. 515-574.

Roedder, E., 1984, Fluid inclusion evidence bearing on the environments of gold deposition: in Foster, R. P., ed., Gold'82; The geology, geochemistry and genesis of gold deposits: Rotterdam, A.A. Balkema Pub., p. 129-164.

Rogers, J. J., 1982, Critia for recognizing environments of formation of volcanic suites; Application of these critia to volcanic suites in the Carolina slate belt: Geological Society of America Special Paper 191, p. 99-107.

Romberger, S. B., 1986, The solution chemistry of gold applied to the origin of hydrothermal deposits: in Clark, L. A., ed., Gold in the western shield, p. 168-112.

Romberger, S. B., 1988, Geochemistry of gold in hydrothermal deposits: U. S. Geological Survey Bulletin 1857-A, p. 9-25.

Rosasco, G. J. and Roedder, E., 1979, Application of a new Raman microprobe spectrometer to nondestructive analysis of sulfate and other ions in individual phases in fluid inclusions in minerals: Geochimica et Cosmochimica Acta, v. 43, p. 1907-1915.

Rushton, R. W., Nesbitt, B. E., Muehlenbachs, K., and Mortensen, J. K., 1993, A fluid inclusion and stable isotope study of Au quartz veins in the Klondike district, Yukon Territory, Canada: A section through a mesothermal vein system: Economic Geology, v. 88, p. 647-678.

Scheetz, J. W., 1991, The geology and alteration of the Brewer gold mine, Jefferson, South Carolina: M.S. Thesis, University of North Carolina, Chapel Hill, 180p.

Scheetz, J. W., Stonehouse, J. M., and Zwaschka, M. R., 1991, Geology of the Brewer gold mine in South Carolina: Mining Engineering, v. p. 38-42.

Schmidt, R. G., 1978, The potential for porphyry copper-molybdenum deposits in the eastern United States: U. S. Geological Survey Professional Paper 907-E, 31 p.

Schmidt, R. G., 1985, High-alumina hydrothermal systems in volcanic rocks and their significance to mineral prospecting in the Carolina slate belt: U. S. Geological Survey Bulletin 1562, 59 p.

Schwartz, M. O., 1989, Determining phase volumes of mixed CO_2-H_2O inclusions using microthermometric measurements: Mineral Deposita, v. 24, p. 43-47.

Secor, D. T., Jr., 1988, Review of the geology of the Carolina Slate Belt: in Secor, D. T., Jr., ed., 1988, Southeastern Geological Excursions: Guidebook for Geological Society of America, p. 1-18.

Secor, D. T., Jr., Samson, S. L., Snoke, A. W., and Palmer, A. R., 1983, Confirmation of the Carolina Slate Belt as an exotic terrane: Science, v. 221, p. 649-651.

Seward, T. M., 1973, Thio complexes of gold and transport of gold in hydrothermal ore solutions: Geochimica Cosmochimica Acta, v 37, 379-399.

Seward, T. M., 1985, The transport and deposition of gold in hydrothermal systems: in Foster, R. P., ed., Gold'82; The geology, geochemistry and genesis of gold deposits: Rotterdam, A. A. Balkema, p. 165-179.

Seward, T. M., 1991, The hydrothermal geochemistry of gold: in Foster, R.P. ed., Gold metallogeny and exploration, p. 37-61.

Shepherd, T. J., Rankin, A. H., and Alderton, D.H.M., 1985, A practical guide to fluid inclusion studies: Blackie, 239p.

Silberman, M. L., and Berger, B. R., 1985, Relationship of trace- element patterns to alteration and morphology in epithermal precious-metal deposits; in Berger, B. R., and Bethke, P. M. (eds), Geology and Geochemistry of Epithermal Systems: Society of Economic Geologists, Reviews in Economic Geology, v. 2, p. 203-232.

Sillitoe, R. H. and Bonham, H. F., Jr., 1984, Volcanic landforms and ore deposits: Economic Geology, v. 79, p. 1286-1298.

Sillitoe, R. H., 1983, Enargite-bearing massive sulfate deposits high in porphyry copper deposits: Economic Geology, v. 78, p. 348-352.

Sillitoe, R. H., 1985, Ore-related breccias in volcanoplutonic arcs: Economic Geology, v. 80, p. 1467-1514.

Sillitoe, R. H., Baker, E. M., and Brook, W. A., 1984, Gold deposits and hydrothermal eruption breccias associated with a Maar volcano at Wau, Papua New Guinea: Economic Geology, v. 79, p. 638-655.

Smith, T. J., Cloke, P. L., and Kelser, S. E., 1984, Geochemistry of fluid inclusions from the McIntyer-Hollinger gold deposit, Tammins, Ontario, Canada: Economic Geology, v. 79, p. 1265-1285.

Sparks, C. J., Jr., 1980, X-ray fluorescence microprobe for chemical analysis: in Winick and Doniach ed. Synchrotron Radiation Research, Plenum, p. 459-512.

Steven, T. A., and Ratte, J. C., 1960, Geology and ore deposits of the Summitville district, San Juan Mountains, Colorado: U. S. Geological Survey Professional Paper 343, 70p.

Stoffregen, R. E., 1987, Genesis of acid-sulfate alteration and Au-Cu-Ag mineralization at Summitville, Colorado: Economic Geology, v. 82, p. 1575-1591.

Tomas, A. V. and Spencer, E.T.C., 1988, Fluid inclusions in the system H_2O-CH_4-NaCl-CO_2 from metasomatic tourmaline within the border unit of the Tanco zoned granitic pegmatite, S.E. Manitiba, Canada: Geochimica et Cosmochimica Acta, v. 52, p. 1065-1075.

Tomas, A. V. and Spencer, E.T.C., 1992, The volatile geochemistry of magmatic H_2O-CO_2 fluid inclusions from the Tanco zoned granitic pegmatite, southeastern Manitiba, Canada: Geochimica et Cosmochimica Acta, v. 56, p. 49-65.

Tomkinson, M. J., 1988, Gold mineralization in phyllonites at the Haile mine, South Carolina: Economic Geology, v. 83, p. 1392-1400.

Touray, J. C., Beny-Bassez, C., Dubessy, J., and Guilhaumou, N., 1985, Scanning electron microscopy, p. 103-118.

Vick, H. K., Channell, J. E. T., and Opdyke, N. D., 1987, Ordovician docking of the Carolina Slate Belt, paleomagnetic data: Tectonics, v. 6, p. 573-583.

Weir, R. H., Jr., and Kerrick, D. M., 1987, Mineralogic, fluid inclusion, and stable isotope studies of several gold mines in the Mother Lode, Tuolumne and Mariposa Counties, California: Economic Geology, v. 82, p. 328-344.

Whitney, J. A., Parks, T. A., Carpenter, R. H., and Hartby, M. E., III, 1978, Volcanic evolution of the southern slate belt of Georgia and South Carolina-- a primitive island arc: Journal of Geology, v. 86, p. 173-192.

Williams, H., and Hatcher, R. D., Jr., 1983, Appalachian suspect terranes: Geological Society of America Memoir 158, p. 33-53.

Worthington, J. T., 1993, The Carolina slate belt and its gold deposits: Reflections after a quartz century: South Carolina Geology, v. 35, p. 1-8.

Worthington, J. T., and Kiff, I. T., 1970, A suggested volcanogenic origin for certain gold deposits in the slate belt of the North Carolina Piedmont: Economic Geology, v. 65, p. 529-537.

Worthington, J. T., Kiff, I. T., Jones, E. M., and Chapman, P. E., 1980, Applications of the hot springs or fumarolic model in prospecting for lode gold deposits: Mining Engineering, v. 32, p. 73-79.

Zhang Y. and Frantz J. D. (1987) Determination of the homogenization temperatures and densities of supercritical fluids in the system NaCl-KCl-$CaCl_2$-H_2O using synthetic fluid inclusions. Chem. Geol. 64, 335-350.

Part 5

Ore-forming Consequences and Gold Precipitation in Hypogene Acid Sulfate Environments--a Numerical Approach

ABSTRACT

Reaction-path modeling of mineralization processes in epithermal acid-sulfate environments of volcanic terranes was carried out to investigate ore-forming consequences and transport and precipitation of gold. The calculations are based on multicomponent heterogeneous chemical equilibria among solids, gases, and an aqueous phase at specific T-P conditions. The fluid composition used was from the fluid inclusion data on the Brewer hydrothermal system and by assuming saturation with sulfide minerals. Calculations involving fluid-rock reaction and fluid-fluid mixing (simultaneous cooling) produced ore mineral assemblages compatible to those observed in the mineralized zone of the Brewer deposit throughout the reaction-path, suggesting that these processes could have been the primary contributing factors for the ore-forming sequence. Gold precipitation from the fluid in such environments appears to be affected by a pH increase due to fluid-rock reaction and desulfidation arising from the precipitation of sulfide minerals. Speciation calculations show that Au is primarily transported as $Au(HS)_2^-$ under reduced conditions, whereas $AuCl_2^-$ becomes more dominant under oxidized conditions. Other metals in the solution are present predominantly as chloride complexes. The common association of gold with pyrite is probably a major constraint on the nature of the dominant gold complex in the ore-forming fluid and the mechanism of gold precipitation.

INTRODUCTION

Field, petrologic, and geochemical studies of a mineral deposit can provide the essential information on its formation environment, mineralization style and association, fluid composition, and P-T condition. From this information, various geochemical processes can be inferred. It is these geochemical processes, involving changes of composition, temperature and pressure in complex multicomponent, multiphase systems that result in the formation of gold and other metal ores.

Metal transport and precipitation in various geologic environments are geochemical processes that can be understood in term of aqueous solution chemistry and chemical thermodynamics and kinetics. These processes can be investigated by numerical calculations by applying experimental data for chemical components to a specific system. Various studies (e.g., Reed, 1982; Reed and Spycher, 1985; Brimhall and Ghiorso, 1983) have shown the usefulness of numerical modeling to understand geochemical processes and dynamic mechanisms.

Gold mineralization at the Brewer Mine was formed in an acid sulfate magmatic hydrothermal environment (see Part 3). The gold mineralization, associated with many sulfide minerals, is hosted by multi-episodic hydrothermal breccias that intruded the rhyolitic volcanic rocks (Scheetz, 1991; Lu et al., 1993). The hydrothermal gold mineralization is suitable for the numerical modeling in that the system can be represented by multicomponent chemical equilibria and reaction processes. The modeling may provide information on effects of various geochemical processes (such as cooling, mixing, oxidation/reduction, and fluid-rock reaction) on the gold precipitation.

This paper reports a preliminary assessment of the reaction-path modeling of the ore-forming processes in an acid-sulfate environment. Although the models described

here are oriented toward the Brewer system, they should also be applicable to many other epithermal deposits similar to the Brewer.

MODELS

Programs SOLVEQ and CHILLER (Reed, 1982) were used for the numerical calculation of the ore-forming fluid composition, speciation, and reaction path. The SOLVEQ is a computer program for computing multicomponent homogeneous chemical equilibria in an aqueous system utilizing mass-balance and mass-action equations by the Newton-Raphson numerical technique. It computes the activities of all aqueous species, the saturation indices of the solid phases, and the fugacities of gases. It also computes partial heterogeneous equilibria, wherein concentration of undetermined species can be calculated by forced equilibria with specific minerals.

CHILLER is a program for computing multicomponent heterogeneous chemical equilibria among solids, gases, and an aqueous phase. It applies a Newton-Raphson numerical method to solve a system of mass-balance and mass-action equations, together with a heat balance equation if needed (Reed, 1982; Reed and Spycher, 1988). CHILLER can be used for modeling various geochemical path calculations, including cooling-heating, boiling and condensation, fluid-fluid mixing, and fluid-rock reaction (Reed, 1982; Reed and Spycher, 1985).

NUMERICAL MODELING OF ORE-FORMING PROCESS AND GOLD PRECIPITATION

A series of calculations were carried out to model various geochemical processes that could have contributed to the gold mineralization and hydrothermal alteration in a hydrothermal system. These calculations utilized different fluid compositions and physiochemical conditions. A few calculations are discussed below in detail.

Composition of Ore-forming Fluid

The fluid compositions used in the model were obtained from fluid inclusion studies and calculations of mineral saturation. The Brewer fluid inclusion data constrain the temperature, composition, and salinity of the fluid responsible for the gold mineralization (see Part 4). A T-P condition of 300 °C and 1000 bars probably prevailed during the mineralization. This information provides essential guidance in building a reasonable initial fluid composition for the numerical model, but it leaves much to be estimated using mineralogical constraints, especially the concentration of metals. Studies of geothermal fluids (Ellis, 1979; Weissberg et al., 1979; Roedder, 1984a, 1984b, 1979; Barnes, 1979; Krupp and Seward, 1987) have presented various compositions. Precipitates formed from well discharge which formed rapidly in response to steam loss, oxidation, and cooling of discharge of the fluid in many geothermal systems, often show high contents of many metals, suggesting that the metals are transported in geothermal fluids in significant quantities. Barnes and Czamanske (1967) argued that the concentration of common base and ferrous metals in ore-forming fluid must be at least 10 ppm.

The computer program SOLVEQ (Reed, 1982) was used to set up the fluid composition (Table 1) as follows:

a) Set Na^+ and Cl^- concentrations at values compatible with the Brewer fluid inclusion salinity, which ranges from 0.2 to 14.8 % NaCl equivalent corresponding to 0.03 to 2.5 molalities.

b) A 4.0 molal CO_2 concentration of the fluid is assumed based on fluid inclusion data.

c) Set SiO_2 concentration for quartz saturation, as quartz is an ubiquitous mineral in the Brewer Mineral assemblages.

d) Assume that Al^{+++} concentration is similar to that in geothermal systems, a value that also provides for aluminum phyllosilicate (kaolinite) saturation.

e) Assume that the concentration of aqueous K^+ to values be saturated with alunite, a characteristic mineral in the acid sulfate environment. The Na^+/K^+ ratio is in the same range as those of volcanic-hosted geothermal systems (Henley and Ellis, 1983; Ellis, 1979).

f) Set Fe^{++} concentration for pyrite saturation, as pyrite is the most abundant and widespread sulfide in the mineralized and alteration zones.

g) Set Cu^+ to saturate with the least soluble Cu sulfide mineral (bornite). Set Zn^{++} and Pb^{++} to values that slightly less than Cu^+ as observed in the Brewer Mine where sphalerite and galena are very minor relative to Cu sulfide minerals.

h) Set Au^+ to a value slightly undersaturated with gold and set Ag^+ to a value slightly smaller than the Au^+.

i) Assume As^{+++} and Sb^{+++} values that are in equilibrium with enargite and tetrahedrite, respectively.

j) Set HS^- concentration to a value in the same magnitude as the molal sum of Cu^+, Pb^{++}, Zn^{++}, and Fe^{++}. Set SO_4^{2-} concentration at values similar to or slightly larger than HS^-. This allows pyrite is closer to saturation than hematite, resulting in precipitation of pyrite instead of hematite when the reaction proceeds.

k) Set pH at 3.5, a value selected based on the advanced argillic alteration and sulfide minerals. Many geothermal waters are acidic, with some fluid having extremely low pH, especially in acid sulfate system, such as at Matsukawa, Japan and Matsao, Taiwan (Ellis, 1979).

Various processes, including fluid-rock reaction, fluid-fluid mixing, and cooling, were modeled using fluid composition given in Table 1 as the starting fluid composition. The calculations were carried out using the computer program CHILLER (Reed, 1982).

Table 1. Composition of ore-forming fluid and reactant used in reaction-path modeling

Parameter	Ore fluid	Determinated by
T (°C)	300	fluid inclusion
P (bar)	1000	fluid inclusion
pH	3.5	acid sulfate system
(in molality)		
Cl^-	1.96E+00	fluid inclusion
SO_4^{2-}	7.00E-03	relation to HS^-
HS^-	5.00E-03	relation to metals
HCO_3^-	4.00E+00	fluid inclusion
Na^+	1.90E+00	fluid inclusion
K^+	5.00E-02	alunite saturation
SiO_2 (aq)	8.76E-03	quartz saturation
Al^{+++}	4.74E-03	kaolinite saturation
Ca^{++}	3.86E-07	estimated based on absence of bearing minerals
Mg^{++}	4.10E-08	estimated based on absence of bearing minerals
Fe^{++}	4.52E-03	pyrite saturation
Cu^+	2.77E-03	bornite saturation
Zn^{++}	2.00E-03	ratios with Cu from the Brewer mine
Pb^{++}	2.00E-03	ratios with Cu from the Brewer mine
Sb^{+++}	2.35E-05	tetrahedrite saturation
Ag^+	8.00E-09	similar to gold
Au^+	2.26E-08	undersaturated slightly to gold
As^{+++}	1.09E-03	enargite saturation
Volcanic rock (in wt%)		
SiO_2	7.37E+01	Chemical analyses of host rock at Brewer
H_2O	2.87E+00	
Al_2O_3	1.46E+01	
FeO	2.79E+00	
MgO	4.50E-01	
CaO	6.00E-02	
Na_2O	1.42E+00	
K_2O	3.03E+00	
ZnO	6.50E-03	
CuO	2.10E-03	
PbO	2.30E-03	

For fluid-rock model, an isothermal reaction of the fluid with host rock was calculated by a stepwise titration into the fluid at 300 °C in a close and in an open system. In the closed system setting, minerals were not fractionated as they formed, thus the calculations can be regarded as applying to a single "reaction front" where early-formed minerals can back-react and where the fluid does not move away from the reaction site. In the open system setting, minerals were removed from the system after they precipitated. The composition of volcanic rock (rhyolitic) used (Table 1) is from the whole-rock chemical analyses of host volcanic rock in the Brewer (Table 1 in Part 2). For fluid-fluid mixing model, the fluid was mixed with pure water of 25 °C incrementally, thus representing a simultaneous cooling and dilution process.

Results

The results of various models are shown in Figs. 1, 2, and 3. Figure 1 shows the progressive titration of rhyolite into the fluid in an open system, expressed in terms of grams of rhyolitic rock per kilogram of initial aqueous phase. Figure 2 is the fluid-rock reaction in a close system. Figure 3 shows the fluid-fluid mixing as the pure water in terms of kilograms is added stepwise to 1 kilogram of the hydrothermal fluid.

As rhyolite is titrated into the fluid that is initially saturated with quartz, pyrite, and alunite (Fig. 1a), these minerals start to precipitate by the following reactions:

$$SiO_2\ (aq) = SiO_2 \qquad (1)$$

(quartz)

$$Fe^{++} + 0.25\ SO_4^{2-} + 1.75\ HS^- + 0.25\ H^+ = FeS_2 + H_2O \qquad (2)$$

(pyrite)

$$K^+ + 3\ Al^{+++} + 2\ SO_4^{2-} + 3\ H_2O = KAl_3(SO_4)_2 + 6\ H^+ \qquad (3)$$

(alunite)

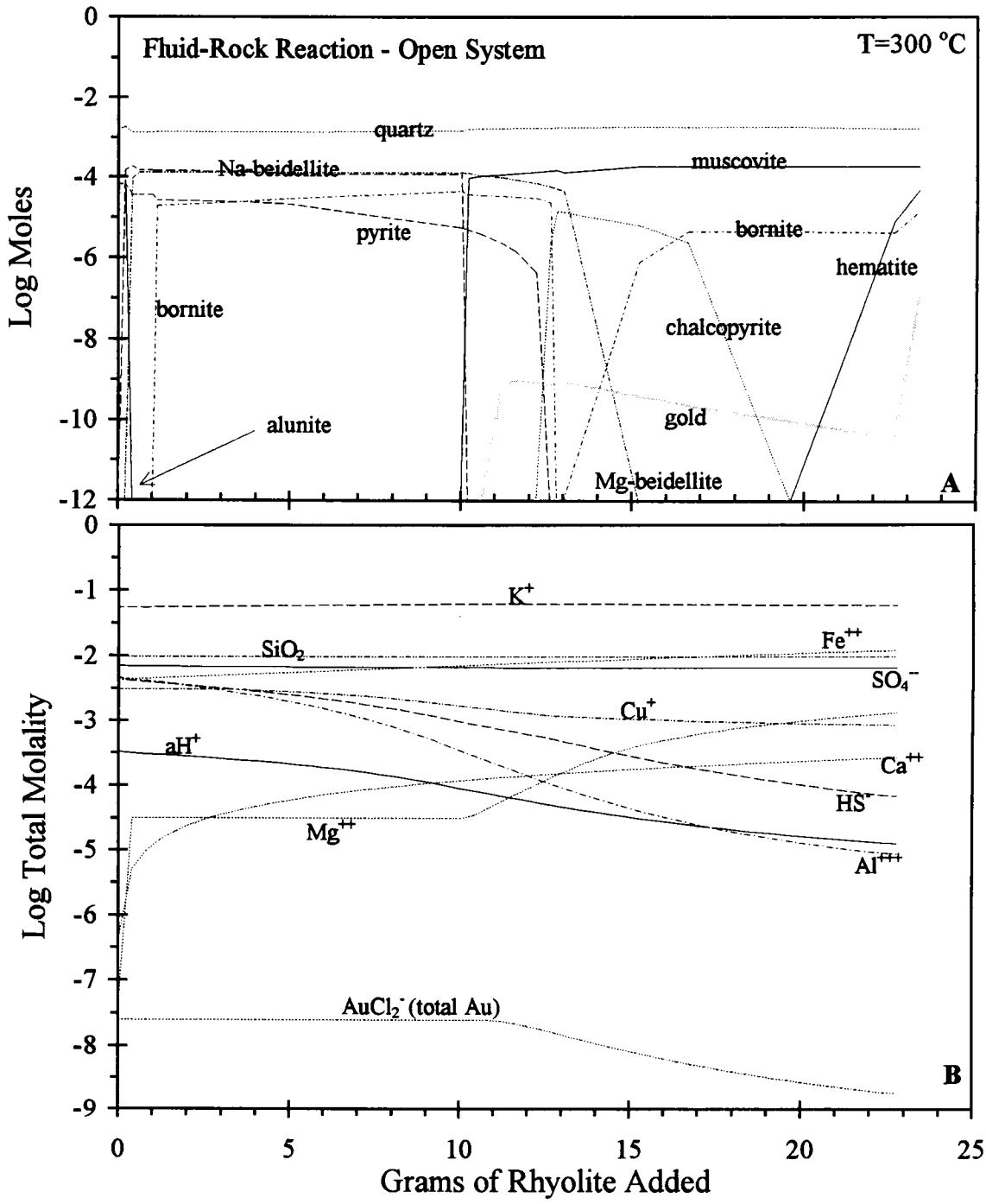

Fig. 1. Results of titration of rhyolite into mineralizing fluid of initial composition given in Table 1 for an open system. a) gold, sulfide, and silicate minerals precipitated along the reaction-path. b) composition of the aqueous phase, showing total molalities of selected component species. Na, Cl^-, and HCO_3^- are off scale at the top. See text for discussion.

The presence of quartz buffers aqueous silica throughout the rest of reactions, as shown by constant SiO_2(aq) molality (Fig. 1b). Alunite stops precipitating as the other Al-bearing minerals start to precipitate. In this model, the other Al-bearing mineral is beidellite, probably due to the high Na concentration in the fluid:

$$0.0825\ Mg^{++} + 0.165\ Na^{+} + 2.33\ Al^{+++} + 3.67\ SiO_2 + 4.66\ H_2O = (Mg_{.0825},Na_{.165})Al_{2.33}Si_{3.67}O_{10}(OH)_2 + 7.32\ H^{+} \quad (4)$$

(beidellite)

Bornite begins to form in response to a decrease in a_{H^+} (increasing pH) because the consumption of H^+ by the dissolution of reactant rock exceeds production of H^+ by the precipitation of sulfides and aluminosilicate minerals.

$$0.125\ SO_4^{2-} + 5\ Cu^{+} + Fe^{++} + 3.875\ HS^{-} = Cu_5FeS_4 + 2.875\ H^{+} + 0.5\ H_2O \quad (5)$$

(bornite)

The precipitation of bornite results in a slight drop in pyrite precipitation rate as both of them compete for Fe^{++} and HS^-. HS^- decreases with the precipitation of bornite and pyrite (Fig. 1b). As 10 gm of rhyolitic rock is added to the fluid, muscovite begins to form and Na-beidellite stops, because the Al^{+++} is used to precipitate muscovite and beidellite is a less stable phase:

$$K^{+} + 3.0\ Al^{+++} + 3.0\ SiO_2(aq) + 6.0\ H_2O = KAl_3Si_3O_{10}(OH)_2 + 10\ H^{+} \quad (6)$$

(muscovite)

Gold starts to precipitate when 11 gm of rhyolite is added to the solution for reasons that will be discussed later. Precipitation of chalcopyrite is the response to the further increase in pH; it consumes Fe^{++} and Cu^+ that results in the termination of pyrite precipitation and a sharp decline in the deposition of bornite:

$$Fe^{++} + Cu^{+} + 1.875\ HS^{-} + 0.125\ SO_4^{2-} = CuFeS_2 + 0.5\ H_2O + 1.875\ H^{+} \quad (7)$$

(chalcopyrite)

Continuous precipitation of muscovite from the solution, which buffers the K^+ in the solution (Fig. 1b), causes Mg-beidellite to stop precipitating as Al^{+++} is consumed. Bornite begins to precipitate, replacing chalcopyrite due to increasing SO_4^{2-}/HS^- ratio in the solution (Fig. 1b). Further decline in HS^- concentration in the solution and increasing SO_4^{2-}/HS^- ratio results in the precipitation of hematite:

$$2\ Fe^{++} + 2.0\ H_2O + 0.25\ SO_4^{2-} = Fe_2O_3 + 0.25\ HS^- + 3.75\ H^+ \quad (8)$$

(hematite)

Figure 1b shows changes of total molality of the components in the fluid along the reaction path. The pH increase throughout the reaction path, from 3.5 at the start to 4.9 at the end of calculation. a_{H^+}, Al^{+++}, Cu, $AuCl_2^-$, HS^-, and SO_4^{2-} decrease because of the precipitation of gold, sulfides and aluminosilicate minerals. The increasing SO_4^{2-}/HS^- ratio suggests that the system become more oxidized along the path. Fe^{++}, Ca^{++}, and Mg^{++} increase because of the addition from the rhyolitic rock, although Fe^{++} is consumed to form sulfide minerals.

Fluid-rock reaction in a closed system (Fig. 2) produces similar mineral assemblages as discussed above. The major differences are the precipitation of pyrite throughout whole reaction path and the precipitation of paragonite at a late stage of the reaction. Because the precipitated mineral can be dissolved by reaction with fluid, formation of new mineral can be considered as replacement of previous mineral-- in the present case (Fig. 2a) chalcopyrite replaces bornite that results in a slightly slower decline of HS^- at the point of replacement (Fig. 2b). The replacement processes are best illustrated by the sudden changes in total molality of chemical components shown in Fig. 2b, corresponding to points of mineral changes (Fig. 2a).

Figure 3 shows the result of fluid (300 °C) mixing with pure water (25 °C) in an open system. Enargite, tetrahedrite-tennantite, covellite, pyrite, bornite, gold, alunite, and quartz precipitate from the fluid as water/fluid ratio increases (Fig. 3a). Molalities of

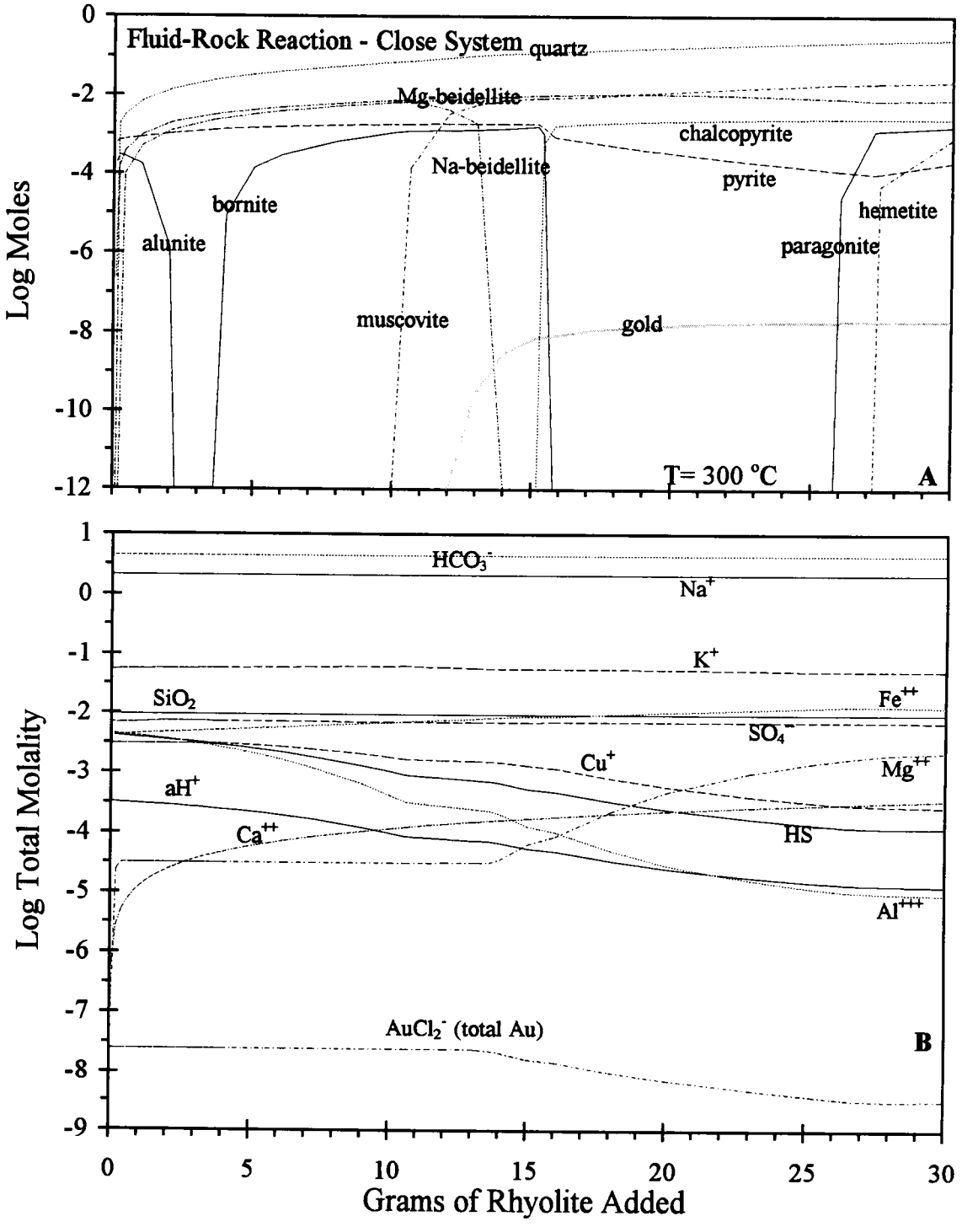

Fig. 2. Results of titration of rhyolite into mineralizing fluid of initial composition given in Table 1 for a close system. a). gold, sulfide, and silicate minerals precipitated along the reaction-path. b). composition of the aqueous phase, showing total molalities of selected component species.

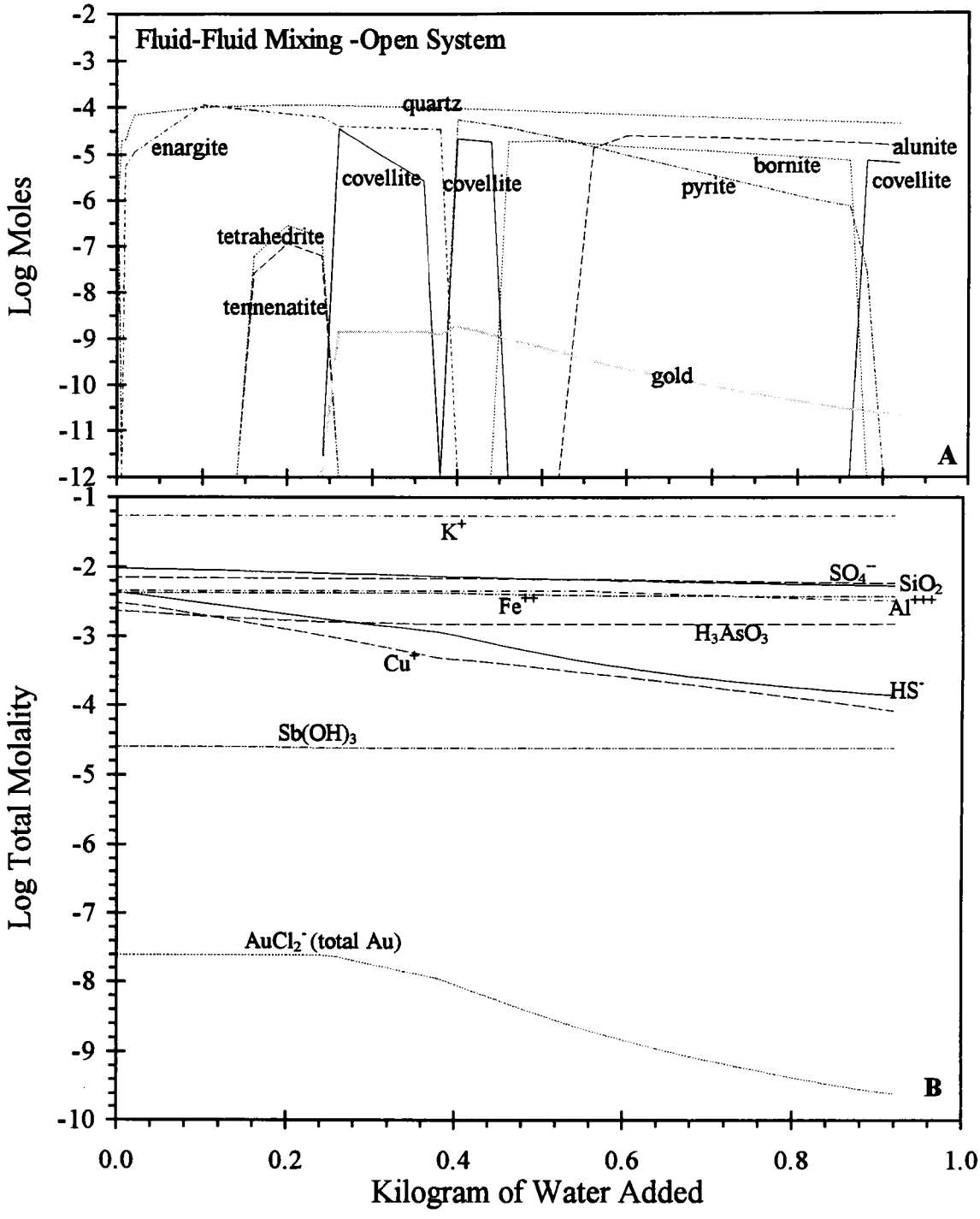

Fig. 3. Results of mixing of water with 1 kilogram of the mineralizing fluid of initial composition given in Table 1 for an open sysyem. a) gold, sulfide, and silicate minerals precipitated along the reaction-path. b) composition of the aqueous phase, showing total molalities of selected component species. Na, Cl^-, and HCO_3^- are off scale at the top.

all components decrease because of mineral precipitation and addition of H_2O (Fig. 3b). The temperature of the system changes from 300 °C at the start to 175 °C at the end of calculation. The precipitation of sulfide minerals is a result of decrease in temperature and dilution of the fluid as complexes of metals become less stable at lower temperature and in diluted fluid.

Discussions

Ore-forming mineral assemblages

Ore-forming mineral assemblages produced in various stages of calculation are observed in the Brewer Mine where pyrite is the dominant sulfide with various amounts of enargite, bornite, chalcopyrite, sphalerite, galena, and tetrahedrite (Fig. 1a, 2a. and 3a.). The calculations suggest that formation and mass of the ore-forming minerals are apparently controlled mainly by the fluid characteristics, particularly concentration in the initial fluid, the stability of mineral relative to other minerals, and concentrations of HS^- and SO_4^{2-} and HS^-/SO_4^{2-} ratio. Sphalerite, galena, and some minor minerals are present in the Brewer Mine, but they are not in the calculated mineral assemblages, primarily due to the fact that the assumed Pb and Zn concentrations are too low for the low-pH fluid. In fact, other trial runs using higher Pb and Zn concentrations produced sphalerite and galena along with pyrite. Calculations indicate that the factors driving the change of fluid composition, and thus controlling the sulfide mineral precipitation include fluid-rock reaction, temperature decrease, and dilution of fluid by fluid mixing. Another factor is contamination of the fluid by gases. Even though a combination of these processes commonly contributes to the precipitation of minerals, any of them may be particularly important for the formation of sulfide and other alteration minerals in certain environments. Pyrite is usually stable throughout the calculations here and other runs, suggesting that different processes could have contributed to its formation. This is in

good agreement with the widespread occurrence of pyrite in the Brewer system. The calculations show that the precipitation of enargite is promoted by a process of fluid-fluid mixing with decreasing temperature. In the mineralized pyrite-quartz breccia at Brewer, enargite occurs in small intrusive breccia pipes, consisting of enargite, pyrite, and quartz. In such an environment, fluid-fluid mixing and decrease in temperature could have played important roles for the formation of enargite, as suggested by the calculations. The limited occurrence of tetrahedrite and tennantite may also be the result of a particular process, such as the fluid-fluid mixing suggested here. Magmatic gas contamination of fluid in hypogene environment could have played a prominent role in the formation of the advanced argillic (acid sulfate) alteration in the Brewer system, as modeled by Brimhall and Ghiorso (1983).

The similarity of the mineral assemblages between in the Brewer deposits and those calculated by the chemical reaction-path models suggests that fluid-rock reaction and mixing with meteoric water with cooling were the likely processes that produced the ore-mineral deposition in the Brewer Mine. Quartz prevails throughout the calculations, consisting of more than 50% of the mass produced.

Although the present study has primarily focused on the ore-forming sulfides, silicate and aluminosilicate minerals produced in the calculations discussed here and in other trial runs are in general agreement with the mineral assemblages in the Brewer Mine. A fluid-rock reaction run using geothermal water analysis from the Rotokawa geothermal system, New Zealand, an active epithermal Au-depositing system which shows many similarities with Brewer, produced alteration mineral assemblages, ranging from argillic, sericitic to propylitic, and sulfide minerals which are similar to those in the Brewer Mine area.

Speciation of metal components in the fluid

Although many ligands can form complexes with metals under hydrothermal conditions, the most important are Cl^-, HS^- or H_2S, and OH^- (Barnes, 1979). Many species may form stable complexes with gold in hydrothermal ore-forming fluids (Seward, 1991; Romberger, 1982). Chloride and sulfide complexes of gold are considered to be the dominant forms in the fluid because chloride and hydrosulfide ions are present in appreciable concentrations in hydrothermal ore fluids (Barnes, 1979; Seward, 1972, 1991; Romberger, 1982, 1986).

In order to examine the dominant complexes of Au and other metals in the fluid, both SOLVEQ and CHILLER programs were used for speciation calculation for the initial fluid and during the reaction path. The speciation calculations show that $Au(HS)_2^-$ is the dominant species for Au in the initial fluid with a $Au(HS)_2^-$:$AuCl_2^-$ ratio of about 4:1. Other complexes include Au^+ and $Au_2H_2S_3$, but they have extremely low concentrations. Ag, Fe, Cu, Pb, and Zn are dominantly chloride-complexed. The dominant As and Sb complexes are H_2AsO_3 and $Sb(OH)_3$, respectively (Table 2). H_2S (aq) is the dominant form of reduced sulfur and HSO_4^- is more abundant than SO_4^{2-} in the initial fluid. H_2CO_3 is the dominant species for CO_2.

The complexes of gold vary along the reaction-path because of changes in sulfur species and gold precipitation (Fig. 4). The $Au(HS)_2^-$ molality decreases slightly with the precipitation of sulfide as a result of decreasing HS^- and H_2S in the fluid. The molalities of $Au(HS)_2^-$ and $AuCl_2^-$, as well as of other complexes, start to decrease rapidly with the precipitation of gold from the solution (Fig. 4). Chloride complexes of metals remain the dominant species for Fe, Cu, Zn, Pb, and Ag throughout the calculations.

Gold precipitation mechanisms

Gold precipitates in all the calculations (Fig. 1, 2, and 3). Because the fluid composition used is based on the fluid characteristics of the Brewer system at T-P

Table 2. Chemical speciation calculation of the fluid

Species	Molality	Log Molality	Activity	Log Activity
H+	1.54E-03	-2.8139	3.29E-04	-3.4823
Cl-	1.64E+00	0.2145	3.65E-01	-0.4379
SO4--	9.56E-04	-3.0197	2.90E-06	-5.5373
H2CO3	4.44E+00	0.6478	8.11E+00	0.9092
HCO3-	2.99E-04	-3.5243	7.81E-05	-4.1073
CO3--	1.21E-10	-9.9162	3.05E-13	-12.5164
HS-	2.54E-06	-5.5953	5.76E-07	-6.2398
S--	8.77E-16	-15.0571	2.20E-18	-17.6572
H2S aq.	4.34E-03	-2.3626	7.92E-03	-2.1011
HSO4-	5.00E-03	-2.3009	1.48E-03	-2.8308
AuCl2-	5.16E-09	-8.2875	1.15E-09	-8.9399
Au+	1.94E-14	-13.7125	5.47E-15	-14.2619
Au(HS)2-	1.99E-08	-7.7007	4.43E-09	-8.3532
Au2H2S3=	3.31E-14	-13.4798	8.32E-17	-16.0800
Ag+	5.92E-14	-13.2273	1.59E-14	-13.7983
AgCl	2.26E-12	-11.6462	2.26E-12	-11.6462
AgCl2-	2.33E-09	-8.6321	5.19E-10	-9.2846
AgCl3--	3.22E-09	-8.4920	8.09E-12	-11.0922
AgCl4---	3.72E-14	-13.4296	4.28E-20	-19.3688
AgHS	1.49E-13	-12.8277	1.49E-13	-12.8277
Ag(HS)2-	7.61E-16	-15.1187	1.69E-16	-15.7712
AgSO4-	1.31E-16	-15.8825	2.92E-17	-16.5350
Fe++	1.58E-05	-4.8004	2.19E-08	-7.6590
FeCl+	5.94E-05	-4.2261	1.68E-05	-4.7755
FeCl2	7.33E-06	-5.1349	7.33E-06	-5.1349
Fe+++	2.49E-14	-13.6033	9.66E-20	-19.0150
FeCl++	2.87E-11	-10.5415	4.88E-14	-13.3117
FeCl2+	4.05E-18	-17.3927	1.14E-18	-17.9421
FeCl3	4.71E-13	-12.3272	4.71E-13	-12.3272
FeCl4-	4.85E-13	-12.3139	1.08E-13	-12.9663
FeCl4--	4.24E-03	-2.3723	1.07E-05	-4.9724
FeOH+	4.05E-11	-10.3931	1.14E-11	-10.9424
Fe(OH)2	1.30E-13	-12.8859	1.30E-13	-12.8859
Fe(OH)3	1.04E-12	-11.9845	1.04E-12	-11.9845
Fe(OH)3-	3.12E-18	-17.5063	6.94E-19	-18.1588
Fe(OH)4-	1.19E-16	-15.9254	2.64E-17	-16.5779
FeSO4+	1.22E-14	-13.9153	3.43E-15	-14.4647
FeSO4	5.28E-09	-8.2770	5.28E-09	-8.2770
Cu+	2.43E-08	-7.6138	5.59E-09	-8.2528
Cu++	5.50E-12	-11.2595	9.34E-15	-14.0297
CuCl+	1.20E-08	-7.9206	3.39E-09	-8.4700
CuCl2	3.87E-09	-8.4118	3.87E-09	-8.4118
CuCl3-	6.38E-09	-8.1955	1.42E-09	-8.8479
CuCl4--	8.29E-08	-7.0816	2.08E-10	-9.6818
CuCl	5.66E-05	-4.2473	5.66E-05	-4.2473
CuCl2-X	8.52E-04	-3.0693	1.90E-04	-3.7218
CuCl3--X	2.16E-03	-2.6649	5.43E-06	-5.2650
Cu(HS)2-	1.49E-09	-8.8258	3.32E-10	-9.4782
CuH4S3-A	1.34E-11	-10.8734	2.98E-12	-11.5258
CuH4S3-B	1.44E-12	-11.8428	3.20E-13	-12.4953
CuOH+	1.02E-12	-11.9911	2.88E-13	-12.5404
CuSO4	3.83E-16	-15.4162	3.83E-16	-15.4162

Table 2. (continued)

Species	Molality	Log Molality	Activity	Log Activity
Pb++	4.50E-07	-6.3463	1.21E-09	-8.9176
PbCl+	1.22E-05	-4.9150	3.43E-06	-5.4644
PbCl2	2.91E-04	-3.5360	2.91E-04	-3.5360
PbCl3-	1.52E-03	-2.8182	3.38E-04	-3.4707
PbCl4--	3.99E-04	-3.3990	1.00E-06	-5.9991
PbCO3	2.47E-11	-10.6072	2.47E-11	-10.6072
Pb(HS)2	1.41E-10	-9.8523	1.41E-10	-9.8523
PbH4S3	3.95E-10	-9.4032	3.95E-10	-9.4032
Pb(HS)3-	4.86E-17	-16.3138	1.08E-17	-16.9662
PbOH+	6.18E-09	-8.2091	1.74E-09	-8.7584
Zn++	8.37E-09	-8.0772	1.16E-11	-10.9359
ZnCl+	7.46E-06	-5.1270	2.11E-06	-5.6764
ZnCl2	2.48E-05	-4.6048	2.48E-05	-4.6048
ZnCl3-	3.11E-04	-3.5070	6.93E-05	-4.1595
ZnCl4=	1.88E-03	-2.7261	4.72E-06	-5.3262
ZnHCO3+	1.13E-10	-9.9461	3.20E-11	-10.4954
Zn(HS)2	3.82E-09	-8.4174	3.82E-09	-8.4174
Zn(HS)3-	1.57E-13	-12.8037	3.50E-14	-13.4562
Zn(HS)4=	5.08E-18	-17.2940	1.28E-20	-19.8941
ZnOH+	1.80E-09	-8.7455	5.07E-10	-9.2949
ZnOH2	7.22E-18	-17.1413	7.22E-18	-17.1413
ZnSO4	7.47E-13	-12.1264	7.47E-13	-12.1264
H3AsO3	2.30E-03	-2.6383	2.30E-03	-2.6383
H2AsO3-	3.98E-09	-8.4006	9.87E-10	-9.0059
HAsO3--	9.91E-16	-15.0040	2.49E-18	-17.6041
AsO+	2.17E-05	-4.6638	6.12E-06	-5.2132
H3AsO4	4.04E-09	-8.3938	4.04E-09	-8.3938
H2AsO4-	6.54E-11	-10.1841	1.62E-11	-10.7894
HAsO4--	8.73E-15	-14.0588	2.19E-17	-16.6590
HAs3S6=	4.32E-13	-12.3647	1.08E-15	-14.9648
H2As3S6-	1.00E-11	-10.9991	2.49E-12	-11.6043
H3As3S6	6.04E-10	-9.2193	6.04E-10	-9.2193
Sb(OH)3	2.61E-05	-4.5840	2.61E-05	-4.5840
Sb(OH)2+	5.60E-09	-8.2520	1.58E-09	-8.8014
Sb(OH)4-	2.45E-11	-10.6117	6.07E-12	-11.2170
Sb2S4=	1.52E-14	-13.8187	3.81E-17	-16.4188
HSb2S4-	1.27E-09	-8.8945	3.16E-10	-9.4998

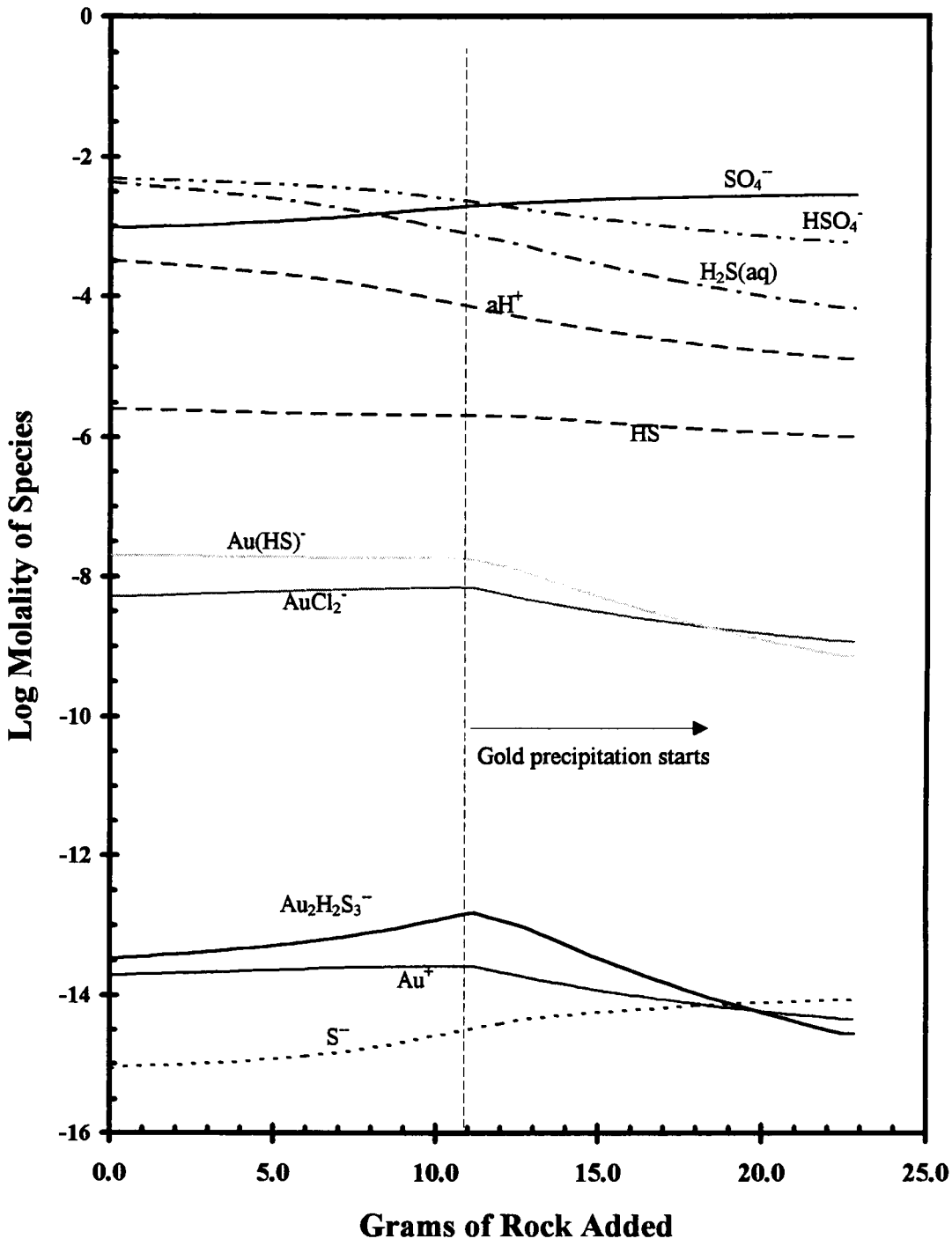

Fig. 4. Variations of molality of individual species of gold and sulfur along the fluid-rock reaction path in an open system (Fig. 1). See text for discussion.

conditions that prevailed during the gold mineralization, the calculations provide insight into the mechanism of gold precipitation at the Brewer Mine. Many geochemical processes may cause gold to precipitate from mineralizing fluids (Romberger, 1986, 1982; Seward, 1982, 1991; Cathles, 1986; Fyfe, 1986, Reed and Spycher, 1985; Spycher and Reed, 1988) -- changes in pH, oxidation and reduction, and desulfidation -- depending on the dissolved gold complexes and fluid composition. If the gold is transported as a chloride complex, reduction, increase in pH, and decrease in temperature may result in gold precipitation. If the gold is transported as a bisulfide complex, oxidation, increase or decrease in pH, and decreasing in sulfur activity will cause gold deposition (Romberger, 1986).

The simultaneous multicomponent calculations of reaction-path involving gold precipitation allow us to model mechanisms for gold precipitation in the Brewer by analyzing the variations of molality of gold complexes, pH, and sulfur species (Fig. 4). Au is held mostly as $Au(HS)^-$ and $AuCl_2^-$ species in the initial fluid. Precipitation of sulfide causes a decrease in HS^- (mostly in H_2S form), resulting in a slightly decrease in molality of $Au(HS)^-$. As a result, some Au transfers to species such as $AuCl_2^-$ and $Au_2H_2S_3^{2-}$, driving the molality up slightly (Fig. 4). When 11 grams of rhyolitic rock are added to the fluid, gold begins to precipitate. The increase in pH that results from dissolution of reactant rock appears to be one of the mechanisms causing gold to precipitate by reactions, such as:

$$8\ Au(HS)_2^- + 4H_2O = 8\ Au + SO_4^{2-} + 15\ S^{2-} + 24\ H^+ \quad (9)$$

$$8\ Au(HS)_2^- + 4H_2O = 8\ Au + SO_4^{2-} + 15\ HS^- + 9\ H^+ \quad (10)$$

$$AuCl_2^- + H_2S + 4\ H_2O = Au + 2\ Cl^- + SO_4^{2-} + 10\ H^+ \quad (11)$$

$$Au^+ + H_2S + 4\ H_2O = Au + SO_4^{2-} + 10\ H^+ \quad (12)$$

$$Au_2H_2S_3^{2-} + 12\ H_2O = 2\ Au + 3\ SO_4^{2-} + 26\ H^+ \quad (13)$$

Due to these reactions, the molalities of all gold complexes begin to decrease and continue decreasing as the reactions progress (Fig. 4).

Desulfidation can also cause gold precipitation from sulfide complexes in accordance with reaction (10). Precipitation of sulfide minerals, such as pyrite, could have led to desulfidation of the aqueous phase, promoting the precipitation of gold. Indeed, gold is associated with pyrite in the Brewer Mine, which can be related by reactions:

$$Fe^{++} + 0.25\ SO_4^{2-} + 1.75\ HS^- + 0.25\ H^+ \Longrightarrow FeS_2 + H_2O$$

(pyrite precipitation)

$$8\ Au(HS)_2^- + 4H_2O \Longrightarrow 8\ Au + SO_4^{2-} + 15\ HS^- + 9\ H^+$$

(gold precipitation)

As the gold released from the bisulfide complex is caused by both pH increase and desulfidation, the molality of $Au(HS)_2^-$ decreases at a faster rate than that of $AuCl_2^-$. $AuCl_2^-$ gradually becomes the dominant complex in the fluid when the fluid becomes more oxidized and hematite starts to precipitate (Fig. 4 and Fig. 3-a). As a result of increasing pH, HSO_4^- decreases, thus driving up the SO_4^{2-} in the fluid.

The speciation calculations shown in Fig. 4 and Table 2 reveal several important points regarding the geochemistry of gold in hydrothermal fluids: 1) the bisulfide and chloride complexes are the most stable species of gold, and thus, are the most capable complexes for hydrothermal transport of gold; 2) the bisulfide complex, $Au(HS)_2^-$, is the dominant complex of gold under reduced conditions; and 3) chloride complexes prevail in more oxidized conditions. These observations agree well with experimental and theoretical studies (Weissberg, 1970; Seward, 1973, 1984, 1991; Barnes, 1979; Romberger, 1982, 1986; Fyfe, 1986). The relative dominance of the bisulfide over chloride complexes is also probably dependent upon temperature. At relatively low temperature (<300 °C), in near-neutral and reduced conditions, sulfide complexes of gold

are the dominant species, whereas chloride complexes of gold are predominant in the fluid at higher temperature (>300 °C) and oxidized conditions (Romberger, 1986).

One observation from the calculations and field study at Brewer, as well as at many other hydrothermal gold deposits, is the common association of gold with pyrite, often because of coprecipitation. This association may be used as a general indicator for the dominant gold complex, fluid composition and conditions for gold precipitation. The gold is most likely released from bisulfide complex due to pyrite precipitation in a less than oxidizing condition.

CONCLUSION AND SUMMARY

Reaction-path calculations of the ore-forming processes in the Brewer Mine suggest that fluid-rock reactions and fluid mixing with cooler and diluted fluids, such as meteoric water, were probably the dominant processes that contributed to the mineralization. These calculations produced sulfide mineral assemblages that are similar to those observed in the mine area. Pyrite is the most abundant mineral produced during calculations. Various amounts of sulfide minerals, including bornite, chalcopyrite, enargite, covellite, tetrahedrite, and tennantite, precipitate at different stages of calculations in response to an increase in pH and decrease in temperature.

Speciation calculations show that chloride complexes are the dominant species for Fe, Cu, Zn, Pb, and Ag. H_2S (aq) is the dominant form of reduced sulfur and HSO_4^- is the most abundant sulfate species. $Au(HS)_2^-$ is the more abundant species for Au in the initial fluid than $AuCl_2^-$. However, $AuCl_2^-$ becomes more abundant during the later stage of fluid-rock reaction. Speciation calculations throughout the reaction-path suggest that bisulfide complex of Au is the dominant complex of gold under reduced conditions and chloride complex appears to be the more stable species under oxidized conditions.

Gold is precipitated in calculations involving fluid-rock reaction as well as fluid-fluid mixing. The calculations show that the primary mechanisms of gold precipitation are desulfidation due to precipitation of sulfide minerals and increase in pH due to fluid-rock reaction, and, to some extent, fluid mixing with less acidic meteoric water.

ACKNOWLEDGMENTS

I like to thank Mark Reed of the University of Oregon for introducing the numerical modeling to me and for providing the PC version program codes. Mark Zwaschka, Jae Stonehouse, and John Scheetz of the Brewer Gold Company provided valuable discussions of the geology at the Brewer Mine.

REFERENCES

Barnes, H. L., 1979, Solubilities of ore-minerals: in Barnes, H. L., ed., 1979, Geochemistry of hydrothermal ore deposits, 2nd ed., p. 404-460.

Barnes, H. L. and Czamanske, G. K., 1967, Solubilities and transport of ore minerals: in Barnes, H. L., ed., 1979, Geochemistry of hydrothermal ore deposits, 1st ed., p. 317-355.

Brimhall, G. H., Jr. and Ghiorso, M., 1983, Origin and ore-forming consequences of the advanced argillic alteration process in hypogene environments by magmatic gas contamination of meteoric fluids: Economic Geology, v. 78, p. 73-90.

Ellis, A. J., 1979, Explored geothermal systems: in Barnes, H. L., ed., 1979, Geochemistry of hydrothermal ore deposits, 2nd ed., p. 632-683.

Fyfe, W. S., 1986, The transport and deposition of gold: in Clark, L. A., ed., Gold in the western shield, p. 156-167.

Fyfe, W. S., and Kerrich, R., 1984, Gold: natural concentration processes: in Foster, R. P., ed., Gold'82; The geology, geochemistry and genesis of gold deposits: Rotterdam, A. A. Balkema, p. 99-127.

Krupp, R. E. and Seward, T. M., 1987, The Rotokawa geothermal system, New Zealand: an active epithermal gold-depositing environment: Economic Geology, v. 82, p. 1109-1129.

Lu, C., Misra, K. C., Stonehouse, J. M., and Zwaschka, M. R., 1993, Geochemical signatures of alterations in Brewer gold mine, South Carolina: South Carolina Geology. v. 35, p. 37-54.

Reed, M. H. 1982, Calculation of multicomponent chemical equilibria and reaction processes in systems involving minerals, gases and an aqueous phase. Geochim. Cosmochim. Acta 46, 513-528.

Reed, M. H. and Spycher, N. F., 1985, Boiling, cooling, and oxidation in epithermal systems: a numerical modeling approach: in Berger, B. R. and Bethke, P. M., eds., Geology and geochemistry of epithermal systems: Society of Economic Geologists, Review in Economic Geology, v. 2, p. 249-272.

Reed, M. H., Spycher N., and Akakuk K., 1988, Numerical models of boiling and mixing in geothermal waters (extended abstr.). International Symposium on Geothermal Energy: Exploration and Development of Geothermal Resources, Kumamoto and Beppu. 51-54.

Reed, M. H. and Spycher N., 1990, SOLTHERM: data base of equilibrium constants for aqueous-mineral-gas equilibria. Dept. of Geol. Sci., Univ. of Oregon, Eugene, 47 p.

Roedder, E., 1984a, Fluid inclusions. Review in Mineralogy No. 12. Mineralogical Sociaty of America. 646p.

Roedder, E., 1984b, Fluid inclusion evidence bearing on the environments of gold deposition: in Foster, R. P., ed., Gold'82; The geology, geochemistry and genesis of gold deposits: Rotterdam, A.A. Balkema Pub., p. 129-164.

Roedder, E., 1979, Fluid inclusions as samples of ore fluids: in Barnes, H. L., ed., 1979, Geochemistry of hydrothermal ore deposits, 2nd ed., p. 684-737.

Romberger, S. B., 1988, Geochemistry of gold in hydrothermal deposits: U. S. Geological Survey Bulletin 1857-A, p. 9-25.

Romberger, S. B., 1986, The solution chemistry of gold applied to the origin of hydrothermal deposits: in Clark, L. A., ed., Gold in the western shield, p. 168-112.

Scheetz, J. W., 1991, The geology and alteration of the Brewer gold mine, Jefferson, South Carolina: M.S. Thesis, University of North Carolina, Chapel Hill, 180p.

Seward, T. M., 1973, Thio complexes of gold and transport of gold in hydrothermal ore solutions: Geochimica Cosmochimica Acta, v 37, 379-399.

Seward, T. M., 1984, The transport and deposition of gold in hydrothermal systems: in Foster, R. P., ed., Gold'82; The geology, geochemistry and genesis of gold deposits: Rotterdam, A. A. Balkema, p. 165-179.

Seward, T. M., 1991, The hydrothermal geochemistry of gold: in Foster, R.P. ed., Gold metallogeny and exploration, p. 37-61.

Spycher, N. F. and Reed, M. H., 1989, Evolution of a Broadlands-type epithermal ore fluid along alternative P-T paths: Implications for the transport and deposition of base, precious, and volatile metals: Economic Geology, v. 84, p. 328-359.

Weissberg, B. G., Browne, P. R. L., and Seward, T. M., 1979, Ore metals in active geothermal systems: in Barnes, H. L., ed., 1979, Geochemistry of hydrothermal ore deposits, 2nd ed., p. 738-780.

List of Appendix

Appendix A

List of Samples from the Brewer Mine

List of the Brewer Samples

Sample	Sample Description	Aspects of Study								
		TS	PS	FI			XRF	XRD	EMP	SI
				H-F	SXRF	LRM				
B-1	quartz vein	TS	PS							
B-2	quartz vein	TS	PS							
B-3	quartz vein	TS	PS							
B-4	quartz vein	TS	PS							
B-5	quartz vein	TS	PS							
B-6	topaz+quartz rock	TS	PS							
B6-AC	quartz-vein across the creek feom B-6			H-F						
B6-QV	quartz-vein from B-6 area									
BB'-1	qtz-als rock									
BB'-2	metavolcanic rock	TS					XRF			
BB'-3	metatuff									
BB'-4	foliated metatuff	TS					XRF			
BB'-5	metatuff	TS					XRF			
BB'-6	chlorotoid metavolcanic rock	TS					XRF			
BB'-6B	oxided version of BB'-6	TS								
BB'-7	chlorotoid-bearing qtz-seicite schist	TS								
BB-1	quartz vein									
BB-2	volcano-sedimentary rock	TS					XRF			
BB-3	metatuff	TS								
BB-4	pyrophyllite-rich metavolcanics	TS					XRF			
BB-5	quartz-ilmenite(?) vein									
BB-6	quartz vein									
BB-7	metavolcanic rock									
BB-8	pebble rock									
BB-9	metavolcanics						XRF			
BB-9B	metavolcanics									
BB-10	metatuff									
BB-11	gossan rock									
BB-11B	quartz-hemetite vein									
BB-12	quartz-hemetite									
BB-13	pyrite-als-rock(oxidized vision)									
BB-13B	pyrite-als-rock	TS						XRD		SI
BB-14	Als-rock									
BB-15	metavolcanic rock									
BB-16	quartz-pyrophyllite									
BB-17	metatuff									
BB-18	meta volcano-flow (similar to BB'-2)	TS								
BB-19	quartz vein									
BB-20	quartz vein									
BB-21	fine-grain py-Als-rock	TS					XRF			
BB-22	qtz-als rock									
BBN-1	als-silicate rock	TS								
BBN-2	als-silicate	TS					XRF			
BBN-3	als-siliacte									
B440-1	metatuff ?						XRF			
B440-2	metavolcanic rock									
B440-3	quartz vein									
B440-4	meta-volcanic rock									
B440-5	pyritic als-silicate	TS					XRF	XRD	EMP	SI
B440-6	pyrite-als-qtz rock	TS						XRD		SI
B440-7	meta-tuff ?									
B440-8	quartz-vein									
B440-9	mylonite (fault rock)									
B440-10	qtz-vein									
B440-11	als-silicate									
B440-12	als-silicate									
B440-13	quartz-vein									
B440-14	qtz-vein									
B440-15	quartz-sericite vein									
B440-16	strongly weathered als-silicate									
B440-17	pyrite-bearing als-silicate									
B440-18	fine-grain qtz rock						XRF			
B440-19	quartz-vein									

Sample	Sample Description	Aspects of Study								
		TS	PS	FI			XRF	XRD	EMP	SI
				H-F	SXRF	LRM				
B440-20	als-silicate w/quartz	TS								
B440-21	qtz-white-mica vein									
B440-22	pyritic siliceous rock									
B440-23	felsic dike									
B440-24	als-siliacte									
B460-1	pyritic als-silicate									
B460-2	foliated pyritic als-silicate						XRF			
BRECCIA	breccia						XRF			
BG-1	breccia						XRF			
BG-2	breccia (als rocks)	TS					XRF			
BN-01	volcanic tuff	TS					XRF			
BN-02	volcanic flow						XRF			
BO-1	meta volcanic flow	TS					XRF			
BO-2	volcanic breccia									
BO-3	volcanic flow	TS					XRF			
BO-4	volcanic rock									
BO-5	volcanic rock									
BO-6	slate	TS					XRF			
BP-1	quartz-vein									
BP-2	breccia	TS					XRF			
BP-3	pyrite-silicate (breccia)	TS								
BP-4	pyrophyllite on als-silicate									
BP-5	mineralized breccia	TS								
BP-6	mineralized breccia									
BP-7	mineralized breccia									
BP-8	als-silicate									
BP-LV	quartz vein			H-F	SXRF	LRM				
BS-1	pebble ?	TS					XRF			
BS-2	qtz-vein									
BS-3	breccia	TS					XRF			
BS-4	breccia-prophyllite-sericite rock	TS					XRF			
BW-1	meta volcano-flow	TS					XRF			
BW-2	qtz-pebble with sedimentary rock	TS					XRF			
BW-3	qtz-ilmenite vein									
BEO-1	qtz-vein									
BEO-2	qtz-vein									
BEO-3	qtz-ilmenite vein									
DIKE-BP	felsic dike in Brewer pit	TS								
WB-1	volcanic flow (thermal metamorphosed ?)	TS					XRF			
WB-2	volcanic flow (thermal metamorphosed ?)	TS					XRF			
WB-3	volcanic rock									
WB-4	volcanic flow						XRF			
WB-5	hornfels	TS					XRF			
WB-6	volcanic flow (thermal metamorphosed ?)	TS					XRF			
WB-10	volcanic flow						XRF			
WB-11	volcanics									
WB-12	hornfels									
WB-13	slate rock (?)						XRF			
WB-14	hornfels (?)	TS					XRF			
BS-10	quartz-vein			H-F		LRM				
BS-11	quartz-vein									
BS-12	metamudstone						XRF			
BS-13	metavolcanic mudstone						XRF			
BS-14	metavolcanic sedimentary rock						XRF			
BS-15	diabate dike (?)	TS								
BS-16	quartz-vein									
BS-17	metavolcanic tuff						XRF			
BS-18	metavolcanics						XRF			
BS-19	metatuff w/quartz						XRF			
BS-20	metavolcanics	TS					XRF			
BS-21	metamudstone						XRF			
BS-22	metavolcanics (breccia ?)						XRF			
Mafic dike	mafic dike	TS								
OB-1	metatuff						XRF			
OB-2	hornfels	TS					XRF			

Sample	Sample Description	Aspects of Study								
		TS	PS	FI			XRF	XRD	EMP	SI
				H-F	SXRF	LRM				
OB-3	fine-grained granite (near contact)	TS					XRF			
OB-4	coarse-grained granite	TS								
OB-5	granite	TS					XRF			
OB-6	hornfels						XRF			
OB-7	metatuff	TS					XRF			
OB-8	metavolcanic clastics	TS					XRF			
OB-9	granite (old name granite, along 40)						XRF			
BN-1	quartz-vein									
BN-2	metavolcaniclastics						XRF			
BN-3	metavolcanics									
BN-4	pyrite-bearing silicified rock	TS					XRF			
BN-5a	metavolcanics									
BN-5b	meta-volcanic tuffs									
BN-6	metavolcanic-sedimentary rock	TS					XRF			
BN-7	metavolcanics	TS					XRF			
BN-8	quartz-vein									
BN-9	metavolcanic clastics						XRF			
BN-10	meatvolcanics	TS					XRF			
BN-11	metavolcanic flow						XRF	XRD		
BN-12	metavolcanics						XRF	XRD		
BN-13	metavolcanics	TS					XRF	XRD		
BPQ										SI
BPQ-1										
BPQ-2										SI
PYCRY										SI
BQ-1	quartz vein			H-F		LRM				
BQ-2	quartz vein									
BQ-3	quartz vein									
BQ-4	quartz vein									
BQ-5	quartz vein					LRM				
BQ-6	quartz vein			H-F						
BQ-7	quartz vein									
BQ-8	quartz vein									
BQ-9	quartz vein			H-F						SI
BQ-10	quartz vein									
BQ-11	quartz vein									
BQ-12	quartz vein									
BQ-13	quartz vein									
BQ-14	quartz vein									
BQ-15	quartz vein									
BQ-16	quartz vein									
BQ-17	quartz vein									
BQ-18	quartz vein									
BQ-19	quartz-topaz vein	TS								
BQ-20	quartz vein									
BQ-21	quartz vein									
BQ-22	quartz vein									
BQ-23	quartz vein									
BQ-24	quartz vein			H-F	SXRF	LRM				
BQ-25	quartz vein									
BQ-26	quartz vein									
BQ-27	quartz vein									
BQ-28	quartz vein									
BQ-29	quartz vein									
BQ-30	quartz vein			H-F						
BQ-31	quartz vein									
BQ-32	quartz vein									
BQ-33	quartz vein									
BQ-34	quartz vein									
BQ-35	quartz vein									
BQ-35b	fine-grain qtz-pyrite rock									
BQ-36	quartz vein			H-F						
BQ-37	quartz vein									
BQ-38	quartz vein									
BQ-39	quartz vein									

Sample	Sample Description	Aspects of Study								
		TS	PS	FI			XRF	XRD	EMP	SI
				H-F	SXRF	LRM				
BQ-40	quartz vein									
BQ-41	quartz vein									
BQ-42	quartz-pyrite breccia w/ quartz									
BQ-43	quartz vein			H-F						
BQ-44	quartz vein									
BQ-45	quartz vein			H-F						
BQ-46	quartz-pyrite vein									
BQ-47	quartz vein									
BQ-48	quartz vein									
BQ-49	qtz-pyrite breccia									
BQ-50	qtz-als-py rock									
BQ-51	quartz vein									
BQ-52	pyrite-quartz breccia									
BQ-53	quartz vein									
BQ-54	qtz-als-py rock w/ small qtz vein									
BQ-55	quartz vein									
BQ-56	quartz vein									
BQ-57	quartz-prophylite vein									
BQ-58	quartz vein									
BNQ-2	fine-grain quartz-pyrite rock	TS								
BNQ-11	andalusite-bearing rock									
BNQ-19	felsic dike									
BNQ-19	fine-grain quartz-pyrite rock w/ dickite vein ?	TS		H-F						
BNQ-29	qtz-pyrite-sericite rock									
BNQ-34	quartz vein									
BNQ-41	topaz									
BNQ-57	qtz-als-py rock									
BNQ-58	qtz-als-py rock									
BNQ-59	mafic dike									
BP pipe	mineralized breccia									
Drill Core Samples										
B3-183	silicic rock									
B3-226	pyrite silicic rock									
B3-236	alunite-bearinf rock	TS						XRD		SI
B3-263	alunite-bearing rock							XRD		SI
B3-800	breccia									
BDH-11-121	foliated quartz-pyrite rock									
BDH-11-150	foliated quartz-pyrite rock									
BDH-11-160	foliated quartz-pyrite rock									
BDH-11-40	foliated quartz-pyrite rock									
BDH-11-53	foliated tuff	TS					XRF			
BDH-11-54	foliated quartz-pyrite rock	TS								
BDH-11-74	foliated quartz-pyrite rock	TS								
BDH-11-85	foliated quartz-pyrite rock									
BDH-110-104	breccia						XRF			
BDH-110-40	breccia	TS					XRF			
BDH-117-104	gossan									
BDH-117-116	breccia									
BDH-117-130	quartz vein									
BDH-117-172	breccia									
BDH-117-42	breccia									
BDH-117-60	breccia									
BDH-117-76	quartz vein									
BDH-117-87	breccia									
BDH-117-98	quartz vein									
BDH-121-135	andalusite-pyrite breccia									
BDH-121-149	andalusite-pyrite breccia									SI
BDH-121-15	quartz vein									
BDH-121-164	andalusite-pyrite breccia									
BDH-121-175	mineralized breccia									
BDH-121-201	pyrite-quartz rock									
BDH-121-205	breccia									
BDH-121-220	quartz-pyrite rock									
BDH-121-241	andalusite quartz rock									

Sample	Sample Description	Aspects of Study								
		TS	PS	FI			XRF	XRD	EMP	SI
				H-F	SXRF	LRM				
BDH-121-34	quartz vein									
BDH-121-66	quartz vein									
BDH-121-94	quartz vein									
BDH-127-129	breccia						XRF			
BDH-127-212	breccia									
BDH-127-340	breccia									
BDH-129-172	breccia									
BDH-129-195	breccia									
BDH-129-50	breccia						XRF			
BDH-129-73	breccia									
BDH-129-91	breccia									
BDH-1A-262	breccia	TS								
BDH-2-262	tuff									
BDH-2-70	quartz-topaz rock									
BDH-2-71	quartz-topaz rock									
BDH-2-72	quartz-topaz rock									
BDH-34-130	quartz vein									
BDH-34-139	quartz vein w/ gossan									
BDH-34-146	foliated breccia									
BDH-34-160	foliated crystal tuff									
BDH-34-165	breccia	TS								
BDH-34-209	andalusite breccia									
BDH-34-214	andalusite-pyrite breccia									
BDH-34-231	fine-grained silicic rock									
BDH-34-98	quartz-hematite vein									
BDH-52-112	fine-grained silicic rock									
BDH-52-122	fine-grained silicic rock									
BDH-52-170	fine-grained silicic rock									
BDH-52-23	quartz vein									
BDH-52-234	fine-grained silicic rock									
BDH-52-243	fine-grained silicic rock	TS								
BDH-52-249	fine grained pyrite quartz rock									
BDH-52-70	massive pyrite rock									
BDH-52-80	andalusite-quartz vein									
BDH-52-88	fine-grained silicic rock									
BDH-52-93	fine-grained silicic rock									
BDH-57-128	fine grained pyrite quartz rock									
BDH-57-150	fine-grained silicic rock									
BDH-57-155	felsic dike									
BDH-57-161	breccia	TS								
BDH-57-170	fine-grained silicic rock									
BDH-57-193	quartz vein									
BDH-57-42	mineralized breccia									
BDH-57-81	silicified rock									
BDH-58-134	breccia									
BDH-61-100	breccia						XRF			
BDH-61-110	breccia									
BDH-61-124	breccia						XRF			
BDH-61-142	porphyry-likr rock									
BDH-61-156	breccia						XRF			
BDH-61-183	breccia									
BDH-61-193	breccia									
BDH-61-198	breccia						XRF			
BDH-61-21	breccia									
BDH-61-222	breccia									
BDH-61-247	breccia									
BDH-61-265	breccia									
BDH-61-293	breccia									
BDH-61-332	breccia	TS					XRF			
BDH-61-333	breccia									
BDH-61-386	breccia									
BDH-61-407	breccia									
BDH-61-421	breccia									
BDH-61-448	porphyry-like rock						XRF			
BDH-61-466	breccia									

Sample	Sample Description	Aspects of Study								
		TS	PS	FI			XRF	XRD	EMP	SI
				H-F	SXRF	LRM				
BDH-61-48	porphyry-like rock									
BDH-61-498	breccia									
BDH-61-513	breccia									
BDH-61-519	breccia									
BDH-61-586	breccia	TS					XRF			
BDH-61-605	breccia									
BDH-61-637	breccia						XRF			
BDH-61-643	breccia									
BDH-61-693	breccia									
BDH-61-715	breccia	TS								
BDH-61-755	breccia									
BDH-61-777	breccia									SI
BDH-61-800	breccia	TS					XRF			
BDH-61-808	breccia									
BDH-61-820	breccia									
BDH-61-839	breccia	TS								
BDH-61-851	breccia									
BDH-61-87	breccia									
BDH-61-884	breccia									
BDH-61-889	breccia						XRF	XRD		
BDH-61-893	breccia			H-F						
BDH-61-949	porphyry-like rock/breccia	TS					XRF			
BDH-61-953	breccia						XRF			
BDH-62-104	andalusite-bearing breccia									
BDH-62-121	tuff	TS								
BDH-62-133	andalusite-bearing breccia									
BDH-62-16	quartz vein									
BDH-62-200	andalusite-bearing breccia									
BDH-62-50	quartz vein									
BDH-62-51	crystal tuff	TS								
BDH-62-64	quartz vein									
BDH-62-80	breccia	TS					XRF			
BDH-62-80	breccia						XRF			
BDH-66-101	volcanic breccia									
BDH-66-121	volcanic breccia						XRF			
BDH-66-132	quartz vein									
BDH-66-14	tuff	TS					XRF			
BDH-66-141	quartz vein									
BDH-66-156	quartz-pyrite vein									
BDH-66-163	silicic rock									
BDH-66-181										
BDH-66-185	breccia	TS								
BDH-66-186	breccia									
BDH-66-202	quartz vein									
BDH-66-205	tuff	TS								
BDH-66-210	breccia									
BDH-66-222	mineralized breccia									
BDH-66-232	quartz vein									
BDH-66-236	massive pyrite rock									
BDH-66-250	massive pyrite rock									
BDH-66-267	massive pyrite rock									
BDH-66-282	mineralized breccia									
BDH-66-287	quartz vein									
BDH-66-29	tuff									
BDH-66-30	tuff									
BDH-66-300	quartz vein									
BDH-66-33	breccia						XRF			
BDH-66-63	breccia									
BDH-66-63	quartz vein									
BDH-66-65	breccia	TS					XRF			
BDH-66-74	quartz vein									
BDH-66-87	fine grained silicic rock									
BDH-66-92	quartz evin									
BDH-67-227	pyrite-quartz rock									
BDH-67-316	pyrite-quartz rock									

Sample	Sample Description	Aspects of Study								
		TS	PS	FI			XRF	XRD	EMP	SI
				H-F	SXRF	LRM				
BDH-67-346	foliated pyrite-quartz rock	TS					XRF			
BDH-68-253	mineralized breccia									
BDH-70-235	breccia									
BDH-70-297	breccia									
BDH-71-193	foliated andalusite-pyrite breccia									
BDH-71-196	breccia	TS								
BDH-71-209	breccia						XRF			
BDH-72-102	breccia									
BDH-72-110	andalusite-bearing breccia									
BDH-72-120	mineralized breccia									
BDH-72-161	mineralized breccia									
BDH-72-238	mineralized breccia	TS								
BDH-72-255	mineralized breccia									
BDH-72-267	mineralized breccia									
BDH-72-71	breccia									
BDH-72-85	andalusite rock									
BDH-74-177	andalusite rock									
BDH-74-178	andalusite rock									
BDH-74-181	andalusite rock	TS								
BDH-75-130	silicic rock									
BDH-75-134	fine grained silicic rock									
BDH-75-164	breccia									
BDH-75-172	fine grained silicic rock									
BDH-75-182	andalusite-kyanite breccia									
BDH-75-192	tuff									
BDH-75-208	breccia									
BDH-75-214	breccia									
BDH-75-284	breccia									
BDH-75-293	breccia									
BDH-75-300	breccia									
BDH-75-65	tuff	TS								
BDH-75-96	breccia	TS								
BDH-76-115	breccia	TS					XRF			
BDH-76-116	silicic rock									
BDH-76-119	quartz-pyrite porphyry-like rock									
BDH-76-128	layered andalusite rock									
BDH-76-147	fine-grained silicic rock									
BDH-76-161	silicic rock						XRF			
BDH-76-199	quartz vein									
BDH-76-65	breccia	TS								
BDH-76-69	breccia	TS								
BDH-76-70	breccia	TS								
BDH-76-76	andalusite quartz rock									
BDH-78-141	mineralized breccia									
BDH-78-159	andalusite-bearing rock	TS								
BDH-78-170	andalusite-bearing rock									
BDH-78-182	breccia									
BDH-78-202	breccia									
BDH-78-300	breccia									
BDH-78-88	breccia									
BDH-79-100	felsic dike	TS					XRF			
BDH-79-111	felsic dike									
BDH-79-116	quartz vein									
BDH-79-122	fine graine dquartz rock									
BDH-79-129	breccia	TS								
BDH-79-135	breccia									
BDH-79-150	silicic rock									
BDH-79-161	quartz vein									
BDH-79-174	andalusite breccia									
BDH-79-175	quartz vein									
BDH-79-179	finegrained silicic rock									
BDH-79-186	quartz vein									
BDH-79-188	breccia	TS					44			
BDH-79-204	breccia	TS								
BDH-79-214	andalusite quartz rock									

Sample	Sample Description	Aspects of Study								
		TS	PS	FI			XRF	XRD	EMP	SI
				H-F	SXRF	LRM				
BDH-79-218	pyrite-quartz rock									
BDH-79-233	pyrite-quartz rock									
BDH-79-238	breccia	TS					XRF			
BDH-79-239	breccia	TS								
BDH-79-252	breccia									
BDH-79-252	andalusite quartz breccia									
BDH-79-259	andalusite quartz breccia									
BDH-79-261	andalusite quartz breccia									
BDH-79-271	breccia	TS					XRF			
BDH-79-277	mineralized breccia									
BDH-79-280	andalusite quartz breccia									
BDH-79-283	andalusite quartz breccia	TS								
BDH-79-287	andalusite quartz breccia									
BDH-79-289	andalusite quartz breccia	TS					XRF			
BDH-79-294	breccia	TS					XRF			
BDH-79-296	breccia	TS								
BDH-79-300	breccia	TS					XRF			
BDH-79-306	breccia									
BDH-79-310	mineralized breccia									
BDH-79-311	breccia	TS					XRF			
BDH-79-315	breccia									
BDH-79-324	quartz									
BDH-79-40	tuff									
BDH-79-58	tuff	TS					XRF			
BDH-79-60	andalusite quartz breccia									
BDH-79-66	fine grained									
BDH-79-76	breccia									
BDH-79-77	silicic rock									
BDH-79-83	breccia									
BDH-79-91	quartz vein			H-F						
BDH-79-98	breccia	TS					XRF			
BDH-80-103	breccia									
BDH-80-115	foliated pyrite-quartz rock									
BDH-80-119	foliated pyrite-quartz rock									
BDH-80-130	andalusite quartz rock									
BDH-80-165	breccia									
BDH-80-169	silicic rock									
BDH-80-178	foliated pyrite-quartz rock									
BDH-80-190	foliated tuff									
BDH-80-192	foliated pyrite-quartz rock									
BDH-80-96	quartz									
BDH-81-260	quartz									
BDH-87-257	breccia						XRF			
BDH-91-187	breccia						XRF			
BDH-94-256	mineralized breccia									
BDH-94-279	breccia									
BDH-94-298	breccia	TS								
BDH-96-102	silicic rock									
BDH-96-108	mineralized breccia									
BDH-96-117	quartz vein			H-F						
BDH-96-121	breccia	TS								
BDH-96-130	mineralized breccia									
BDH-96-135	massive pyrite rock									
BDH-96-142	andalusite-pyriet rock									
BDH-96-160	quartz vein			H-F						
BDH-96-19	quartz vein			H-F						
BDH-96-196	mineralized breccia									
BDH-96-202	breccia	TS								
BDH-96-21	breccia									
BDH-96-215	breccia	TS					XRF			
BDH-96-220	breccia	TS								
BDH-96-226	quartz vein			H-F						
BDH-96-233	breccia									
BDH-96-239	breccia									
BDH-96-244	breccia	TS								

Sample	Sample Description	Aspects of Study								
		TS	PS	FI			XRF	XRD	EMP	SI
				H-F	SXRF	LRM				
BDH-96-245	quartz vein									
BDH-96-247	silicic rock									
BDH-96-265	massive pyrite rock									
BDH-96-269	breccia	TS								
BDH-96-275	tuff	TS								
BDH-96-275	tuff						XRF			
BDH-96-278	breccia									
BDH-96-280	quartz vein			H-F						
BDH-96-280	breccia						XRF			
BDH-96-286	breccia									
BDH-96-294	quartz vein			H-F						
BDH-96-300	pyrite quartz breccia									
BDH-96-36	silicic rock									
BDH-96-45	quartz vein			H-F						
BDH-96-50	quartz vein									
BDH-96-58	gossan (breccia)									
BDH-96-70	quartz vein			H-F						
BDH-96-9	quartz vein			H-F						
BDH-96-97	pyrite-quartz breccia									
CD-14-33	breccia									
CD-14-56	breccia	TS					XRF	XRD		SI
CD-16-100	alunite-bearing volcanic rock	TS					XRF	XRD		
CD-16-28	alunite-bearing volcanic rock									SI
CD-16-31	alunite-bearing volcanic rock									
CD-16-36	alunite-bearing volcanic rock	TS						XRD		SI
CD-16-40	alunite-bearing volcanic rock									SI
CD-16-48	alunite-bearing volcanic rock									
CD-16-49	alunite-bearing volcanic rock									
CD-16-50	alunite-bearing volcanic rock									
CD-16-60	alunite-bearing volcanic rock									
CD-16-61	alunite-bearing volcanic rock	TS					XRF	XRD		SI
CD-16-79	alunite-bearing volcanic rock									
CD-16-84	alunite-bearing volcanic rock	TS					XRF	XRD	EMP	
CD-16-85	alunite-bearing volcanic rock									
CD-24-49	volcanci rock						XRF			
CD-26-33	volcanci rock						XRF			
CD-26-59	volcanci rock						XRF			
CD-7-40	volcanci rock									
CD-7-84	volcanci rock						XRF			
CD-9-64	volcanci rock									
CD-9-88	volcanci rock						XRF			
Abbrevation:	TS-thin section; PS-polished slab or thin sections;									
	FI-fluid inclusion; H-F-heating-freezing; SXRF-synchrotron X-ray microprobe; LMP-laser Raman microprobe									
	XRF-X-ray fluorencence; XRD-X-ray diffetometry; EMP-electron microprobe; SI-sulfur stable isotope.									

Appendix B

XRF Analysis of the Brewer Rocks

Sample #	unit	Protocol calibration range	B-11-53	B-110-40	B-117-60	B-127-129	B-129-195	B-129-50	B-61-48	B-61-100	B-61-124	B-61-156	B-61-198	B-61-332	B-61-448	B-61-586
Na_2O	%	0.07-6.20	1.35	1.62	.00	.09	.64	.21	.44	.90	1.16	1.89	1.99	.54	.70	.63
K_2O	%	0.62-15.35	2.70	.00	.13	.00	.00	.00	.00	.22	.00	.25	.00	.00	.00	.00
Al_2O_3	%	6.18-39.2	14.2	3.91	23.7	11.1	2.33	21.0	18.1	24.4	2.71	3.02	3.62	9.14	11.1	8.99
TiO_2	%	0.02-2.39	.41	.44	1.36	.30	.22	.47	.35	.29	.29	.21	.27	.25	.32	.30
SiO_2	%	48.9-88.2	74.1	92.4	15.4	82.0	99.8	70.9	74.2	60.8	98.2	97.1	95.1	87.2	81.4	89.0
MgO	%	0.02-3.83	.26	.67	.88	.00	.13	.00	.16	.28	.35	.76	.86	.23	.18	.18
CaO	%	0.03-2.74	.04	.00	.00	.00	.00	.00	.00	.00	.00	.00	.00	.00	.00	.00
Fe_2O_3	%	0.07-8.58	1.26	6.93	*39.10*	.00	1.71	.55	2.06	1.07	4.21	7.11	8.11	2.64	2.47	2.26
MnO	%	0.002-0.17	.01	.07	.23	.00	.06	.00	.02	.00	.09	.10	.10	.04	.03	.04
P_2O_5	%	0.01-0.69	.21	.80	.64	.01	.17	.22	.35	.48	.48	.84	1.00	.35	.29	.28
Cu	ppm	5-120	14	43	0	9	37	9	18	21	55	50	68	35	30	26
V	ppm	2-550	98	173	8558	68	71	144	98	104	112	129	171	91	97	105
Cr	ppm	4-438	0	0	0	0	0	27	0	56	0	0	0	0	0	0
Co	ppm	1-49	4	20	>>>	4	10	4	6	5	24	25	46	11	8	7
Ni	ppm	4-94	4	13	66	4	11	6	9	10	15	15	20	13	9	9
Zn	ppm	5-145	46	252	>>>	48	949	56	91	146	992	>>	1074	199	104	114
Pb	ppm	5-69	39	16	4291	8	83	17	13	54	66	140	52	30	13	17
Rb	ppm	33-2000	90	0	23	0	0	0	0	0	0	0	0	0	0	0
Sr	ppm	10-480	209	26	629	3	1	132	40	315	3	2	0	58	16	52
Y	ppm	11-145	20	0	0	0	0	1	0	0	0	0	0	0	0	0
Zr	ppm	33-790	267	113	60	154	99	242	146	206	98	53	58	114	165	149
Nb	ppm	4-90	11	8	69	9	9	13	10	10	10	6	8	10	10	11
Mo	ppm	1-100	19	21	45	12	7	14	13	20	16	3	4	17	15	34
Ba	ppm	47-2400	551	0	0	149	96	221	132	319	51	0	0	120	133	124
Total (c)	%		94.7	106.9	82.8	93.6	105.2	93.4	95.7	88.6	107.6	111.3	111.2	100.5	96.5	101.7
S*	%		1.07	5.30	.46	.11	1.32	.51	1.53	2.06	3.43		5.37	2.13	1.91	1.86
L.O.I.	%		4.07		13.95	2.91		5.98	3.39	10.07				2.87	4.37	2.33
Total (T)	%		99.8	112.2	97.2	96.6	106.5	99.9	100.7	100.8	111.1	111.3	116.6	105.5	102.8	105.9
	Note: * - sulfur analyzed by sulfur analyzer; >>> - much greater than the upper calibration range;															

Sample #	B-61-637	B-61-800	B-61-889	B-61-953	B-62-80	B-66-14	B-66-33	B-66-65	B-66-121	B-67-346	B-69-50	B-71-209	B-76-115	B-76-161	B-79-58	B-79-98
Na_2O	.29	.00	.36	.50	.47	.62	.51	.40	.44	.99	.60	.80	.23	.50	.36	.90
K_2O	.00	.00	.00	.00	.00	3.40	1.88	.67	.62	3.82	.00	3.04	.00	.12	.38	3.39
Al_2O_3	15.8	43.9	12.4	9.02	4.52	15.1	12.2	4.63	6.03	20.7	2.62	15.3	4.43	2.91	9.31	15.0
TiO_2	.45	.50	.39	.29	.34	.60	.44	.21	.86	.40	.48	.41	.28	.34	.27	.31
SiO_2	72.1	46.6	81.8	85.7	91.1	72.5	74.1	92.0	86.8	65.6	*100.4*	72.6	91.2	*100.1*	81.6	73.9
MgO	.05	.00	.02	.17	.00	.36	.25	.00	.05	.27	.00	.25	.00	.00	.08	.18
CaO	.00	.00	.00	.00	.00	.00	.33	.00	.00	.08	.00	.05	.00	.00	.00	.05
Fe_2O_3	.91	.47	.65	2.11	.76	4.90	4.79	.56	2.20	2.17	.32	1.49	.34	.00	2.22	.30
MnO	.01	.00	.01	.03	.03	.03	.04	.02	.04	.01	.03	.01	.02	.02	.04	.00
P_2O_5	.21	.39	.11	.33	.41	.15	.92	.10	.23	.34	.15	.31	.03	.02	.37	.14
Cu	18	6	17	20	25	15	27	20	23	13	19	12	14	26	27	9
V	118	162	77	91	128	195	150	49	217	97	101	87	69	66	111	87
Cr	2	145	0	0	0	5	0	0	0	16	0	0	0	0	0	0
Co	4	4	5	7	5	8	7	4	5	4	4	4	4	5	5	4
Ni	6	10	9	9	5	9	7	5	4	5	6	5	4	8	6	4
Zn	141	2419	99	103		59	71	39		29	>>>	26	69	51		70
Pb	44	124	15	13	315	1	21	11	400	19	219	12	25	7	463	58
Rb	0	0	0	0	3	54	33	0	4	49	0	64	0	0	9	72
Sr	112	942	169	58	1882	0	395	33	702	252	665	42	192	0	1152	202
Y	0	23	0	0	47	18	22	0	33	42	15	14	0	0	30	5
Zr	252	697	155	115	1480	86	217	141	707	201	416	136	199	195	697	166
Nb	15	13	10	8	10	9	9	8	17	10	13	8	12	11	9	7
Mo	60	5	25	12	0	3	9	27	23	6	18	9	40	13	59	10
Ba	235	311	140	81	330	192	527	166	204	513	284	673	139	164	455	537
Total (c)	90.0	92.3	95.8	98.2	98.1	97.7	95.6	98.6	97.5	94.5	104.8	94.4	96.6	104.1	94.9	94.3
S*	.68	.30	.46	1.57	.61	.14	.00	.50	.00	1.91	.00	1.17	.01	.01	.00	.03
L.O.I.	6.13	5.60	2.35	2.37	1.94	3.29	3.22	1.11	1.69	4.30		4.45	1.33		3.73	3.39
Total (T)	96.8	98.2	98.6	102.1	100.6	101.1	98.8	100.2	99.2	100.7	104.8	100.0	97.9	104.1	98.7	97.7

Sample #	B-79-100	B-79-188	B-79-238	B-79-271	B-79-289	B-79-294	B-79-300	B-79-311	B-87-257	B-91-187	B-96-142	B-96-202	B-96-215	B-96-220	B-96-244	B-96-269
Na_2O	.16	2.30	.00	.06	.00	1.11	.63	.00	.47	2.14	3.63	1.03	.87	2.25	1.78	4.99
K_2O	1.78	.00	.00	.00	.00	.14	1.52	.35	.00	.68	.00	.00	.81	.00	.00	.00
Al_2O_3	13.7	16.0	47.2	14.6	48.2	7.85	9.91	25.3	2.09	17.4	30.6	25.9	5.99	17.6	6.22	24.1
TiO_2	.18	.64	.20	.42	.35	.60	.40	.24	.44	.33	2.00	.53	.37	.79	.54	1.28
SiO_2	73.2	64.3	46.6	77.7	43.4	84.1	82.1	66.7	*104.4*	68.3	53.6	61.9	89.2	61.1	88.4	56.4
MgO	.19	1.37	.00	.02	.00	.37	.03	.00	.00	.68	2.01	.51	.21	1.22	.84	2.87
CaO	.00	.00	.00	.00	.00	.00	.00	.00	.00	.00	.00	.00	.00	.00	.00	.00
Fe_2O_3	.66	11.9	.21	.00	.68	3.58	.14	.07	.05	1.24	12.1	4.22	2.45	8.60	7.21	16.2
MnO	.01	.05	.00	.00	.00	.05	.00	.00	.02	.00	.04	.02	.04	.03	.08	.05
P_2O_5	.04	1.58	.09	.19	.17	.56	.27	.08	.06	.89	2.87	.09	.41	.31	1.13	3.19
Cu	11	38	0	12	2	32	9	3	31	13	37	17	25	87	60	31
V	64	74	92	116	131	294	143	100	88	108	1030	94	113	38	250	774
Cr	0	6	150	0	165	0	0	34	0	25	0	50	0	0	0	0
Co	4	43	3	4	4	7	4	4	6	4	36	15	5	67	27	68
Ni	4	29	9	5	9	7	3	6	11	8	35	0	5	0	17	45
Zn	79	93	741		>>>	508		1285	132	80	>>>	0	211	29	>>>	>>>
Pb	53	19	116	260	215	94	265	129	28	49	777	124	72	64	285	240
Rb	83	0	0	2	0	0	10	0	0	0	0	9	0	21	0	0
Sr	0	418	402	989	603	198	697	403	154	425	2179	861	340	459	820	728
Y	5	0	1	25	9	0	21	4	0	0	49		1		15	4
Zr	132	170	217	590	165	162	340	191	226	257	1831	723	168	400	281	290
Nb	6	10	7	10	8	9	7	8	11	8	25		7		10	17
Mo	35	1	16	11	11	7	6	12	9	12	0		7		0	0
Ba	841	24	449	330	367	1588	918	330	225	569	901	1582	477	456	205	373
Total (c)	90.0	98.3	94.5	93.2	93.0	98.7	95.3	93.0	107.6	91.8	107.5	94.5	100.5	92.1	106.4	109.3
S*	.01		.15	.09	.59	3.24	.20	.07	2.06	4.46		5.15	2.36			
L.O.I.	5.52		5.01	2.85		4.85	3.29	2.95		12.7		10.6	3.01			
Total (T)	95.6	98.3	99.7	96.1	93.6	106.8	98.7	96.0	109.7	108.9	107.5	110.3	105.9	92.1	106.4	109.3

Sample #	B-96-275	B-96-280	B440-1	B440-5	B440-7	B440-18	B440-24	B460-2	BB'-2	BB'-4	BB'-5	BB'-6	BB-2	BB-4	BB-9	BB-21
Na_2O	.45	.44	2.40	6.63	6.09	.71	.65	9.77	.81	.76	1.08	1.88	.75	.56	.37	2.04
K_2O	.00	.00	.00	.21	2.82	.00	.00	1.91	4.09	3.24	3.10	2.97	4.94	6.01	.00	.00
Al_2O_3	2.08	2.06	25.6	16.0	26.4	.43	2.50	41.4	16.5	15.9	15.8	19.6	22.2	25.9	2.5	3.2
TiO_2	.43	.57	.85	1.10	.65	2.58	.51	.63	.45	.49	.62	.45	.90	.89	.77	.33
SiO_2	99.0	*103.0*	71.3	59.4	48.2	*103.8*	*103.2*	*26.6*	73.6	72.6	74.6	68.6	64.0	61.2	99.4	99.9
MgO	.00	.00	.32	2.79	1.70	.00	.00	3.11	.17	.27	.15	.11	.45	.53	.00	.75
CaO	.00	.00	.00	.00	.13	.00	.00	.18	.08	.04	.02	.06	.14	.15	.00	.00
Fe_2O_3	.06	.01	8.49	12.4	3.54	.13	.00	7.42	1.82	6.01	3.69	1.21	7.67	5.77	.88	6.21
MnO	.02	.02	.02	.04	.00	.00	.00	.00	.01	.02	.02	.04	.01	.03	.04	.03
P_2O_5	.07	.08	.19	3.10	1.90	.03	.00	3.69	.04	.12	.01	.06	.03	.06	.08	.53
Cu	29	19	13	30	10	13	17	15	8	13	11	6	16	19	16	49
V	86	123	91	475	42	19	20	239	24	44	37	160	102	279	178	31
Cr	0	0	0	0	171	0	0	168	0	0	0	39	28	51	0	0
Co	6	5	12	27	5	3	4	8	4	8	5	4	9	7	5	3
Ni	10	10	14	30	13	5	6	34	5	9	5	4	11	11	6	16
Zn	146	191	179	290	>>>	113	39	3684	24	86	41	32	259	47	72	>>>
Pb	26	36	26	10	981	47	12	301	12	11	11	13	79	12	9	104
Rb	0	0	0	0	6	0	0	0	75	54	84	123	72	114	0	0
Sr	156	169	148	113	2034	221	0	632	61	22	228	279	19	16	18	0
Y	0	7	0	0	109	5	0	2	13	11	8	95	23	78	26	0
Zr	229	315	221	174	1242	308	318	259	173	108	200	254	137	172	663	63
Nb	11	15	13	14	9	12	12	7	9	8	9	14	12	17	22	8
Mo	11	9	1	0	0	7	7	0	9	2	5	8	5	4	2	33
Ba	220	277	122	95	1072	151	139	974	447	570	1014	1209	316	451	208	0
Total (c)	102.2	106.3	109.3	101.8	92.0	107.8	106.9	95.3	97.7	99.5	99.3	95.1	101.2	101.2	104.1	113.1
S*	.00	.02	.00	14.40	.00	.08	.00	16.5	.00	.00	.00	.00	.00	.00	.00	5.25
L.O.I.			5.13		23.9	.66	.71		3.46	3.84	3.37	2.97	3.78	3.39	.62	5.42
Total (T)	102.2	106.3	114.4	116.2	115.9	108.5	107.6	111.8	101.1	103.4	102.6	98.1	105.0	104.6	104.8	123.7

Sample #	BB-23	BB-24	BB-25	BB-26	BBN-2	BG-1	BG-2	BN-01	BN-02	BN-2	BN-4	BN-6	BN-7	BN-9	BN-10	BN-11
Na_2O	.39	.00	.79	.49	.36	.54	.76	1.14	.75	.00	1.44	.63	.74	.55	1.29	.79
K_2O	.00	.00	2.73	4.19	.00	.00	.14	3.51	2.48	.00	.00	2.55	3.20	.82	.00	4.27
Al_2O_3	17.4	16.4	11.8	24.2	50.2	24.1	14.1	18.0	12.0	14.3	13.2	13.6	13.7	15.5	16.1	19.1
TiO_2	.40	.68	.33	.80	.56	.75	.23	.42	.27	.50	.39	.36	.32	.48	.38	.34
SiO_2	72.3	76.2	80.5	64.6	44.2	67.1	78.5	70.5	79.9	76.1	72.8	76.0	76.2	78.2	78.5	69.4
MgO	.00	.10	.14	.39	.00	.12	.03	.22	.14	.06	.76	.14	.14	.06	.12	.18
CaO	.00	.00	.00	.11	.00	.00	.00	.14	.00	.00	.00	.20	.05	.00	.00	.08
Fe_2O_3	.05	7.69	1.56	13.5	.09	5.02	1.33	2.27	2.23	5.40	6.51	2.50	1.15	2.50	3.47	1.71
MnO	.00	.03	.00	.03	.00	.01	.02	.01	.03	.06	.02	.03	.00	.03	.01	.01
P_2O_5	.05	.05	.00	.20	.24	.09	.05	.07	.03	.05	.25	.02	.00	.24	.11	.03
Cu	9	25	9	21	0	12	12	14	20	33	109	18	9	13	9	9
V	21	67	22	181	28	56	95	104	86	242	33	106	22	157	30	89
Cr	0	0	0	0	270	2	0	0	0	0	9	0	0	0	0	1
Co	3	10	3	17	3	7	4	4	5	11	28	5	3	5	5	4
Ni	4	12	3	17	8	9	5	5	6	8	0	6	4	8	8	4
Zn	185	181	33	849	>>>	74	38	29	37	214	44	68	27	117	73	23
Pb	66	16	17	79	247	9	6	15	14	40	12	35	17	40	17	11
Rb	0	0	68	28	0	0	0	96	68	0	10	81	101	14	0	92
Sr	972	98	53	378	1317	150	107	235	110	166	102	192	181	819	418	4
Y	5	10	6	2	51	7	1	19	9	0	0	35	26	14	0	7
Zr	302	148	116	150	847	253	132	234	152	190	251	180	199	414	236	145
Nb	7	13	7	12	13	15	9	9	8	12	0	9	6	11	9	8
Mo	3	5	11	0	0	3	14	6	9	7	0	8	4	5	4	8
Ba	232	204	561	164	373	155	313	537	353	219	0	642	550	255	176	674
Total (c)	90.8	101.2	97.9	108.7	96.0	97.8	95.2	96.4	97.9	96.6	95.4	96.1	95.6	98.6	100.1	96.0
S*	.11	.00	.00	.00	.10	.00	.01	.00	.00	.00	6.36	.04	.00	.00	.05	.00
L.O.I.	2.15	2.92	2.75	4.29	5.10	4.52	3.43	3.17	2.45	3.47	5.52	2.95	3.44	4.02	4.13	3.24
Total (T)	93.0	104.1	100.7	113.0	101.2	102.3	98.7	99.6	100.4	100.0	107.3	99.1	99.1	102.6	104.3	99.2

Sample #	BN-12	BN-13	BO-1	BO-3	BO-6	BPB	BRECCIA	BS-1	BS-3	BS-4	BS-12	BS-13	BS-14	BS-17	BS-18	BS-20
Na_2O	3.64	3.14	.70	.91	1.66	3.27	.85	.45	.18	5.19	.00	.00	.00	2.36	3.32	.41
K_2O	2.13	2.18	3.48	2.58	2.15	.00	.00	2.10	.00	.00	1.98	2.97	1.34	.00	1.64	1.92
Al_2O_3	16.9	15.2	14.2	13.4	16.9	4.48	19.1	10.6	16.8	29.6	24.7	36.3	21.6	23.6	23.7	7.9
TiO_2	.28	.27	.47	.43	.80	.35	.39	.49	.63	.56	1.12	1.54	1.05	.48	.64	.38
SiO_2	64.2	66.0	74.7	77.4	59.3	88.7	70.5	78.1	78.8	70.0	52.9	45.8	51.9	65.3	66.2	86.0
MgO	.93	1.08	.47	.13	1.99	1.69	.25	.05	.00	.36	3.10	1.96	4.28	.23	.10	.17
CaO	.01	.02	.02	.00	4.25	.00	.00	.00	.00	.00	.00	.05	.00	.00	.05	.00
Fe_2O_3	1.50	1.84	4.35	3.45	6.83	12.0	5.54	2.67	2.44	3.52	12.5	19.6	12.3	4.66	3.60	1.20
MnO	.00	.01	.02	.03	.09	.10	.05	.03	.02	.02	.04	.06	.09	.01	.02	.02
P_2O_5	1.14	1.07	.06	.09	.13	1.70	.19	.08	.07	.35	.12	.14	.19	.09	.00	.01
Cu	10	17	13	20	35	57	23	18	11	2	81	36	57	11	27	18
V	85	80	35	146	0	253	200	140	166	194	646	5532	947	42	188	83
Cr	24	9	0	0	30	0	21	0	0	40	66	15	19	49	51	0
Co	4	4	6	5	10	57	9	5	5	6	47	43	119	6	7	4
Ni	8	10	9	5	31	25	9	3	7	11	90	55	130	9	8	5
Zn	105	56	234	97	98	2498	211	54	82	55	275	560	524	77	96	50
Pb	68	36	84	46	30	72	48	24	8	4	6	0	0	13	39	27
Rb	0	0	123	70	99	0	0	36	0	0	37	46	19	0	37	58
Sr	289	193	57	136	384	2	231	18	0	8	12	0	0	65	948	32
Y	0	0	26	20	25	0	75	8	0	0	2	34	35	0	100	9
Zr	185	142	177	185	190	45	174	199	238	202	93	38	45	154	670	195
Nb	8	7	11	12	10	6	16	13	15	14	10	14	13	11	18	10
Mo	8	10	20	9	0	3	12	44	11	12	0	0	0	7	1	16
Ba	628	545	646	347	632	0	113	514	120	182	98	590	406	148	290	388
Total (c)	90.8	90.9	98.6	98.6	94.3	112.6	97.0	94.6	99.0	109.7	96.6	109.1	93.1	96.8	99.5	98.1
S*	4.97	4.75	.00	.01	.00		.00	.00	.00	.00	.00	.00	.00	.00	.00	.00
L.O.I.	15.6	16.6	3.30	2.54	2.80		4.26	2.14	1.60	5.11	8.14	10.3	8.92	5.24	3.46	1.68
Total (T)	111.4	112.2	101.9	101.1	97.1	112.6	101.2	96.8	100.6	114.8	104.7	119.4	102.0	102.0	103.0	99.8

Sample #	BS-21	BS-22	BW-1	BW-2	CD-14-56	CD-16-84	CD-26-33	OB-9	NW	OB-1	OB-2	OB-3	OB-5	OB-7	OB-8	topaz Rx
Na_2O	.00	.83	.38	.34	2.34	2.55	.90	4.10	.20	.05	2.97	3.92	3.85	2.34	5.10	.04
K_2O	3.51	2.25	3.71	3.06	.30	1.37	3.31	4.93	.00	2.80	.48	4.25	4.35	3.92	2.14	.00
Al_2O_3	23.1	12.7	16.8	13.9	11.3	10.6	12.9	13.1	16.2	15.0	15.1	12.2	14.5	16.1	13.7	57.0
TiO_2	1.04	.29	.36	.37	.25	.29	.25	.05	.48	.33	.58	.05	.42	.40	.26	.76
SiO_2	55.9	77.7	68.9	74.4	78.1	73.9	80.6	73.6	76.5	73.1	50.5	79.0	70.8	70.4	76.9	32.0
MgO	1.59	.13	.38	.27	.86	.54	.36	.24	.03	.47	7.72	.15	.71	.87	.71	.00
CaO	.03	.00	.00	.00	.00	.00	.02	.73	.00	.00	11.3	.45	1.86	.16	.09	.00
Fe_2O_3	8.55	2.76	6.36	5.64	5.44	.00	2.26	1.08	1.09	2.00	8.24	1.12	3.16	2.47	3.03	.00
MnO	.05	.03	.03	.03	.05	.00	.02	.02	.01	.03	.20	.02	.04	.03	.05	.00
P_2O_5	.14	.04	.15	.02	1.07	.78	.27	.12	.29	.04	.10	.01	.12	.03	.03	.44
Cu	38	14	23	20	39	12	16	21	8	13	63	16	18	14	18	18
V	477	117	173	1360	126	73	69	0	25	107	59	0	0	103	95	350
Cr	38	0	0	0	0	0	0	0	0	0	147	0	18	7	16	437
Co	21	5	9	7	12	3	4	4	4	4	26	4	5	4	5	3
Ni	28	5	8	6	14	5	7	5	6	7	56	5	10	9	9	9
Zn	150	61	65	53	1783	56	58	30	63	34	113	31	40	24	44	>>>
Pb	10	27	4	5	147	41	33	35	18	10	2	20	22	2	9	397
Rb	97	55	53	44	0	0	43	288	0	93	16	260	131	141	87	35
Sr	0	110	68	0	215	472	34	48	78	0	326	31	198	42	123	969
Y	42	45	12	3	0	2	39	68	0	23	0	89	23	13	33	52
Zr	133	140	96	65	112	272	144	62	230	159	77	97	284	157	137	1096
Nb	17	12	7	6	7	9	10	41	15	11	0	35	14	8	9	17
Mo	4	7	1	0	2	10	6	8	20	11	0	9	7	10	10	4
Ba	340	465	537	227	232	466	189	302	236	472	0	259	780	674	459	290
Total (c)	94.0	96.8	97.1	98.2	100.0	90.1	100.9	98.1	94.9	93.9	97.3	101.3	100.0	96.8	102.1	90.6
S*	.01	.00	.00	.01	6.16	3.48	2.01	.00	.00	.00	.37	.00	.02	.00	.00	.30
L.O.I.	6.73	2.53	2.74	1.83	11.1	12.7	4.27	.74	1.87	4.05	1.42	1.08	.98	3.04	1.76	
Total (T)	100.8	99.3	99.9	100.0	117.2	106.3	107.2	98.8	96.7	98.0	99.1	102.4	101.0	99.8	103.9	90.9

Sample #	vol-cal	WB-1	WB-2	WB-4	WB-5	WB-6	WB-10	WB-13	WB-14
Na_2O	.27	4.78	3.34	.00	3.05	2.83	.46	1.28	4.91
K_2O	2.75	1.24	3.91	3.83	3.67	2.43	10.17	3.55	.23
Al_2O_3	14.8	16.4	15.3	14.4	14.4	16.7	36.4	18.9	13.5
TiO_2	.44	.45	.33	.41	.34	.69	.74	.88	.30
SiO_2	72.0	66.2	68.8	71.3	71.8	65.6	46.2	56.3	74.5
MgO	.19	1.95	1.33	.65	.90	2.01	.63	2.31	.50
CaO	.00	3.81	2.83	.03	3.67	2.59	.44	2.14	2.51
Fe_2O_3	8.36	3.93	3.59	4.12	3.06	6.25	.54	8.12	2.89
MnO	.06	.15	.11	.04	.08	.11	.00	.10	.06
P_2O_5	.14	.10	.18	.10	.13	.10	.00	.11	.00
Cu	37	11	12	19	13	12	2	29	20
V	217	18	16	131	14	33	101	100	0
Cr	0	43	0	0	0	8	90	49	0
Co	16	6	5	6	5	7	3	15	5
Ni	9	22	14	10	11	25	8	37	8
Zn	116	90	55	100	43	87	10	134	39
Pb	2	39	29	46	23	14	21	20	6
Rb	28	47	123	85	126	74	263	144	9
Sr	37	302	217	0	229	273	277	272	365
Y	9	26	19	4	36	27	31	45	0
Zr	85	178	123	119	220	160	215	166	164
Nb	9	9	6	7	9	9	6	12	7
Mo	2	0	0	8	3	0	6	0	2
Ba	256	681	939	489	871	705	1259	789	359
Total (c)	99.1	99.2	99.9	95.0	101.3	99.5	95.8	93.8	99.5
S^	.00	.00	.92	.00	.88	.01	.00	.00	.03
L.O.I.	2.75	2.69	3.36	3.08	2.84	3.66	4.72	3.57	1.49
Total (T)	101.9	101.8	104.2	98.1	105.0	103.1	100.5	97.4	101.0

Appendix C

Mineralogy of the Brewer Samples based on Petrographic Study

Mineralogy of the Brewer samples based on petrographic study

Sample #	Rock Type	Mineralogy																				
		silicates and non-opaque															*sulfides, sulfates, and oxides*					
		qtz	and	kya	ser	pp	kaol	tz	epi	chl	calc	plag	ksp	cht	hb	bio	alu	py	ena	ilm	hem	others
Als-rock	breccia																	py	ena			
B-1	quartz-pyrite breccia	qtz			ser													py				
B-2	quartz vein	qtz																py				
B-3	quartz vein	qtz																py				
B-4	quartz vein	qtz																py				
B-5	quartz-pyrite breccia	qtz	and		ser													py				
B-6	quartz-topaz vein	qtz						tz														
B3-263	tuff	qtz															alu					
B440-20	tuff	qtz			ser																	
B440-5	breccia	qtz			ser												alu	py				
B440-6	breccia	qtz															alu	py				
BB'-2	tuff	qtz			ser																hem	
BB'-4	volcanic flow	qtz			ser																hem	cor
BB'-5	crystal tuff	qtz			ser																	
BB'-6	tuff	qtz			ser									cht								
BB'-6B	weld tuff	qtz			ser						calc			cht								
BB'-7	tuff	qtz			ser									cht							hem	
BB-13B	breccia	qtz			ser												alu	py				
BB-18	tuff	qtz			ser																	
BB-2	breccia	qtz	and		ser																hem	
BB-21	sil;icified rock	qtz			ser													py				
BB-3	tuff	qtz			ser																hem	
BB-4	phyllite	qtz	and		ser	pp															hem	
BB-5	quartz-hematite vein	qtz																		ilm	hem	
BBN-01	breccia		and			pp			epi												hem	
BBN-02	breccia	qtz	and	kya																		
BDH-11-53	pyrite-quartz rock	qtz			ser													py			hem	
BDH-11-54	mineralized tuff	qtz			ser													py				
BDH-11-74	foliated breccia	qtz			ser													py				
BDH-110-40	breccia	qtz			ser													py				
BDH-121-66	tuff	qtz			ser																hem	
BDH-1A-262	breccia	qtz																				
BDH-34-165	tuff	qtz			ser													py				
BDH-52-243	breccia	qtz	and															py				lazulite(?)
BDH-57-161	breccia	qtz	and		ser																	
BDH-61-156	breccia																					
BDH-61-332	breccia	qtz	and		ser													py				
BDH-61-586	breccia	qtz	and															py				

Sample #	Rock Type	Mineralogy																				
		silicates and non-opaque															*sulfides, sulfates, and oxides*				
		qtz	and	kya	ser	pp	kaol	tz	epi	chl	calc	plag	ksp	cht	hb	bio	alu	py	ena	ilm	hem	others
BDH-61-715	breccia	qtz																py	ena			cove
BDH-61-800	breccia	qtz			ser													py				
BDH-61-839	breccia	qtz			ser		kaol	tz														cor
BDH-61-949	breccia	qtz	and					tz										py				cor
BDH-62-51	crystal tuff	qtz						tz														
BDH-62-80	breccia	qtz	and		ser																	
BDH-66-121	tuff	qtz			ser																hem	
BDH-66-14	tuff	qtz			ser															ilm	hem	
BDH-66-185	breccia	qtz			ser	pp												py				
BDH-66-205	tuff	qtz			ser	pp																
BDH-66-65	breccia	qtz			ser													py			hem	
BDH-67-346	volcanic flow	qtz	and		ser													py				
BDH-71-196	breccia	qtz	and		ser													py				
BDH-72-238	breccia	qtz	and		ser	pp		tz														
BDH-74-181	volcanic flow	qtz	and																			
BDH-76-115	breccia	qtz			ser																hem	
BDH-76-65	breccia	qtz	and		ser													py				
BDH-76-69	breccia	qtz	and		ser	pp												py				
BDH-76-70	breccia	qtz	and		ser													py				
BDH-78-159	breccia	qtz	and		ser													py				
BDH-79-100	tuff	qtz			ser			tz													hem	
BDH-79-129	breccia	qtz	and	kya	ser			tz													hem	
BDH-79-188	breccia	qtz	and		ser			tz				cht						py				
BDH-79-204	breccia	qtz	and	kya	ser													py				
BDH-79-238	breccia	qtz	and	kya	ser																	
BDH-79-239	breccia	qtz	and	kya	ser																	
BDH-79-271	breccia	qtz	and	kya	ser																	
BDH-79-283	breccia		and	kya		pp												py			hem	
BDH-79-289	breccia	qtz	and	kya	ser																	
BDH-79-294	breccia	qtz				pp															hem	
BDH-79-296	breccia	qtz	and	kya	ser																	
BDH-79-300	breccia	qtz			ser		kaol	tz														
BDH-79-311	breccia	qtz	and	kya	ser	pp																
BDH-79-58	breccia	qtz			ser	pp															hem	
BDH-79-95	breccia	qtz			ser	pp												py				
BDH-79-98	breccia	qtz	and		ser	pp																
BDH-94-298	breccia ?	qtz																py	ena			chal
BDH-96-121	breccia	qtz															alu	py				
BDH-96-202	breccia	qtz	and		ser													py				
BDH-96-215	breccia	qtz				pp												py				

Sample #	Rock Type	Mineralogy																				
		silicates and non-opaque															*sulfides, sulfates, and oxides*					
		qtz	and	kya	ser	pp	kaol	tz	epi	chl	calc	plag	ksp	cht	hb	bio	alu	py	ena	ilm	hem	others
BDH-96-220	breccia	qtz	and		ser													py				
BDH-96-244	breccia	qtz																py				
BDH-96-269	breccia	qtz	and	kya	ser	pp												py				
BDH-96-275	tuff	qtz																				
BG-02	breccia	qtz	and		ser	pp												py			hem	
BN-01	tuff	qtz			ser																hem	
BN-10	tuff	qtz			ser																hem	
BN-13	tuff	qtz															alu				hem	
BN-4	breccia	qtz	and		ser													py				
BN-6	volcanic tuff	qtz			ser																hem	
BN-7	volcanic tuff	qtz			ser																hem	
BNQ-19	breccia	qtz			ser		kaol?	tz										py				
BNQ-2	breccia	qtz																py				
BO-01	volcanic flow	qtz			ser							chl									hem	
BO-03	tuff	qtz			ser													py			hem	
BO-06	slate	qtz			ser				epi		plag	chl									hem	
BP breccia	breccia	qtz																py				
BP Breccia	breccia																	py				bornite+cove
BP PIT	breccia	qtz																py				
BP-02	breccia	qtz																py				
BP-03	breccia																					
BP-05	breccia	qtz	and	kya	ser													py				
BP-breccia	breccia																	py	ena			spha
BP-LV	quartz-pyrite vein																	py	ena		hem	
BP-SV	quartz-pyrite vein																	py	ena			spha+cove
BPB-3	breccia	qtz	and	kya	ser		kaol											py				
BPB1	breccia	qtz																py				spha
BPB3	breccia	qtz	and	kya	ser		kaol											py	ena			
BPQ-4	breccia																	py	ena		hem	
BPQ-7	breccia																	py	ena			
BPZ	breccia	qtz	and		ser													py	ena			spha
BQ-19	quartz rock	qtz	and		ser																	
BQ-42	breccia																	py	ena			
BQ-45	breccia																	py	ena			
BQ-5	quartz-pyrite vein(?)																	py			hem	cove
BQ-52	breccia	qtz																py				
BQ-52	Breccia																	py	ena			
BQZ	breccia	qtz	and		ser													py				

Sample #	Rock Type	Mineralogy																			
		silicates and non-opaque														*sulfides, sulfates, and oxides*					
		qtz	and	kya	ser	pp	kaol	tz	epi	chl	calc	plag	ksp	cht	hb	bio	alu	py	ena	ilm	hem	others
Breccia	breccia																	py	ena			spha+cove
BS-01	volcanic breccia	qtz				pp																
BS-03	volcanic breccia	qtz	and	kya	ser	pp												py			hem	
BS-04	breccia	qtz	and	kya		pp															hem	
BS-15	metamudstone	qtz			ser																hem	
BS-18	metased. rock	qtz			ser																hem	
BS-20	foliated volcanic tuff	qtz			ser																	
BW-01	metavolcanic breccia	qtz			ser																hem	
BW-02	volcanic breccia	qtz																			hem	
CD-14-56	breccia	qtz	and		ser												alu	py				
CD-16-100	breccia	qtz	and	kya	ser												alu					
CD-16-36	crystal tuff	qtz															alu				hem	
CD-16-61	breccia	qtz															alu					
CD-16-84	crystal tuff	qtz			ser							plag					alu				hem	
DIKE-BP	felsic dike	qtz			ser																	
MAFIC-DIKE	mafic dike	qtz			ser																hem	
OB-2	hornfels	qtz							epi						amp	bio						
OB-3	granite	qtz							epi			plag	ksp			bio						
OB-4	granite	qtz										plag	ksp			bio						
OB-5	granite	qtz										plag	ksp		hb	bio						
OB-7	tuff	qtz			ser							plag										
OB-8	tuff	qtz			ser											bio						
WB-01	metavolcanic flow	qtz							epi	chl		plag										
WB-02	hornfels	qtz			ser				epi		calc	plag	ksp									
WB-05	hornfels	qtz			ser						calc				amp	bio		py				
WB-06	meta tuff	qtz			ser					chl		plag	ksp			bio						
WB-07	granite	qtz								chl		plag	ksp			bio						
WB-14	meta-tuff	qtz							epi			plag				bio						
Abbrevations:	qtz-quartz; and-andalusite; kya-kyanite; ser-sericite; phy-pyrophyllite; kaol-kaolinite; tz-topaz; epi-epidote; chl-chlorite; calc-calcite; plag-plagioclase; ksp-feldspar; cht-chloritoid;																					
	hb-hornblend; amp-amphibole; bio-biotite; alu-alunite;py-pyrite; ena-enargite; ilm-ilmenite; hem-hematite; spha-sphalerite; cove-covellite; chal-chalcopyrite; cor-corundum																					

Appendix D

Microthermometric Analysis Data

of Fluid Inclusions from the Brewer Mine

Microthermometric analysis of fluid inclusion

Phase & Type		Microthermometric data							Geochemical data						
T(room)=20 °C	CO_2 or vapor %	Tm-CO_2	Te	Tm-ice	Tm-clath	Th-CO_2	Th	Td	X(H_2O)	X(CO_2)	X(NaCl)	ρ (CO_2)	ρ (aq.)	ρ (bulk)	wt% NaCl eq.
BDH-61-893 -- quartz in deep porphyry rock															
Lc		-56.0				4.5				1.000		0.90	0.90	0.90	
Lc						1.8				1.000		0.92	0.92	0.92	
Lc		-56.0				0.0				1.000		0.93	0.93	0.93	
Lc		-55.9				0.0				1.000		0.93	0.93	0.93	
Lc						-3.0				1.000		0.95	0.95	0.95	
Lc		-55.8				-2.2				1.000		0.94	0.94	0.94	
Lc+Vc		-56.0				24.0				1.000		0.73	0.73	0.73	
Lc+Vc		-56.0				23.0				1.000		0.74	0.74	0.74	
Lc+Vc		-56.0				24.0				1.000		0.73	0.73	0.73	
L+Lc	20						231.5								
L+Lc	25						220.0								
L+Lc	15						198.3								
L+Lc	20						198.9								
L+Lc	15						200.8								
L+Lc	20						201.5								
L+Lc	15						200.0								
L+Lc	5						216.0								
L+Lc	15	-60.0	-35.0	-5.0	8.0	14.0	228.0		0.931	0.057	0.012	0.83	1.02	0.99	3.95
L+Lc	70	-55.7				4.4			0.537	0.463		0.90		0.93	
L+Lc	40	-55.7				4.9			0.803	0.197		0.90		0.96	
L+Lc	80					4.6			0.404	0.596		0.90		0.92	
L+Lc	25	-56.0		-1.0		1.0	240.0		0.888	0.112		0.92		0.98	1.65
L+Lc	25	-56.0		-0.6		1.0	242.0		0.888	0.112		0.92		0.98	0.99
L+Lc	20						240.0								
L+Lc	20				1.1		240.0								
L+Lc	20							302.0							
L+Lc	60						232.0								
L+Lc	15						218.6								
L+Lc+Vc	10						195.6								
BP-B1 -- quartz in breccia															
L+Lc	10						205								
L+Lc	5						220.0								
L+Lc	15						206.2								
L+Lc	10						206.3								
L+Lc	10						206.0								
L+Lc	60						290.2								
L+Lc	70						288.2								
L+Lc	80						280.0								
L+Lc	70						280.0								
L+Lc+Vc	70					30.9	288.0		0.661	0.339		0.53		0.67	
QV-E -- quartz in breccia from BP															
L+Lc	60							250.2							
L+Lc+Vc	10					28.4		295.1	0.971	0.029		0.65		0.96	
L+Lc+Vc	10					30.2		336.0	0.974	0.026		0.59		0.95	

Phase & Type		Microthermometric data							Geochemical data						
T(room)=20 °C	CO_2 or vapor %	Tm-CO_2	Te	Tm-ice	Tm-clath	Th-CO_2	Th	Td	X(H_2O)	X(CO_2)	X(NaCl)	ρ (CO_2)	ρ (aq.)	ρ (bulk)	wt% NaCl eq.
L+Lc+Vc	10					30.0		337.6	0.973	0.027		0.60		0.95	
L+Lc+Vc	10					29.0		330.6	0.972	0.028		0.63		0.96	
BPQ-X -- quartz in breccia															
L+Lc	60							271.9							
L+Lc	60							257.0							
L+Lc	60						226.0								
L+Lc	60	-57.8				4.8	249.0		0.644	0.356		0.90		0.94	
L+Lc	70	-57.0				9.7	248.0		0.547	0.453		0.86		0.90	
L+Lc	60	-57.0				11.7	249.2		0.657	0.343		0.85		0.91	
L+Lc	70	-57.0					249.0								
L+Lc	80	-56.0													
L+Lc+Vc	10					28.7		215.0	0.972	0.028		0.64		0.96	
L+Lc+Vc	10					27.8		210.3	0.971	0.029		0.66		0.96	
L+Lc+Vc	20					28.0	227.0		0.937	0.063		0.66		0.93	
L+Lc+Vc	20					28.0	230.0		0.937	0.063		0.66		0.93	
L+Lc+Vc	25					28.0	236.2		0.917	0.083		0.66		0.91	
L+Lc+Vc	20					28.0	230.0		0.937	0.063		0.66		0.93	
L+Lc+Vc	10					23.4	238.2		0.967	0.033		0.73		0.97	
L+Lc+Vc	15					24.5		245.0	0.950	0.050		0.72		0.95	
L+Lc+Vc	15					25.3		240.0	0.951	0.049		0.71		0.95	
L+Lc+Vc	15					22.7		225.0	0.949	0.051		0.74		0.96	
L+Lc+Vc	15					22.9		197.0	0.949	0.051		0.74		0.96	
L+Lc+Vc	5					23.5		240.0	0.984	0.016		0.73		0.98	
L+Lc+Vc	15					22.7		210.0	0.945	0.051		0.74		0.96	
L+Lc+Vc	15					27.0		195.0	0.953	0.047		0.67		0.95	
L+Lc+Vc	5					23.5		240.0	0.984	0.016		0.73		0.98	
L+Lc+Vc	10	-57.0				24.1		245.0	0.968	0.032		0.73		0.97	
L+Lc+Vc	30	-57.0				23.2	245.0		0.885	0.115		0.74		0.92	
L+V	2		-31.0	-7.8			110.4				0.038			1.02	11.46
L+V	2		-30.0	-8.4			109.8				0.041			1.02	12.17
L+V	2						106.0								
L+V	2			-11.0			108.0				0.052			1.04	14.98
L+V	2						107.0								
L+V	2						106.7								
L+V	2		-30.0	-3.1			107.8				0.016			0.98	5.01
L+V	2		-30.0	-3.0			106.8				0.015			0.98	4.86
L				-9.7			106.0				0.046			1.03	13.62
L+V	2		-30.0	-3.5			106.8				0.018			0.99	5.62
L			-30.0	-8.0			109.8				0.039			1.02	11.70
BPQ-4 -- small quartz vein in breccia															
Lc						14.0						0.83			
Lc						13.6						0.83			
Lc						14.1						0.83			
L+Lc	10		-30.0	-5.1	8.0	18.1			0.953	0.035	0.012	0.79	1.02	1.00	3.95
L+Lc+Vc	10		-28.0		1.5										
L+Lc+Vc	10		-25.0			25.7						0.70			
L+Lc+Vc	20					30.0			0.942	0.058		0.60		0.92	

Phase & Type		Microthermometric data							Geochemical data						
T(room)=20 °C	CO_2 or vapor %	$Tm\text{-}CO_2$	Te	Tm-ice	Tm-clath	$Th\text{-}CO_2$	Th	Td	$X(H_2O)$	$X(CO_2)$	X(NaCl)	$\rho\ (CO_2)$	ρ (aq.)	ρ (bulk)	wt% NaCl eq.
L+Lc+Vc	10					23.1						0.74			
L+Lc+Vc	10					26.6						0.69			
L+Lc+Vc	10					21.0						0.76			
L+V	10		-26.0												
BPQ-7 -- small quartz vein in breccia															
L+Lc	20							187.4							
L+Lc	5						226.2								
L+Lc+Vc	10		-28.0				213.7								
L+Lc+Vc	25	-55.0				21.0		206.3	0.905	0.095		0.76		0.94	
L+Lc+Vc	25					23.5			0.909	0.091		0.73		0.93	
L+Lc+Vc	10		-28.0		7.8	25.0	217.8		0.955	0.032	0.013	0.71	1.02	0.99	4.26
L+Lc+Vc	20					24.0	260.7		0.931	0.069		0.73		0.94	
L+Lc+Vc	10		-28.0	-11.2	6.1	24.0	220.3		0.945	0.032	0.023	0.73	1.05	1.02	7.31
L+Lc+Vc	30					24.0	271.0		0.886	0.114		0.73		0.91	
L+Lc+Vc	20		-28.0	-3.0	8.0	29.8		230.0	0.930	0.059	0.012	0.60	1.02	0.94	3.95
L+Lc+Vc	20					24.0		270.0	0.930	0.070		0.73		0.94	
L+Lc+Vc	20														
L+V	5						141.7								
L+V	5						117								
L+V	2						108								
BPQ-SV -small mineralized vein in breccia															
L+Lc+Vc	15		-25.0	-4.2	3.1	25.0	196.3		0.913	0.049	0.038	0.71	1.08	1.02	11.74
L+Lc+Vc	15		-25.0	-4.2	3.1	25.0	195.2		0.913	0.049	0.038	0.71	7.08	1.02	11.74
L+Lc+Vc	15						211.4								
L+Lc+Vc	10				8.6	27.0			0.961	0.030	0.008	0.68	0.68	0.98	2.77
L+Lc+Vc	15						223.9								
L+Lc+Vc	15				4.0	24.5	242.9		0.917	0.050	0.033	0.72	0.72	1.01	10.47
L+Lc+Vc	10			-5.0	3.2	24.0	193.0		0.930	0.032	0.038	0.73	0.73	0.04	11.61
L+Lc+Vc	10						205.0								
L+V	5			-1.3			165.0								2.14
L+V	7		-30.0	-3.5			165.0								5.62
BP-LV -- mineralized quartz vein in breccia															
L+LC	15	-56.7			4.0	10.2	200.0		0.908	0.058	0.033	0.86	1.08	1.04	10.58
L+Lc	40	-58.9			6.0	18.6	197.0		0.803	0.177	0.020	0.79	1.05	0.95	7.48
L+Lc	20							283.2							
L+Lc	15							222.8							
L+Lc	15						308.0								
L+Lc	10							245.0							
L+Lc	10							326.8							
L+Lc	10							255.0							
L+Lc+Vc	25	-57.6			4.0	26.0	192.0		0.881	0.088	0.032	0.70	1.07	0.97	10.47
L+Lc+Vc	15	-56.7		-6.0				197.0							9.19
L+Lc+Vc	20	-56.0	-31.0	-8.8	6.1	26.7		196.7	0.912	0.065	0.022	0.68	1.05	0.97	7.31
L+Lc+Vc	25	-58.8		-8.0	5.0	26.1	197.0		0.886	0.087	0.027	0.69	1.06	0.97	9.08
L+Lc+Vc	20	-56.0	-30.0	-8.0	6.0	26.3	197.0		0.911	0.066	0.023	0.69	1.05	0.98	7.48
L+Lc+Vc	5		-30.0	-6.8		30.0	224.9	255.0	0.954	0.013	0.034	0.60	1.07	1.05	10.23
L+V	5		-26.0	-1.1			151.0								1.82

Phase & Type		Microthermometric data							Geochemical data						
T(room)=20 °C	CO_2 or vapor %	Tm-CO_2	Te	Tm-ice	Tm-clath	Th-CO_2	Th	Td	X(H_2O)	X(CO_2)	X(NaCl)	ρ (CO_2)	ρ (aq.)	ρ (bulk)	wt% NaCl eq.
BPV -- quartz in quartz-andalusite-pyrite rock															
L+Lc	40							281.2							
L+Lc	15		-24.0		1.1			245.0							
L+Lc	5							288.8							
L+Lc	5						271.0								
L+Lc+Vc	15	-56.0	-26.0	-1.2		25.2		245.0	0.945	0.049	0.006	0.71	1.01	0.96	1.98
L+Lc+Vc	15					28.2		245.0	0.955	0.045		0.65		0.94	
L+Lc+Vc	30			-10.8		30.5	280.0		0.863	0.091	0.046	0.57	1.10	0.94	14.77
L+Lc+Vc	10	-56.0				30.9			0.977	0.023		0.51		0.95	
L+Lc+Vc	25	-56.0	-28.0	-3.1		28.2			0.903	0.082	0.015	0.65	1.03	0.93	5.01
L+Lc+Vc	15	-56.0		-5.6		27.8		271.1	0.927	0.046	0.027	0.66	1.06	1.00	8.65
L+Lc+Vc	15		-30.0			30.8			0.962	0.038		0.54		0.93	
L+Lc+Vc	15	-56.1		-13.7	2.9	28.2		277.0	0.916	0.045	0.039	0.65	1.08	1.02	12.10
L+Lc+Vc	10					30.9	223.4		0.977	0.023		0.51		0.95	
L+Lc+Vc	15					26.1		277.0	0.952	0.048		0.69		0.95	
L+Lc+Vc	10		-26.0	-11.3	6.0	27.6	234.0		0.947	0.030	0.024	0.67	1.05	1.01	7.48
BQ-36 -- quartz vein in breccia															
Lc+Vc	15					29.0									
Lc+Vc	10					28.4									
Lc+Vc	15					26.7									
L+Lc	25						215.9								
L+Lc	20						220.0								
L+Lc	7							226.1							
L+Lc	15						233.4								
L+Lc	10						212.2								
L+Lc	10						210.0								
L+Lc	25					20.0		223.6	0.904	0.096		0.77		0.94	
L+Lc	30						235.0								
L+Lc	15							250.0							
L+Lc	15						214.3								
L+Lc	20						199.9								
L+Lc	35						260.6								
L+Lc	20							228.0							
L+Lc	20						198.2								
L+Lc	30						185.0								
L+Lc	20						251.3								
L+Lc	30						257.6								
L+Lc	20						262.4								
L+Lc	25	-57.0													
L+Lc+Vc	20						238.5								
L+Lc+Vc	15	-57.0	-30.0	-0.5			225.1								0.83
L+Lc+Vc	20						242.5								
L+V	10			-0.7			190.0								1.16
L+V	10		-30.0	-2.4			190.0								3.92
BQ-45 -- quartz vein in breccia															
Lc		-57.0				17.4						0.80			
L+Lc	30							280.0							

Phase & Type		Microthermometric data							Geochemical data						
T(room)=20 °C	CO_2 or vapor %	Tm-CO_2	Te	Tm-ice	Tm-clath	Th-CO_2	Th	Td	X(H_2O)	X(CO_2)	X(NaCl)	ρ (CO_2)	ρ (aq.)	ρ (bulk)	wt% NaCl eq.
L+Lc	25						276.0								
L+Lc	30						265.8								
L+Lc	20						264.7								
L+Lc	25						310.0								
L+Lc	20							300.0							
L+Lc	15						255.7								
L+Lc	30						280.0								
L+Lc	30						314.6								
L+Lc	15			-0.2			184.0								
L+Lc	70	-56.6													
L+Lc	60						320.0								
L+Lc+Vc	30	-57.0				25.6			0.890	0.110		0.70		0.91	
L+Lc+Vc	60	-57.0				29.6			0.725	0.275		0.61		0.76	
BQ-43 -- quartz vein in breccia															
L+Lc	30					1.8	326.2		0.861	0.139		0.92		0.97	
L+Lc	7					2.0	168.8		0.973	0.027		0.92		0.99	
L+Lc	5					2.0	150.0		0.973	0.027		0.92		0.99	
L+Lc	30						286.8								
L+Lc	40						300.0								
L+Lc+Vc	20				9.9	30.9	242.5		0.947	0.052	0.001	0.53	0.99	0.90	0.22
BNQ-19 -- quartz vein in andalusite-bearing rock															
L+Lc	20						209.0								
L+Lc	20						208.6								
L+Lc	20						209.2								
L+Lc	20							226.6							
L+Lc	20						266.2								
L+Lc	20							260.0							
L+Lc	10		-32.0				280.0								
L+Lc	15						288.0								
L+Lc	15						283.0								
L+Lc	15						264.9								
L+Lc	25			-1.0			326.7								1.65
L+Lc	80	-57.0				12.0			0.417	0.583		0.85		0.88	
L+Lc	20	-57.0													
L+Lc	20		-33.0	-10.1			275.6								14.05
L+Lc	10		-30.0	-8.4			236.0								12.17
L+Lc	60						270.0								
L+Lc	60					10.0			0.654	0.346		0.86		0.92	
L+Lc	40							300.0							
L+Lc+Vc	10		-30.0	-8.5	4.3		301.8								12.29
L+V	15			-8.0											11.70
BDH-121-X -- quartz in massive pyrite															
L+Lc	10		-28.0	-2.8	9.5	15.0			0.961	0.036	0.003	0.82	1.00	0.98	1.03
L+Lc	20	-57.0	-25.0		6.5	19.1			0.906	0.074	0.020	0.78	1.04	0.99	6.63
L+Lc	25				9.6		231.0								
L+Lc	15		-28.0		10.0		240.9								
L+Lc	10						243.2								

Phase & Type		Microthermometric data						Geochemical data						
T(room)=20 °C	CO_2 or vapor %	Tm-CO_2	Te	Tm-ice	Tm-clath	Th-CO_2	Th	Td	X(H_2O)	X(CO_2)	X(NaCl)	ρ (CO_2)	ρ (aq.)	ρ (bulk)	wt% NaCl eq.
L+Lc	10						220.0								
L+Lc	15						242.5								
L+Lc	15							322.0							
L+Lc	20			-0.1		15.0			0.921	0.078	0.001	0.82	0.99	0.96	0.17
L+Lc+Vc	20				10.0		233.9								
L+Lc+Vc	20				8.5	30.0	210.0		0.933	0.058	0.009	0.60	1.01	0.93	3.00
L+Lc+Vc	20					30.9	211.9		0.950	0.050		0.51		0.90	
L+Lc+Vc	15						215.4								
L+Lc+Vc	10					30.0	224.5		0.974	0.026		0.60		0.96	
L+Lc+Vc	10					30.6			0.975	0.025		0.56		0.95	
L+Lc+Vc	15	-54.9	-30.0	-3.6	8.7	30.1	227.8		0.951	0.041	0.008	0.59	1.01	0.95	2.62
L+V	10		-28.0												
BQ-5 -- quartz in breccia															
Lc+Vc	25	-55.7				28.5						0.64			
L+Lc	10		-30.0		6.0		194.5								
L+Lc+Vc	15					29.0		249.0	0.956	0.044		0.63		0.94	
L+Lc+Vc	10					29.0		247.0	0.972	0.028		0.63		0.96	
L+V	5			-6.0			196.2		9.970		0.030			0.94	9.19
L+V	10		-26.0	-3.0			190.0		9.985		0.015			0.92	4.86
L+V	7		-25.0	0.0			201.6								
L+V	5		-28.0	0.2											
L+V	5		-25.0	0.0			126.9								
L+V	5		-30.0	-2.0			190.0		9.990		0.010			0.90	3.28
L+V	7						194.2								
L+V	5		-30.0				192.1								
BQ-1 -- quartz vein in altered volcanic rock															
L+Lc	30						226.6								
L+Lc	40						270.1								
L+Lc	60						240.0								
L+Lc	20						216.4								
L+Lc	50						234.5								
L+Lc	20						209.2								
L+Lc	15						319.4								
L+Lc	15						263.7								
L+Lc	15						314.2								
L+Lc	15						251.0								
L+Lc+Vc	15							323.0							
BQ-30 -- quartz vein in altered volcanic rock															
L+Lc	25						227.4								
L+Lc	15						243.5								
L+Lc	10						249.3								
L+Lc	30							271.0							
L+Lc	20							267.0							
L+Lc	5						190.0								
BQ-24 -- quartz vein in B-6 area															
L+Lc	10							230.0							
L+Lc	10						235.0								

Phase & Type		Microthermometric data							Geochemical data						
T(room)=20 °C	CO_2 or vapor %	Tm-CO_2	Te	Tm-ice	Tm-clath	Th-CO_2	Th	Td	X(H_2O)	X(CO_2)	X(NaCl)	ρ (CO_2)	ρ (aq.)	ρ (bulk)	wt% NaCl eq.
L+Lc	20						225.4								
L+Lc	15						232.0								
L+Lc	30						226.0								
L+Lc	40						220.0								
L+Lc	40						228.3								
L+Lc+Vc	20					29.6	207.3		0.941	0.059		0.61		0.92	
L+Lc+Vc	20					29.6	205.0		0.941	0.059		0.61		0.92	
L+Lc+Vc	25					29.6	206.3		0.941	0.059		0.61		0.92	
L+Lc+Vc	20					29.6	156.0		0.941	0.059		0.61		0.92	
L+Lc+Vc	20					29.6	191.0		0.941	0.059		0.61		0.92	
L+Lc+Vc	15						208.6								
L+Lc+Vc	10	-55.0	-32.0	-5.5			235.0								8.51
L+Lc+Vc	15	-55.0	-26.0	-3.9	8.0	29.4	227.8		0.945	0.043	0.012	0.62	1.02	0.96	3.89
L+Lc+Vc	20	-55.0	-22.0	-6.0	6.0	29.0	230.0		0.916	0.061	0.023	0.63	1.04	0.96	7.38
L+Lc+Vc	20	-54.5	-30.0	-5.0	5.0	29.0	232.0		0.911	0.061	0.028	0.63	1.06	0.97	8.97
L+Lc+Vc	20	-54.0	-25.0	-3.5	10.0	29.5	230.0		0.940	0.060	0.000	0.62	0.99	0.91	0.02
L+Lc+Vc	15	-55.0	-24.0	-5.0		29.5	231.0		0.957	0.043		0.62		0.94	7.82
L+Lc+Vc	15			-5.0	9.0	29.6	236.0		0.951	0.043	0.006	0.61	1.00	0.94	2.00
BQ-6 -- quartz vein in B-6 altered volcanic rock															
L+Lc	10						188.3								
L+Lc	10						222.7								
L+Lc	10						188.2								
L+Lc	15							223.0							
L+Lc	10							223.0							
BQ-9(S) -- pyrite-quartz vein in B-6 area															
L+Lc	15						244.4								
L+Lc	15						270.8								
L+Lc	15						284.6								
L+Lc	25						270.0								
L+Lc	20						227.1								
L+Lc	20						233.4								
L+Lc	25						229.0								
L+Lc	15						251.0								
L+Lc	20						258.2								
L+Lc	25						288.0								
L+Lc	15						260.6								
L+Lc	30							300.0							
L+Lc+Vc	20						253.2								
L+Lc+Vc	20						229.3								
L+Lc+Vc	15						225.0								
BDH-96-45 -- quartz vein in volcanic rock															
L+Lc	20						204.0								
L+Lc	20						206.4								
L+Lc	15						205.0								
L+Lc	20						204.0								
L+Lc+Vc	10						205.5								
L+Lc+Vc	20						208.8								

Phase & Type		Microthermometric data							Geochemical data						
T(room)=20 °C	CO_2 or vapor %	Tm-CO_2	Te	Tm-ice	Tm-clath	Th-CO_2	Th	Td	X(H_2O)	X(CO_2)	X(NaCl)	ρ (CO_2)	ρ (aq.)	ρ (bulk)	wt% NaCl eq.
L+Lc+Vc	5						189.5								
L+V	5						180.0								
L+V	5						198.1								
BDH-96-70 -- quartz in pyrite-als rock															
L+Lc	20						297.9								
L+Lc	10						286.5								
L+Lc	10							320.0							
L+Lc	15							238.6							
BDH-96-160 -- quartz vein in breccia															
L+Lc	5						199.9								
L+Lc	10						229.4								
L+Lc	10						218.0								
L+Lc	15						216.0								
L+Lc	15						228.7								
L+Lc	15						226.0								
BDH-96-226 -- vein in pyritic silicified rock															
L+Lc+Vc	20	-55.7		-3.0	8.2	29.5	240.1		0.930	0.059	0.011	0.62	1.02	0.94	3.57
L+Lc+Vc	10	-55.7		-2.9	8.0	28.9	250.0		0.960	0.028	0.012	0.63	1.02	0.98	3.95
L+Lc+Vc	20	-55.7		-5.0	8.2	27.8		240.1	0.926	0.064	0.011	0.66	1.02	0.95	3.57
L+Lc+Vc	25	-55.9		-4.7	8.2	29.2		278.3	0.911	0.079	0.010	0.63	1.02	0.92	3.57
L+Lc+Vc	25	-55.9		-5.7	7.9	28.6		278.0	0.907	0.081	0.012	0.64	1.02	0.93	4.14
L+Lc+Vc	20	-55.9		-5.0	7.2	29.0	264.9		0.923	0.061	0.016	0.63	1.03	0.95	5.41
L+Lc+Vc	10						251.8								
L+Lc+Vc	20	-55.6													
QV -- quartz vein in B-6															
L+Lc+Vc	25					28.4		311.0	0.919	0.081		0.65		0.91	
L+Lc+Vc	25						313.0								
L+Lc+Vc	25					28.4		311.0	0.919	0.081		0.65		0.91	
BDH-96-117(b) -- quartz vein in B-6 breccia															
L+V	5		-25.8	-5.1			122.3								7.96
L+V	5		-25.0	-4.5			110.6								7.10
L+V	10		-26.0				229.5								
L+V	10						224.7								
L+V	5						266.4								
BS-10 -- quartz vein in volcaniclastic rock (clay pit)															
L+Lc	10						196.3								
L+Lc	15						195.1								
L+Lc	10						199.1								
L+Lc	10						214.0								
L+Lc	10						198.0								
L+Lc	10						171.0								
L+Lc	15						176.0								
L+Lc	10						195.0								
L+Lc	10						171.6								
L+Lc	10						169.0								
L+V	10		-28.0	-5.3											8.24
L+V	15		-30.0	-7.0											10.48
L+V	10		-28.0	-5.7											8.79

Appendix E

Orientation of Quartz Veins at Brewer Mine

Quartz vein orientation in the Brewer mine				
Sample #	**Vein type**	**Host rock**	**Stike**	**Dip**
BQ-1	buck quartz	als-silicate	N15W	70NE
			N82W	27SW
BQ-2	quartz	als-silicate	N20W	82SW
BQ-3	quartz		N53E	47SE
			N20W	80NE
			N70E	30SE
BQ-4	quartz+muscovite		S85E	70SW
BQ-5	quartz		N60E	60SE
BQ-6	quartz		N55E	30SE
BQ-7	quartz	als-silicate		
BQ-8	quartz+pyrite	als-silicate		
BQ-9(sulfide)	quartz+pyrite		N40W	70NE
BQ-9(center)	quartz			
BQ-9(margin)	quartz+muscovite			
BQ-10	quartz	phyllite(s bearing)		
BQ-11	quartz	massive pyrite		
BQ-12	quartz+-pyrite			
BQ-13	quartz	py als-silicate		
BQ-14	quartz		N42E	30SE
BQ-15	quartz+pyrophyllite			
BQ-16	quartz+pyrophyllite	als-silicate	N60E	50SE
			N50E	45SE
BQ-17	bulk milky quartz	als-silicate		
BQ-18	quartz+pyrite			
	quartz	als-silicate	N53E	47SE
BQ-19	quartz+topaz ?	topaz rock (?)	NS	40E
	quartz	tuffceous rock	N47E	50SE
BQ-20	quartz+pyrophyllite	tuffceous rock	N57E	49SE
BQ-21	quartz		N5W	78SW
	quartz	volcanic rock	N52E	52SE
BQ-22	quartz	volcanic rock		
BQ-23	massive quartz			
BQ-24	quartz		N20E	83SE
BQ-24b				
BQ-25	quartz	als-silicate		
BQ-26	quartz+muscovite		N85E	82SE
BQ-27	quartz+pyrite	py-als-rock		
BQ-28	quartz	volcanic rock	EW	34S
BQ-29	quartz	py-als-rock		
BQ-30	quartz	volcanic tuff	N75W	32SW
BQ-31	quartz	als-silicate	N57E	42SE
BQ-32	quartz+pyrophyllite	als-silicate	N45E	36SE
BQ-33	quartz		N15W	84NE
BQ-34	quartz+pyrophyllite+pyrite	als-silicate	NS	68W
BQ-35a	breccia			
BQ-35b	silicate rock			
BQ-36	quartz	breccia	N45E	58SE
BQ-37	quartz+pyrophyllite	breccia		
BQ-38	quartz+pyrite	breccia		
BQ-39a	quartz			
BQ-39b	quartz in breccia ?			

Sample #	Vein type	Host rock	Stike	Dip
BQ-40	quartz	topaz rock		
BQ-41	topaz rock			
BQ-42	quartz+pyrite breccia			
BQ-43	quartz		N15W	80SW
BQ-44	quartz+pyrite			
BQ-45	quartz		N43E	71SE
BQ-46	quartz+pyrite			
BQ-47	quartz	als-rock		
BQ-48	quartz+pyrophyllite	als-silicate	N55E	60SE
BQ-49	breccia			
BQ-50	pyrite vein	breccia		
BQ-51	quartz	py-breccia		
BQ-52	silica-py-enargite breccia			
BQ-53	quartz			
BQ-54	quartz	breccia		
BQ-55	quartz+pyrophyllite+sulfide ?			
BQ-56	quartz	py-breccia	N75W	20SW
BQ-57	quartz+pyrophyllite	als-silicate		
BQ-58	quartz	py-als-rock	N35W	72NE
BN-1	quartz vein			
BN-8	quartz vein			
BS-10	quartz	metasedimentary	N40W	83NE
			N38W	80NE
BS-11	quartz	metasedimentary	N27E	80SE
BS-16	quartz		NS	78E
BS-19 ?	quartz		N30E	62SE

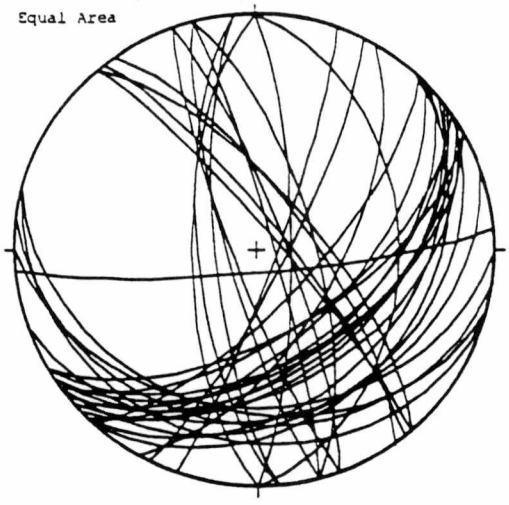
Equal Area

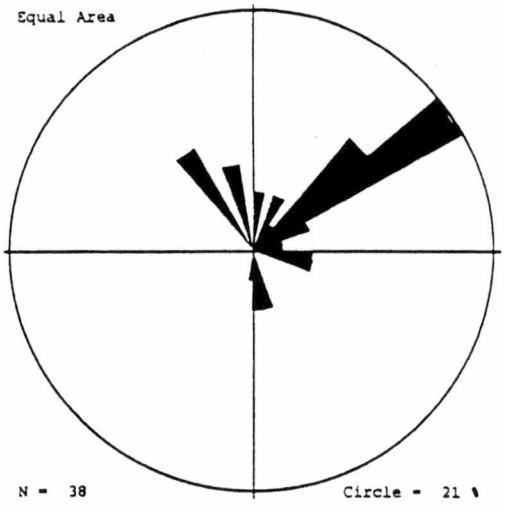
Equal Area
N = 38
Circle = 21 %

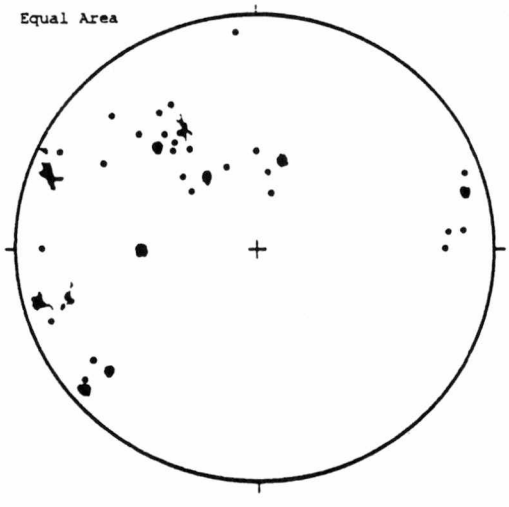
Equal Area

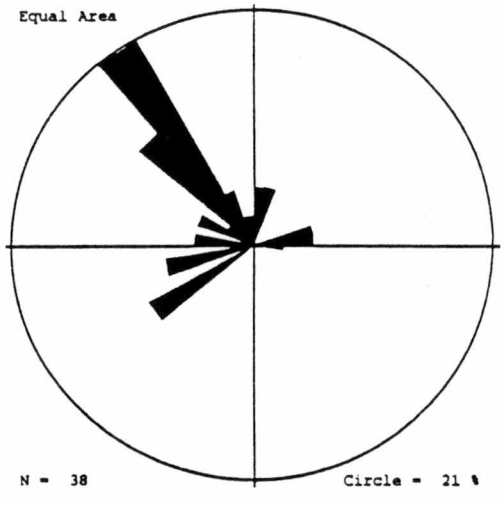
Equal Area
N = 38
Circle = 21 %

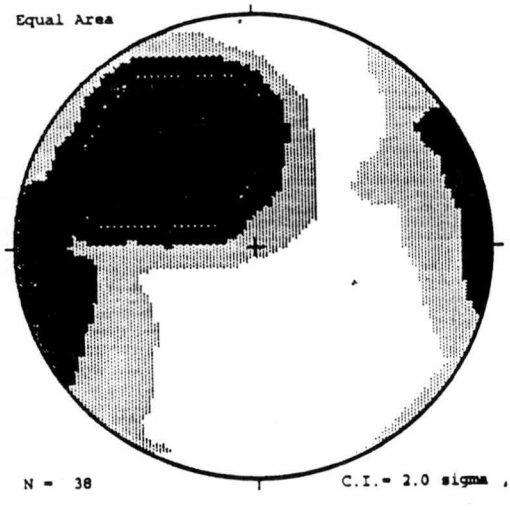
Equal Area
N = 38
C.I.= 2.0 sigma

Vita

Changsheng Lu was born in Guangdong Province, southern China. He moved with his parents to Xiuwu, Henan Province, central China and grew up there. After graduated from high school in 1979, he went to the Lanzhou University, Lanzhou, Gansu Province in northwestern China in the September, 1979 and graduated in July, 1983 with a B.S. in Geology. He worked in the Department of Geology of the Lanzhou University as a Teaching and Research Associate between 1983 and 1985.

In September, 1985, he enrolled the graduate program in the Department of Geological Sciences of the University of Oregon. He graduated in June, 1988 with a M.S. in Geology. The following August, he started his Ph.D. program in the Department of Geological Sciences of the University of Tennessee and was awarded a Graduate Teaching Assistantship. He worked in the TVA Engineering Laboratory on a Graduate Internship between May, 1992 and April, 1993. During the last year of his graduate school, he worked as a geologist and geoscientist in two Oak Ridge-Knoxville companies while finishing up his dissertation. In August, 1994, he received the Doctor of Philosophy degree with a major in Geology from the University of Tennessee, Knoxville, and finally finished his long school career.

Photography is his "big" hobby that he has spent a great time and effort.